

Instrumentation for Flexible Pavements—Field Performance of Selected Sensors

Volume I: Final Report



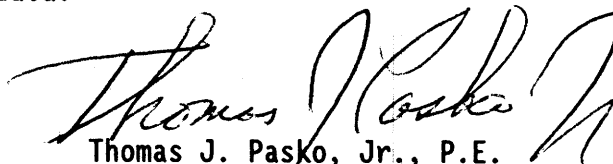
U.S. Department of Transportation
Federal Highway Administration

Research and Development
Turner-Fairbank Highway Research Center
6300 Georgetown Pike
McLean, Virginia 22101-2296

FOREWORD

Deflections measured at the pavement surface under known loads are the most widely used method for estimating the structural condition of pavements. In-situ resilient moduli are derived by back calculation methods. The availability of pavement response data at and below the pavement surface enhances the accuracy of these estimates. A computer model, PENMOD, has been developed and is documented in the report. This model can use stress, strain and deflection data, or a combination of these, for back calculating the resilient modulus. A further advantage of embedded sensors is that continuous response data can be collected without interfering with traffic. However, installation of an adequate number of sensors is costly and therefore must be well planned and executed.

The information in this report, and in a previous report generated under this research (FHWA-RD-89-084, "Instrumentation for Flexible Pavements") are valuable guides for selecting, installing, and monitoring in-situ instrumentation. A companion (not printed) report, FHWA-RD-91-095, contains a compilation of the test data.



Thomas J. Pasko, Jr., P.E.
Director, Office of Engineering and Highway
Operations Research and Development

NOTICE

This document is disseminated under the sponsorship of the Department of Transportation in the interest of information exchange. The United States Government assumes no liability for its contents or use thereof. The contents of this report reflect the views of the contractor, who is responsible for the accuracy of the data presented herein. The contents do not necessarily reflect the official policy of the Department of Transportation. This report does not constitute a standard, specification, or regulation.

The United States Government does not endorse products or manufacturers. Trade or manufacturers' names appear herein only because they are considered essential to the object of this document.

1. Report No. FHWA-RD-91-094		2. Government Accession No.		3. Recipient's Catalog No.	
4. Title and Subtitle INSTRUMENTATION FOR FLEXIBLE PAVEMENTS--FIELD PERFORMANCE OF SELECTED SENSORS, Volume I: Final Report				5. Report Date June 1992	
				6. Performing Organization Code	
7. Author(s) P. Sebaaly, N. Tabatabaee, B. Kulakowski, T. Scullion				8. Performing Organization Report No. PTI 9118	
9. Performing Organization Name and Address Pennsylvania Transportation Institute The Pennsylvania State University Research Office Building University Park, PA 16802				10. Work Unit No. (TRAIS) 3C3A-2312	
				11. Contract or Grant No. DTFH61-88-R-00052	
12. Sponsoring Agency Name and Address Office of Engineering and Highway Operations R & D Federal Highway Administration 6300 Georgetown Pike McLean, VA 22101-2296				13. Type of Report and Period Covered Final Report July 1988 - May 1991	
				14. Sponsoring Agency Code	
15. Supplementary Notes FHWA Contracting Officer's Technical Representative (COTR): R. R. Hegmon, HNR-20					
16. Abstract <p>This report presents the results of a research study on methods for measuring strain and stress in bituminous pavements subjected to dynamic vehicle loading. The research program was divided into two phases. In the first phase, an extensive literature search was conducted to identify the existing pavement instrumentation and to select the most promising types of gauges for a field testing program. Two sections of bituminous pavement 6 and 10 in (152 and 254 mm) thick were constructed and instrumented with the selected gauges. The response of the gauges to dynamic loading applied by a tractor-semitrailer at different levels of axle loading, tire pressure, and speed was investigated. In the second phase, new concepts in pavement instrumentation were investigated. Prototype gauges were built and evaluated, first in the laboratory and then in a field testing program similar to the one conducted in the first phase. Two new gauges, an inductive sensor and the Hall effect sensor, performed very well in the tests. The pavement response data, collected in the field testing program, were used to evaluate methods for backcalculating pavement material properties. It was demonstrated that the backcalculated moduli are much more accurate if data from multiple sensors placed throughout the pavement structure, rather than a single sensor measurements, are used in the analysis.</p> <p>This volume is the first in a series. The other volume in the series is:</p> <p style="text-align: center;">FHWA-RD-91-095 Volume II: Appendixes</p>					
17. Key Words H-gauges, pressure cells, LVDT, geophone, SLD, MDD, Hall effect sensor, inductive gauges, thermocouples, solid state sensors			18. Distribution Statement This document is available to the public through the National Technical Information Service, Springfield, Virginia 22161.		
19. Security Classif. (of this report) Unclassified		20. Security Classif. (of this page) Unclassified		21. No. of Pages 314	22. Price

SI* (MODERN METRIC) CONVERSION FACTORS

APPROXIMATE CONVERSIONS TO SI UNITS

APPROXIMATE CONVERSIONS FROM SI UNITS

Symbol	When You Know	Multiply By	To Find	Symbol	Symbol	When You Know	Multiply By	To Find	Symbol
LENGTH					LENGTH				
in	inches	25.4	millimeters	mm	mm	millimeters	0.039	inches	in
ft	feet	0.305	meters	m	m	meters	3.28	feet	ft
yd	yards	0.914	meters	m	m	meters	1.09	yards	yd
mi	miles	1.61	kilometers	km	km	kilometers	0.621	miles	mi
AREA					AREA				
in ²	square inches	645.2	millimeters squared	mm ²	mm ²	millimeters squared	0.0016	square inches	in ²
ft ²	square feet	0.093	meters squared	m ²	m ²	meters squared	10.764	square feet	ft ²
yd ²	square yards	0.836	meters squared	m ²	m ²	meters squared	1.195	square yards	ac
ac	acres	0.405	hectares	ha	ha	hectares	2.47	acres	mi ²
mi ²	square miles	2.59	kilometers squared	km ²	km ²	kilometers squared	0.386	square miles	
VOLUME					VOLUME				
fl oz	fluid ounces	29.57	milliliters	ml	ml	milliliters	0.034	fluid ounces	fl oz
gal	gallons	3.785	liters	l	l	liters	0.264	gallons	gal
ft ³	cubic feet	0.028	meters cubed	m ³	m ³	meters cubed	35.71	cubic feet	ft ³
yd ³	cubic yards	0.765	meters cubed	m ³	m ³	meters cubed	1.307	cubic yards	yd ³
MASS					MASS				
oz	ounces	28.35	grams	g	g	grams	0.035	ounces	oz
lb	pounds	0.454	kilograms	kg	kg	kilograms	2.202	pounds	lb
T	short tons (2000 lb)	0.907	megagrams	Mg	Mg	megagrams	1.103	short tons (2000 lb)	T
TEMPERATURE (exact)					TEMPERATURE (exact)				
°F	Fahrenheit temperature	5(F-32)/9 or (F-32)/1.8	Celcius temperature	°C	°C	Celcius temperature	1.8C + 32	Fahrenheit temperature	°F
ILLUMINATION					ILLUMINATION				
fc	foot-candles	10.76	lux	l	lx	lux	0.0929	foot-candles	fc
fl	foot-Lamberts	3.426	candela/m ²	cd/m ²	cd/m ²	candela/m ²	0.2919	foot-Lamberts	fl
FORCE and PRESSURE or STRESS					FORCE and PRESSURE or STRESS				
lbf	poundforce	4.45	newtons	N	N	newtons	0.225	poundforce	lbf
psi	poundforce per square inch	6.89	kilopascals	kPa	kPa	kilopascals	0.145	poundforce per square inch	psi

* SI is the symbol for the International System of Units

(Revised January 1992)

VOLUME I: FINAL REPORT

TABLE OF CONTENTS

<u>Chapter</u>	<u>Page</u>
1. INTRODUCTION	1
BACKGROUND	1
OBJECTIVES	1
OUTLINE OF THE REPORT	2
 2. TESTING OF EXISTING FLEXIBLE PAVEMENTS	
INSTRUMENTATION: PHASE I	3
SELECTION OF INSTRUMENTATION	3
EXPERIMENTAL PLAN	5
PAVEMENT DESIGN	5
INSTRUMENTATION LAYOUT	5
DATA COLLECTION PLAN	6
DATA ANALYSIS PLAN	10
PAVEMENT CONSTRUCTION	11
INSTALLATION OF INSTRUMENTATION	15
SOIL STRAIN GAUGES	18
H-GAUGES	19
PRESSURE CELLS	19
GEOPHONES	20
Unbonded Layers	20
Bonded Layers	21
INSTRUMENTED CORES	21
SINGLE-LAYER DEFLECTOMETER	22
MULTIDEPTH DEFLECTOMETER	22
DATA ACQUISITION AND REDUCTION	24
FIELD TESTING	27
 3. DATA ANALYSIS: PHASE I	31
STRAIN MEASUREMENTS IN THE ASPHALT CONCRETE LAYER	31
SURVIVABILITY	31
REPEATABILITY	34
EFFECTS OF TEST VARIABLES ON THE RESPONSE OF GAUGES	40
Effect of Axle Load on the Response of Strain Gauges	41
Effect of Truck Speed on the Response of Strain Gauges	41
UNCERTAINTY	46
REGRESSION ANALYSIS OF STRAIN MEASUREMENTS	54
STRAIN MEASUREMENT IN THE SUBGRADE LAYER	60
SURVIVABILITY	61
REPEATABILITY	61
EFFECTS OF TEST VARIABLES ON THE RESPONSE OF SOIL STRAIN GAUGES	62
UNCERTAINTY	68

**VOLUME I: FINAL REPORT
TABLE OF CONTENTS (Continued)**

<u>Chapter</u>	<u>Page</u>
COMPRESSIVE STRESS MEASUREMENTS	72
SURVIVABILITY OF THE PRESSURE CELLS	72
REPEATABILITY	72
EFFECT OF TEST VARIABLES ON THE PRESSURE CELL MEASUREMENTS	72
UNCERTAINTY	77
ANALYSIS OF DEFLECTION DATA	79
SURVIVABILITY	79
REPEATABILITY	80
EFFECTS OF TEST VARIABLES ON THE RESPONSE OF GAUGES	85
UNCERTAINTY OF THE MEASURED DEFLECTIONS	94
AUXILIARY MEASUREMENTS	94
MOISTURE MEASUREMENTS	94
TEMPERATURE MEASUREMENTS	98
4. EVALUATION OF IN SITU RESILIENT MODULI FROM SENSORS DATA	101
DESCRIPTION OF THE GENERALIZED MODULUS BACKCALCULATION PROCEDURE	101
INPUTS TO THE GENERALIZED BACKCALCULATION PROCEDURE	104
Strain Gauge	104
Stress Sensor	104
Multidepth Deflectometer	106
SENSITIVITY ANALYSIS	106
SYSTEMATIC ERROR ANALYSIS	109
RANDOM ERROR ANALYSIS	115
MODULUS BACKCALCULATION USING MDD DATA COLLECTED UNDER A FALLING WEIGHT DEFLECTOMETER	120
MODULUS BACKCALCULATION USING SENSOR DATA COLLECTED UNDER TRUCK LOADING	128
BACKCALCULATION OF IN SITU MODULI FROM THE MEASURED STRAIN BASINS	128
BACKCALCULATION OF IN SITU MODULI FROM THE MEASURED MDD DEFLECTIONS	129
BACKCALCULATION OF IN SITU MODULI FROM THE COMBINATION OF THE MEASURED STRAIN BASINS AND MDD DEFLECTIONS	129
CONCLUSIONS AND RECOMMENDATIONS	135
5. INVESTIGATION OF NEW INSTRUMENTATION IDEAS	141
INVESTIGATION OF GAUGES USED IN PORTLAND CEMENT CONCRETE	141
CARLSON GAUGE	141
Principles of Measurement	141
Cost and Availability	143
Operating Temperature	143

**VOLUME I: FINAL REPORT
TABLE OF CONTENTS (Continued)**

<u>Chapter</u>	<u>Page</u>
Moisture Effects	144
Linearity and Range	144
Applications	144
Recommendations	144
TML EMBEDMENT STRAIN GAUGE	145
Principles of Measurement	145
Cost and Availability	145
Operating Temperature	145
Moisture Effects	147
Linearity and Range	147
Applications	147
Recommendations	147
NEW INSTRUMENTATION CONCEPTS	147
HALL EFFECT SENSOR	148
Principles of Measurement	148
Cost and Availability	150
Operating Temperature	150
Moisture Effects	152
Linearity and Range	152
Applications	152
Recommendations	152
PIEZOELECTRIC FILM	154
Principles of Measurement	154
Cost and Availability	154
Operating Temperature	155
Linearity and Range	155
Applications	157
Recommendations	157
INDUCTIVE DISPLACEMENT TRANSDUCER	157
Principles of Measurement	157
Cost and Availability	158
Operating Environment	158
Linearity and Range	158
Applications	159
Recommendations	159
INVESTIGATION OF WIRELESS GAUGES	159
RECOMMENDATIONS	161
6. TESTING OF NEW INSTRUMENTATION: PHASE II	163
LABORATORY TESTING OF NEW INSTRUMENTATION	163
MEASUREMENT OF THE MODULUS OF ELASTICITY OF EXISTING GAUGES	163
LABORATORY TESTING OF THE NEW INSTRUMENTATION CONCEPTS GAUGES	166
Effect of Temperature	166
Dynamic Characteristics	166
Measurement of Modulus of Elasticity	167
Effect of Bending	167

**VOLUME I: FINAL REPORT
TABLE OF CONTENTS (Continued)**

<u>Chapter</u>	<u>Page</u>
THE USE OF HALL EFFECT SENSORS IN THE MULTIDEPTH DEFLECTOMETER	167
PURPOSE OF TESTING	167
HARDWARE SETUP	175
CALIBRATION OF SENSORS	175
EXPERIMENTAL PLAN	178
PAVEMENT DESIGN	178
DATA COLLECTION PLAN	178
INSTRUMENTATION LAYOUT	180
DATA ANALYSIS PLAN	184
PAVEMENT CONSTRUCTION	185
INSTALLATION OF INSTRUMENTATION	185
DATA ACQUISITION AND REDUCTION	186
 7. DATA ANALYSIS: PHASE II	 187
STRAIN MEASUREMENTS IN THE ASPHALT CONCRETE LAYER	187
SURVIVABILITY	188
REPEATABILITY	188
EFFECT OF TEST VARIABLES ON THE RESPONSE OF GAUGES	189
Effect of Axle Load on the Response of Strain Gauges	189
Effect of Truck Speed on the Response of Strain Gauges	192
UNCERTAINTY	192
REGRESSION ANALYSIS OF STRAIN MEASUREMENTS	194
STRAIN MEASUREMENTS IN THE UNBONDED LAYERS	203
SURVIVABILITY	203
REPEATABILITY	207
EFFECTS OF TEST VARIABLES ON THE RESPONSE OF SOIL STRAIN GAUGES	210
ANALYSIS OF DEFLECTION DATA	210
SURVIVABILITY	210
REPEATABILITY	210
EFFECT OF TEST VARIABLES ON THE RESPONSE OF SLD	214
UNCERTAINTY	214
ANALYSIS OF MDD DATA	215
 8. SUMMARY AND RECOMMENDATIONS	 227
FIELD EVALUATION OF EXISTING GAUGES	228
EXISTING GAUGES TO MEASURE STRAINS IN THE ASPHALT CONCRETE LAYER	228
EXISTING GAUGES TO MEASURE STRAINS IN THE SUBGRADE LAYER	229
EXISTING GAUGES TO MEASURE STRESS	229
EXISTING GAUGES TO MEASURE DEFLECTION	229
EVALUATION OF IN SITU RESILIENT MODULI FROM SENSOR DATA	230
INVESTIGATION OF NEW INSTRUMENTATION IDEAS	231
LABORATORY TESTING OF NEW INSTRUMENTATION	232

**VOLUME I: FINAL REPORT
TABLE OF CONTENTS (Continued)**

<u>Chapter</u>	<u>Page</u>
FIELD EVALUATION OF NEW INSTRUMENTATION	233
NEW GAUGES TO MEASURE STRAINS IN THE ASPHALT CONCRETE LAYER	233
NEW GAUGES TO MEASURE STRAINS IN UNBONDED LAYERS	233
NEW GAUGES TO MEASURE DEFLECTION	234
 APPENDIX A: GENERAL PURPOSE MODULUS BACKCALCULATION (PENMOD) USER MANUAL	 235
 APPENDIX B: DESIGN DRAWING AND CIRCUIT DIAGRAMS FOR THE HALL EFFECT GAUGES	 261
 REFERENCES	 285

VOLUME I: FINAL REPORT

LIST OF FIGURES

<u>Figure No.</u>		<u>Page</u>
1	Cross sections of thin and thick sections	7
2	Layout of instrumentations for the thick section	8
3	Layout of instrumentations for the thin section	9
4	Design chart for flexible pavements based on using mean values for each input	13
5	Thickness of asphalt concrete layer of the thick section	16
6	Thickness of asphalt concrete and crushed aggregate base layers of the thin section	17
7	Multidepth deflectometers installed in the test track	23
8	Typical response of asphalt concrete longitudinal strain gauge (thick section)	32
9	Effects of load, tire pressure, and speed on the response of the Kyowa gauge at station 18 of the thick section, drive single axle	42
10	Effects of load, tire pressure, and speed on the response of the Kyowa gauge at station 10 of the thin section, drive single axle	43
11	Effects of load, tire pressure, and speed on the response of the Kyowa gauge at station 18 of the thick section, trailer tandem axles	44
12	Effects of load, tire pressure, and speed on the response of the Kyowa gauge at station 10 of the thin section, trailer tandem axles	45
13	Profile of the test track	49
14	Comparison of measured and calculated strains under a drive single axle load of 20,000 lb (9 080 kg) for the thin section	50
15	Comparison of measured and calculated strains under a drive single axle load of 12,000 lb (5 448 kg) for the thin section	51
16	Comparison of measured and calculated strains under a drive single axle load of 20,000 lb (9 080 kg) for the thick section	52
17	Comparison of measured and calculated strains under a drive single axle load of 12,000 lb (5 448 kg) for the thick section	53
18	Correlation between Dynatest gauges and overall mean of all gauges--phase I	57
19	Correlation between Kyowa gauges and overall mean of all gauges--phase I	58
20	Correlation between core gauges and overall mean of all gauges--phase I	59
21	Effect of load and speed on the response of the soil strain gauge at 6.5 in (165 mm) from top of subgrade of the thin section, drive single axle	63

VOLUME I: FINAL REPORT

LIST OF FIGURES (Continued)

<u>Figure No.</u>		<u>Page</u>
22	Effect of load and speed on the response of the soil strain gauge at 6.5 in (165 mm) from top of subgrade of the thin section, trailer tandem axles	64
23	Effect of speed on the response of the soil strain gauge at 6.5 in (165 mm) from top of subgrade of the thick section, drive single axle, fully loaded	65
24	Effect of speed on the response of the soil strain gauge at 6.5 in (165 mm) from top of subgrade of the thick section, trailer tandem axles, fully loaded	66
25	Effects of load and speed on the response of the soil strain gauge at 2.5 in (64 mm) from top of subgrade of the thick section, drive single axle	67
26	Comparison of the measured and calculated soil strains under the drive single axle of the thick section, 2.5 in (64 mm) from top of subgrade	69
27	Comparison of the measured and calculated soil strains under the drive single axle of the thick section, 6.5 in (165 mm) from top of subgrade	70
28	Comparison of the measured and calculated soil strains under the drive single axle of the thin section, 6.5 in (165 mm) from top of subgrade	71
29	Typical response from the diaphragm pressure cell, thin section	73
30	Effects of load, tire pressure, and speed on the response of the pressure cell, thin section, drive single axle	75
31	Effects of load, tire pressure, and speed on the response of the pressure cell, thin section, trailer tandem axles	76
32	Comparison of measured and calculated pressures under the drive single axle at the thin section	78
33	Effects of load, tire pressure, and speed on the response of the SLD at the surface/base interface of the thick section, drive single axle	89
34	Effect of load, tire pressure, and speed on the response of the SLD at the surface/base interface of the thick section, trailer tandem axles	90
35	Effect of test variables on multidepth deflectometer output (thin pavement/single axle)	92
36	Effects of test variables on multidepth deflectometer output (thick pavement/single axle)	93
37	Comparison of calculated and measured deflections under the drive single axle at the thick section	95
38	Typical strain response under a fully loaded single axle. The table shows the measured strains at various offsets	105
39	Test configurations for single and dual tire wheels	107
40	Typical responses of the top MDD for different truck speeds	134

VOLUME I: FINAL REPORT LIST OF FIGURES (Continued)

<u>Figure No.</u>		<u>Page</u>
41	Setup of MDD and strain gauge for pavement layers moduli evaluation	136
42	Physical characteristics of the Carlson gauge	142
43	Physical characteristics of the TML gauge	146
44	Configurations of the Hall effect sensor	149
45	Effect of high construction temperature on the Hall effect sensor. Magnet was heated at 300 °F for 24 hours	151
46	Effect of inservice temperature on the Hall effect sensor	153
47	Relationship between gain and sensor life at different temperatures for the piezoelectric film	156
48	Effect of lateral force on Hall effect gauges	174
49	Multidepth deflectometer configurations	176
50	LVDT and Hall effect setups at TTI research annex	177
51	Field calibration of Hall effect multidepth deflectometer	179
52	Layout of instrumentation for the thin section, outer wheel path	182
53	Layout of instrumentation for the thick section, outer wheel path	183
54	Comparison of measured and calculated strains under a single drive axle load of 13,500 lb (6 129 kg) for the thin section	195
55	Comparison of measured and calculated strains under a single drive axle load of 18,500 lb (8 399 kg) for the thin section	196
56	Comparison of measured and calculated strains under a single drive axle load of 13,500 lb (6 129 kg) for the thick section	197
57	Comparison of measured and calculated strains under a single drive axle load of 18,500 lb (8 399 kg) for the thick section	198
58	Correlation between the Kyowa gauges and the overall mean of all gauges--phase II	200
59	Correlation between the Hall effect gauges and the overall mean of all gauges--phase II	201
60	Correlation between the PML gauges and the overall mean of all gauges--phase II	202
61	Correlation between the Kyowa gauges and the overall mean of all gauges, thick section	204
62	Correlation between the Hall effect gauges and the overall mean of all gauges, thick section	205
63	Correlation between the PML gauges and the overall mean of all gauges, thick section	206
64	Comparison of measured and calculated surface deflection from the inductive displacement SLD, thick section	216
65	Comparison of measured and calculated surface deflection from the Hall effect SLD, thin section	217

VOLUME I: FINAL REPORT

LIST OF FIGURES (Continued)

<u>Figure No.</u>		<u>Page</u>
66	Comparison of measured and calculated surface deflection from the inductive displacement SLD, thin section	218
67	Typical raw sensor output for falling weight loads	219
68	Typical sensor output for truck loads	220
69	Power spectral analysis displaying the frequency components of the Hall effect sensors displacement output under truck loading	222
70	Power spectral analysis displaying the frequency components of the Hall effect sensors displacement output under FWD loading	223
71	Hall effect output with high-frequency noise removed	224
72	Example of TMP.WES file	237
73	Example of TMP.DEF file	238
74	Example of WES.RES file	240
75	Example output	241
76	Example of output LOADOPT	245
77	Example of output DATAOPT	247
78	Example of output SINGLINPT	249
79	Example of output DUALINPT	251
80	Example of output ISMBDEFL	252
81	Screen displayed while WESLEA is running	254
82	Screen displaying the option for the user to define if the output should go to a file or to the printer	255
83	Display of the number of bowls being used in backcalculation	256
84	Completed sensor assembly drawings--SLD and soil transducer	261
85	Magnet assembly drawings--SLD and soil transducer	262
86	Assembly drawings--SLD and soil transducer	263
87	Assembly drawings--soil transducer	264
88	Completed sensor assembly drawings--soil transducer	265
89	Magnet assembly drawing--soil transducer	266
90	Assembly drawings--SLD transducer (components)	267
91	Assembly drawings--SLD transducer (dimensions)	268
92	Assembly drawings--SLD transducer (installed)	269
93	Completed sensor assembly drawings--asphalt transducer	271
94	Magnet assembly drawings--asphalt transducer	271
95	Assembly drawings(without sensor and cables)--asphalt transducer	272
96	Assembly drawings--asphalt transducer	273
97	Manufacturing drawings--transducer assembly (magnet tube)	274
98	Manufacturing drawings--transducer assembly (outer sleeve)	275
99	Manufacturing drawings--transducer assembly (SLD and soil gauge inner sleeve)	276
100	Manufacturing drawings--basic transducer assemblies	277
101	Manufacturing drawings--transducer assembly (bearing shield)	278

**VOLUME I: FINAL REPORT
LIST OF FIGURES (Continued)**

<u>Figure No.</u>		<u>Page</u>
102	Manufacturing drawings--transducer assembly (soil anchors) .	279
103	Manufacturing drawings--transducer assembly (sensor anchor)	280
104	Manufacturing drawings--transducer assembly (magnet anchor)	281
105	Manufacturing drawings--transducer assembly (SLD disk) . . .	282
106	Manufacturing drawings--transducer assembly (SLD and soil gauge mounting stud)	283
107	Assembly drawings--transducer conditioner for all three variations of transducers	284

VOLUME I: FINAL REPORT

LIST OF TABLES

<u>Table No.</u>		<u>Page</u>
1	Summary of gauges for phase I field testing	4
2	Structures of the instrumented sections	6
3	Experimental plan for field testing in phase I	28
4	Static load levels for the test track in pounds	28
5	Strain values under drive axle with 20 kips/axle, tire pressure of 125 psi (863 kPa), thick section	36
6	Strain values under drive axle with 20 kips/axle, tire pressure of 105 psi (725 kPa), thick section	37
7	Summary of the pooled standard deviations of the strain measurements under the single drive axle, thin section	38
8	Summary of the pooled standard deviations of the strain measurements under the tandem trailer axle, thin section	38
9	Summary of the pooled standard deviations of the strain measurements under the single drive axle, thick section	39
10	Summary of the pooled standard deviations of the strain measurements under the tandem trailer axle, thick section	39
11	Percent reductions in the measured strains (with respect to strain measured at 20 mi/h [32 km/h]) as a function of vehicle speed	47
12	Statistical summary of the regression analysis for the thin and thick section, drive and trailer axles, stage I and II, phase I	56
13	Summary of the means, standard deviations, and coefficients of variation for the Nottingham-type pressure cell	74
14	Geophone data under FWD	81
15	Summary of the means, standard deviations, and coefficients of variation for the surface geophones under the single drive axle	83
16	Summary of the means, standard deviations, and coefficients of variation for the single-layer deflectometer	84
17	Summary of the means, standard deviations, and coefficients of variation for the multidepth deflectometer on the thin section	86
18	Summary of the means, standard deviations, and coefficients of variation for the multidepth deflectometer on the thick section	87
19	Summary of the means of the surface geophones and the first LVDT of the MDD	88
20	Sensitivity analysis on thin pavement--predicted MDD values versus measured MDD values	96
21	Sensitivity analysis on thick pavement--predicted MDD values versus measured MDD values	96
22	Suction and temperature readings from the thin and thick test sections	97
23	Temperature measurements from the controlled laboratory experiment	100

**VOLUME I: FINAL REPORT
LIST OF TABLES (Continued)**

<u>Table No.</u>		<u>Page</u>
24	Calculated strains and deflections for the single tire loading configuration	108
25	Calculated strains for the 3-in (76-mm) lateral offset	109
26	Descriptions of sensitivity analysis runs	110
27	Sensitivity analysis on strain data/single tire used to backcalculate layer moduli (known: $E_1 = 400$ ksi, $E_2 = 30$ ksi, $E_3 = 15$ ksi)	111
28	Sensitivity analysis on multidepth deflectometer data/single tire used to backcalculate layer moduli (known: $E_1 = 400$ ksi, $E_2 = 30$ ksi, $E_3 = 15$ ksi)	112
29	Sensitivity analysis on strain data/dual tires used to backcalculate layer moduli (known: $E_1 = 400$ ksi, $E_2 = 30$ ksi, $E_3 = 15$ ksi)	113
30	Sensitivity analysis on multidepth deflectometer data/dual tires used to backcalculate layer moduli (known: $E_1 = 400$ ksi, $E_2 = 30$ ksi, $E_3 = 15$ ksi)	114
31	Strain basins generated from random errors for single tire load	116
32	Effect of random errors on the backcalculated moduli for single tire load (known moduli: $E_1 = 40$ ksi, $E_2 = 30$ ksi, $E_3 = 15$ ksi)	117
33	Strain basins generated from random errors for dual tire load	118
34	Effect of random errors on the backcalculated moduli for dual tire load (known moduli: $E_1 = 40$ ksi, $E_2 = 30$ ksi, $E_3 = 15$ ksi)	119
35	FWD and MDD test results from the thin pavement section	121
36	FWD and MDD test results from the thick pavement section	122
37	Layer moduli backcalculated using surface deflections only	123
38	Layer moduli backcalculated using a three-layer system and surface deflections only (thin pavement)	124
39	Layer moduli backcalculated using a four-layer system and both surface and depth deflections (thin pavement)	125
40	Layer moduli backcalculated using a three-layer system and surface deflections only (thick pavement)	126
41	Layer moduli backcalculated using a four-layer system and both surface and depth deflections (thick pavement)	127
42	Backcalculated moduli for the thick section under the single drive axle, based on the strain measurements	130
43	Backcalculated moduli for the thin section under the single single drive axle, based on the strain measurements	131
44	Backcalculated moduli for the thick section under the single drive axle, based on the MDD measurements	132
45	Backcalculated moduli for the thin section under the single drive axle, based on the MDD measurements	132
46	Strain and deflection data used in analysis	133

**VOLUME I: FINAL REPORT
LIST OF TABLES (Continued)**

<u>Table No.</u>		<u>Page</u>
47	Layer moduli values backcalculated using both deflection and strain data	137
48	Laboratory-measured data on the Hall effect sensor	150
49	Modulus of elasticity values for various types of gauges	164
50	Response of the Hall effect gauges to sine input under MTS loading frame	168
51	Response of the Hall effect gauges to haversine input under MTS loading frame	171
52	Summary of gauges for phase II field testing	181
53	Strain values under drive axle with 18.5 kips/axle, tire pressure of 100 psi (690 kPa), thick section	190
54	Strain values under drive axle with 18.5 kips/axle, tire pressure of 135 psi (932 kPa), thin section	191
55	Summary of the WIM measurements	193
56	Statistical summary of the regression analysis for the thin and thick section, drive and trailer axles, phase II	199
57	Strain values in unbonded layers under drive and tandem axles, heavy load level, tire pressure of 100 psi (690 kPa), thick section	208
58	Strain values in unbonded layers under drive and tandem axles, intermediate load level, tire pressure of 100 psi (690 kPa), thin section	209
59	Summary of the means, standard deviations, and coefficients of variation for the single-layer deflectometer with inductive displacement sensor, thick section	211
60	Summary of the means, standard deviations, and coefficients of variation for the single-layer deflectometer with Hall effect sensor, thin section	212
61	Summary of the means, standard deviations, and coefficients of variation for the single-layer deflectometer with inductive displacement sensor, thin section	213
62	Repeatability assessments of sensors	225



**VOLUME II: APPENDIXES
TABLE OF CONTENTS**

<u>Chapter</u>	<u>Page</u>
APPENDIX C: LONGITUDINAL STRAIN MEASUREMENTS AT THE BOTTOM OF ASPHALT CONCRETE	1
APPENDIX D: STRAIN MEASUREMENTS AT THE BOTTOM OF ASPHALT CONCRETE	71
APPENDIX E: STRAIN MEASUREMENTS IN UNBONDED LAYERS	137
APPENDIX F: DEFLECTION MEASUREMENTS AT THE SURFACE FROM THE SINGLE-LAYER DEFLECTOMETER	147

VOLUME II: APPENDIXES LIST OF FIGURES

<u>Figure No.</u>		<u>Page</u>
1	Effects of load, tire pressure, and speed on the response of the Kyowa gauge at station 6 of the thick section, single drive axle	48
2	Effects of load, tire pressure, and speed on the response of the core gauge at station 12 of the thick section, single drive axle	49
3	Effects of load, tire pressure, and speed on the response of the core gauge at station 16 of the thick section, single drive axle	50
4	Effects of load, tire pressure, and speed on the response of the Kyowa gauge at station 18 of the thick section, single drive axle	51
5	Effects of load, tire pressure, and speed on the response of the ARC gauge at station 21 of the thick section, single drive axle	52
6	Effects of load, tire pressure, and speed on the response of the Dynatest gauge at station 9 of the thin section, single drive axle	53
7	Effects of load, tire pressure, and speed on the response of the Kyowa gauge at station 10 of the thin section, single drive axle	54
8	Effects of load, tire pressure, and speed on the response of the core gauge at station 12 of the thin section, single drive axle	55
9	Effects of load, tire pressure, and speed on the response of the Kyowa gauge at station 29 of the thin section, single drive axle	56
10	Effects of load, tire pressure, and speed on the response of the Dynatest gauge at station 30 of the thin section, single drive axle	57
11	Effects of load, tire pressure, and speed on the response of the ARC gauge at station 34 of the thin section, single drive axle	58
12	Effects of load, tire pressure, and speed on the response of the Kyowa gauge at station 6 of the thick section, tandem trailer axles	59
13	Effects of load, tire pressure, and speed on the response of the core gauge at station 12 of the thick section, tandem trailer axles	60
14	Effects of load, tire pressure, and speed on the response of the core gauge at station 16 of the thick section, tandem trailer axles	61
15	Effects of load, tire pressure, and speed on the response of the Kyowa gauge at station 18 of the thick section, tandem trailer axles	62

VOLUME II: APPENDIXES
LIST OF FIGURES (Continued)

<u>Figure No.</u>		<u>Page</u>
16	Effects of load, tire pressure, and speed on the response of the ARC gauge at station 21 of the thick section, tandem trailer axles	63
17	Effects of load, tire pressure, and speed on the response of the Dynatest gauge at station 9 of the thin section, tandem trailer axles	64
18	Effects of load, tire pressure, and speed on the response of the Kyowa gauge at station 10 of the thin section, tandem trailer axles	65
19	Effects of load, tire pressure, and speed on the response of the core gauge at station 12 of the thin section, tandem trailer axles	66
20	Effects of load, tire pressure, and speed on the response of the Kyowa gauge at station 29 of the thin section, tandem trailer axles	67
21	Effects of load, tire pressure, and speed on the response of the Dynatest gauge at station 30 of the thin section, tandem trailer axles	68
22	Effects of load, tire pressure, and speed on the response of the ARC gauge at station 34 of the thin section, tandem trailer axles	69

VOLUME II: APPENDIXES LIST OF TABLES

<u>Table No.</u>		<u>Page</u>
1	Strain values under drive axle with 20 kips/axle (38 kips/tandem axle), tire pressure of 105 psi (725 kPa), thin section--phase I, stage I	2
2	Strain values under drive axle with 20 kips/axle (38 kips/tandem axle), tire pressure of 125 psi (863 kPa), thin section--phase I, stage I	3
3	Strain values under tandem axle load of 38 kips, tire pressure of 105 psi (725 kPa), thin section--phase I, stage I	4
4	Strain values under tandem axle load of 38 kips, tire pressure of 125 psi (863 kPa), thin section--phase I, stage I	5
5	Strain values under drive axle with 20 kips/axle (31 kips/tandem axle), tire pressure of 105 psi (725 kPa), thin section--phase I, stage I	6
6	Strain values under drive axle with 20 kips/axle (31 kips/tandem axle), tire pressure of 125 psi (863 kPa), thin section--phase I, stage I	7
7	Strain values under tandem axle load of 31 kips, tire pressure of 105 psi (725 kPa), thin section--phase I, stage I	8
8	Strain values under tandem axle load of 31 kips, tire pressure of 125 psi (863 kPa), thin section--phase I, stage I	9
9	Strain values under drive axle with 20 kips/axle (9 kips/tandem axle), tire pressure of 105 psi (725 kPa), thin section--phase I, stage I	10
10	Strain values under drive axle with 20 kips/axle (9 kips/tandem axle), tire pressure of 125 psi (863 kPa), thin section--phase I, stage I	11
11	Strain values under tandem axle load with 9 kips, tire pressure of 105 psi (725 kPa), thin section--phase I, stage I	12
12	Strain values under tandem axle load with 9 kips, tire pressure of 125 psi (863 kPa), thin section--phase I, stage I	13
13	Strain values under drive axle with 20 kips/axle (38 kips/tandem axle), tire pressure of 125 psi (863 kPa), thick section--phase I, stage I	14
14	Strain values under tandem axle load with 38 kips, tire pressure of 125 psi (863 kPa), thick section--phase I, stage I	15
15	Strain values under drive axle with 20 kips/axle (31 kips/tandem axle), tire pressure of 105 psi (725 kPa), thick section--phase I, stage I	16

VOLUME II: APPENDIXES
LIST OF TABLES (Continued)

<u>Table No.</u>		<u>Page</u>
16	Strain values under drive axle with 20 kips/axle (31 kips/tandem axle), tire pressure of 125 psi (863 kPa), thick section--phase I, stage I	17
17	Strain values under tandem axle load with 31 kips, tire pressure of 105 psi (725 kPa), thick section--phase I, stage I	18
18	Strain values under tandem axle load with 31 kips, tire pressure of 125 psi (863 kPa), thick section--phase I, stage I	19
19	Strain values under drive axle with 20 kips/axle (9 kips/tandem axle), tire pressure of 105 psi (725 kPa), thick section--phase I, stage I	20
20	Strain values under drive axle with 20 kips/axle (9 kips/tandem axle), tire pressure of 125 psi (863 kPa), thick section--phase I, stage I	21
21	Strain values under tandem axle load with 9 kips, tire pressure of 105 psi (725 kPa), thick section--phase I, stage I	22
22	Strain values under tandem axle load of 9 kips, tire pressure of 125 psi (863 kPa), thick section--phase I, stage I	23
23	Strain values under drive axle with 20 kips/axle, tire pressure of 100 psi (690 kPa), thin section--phase I, stage II	24
24	Strain values under drive axle with 20 kips/axle, tire pressure of 125 psi (863 kPa), thin section--phase I, stage II	25
25	Strain values under tandem axle load of 38 kips, tire pressure of 100 psi (690 kPa), thin section--phase I, stage II	26
26	Strain values under tandem axle load of 38 kips, tire pressure of 125 psi (863 kPa), thin section--phase I, stage II	27
27	Strain values under drive axle with 12 kips/axle, tire pressure of 100 psi (690 kPa), thin section--phase I, stage II	28
28	Strain values under drive axle with 12 kips/axle, tire pressure of 125 psi (863 kPa), thin section--phase I, stage II	29
29	Strain values under tandem axle load of 21 kips, tire pressure of 100 psi (690 kPa), thin section--phase I, stage II	30
30	Strain values under tandem axle load of 21 kips, tire pressure of 125 psi (863 kPa), thin section--phase I, stage II	31

VOLUME II: APPENDIXES
LIST OF TABLES (Continued)

<u>Table No.</u>		<u>Page</u>
31	Strain values under drive axle with 8 kips/axle, tire pressure of 100 psi (690 kPa), thin section--phase I, stage II	32
32	Strain values under drive axle with 8 kips/axle, tire pressure of 125 psi (863 kPa), thin section--phase I, stage II	33
33	Strain values under tandem axle load of 9 kips, tire pressure of 100 psi (690 kPa), thin section--phase I, stage II	34
34	Strain values under tandem axle load of 9 kips, tire pressure of 125 psi (863 kPa), thin section--phase I, stage II	35
35	Strain values under drive axle with 20 kips/axle, tire pressure of 100 psi (690 kPa), thick section--phase I, stage II	36
36	Strain values under drive axle with 20 kips/axle, tire pressure of 125 psi (863 kPa), thick section--phase I, stage II	37
37	Strain values under tandem axle load of 38 kips, tire pressure of 100 psi (690 kPa), thick section--phase I, stage II	38
38	Strain values under tandem axle load of 38 kips, tire pressure of 125 psi (863 kPa), thick section--phase I, stage II	39
39	Strain values under drive axle with 12 kips/axle, tire pressure of 100 psi (690 kPa), thick section--phase I, stage II	40
40	Strain values under drive axle with 12 kips/axle, tire pressure of 125 psi (863 kPa), thick section--phase I, stage II	41
41	Strain values under tandem axle load of 21 kips, tire pressure of 100 psi (690 kPa), thick section--phase I, stage II	42
42	Strain values under tandem axle load of 21 kips, tire pressure of 125 psi (863 kPa), thick section--phase I, stage II	43
43	Strain values under drive axle with 8 kips/axle, tire pressure of 100 psi (690 kPa), thick section--phase I, stage II	44
44	Strain values under drive axle with 8 kips/axle, tire pressure of 125 psi (863 kPa), thick section--phase I, stage II	45
45	Strain values under tandem axle load of 9 kips, tire pressure of 100 psi (690 kPa), thick section--phase I, stage II	46

**VOLUME II: APPENDIXES
LIST OF TABLES (Continued)**

<u>Table No.</u>		<u>Page</u>
46	Strain values under tandem axle load of 9 kips, tire pressure of 125 psi (863 kPa), thick section--phase I, stage II	47
47	Strain values under drive axle with 13.5 kips/axle, tire pressure of 100 psi (690 kPa), thin section	71
48	Strain values under drive axle with 13.5 kips/axle, tire pressure of 135 psi (932 kPa), thin section	72
49	Strain values under drive axle with 8 kips/axle, tire pressure of 100 psi (690 kPa), thin section	73
50	Strain values under drive axle with 8 kips/axle, tire pressure of 135 psi (932 kPa), thin section	74
51	Strain values under front tandem axle with 22 kips/axle, tire pressure of 100 psi (690 kPa), thin section	75
52	Strain values under front tandem axle with 22 kips/axle, tire pressure of 135 psi (932 kPa), thin section	76
53	Strain values under front tandem axle with 9 kips/axle, tire pressure of 100 psi (690 kPa), thin section	77
54	Strain values under front tandem axle with 9 kips/axle, tire pressure of 135 psi (932 kPa), thin section	78
55	Strain values under rear tandem axle with 22 kips/axle, tire pressure of 100 psi (690 kPa), thin section	79
56	Strain values under rear tandem axle with 22 kips/axle, tire pressure of 135 psi (932 kPa), thin section	80
57	Strain values under rear tandem axle with 9 kips/axle, tire pressure of 100 psi (690 kPa), thin section	81
58	Strain values under rear tandem axle with 9 kips/axle, tire pressure of 135 psi (932 kPa), thin section	82
59	Strain values under drive axle with 18.5 kips/axle, tire pressure of 100 psi (690 kPa), thin section	83
60	Strain values under drive axle with 18.5 kips/axle, tire pressure of 135 psi (932 kPa), thin section	84
61	Strain values under drive axle with 13.5 kips/axle, tire pressure of 100 psi (690 kPa), thin section	85
62	Strain values under drive axle with 13.5 kips/axle, tire pressure of 135 psi (932 kPa), thin section	86
63	Strain values under front tandem axle with 41 kips/axle, tire pressure of 100 psi (690 kPa), thin section	87
64	Strain values under front tandem axle with 41 kips/axle, tire pressure of 135 psi (932 kPa), thin section	88
65	Strain values under front tandem axle with 22 kips/axle, tire pressure of 100 psi (690 kPa), thin section	89
66	Strain values under front tandem axle with 22 kips/axle, tire pressure of 135 psi (932 kPa), thin section	90
67	Strain values under rear tandem axle with 41 kips/axle, tire pressure of 100 psi (690 kPa), thin section	91
68	Strain values under rear tandem axle with 41 kips/axle, tire pressure of 135 psi (932 kPa), thin section	92

VOLUME II: APPENDIXES
LIST OF TABLES (Continued)

<u>Table No.</u>		<u>Page</u>
69	Strain values under rear tandem axle with 22 kips/axle, tire pressure of 100 psi (690 kPa), thin section	93
70	Strain values under rear tandem axle with 22 kips/axle, tire pressure of 135 psi (932 kPa), thin section	94
71	Strain values under drive axle with 18.5 kips/axle, tire pressure of 100 psi (690 kPa), thin section	95
72	Strain values under drive axle with 18.5 kips/axle, tire pressure of 135 psi (932 kPa), thin section	96
73	Strain values under drive axle with 13.5 kips/axle, tire pressure of 100 psi (690 kPa), thin section	97
74	Strain values under drive axle with 13.5 kips/axle, tire pressure of 135 psi (932 kPa), thin section	98
75	Strain values under drive axle with 8 kips/axle, tire pressure of 100 psi (690 kPa), thin section	99
76	Strain values under drive axle with 8 kips/axle, tire pressure of 135 psi (932 kPa), thin section	100
77	Strain values under front tandem axle with 41 kips/axle, tire pressure of 100 psi (690 kPa), thin section	101
78	Strain values under front tandem axle with 41 kips/axle, tire pressure of 135 psi (932 kPa), thin section	102
79	Strain values under front tandem axle with 22 kips/axle, tire pressure of 100 psi (690 kPa), thin section	103
80	Strain values under front tandem axle with 22 kips/axle, tire pressure of 135 psi (932 kPa), thin section	104
81	Strain values under front tandem axle with 9 kips/axle, tire pressure of 100 psi (690 kPa), thin section	105
82	Strain values under front tandem axle with 9 kips/axle, tire pressure of 135 psi (932 kPa), thin section	106
83	Strain values under rear tandem axle with 41 kips/axle, tire pressure of 100 psi (690 kPa), thin section	107
84	Strain values under rear tandem axle with 41 kips/axle, tire pressure of 135 psi (932 kPa), thin section	108
85	Strain values under rear tandem axle with 22 kips/axle, tire pressure of 100 psi (690 kPa), thin section	109
86	Strain values under rear tandem axle with 22 kips/axle, tire pressure of 135 psi (932 kPa), thin section	110
87	Strain values under rear tandem axle with 9 kips/axle, tire pressure of 100 psi (690 kPa), thin section	111
88	Strain values under rear tandem axle with 9 kips/axle, tire pressure of 135 psi (932 kPa), thin section	112
89	Strain values under drive axle with 18.5 kips/axle, tire pressure of 100 psi (690 kPa), thick section	113
90	Strain values under drive axle with 18.5 kips/axle, tire pressure of 125 psi (863 kPa), thick section	114
91	Strain values under drive axle with 13.5 kips/axle, tire pressure of 100 psi (690 kPa), thick section	115

VOLUME II: APPENDIXES
LIST OF TABLES (Continued)

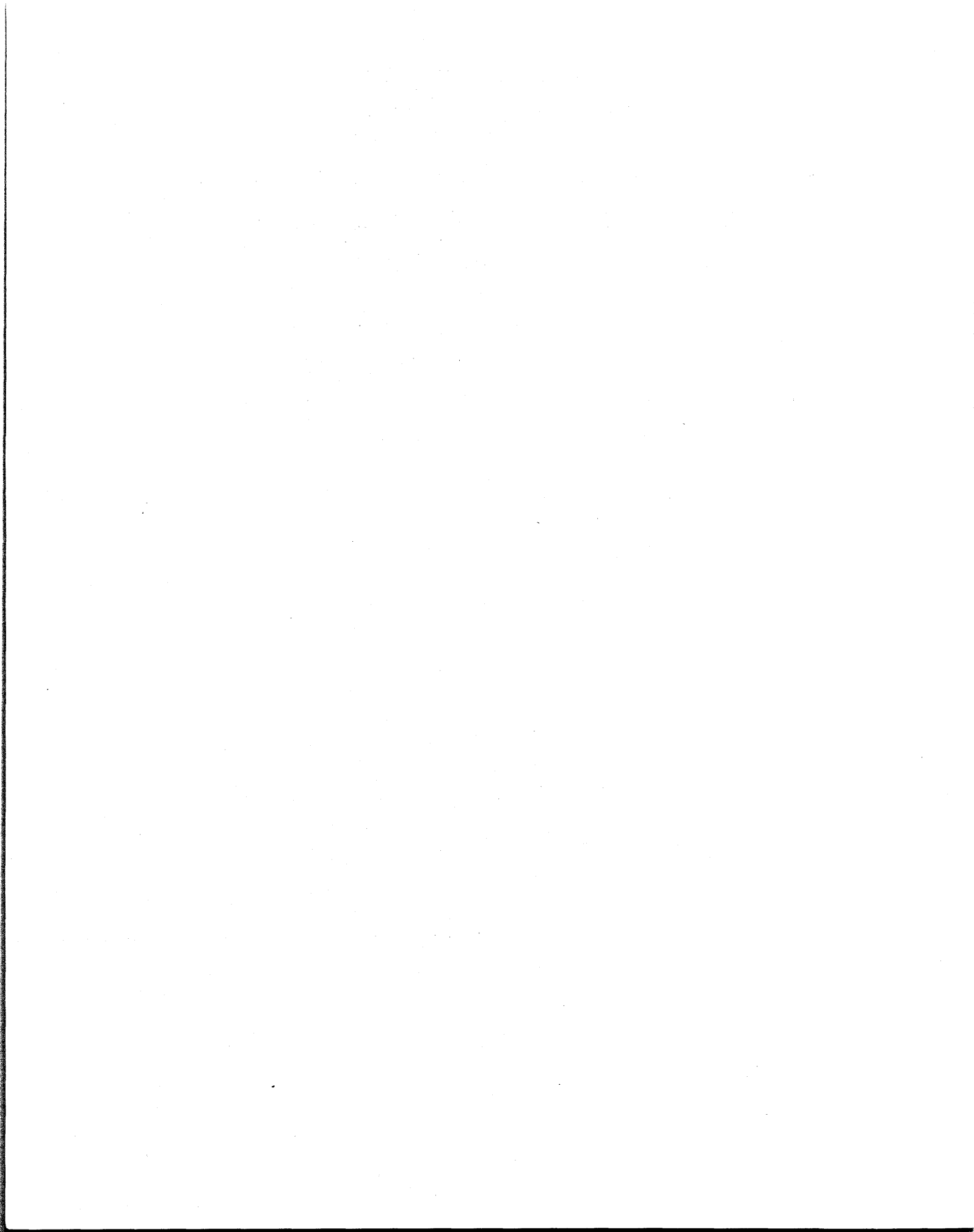
<u>Table No.</u>		<u>Page</u>
92	Strain values under drive axle with 13.5 kips/axle, tire pressure of 125 psi (863 kPa), thick section	116
93	Strain values under front tandem axle with 41 kips/axle, tire pressure of 100 psi (690 kPa), thick section	117
94	Strain values under front tandem axle with 41 kips/axle, tire pressure of 125 psi (863 kPa), thick section	118
95	Strain values under front tandem axle with 22 kips/axle, tire pressure of 100 psi (690 kPa), thick section	119
96	Strain values under front tandem axle with 22 kips/axle, tire pressure of 125 psi (863 kPa), thick section	120
97	Strain values under rear tandem axle with 41 kips/axle, tire pressure of 100 psi (690 kPa), thick section	121
98	Strain values under rear tandem axle with 41 kips/axle, tire pressure of 125 psi (863 kPa), thick section	122
99	Strain values under rear tandem axle with 22 kips/axle, tire pressure of 100 psi (690 kPa), thick section	123
100	Strain values under rear tandem axle with 22 kips/axle, tire pressure of 125 psi (863 kPa), thick section	124
101	Strain values under drive axle with 18.5 kips/axle, tire pressure of 100 psi (690 kPa), thick section	125
102	Strain values under drive axle with 13.5 kips/axle, tire pressure of 100 psi (690 kPa), thick section	126
103	Strain values under drive axle with 13.5 kips/axle, tire pressure of 135 psi (932 kPa), thick section	127
104	Strain values under drive axle with 8 kips/axle, tire pressure of 135 psi (932 kPa), thick section	128
105	Strain values under front tandem axle with 41 kips/axle, tire pressure of 100 psi (690 kPa), thick section	129
106	Strain values under front tandem axle with 22 kips/axle, tire pressure of 100 psi (690 kPa), thick section	130
107	Strain values under front tandem axle with 22 kips/axle, tire pressure of 135 psi (932 kPa), thick section	131
108	Strain values under front tandem axle with 9 kips/axle, tire pressure of 135 psi (932 kPa), thick section	132
109	Strain values under rear tandem axle with 41 kips/axle, tire pressure of 100 psi (690 kPa), thick section	133
110	Strain values under rear tandem axle with 22 kips/axle, tire pressure of 100 psi (690 kPa), thick section	134
111	Strain values under rear tandem axle with 22 kips/axle, tire pressure of 135 psi (932 kPa), thick section	135
112	Strain values under rear tandem axle with 9 kips/axle, tire pressure of 135 psi (932 kPa), thick section	136
113	Strain values in unbonded layers under drive and tandem axles, intermediate load level, tire pressure of 100 psi (690 kPa), thin section	137

**VOLUME II: APPENDIXES
LIST OF TABLES (Continued)**

<u>Table No.</u>		<u>Page</u>
114	Strain values in unbonded layers under drive and tandem axles, intermediate load level, tire pressure of 135 psi (932 kPa), thin section	138
115	Strain values in unbonded layers under drive and tandem axles, heavy load level, tire pressure of 100 psi (690 kPa), thick section. Date of testing: 8/29/90	139
116	Strain values in unbonded layers under drive and tandem axles, heavy load level, tire pressure of 125 psi (863 kPa), thick section	140
117	Strain values in unbonded layers under drive and tandem axles, intermediate load level, tire pressure of 100 psi (690 kPa), thick section. Date of testing: 8/29/90	141
118	Strain values in unbonded layers under drive and tandem axles, intermediate load level, tire pressure of 125 psi (863 kPa), thick section	142
119	Strain values in unbonded layers under drive and tandem axles, heavy load level, tire pressure of 100 psi (690 kPa), thick section. Date of testing: 9/25/90	143
120	Strain values in unbonded layers under drive and tandem axles, intermediate load level, tire pressure of 100 psi (690 kPa), thick section. Date of testing: 9/25/90	144
121	Strain values in unbonded layers under drive and tandem axles, intermediate load level, tire pressure of 135 psi (932 kPa), thick section	145
122	Strain values in unbonded layers under drive and tandem axles, empty load level, tire pressure of 135 psi (932 kPa), thick section	146
123	Peak surface deflection values under drive and tandem axles, empty load level, tire pressure of 100 psi (690 kPa), thin section	147
124	Peak surface deflection values under drive and tandem axles, intermediate load level, tire pressure of 135 psi (932 kPa), thin section	148
125	Peak surface deflection values under drive and tandem axles, heavy load level, tire pressure of 100 psi (690 kPa), thin section	149
126	Peak surface deflection values under drive and tandem axles, heavy load level, tire pressure of 135 psi (932 kPa), thin section	150
127	Peak surface deflection values under drive and tandem axles, intermediate load level, tire pressure of 100 psi (690 kPa), thin section	151
128	Peak surface deflection values under drive and tandem axles, intermediate load level, tire pressure of 135 psi (932 kPa), thin section	152

**VOLUME II: APPENDIXES
LIST OF TABLES (Continued)**

<u>Table No.</u>		<u>Page</u>
129	Peak surface deflection values under drive and tandem axles, heavy load level, tire pressure of 100 psi (690 kPa), thick section	153
130	Peak surface deflection values under drive and tandem axles, heavy load level, tire pressure of 125 psi (863 kPa), thick section	154
131	Peak surface deflection values under drive and tandem axles, intermediate load level, tire pressure of 125 psi (863 kPa), thick section	155
132	Peak surface deflection values under drive and tandem axles, intermediate load level, tire pressure of 100 psi (690 kPa), thick section	156



1. INTRODUCTION

BACKGROUND

The in situ measurements of strains and deflections throughout the pavement structure provide valuable information for pavement evaluation and design. The responses of the gauges can be used to evaluate the in situ moduli of the various pavement layers. Currently, these moduli are backcalculated from surface deflection basins using nondestructive testing (NDT). Unless a perfect match is achieved (i.e., zero error) between the measured and calculated deflection basins, multiple sets of moduli may be generated depending on the assumptions used in the backcalculation analysis. Therefore, the use of strain gauges and deflection devices throughout the pavement structure would provide additional information needed to verify the validity of the evaluated moduli.

Considerable progress has been made in recent years toward the development of accurate and reliable in situ pavement instrumentation. In particular, strain gauges, pressure cells, and deflection-measuring devices have been used in various field trials in the United States and Europe. There are, however, considerable concerns regarding the repeatability, uncertainty, and long-term performance of these gauges. In addition to the measurement of strains and deflections, other ancillary measurements such as moisture and temperature must be made for a complete presentation of the response of the pavement system to traffic loading.

OBJECTIVES

The main objectives of this study were:

1. To review and evaluate methods of measuring strain, stress, and deflection in bituminous pavements and procedures that use these data to determine layer moduli and to estimate performance measures such as fatigue cracking and rutting.
2. To perform field testing programs and to compare the measured strains with expected strains computed by mechanistic models.

3. To investigate and test new concepts of pavement response measurements suitable for field installation.

OUTLINE OF THE REPORT

The results of the research conducted to accomplish the first objective were described in detail in the interim report and are only summarized briefly here. The findings from the work towards the second and third main objectives are fully documented in this report.

The selection of pavement instrumentation from existing devices along with the design and construction of new pavement sections, installation of instrumentation, and field testing conducted in phase I of the project are reported in chapter 2.

Analysis of the measured pavement response under various test conditions, evaluation of performance of the gauges, and effects of test variables are discussed in chapter 3.

Chapter 4 describes the method of estimation of in situ resilient moduli of pavement layers. The moduli are backcalculated using the measured response of pavement under actual truck loading.

Chapter 5 includes new instrumentation ideas for measuring the response of flexible pavements, as well as laboratory testing to examine this operation at different environmental conditions.

Chapters 6 and 7 document pavement construction and field installation and testing, as well as the analysis of the data for phase II of the field testing.

2. TESTING OF EXISTING FLEXIBLE PAVEMENT INSTRUMENTATION: PHASE I

SELECTION OF INSTRUMENTATION

As a part of this project, various types of pavement instrumentation were selected for field evaluation under actual truck loading. The following list presents the different types of each instrumentation group that were selected:

<u>Pavement Response</u>	<u>Sensor Type</u>
Stress	Nottingham diaphragm-type pressure cell
Deflection	Geophones Single-layer deflectometer Multidepth deflectometer
Strain	Dynatest H-gauge Kyowa H-gauge Alberta Research Council (ARC) asphalt carrier block gauge Core gauge

Table 1 shows the location of these gauges within the pavement structure and their corresponding orientation.

In addition to the pavement response-measuring gauges, several other gauges were selected to collect ancillary measurements. The following list presents the additional gauges that were selected:

<u>Measurement</u>	<u>Sensor Type</u>
Temperature	Thermocouples Solid state sensors
Moisture	Nuclear dual tube Moisture/suction-AGWATRONIX
Transverse vehicle location	Ultrasonic sensor

Table 1. Summary of gauges for phase I field testing.

Gauge Type	Number of Gauges/Section	Orientation	Location
Nottingham pressure cell	2/thin	Vertical	At the top of base course
Geophones	3/thin and thick	Vertical	At the pavement surface
Geophones	3/thin and thick	Vertical	At the top of base course
Geophones	3/thin and thick	Vertical	At the top of subgrade
Single-layer deflectometer	1/thick	Vertical	At the top of base course
Single-layer deflectometer	1/thick	Vertical	At the top of subgrade
Multidepth deflectometer	1/thin and thick	Vertical	Throughout the depth of pavement
Dynatest strain gauge (H)	2/thin and thick	Longitudinal	At the bottom of asphalt concrete
Kyowa strain gauge (H)	4/thin and thick	Longitudinal	At the bottom of asphalt concrete
Asphalt carrier block gauge (ARC)	1/thin and thick	Longitudinal	At the bottom of asphalt concrete
Core gauge	4/thin and thick	Longitudinal	At the bottom of asphalt concrete
Core gauge	2/thin and thick	Vertical	At the lower one-third of asphalt concrete
Core gauge	2/thin and thick	Transverse	At the bottom of asphalt concrete
Thermocouples	8/thin and thick	N/A	Throughout the depth of pavement
Solid state temperature sensors	8/thin and thick	N/A	Throughout the depth of pavement

EXPERIMENTAL PLAN

The development of the overall experimental plan involved four subtasks: pavement design, instrumentation layout and installation, data collection plan, and data analysis plan.

PAVEMENT DESIGN

To effectively evaluate the performance of the selected gauges, they must be tested under various levels of expected pavement response. For instance, strain gauges should be tested under both high and low strain levels. A certain type of gauge might be good enough to measure medium level strains but might be too stiff to measure high strain levels or too loose to measure low strain levels. Therefore, a combination of pavement structures and axle load levels was selected to ensure that the various levels of pavement responses would be encountered.

Two pavement structures (one thin, one thick) were selected. The properties of these sections are listed in table 2, and their cross sections are shown in figure 1. The American Association of State Highway and Transportation Officials' (AASHTO) design of these sections and the actual construction are discussed in the next section. The variation in pavement structure (thin and thick) combined with other test variables (i.e., load, axle configuration, and speed) yield a wide range of pavement responses, which will provide an extensive evaluation program for the various gauges.

INSTRUMENTATION LAYOUT

The layouts of the instrumentation in the test sections are shown in figures 2 and 3. The failure rate in a full-scale installation is expected to be on the order of 20 to 50 percent. Therefore, replicates of the various gauges, except the very costly ones, were installed. The replicate gauges were randomly distributed along the length of the test section to account for the variability in the pavement and the dynamic load profile along the section length.

Table 2. Structures of the instrumented sections.

Section	Layer Type	Layer Thickness (in)
Thin	Asphalt concrete surface	6
	Crushed aggregate base	8
	Natural soil subgrade	150*
Thick	Asphalt concrete surface	10
	Crushed aggregate base	10
	Natural soil subgrade	150*

1 in = 25.4 mm

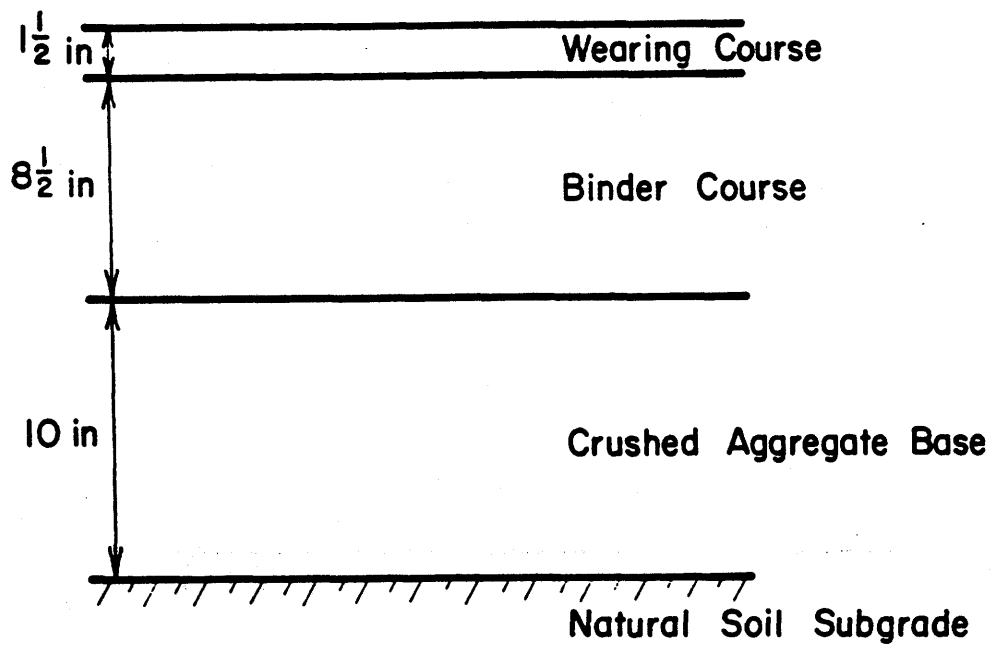
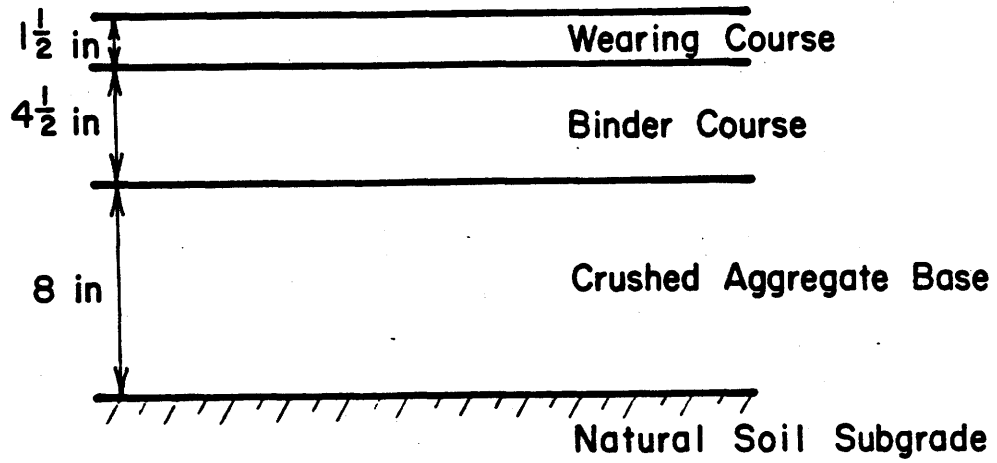
* Depth of subgrade was estimated from geological records and falling weight deflectometer (FWD) testing.

DATA COLLECTION PLAN

In addition to the pavement structure, the following test conditions were also varied:

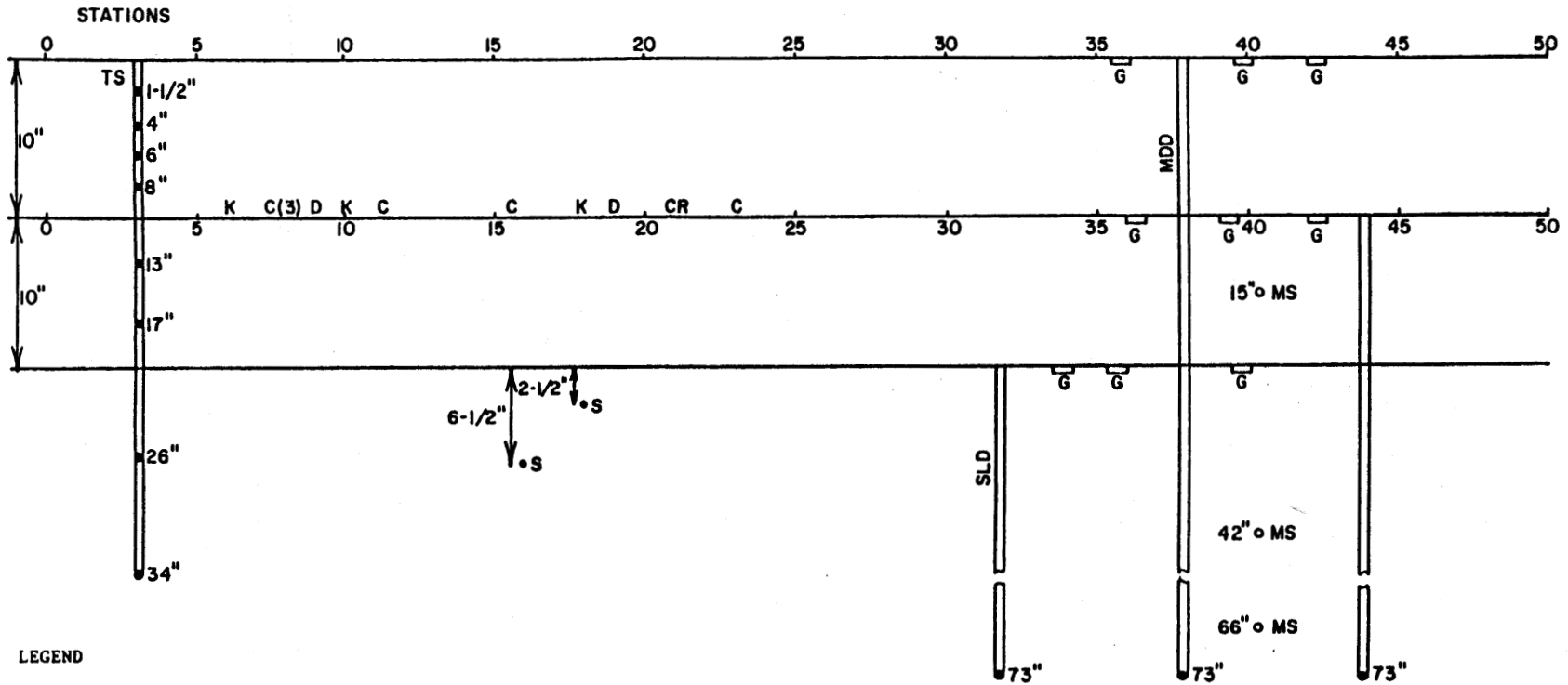
- Load level: empty, intermediate, and fully loaded.
- Axle configuration: single drive axle and tandem trailer axles.
- Testing speeds: 20, 35, and 50 mi/h (32, 56, and 80 km/h).
- Tire pressure: manufacturer's suggested pressure of 100 psi (690 kPa) and suggested plus 25 psi (172 kPa) (i.e., 125 psi [862 kPa]) inflation pressure.

To ensure the statistical validity of the experimental program, four replicate measurements were planned for each combination of test variables. An ultrasonic device for measuring truck transverse location was used to select four valid replicates based on the measured truck's location relative to the gauges. The total number of measurements collected from each gauge during one testing phase equals:



1 in = 25.4 mm

Figure 1. Cross sections of thin and thick sections.

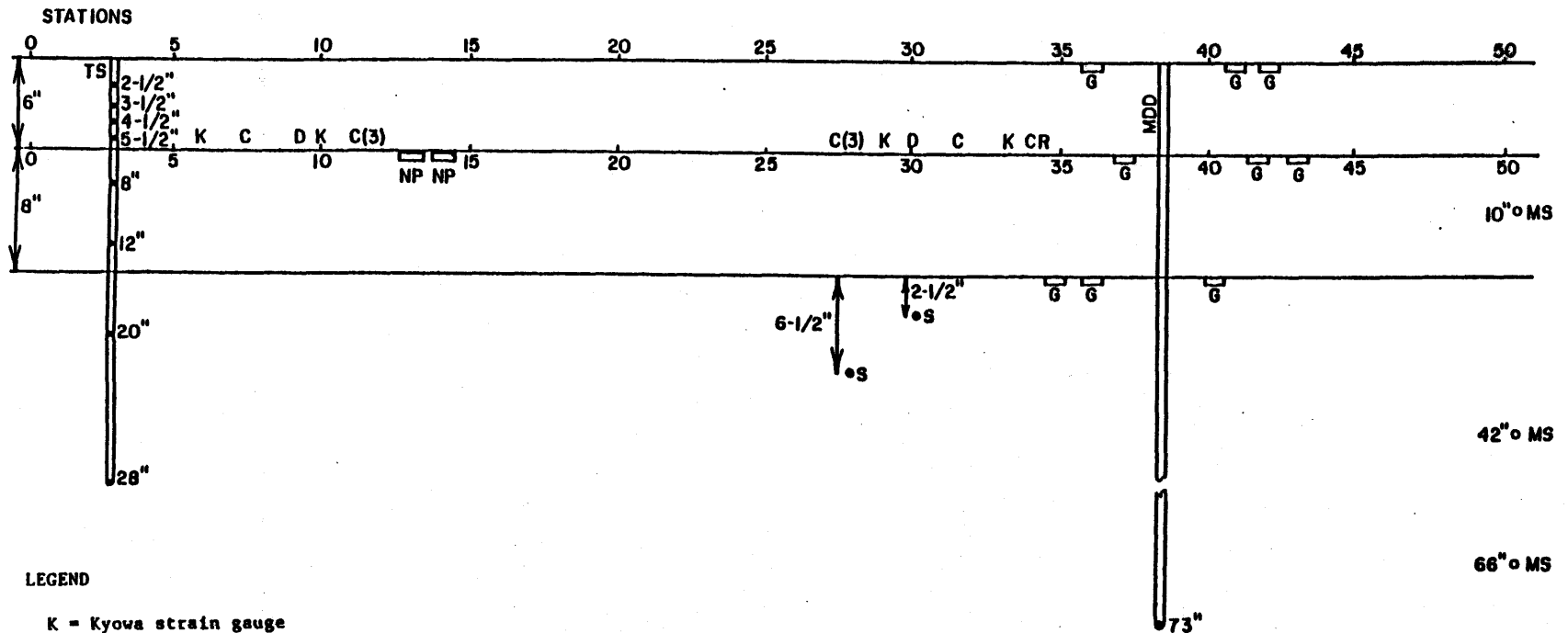


LEGEND

- K = Kyowa strain gauge
- C = Instrumented core strain gauge (3 = three-directional)
- D = Dynatest strain gauge
- S = Soil strain gauge
- NP = Nottingham pressure cell
- TS = Thermocouples and solid state temperature sensors
- G = Geophone
- SLD = Single-layer deflectometer
- MDD = Multidepth deflectometer
- MS = Moisture sensor
- CR = ARC block gauge

1 in = 25.4 mm

Figure 2. Layout of instrumentations for the thick section.



6

LEGEND

- K - Kyowa strain gauge
- C - Instrumented core strain gauge (3 = three-directional)
- D - Dynatest strain gauge
- S - Soil strain gauge
- NP - Nottingham pressure cell
- TS - Thermocouples and solid state temperature sensors
- G - Geophone
- SLD - Single-layer deflectometer
- MDD - Multidepth deflectometer
- MS - Moisture sensor
- CR - ARC block gauge

1 in = 25.4 mm

Figure 3. Layout of instrumentations for the thin section.

$$3(\text{loads}) \times 2(\text{axles}) \times 3(\text{speeds}) \times 2(\text{tire pressures}) \times 4(\text{replicates}) \\ = 144 \text{ measurements/gauge}$$

A total of 144 measurements were collected from every gauge in each of the 2 test pavement sections.

DATA ANALYSIS PLAN

The purpose of phase I of the research project was to evaluate the effectiveness of the instruments currently available for measuring pavement response to the stress levels encountered under typical truck loading conditions. The performance of the available gauges was evaluated based on the following criteria: survivability, repeatability, response under various combinations of test variables, and uncertainty. The following definitions of the evaluation criteria will apply throughout this report.

Survivability is represented by the number of gauges that remain operational after construction and testing relative to the number of gauges that were initially installed. Due to the small number of gauges installed in each test section, this measure can only be considered as the estimate of true survivability rate of the various gauges.

Repeatability (or precision) is a measure of dispersion of measuring results obtained from a specific gauge for specific test conditions.

Effect of test variables will be evaluated based on the sensitivity of each type of gauge to various combinations of load, speed, tire pressure, and axle configuration.

Uncertainty is an estimate of measuring error. It will be determined by the difference between the measured response and the theoretically calculated values. The theoretical values represent the estimated pavement responses based on the predetermined material properties and should not be considered as the true values.

Because four different types of strain gauges were installed at the same level and in the same direction at the bottom of the asphalt concrete layer, a regression analysis of the strain measurements obtained from all these gauges was conducted. The analysis investigated the relationship between the measurements from the individual gauges and the average measurements of the entire groups of gauges.

PAVEMENT CONSTRUCTION

The original plan for the instrumentation of the pavement sections assumed retrofitting the gauges into the existing pavements at the contractor's test track. However, some of the transducers could not be retrofitted without substantially disturbing the pavement layers. Therefore, two pavement sections at the test track--one thin, one thick--were reconstructed, which allowed more accurate installation of the instrumentation.

To accommodate all of the gauges without disturbing the pavement structure, the gauges should not be installed too close to each other. The test sections, each 50 ft (15.2 m) in length, are located at the straight portion of the test track where the truck could easily accelerate to a high speed and where the slope and grade are minimal.

The test pavement sections were designed based on AASHTO's *Guide for Design of Pavement Structures*.⁽¹⁾ The criteria for pavement design are as follows:

- **Traffic:** The pavement section must be strong enough to sustain the heavy truck loading without any damage to the gauges. Furthermore, the traffic from other research activities at the facilities must be taken into account. Therefore, 200,000 18-kip (80-kN) equivalent single-axle loads (ESAL's) were selected as the minimum for the thin pavement structure.
- **Reliability:** According to AASHTO design procedure, the acceptable range for a reliability factor is 85 to 99.9 percent. Consequently, 90 percent was used for reliability factor, R.

- Standard deviation: AASHTO requires a value of standard deviation, S_o , to be used for design. Therefore, an average value of 0.45 was used for the section design.
- Serviceability loss: An initial present serviceability index (PSI) of 4.2 was assumed, with a terminal serviceability index of 3.0. Thus, the serviceability loss for the design is 1.2.
- Resilient modulus of subgrade material: For the design of these sections, a modulus value for the supporting soil should be assumed. Based on the material testing for the previous reconstruction of the test track, a conservative value of 7,500 psi (52 MPa) was assumed for the resilient modulus of the soil.
- Structural number: AASHTO procedure requires calculation of structural number (SN) for the pavement using equation 1:

$$SN = a_1D_1 + a_2D_2m_2 + a_3D_3m_3 \quad (1)$$

where

- a_1, a_2, a_3 = structural coefficients for layers 1, 2, and 3
- D_1, D_2, D_3 = thicknesses of layers 1, 2, and 3
- m_2, m_3 = drainage coefficients for layers 2 and 3

Using the AASHTO procedure, drainage coefficients of 1 were assumed, which represents fair drainage. The structural coefficient values of 0.4 and 0.1 were used for the asphalt concrete layer (wearing course and bituminous concrete base course combined) and crushed aggregate base. The following values were assumed for initial thickness of the pavement layers:

- Thick section:
 - Asphalt concrete = 10 in (254 mm).
 - Crushed aggregate base = 10 in (254 mm).
- Thin section:
 - Asphalt concrete = 6 in (152 mm).
 - Crushed aggregate base = 8 in (203 mm).

Using the nomograph for flexible pavement design (figure 4), 5 million and 450,000 total 18-kip (80-kN) ESAL applications, respectively, were estimated for the two assumed design parameters. These traffic values were

NOMOGRAPH SOLVES:

$$\log_{10} W_{18} = z_R \cdot S_o + 9.36 \cdot \log_{10} (SN+1) - 0.20 + \frac{\log_{10} \left[\frac{\Delta \text{PSI}}{4.2 - 1.5} \right]}{0.40 + \frac{1094}{(SN+1)^{5.19}}} + 2.32 \cdot \log_{10} M_R - 8.07$$

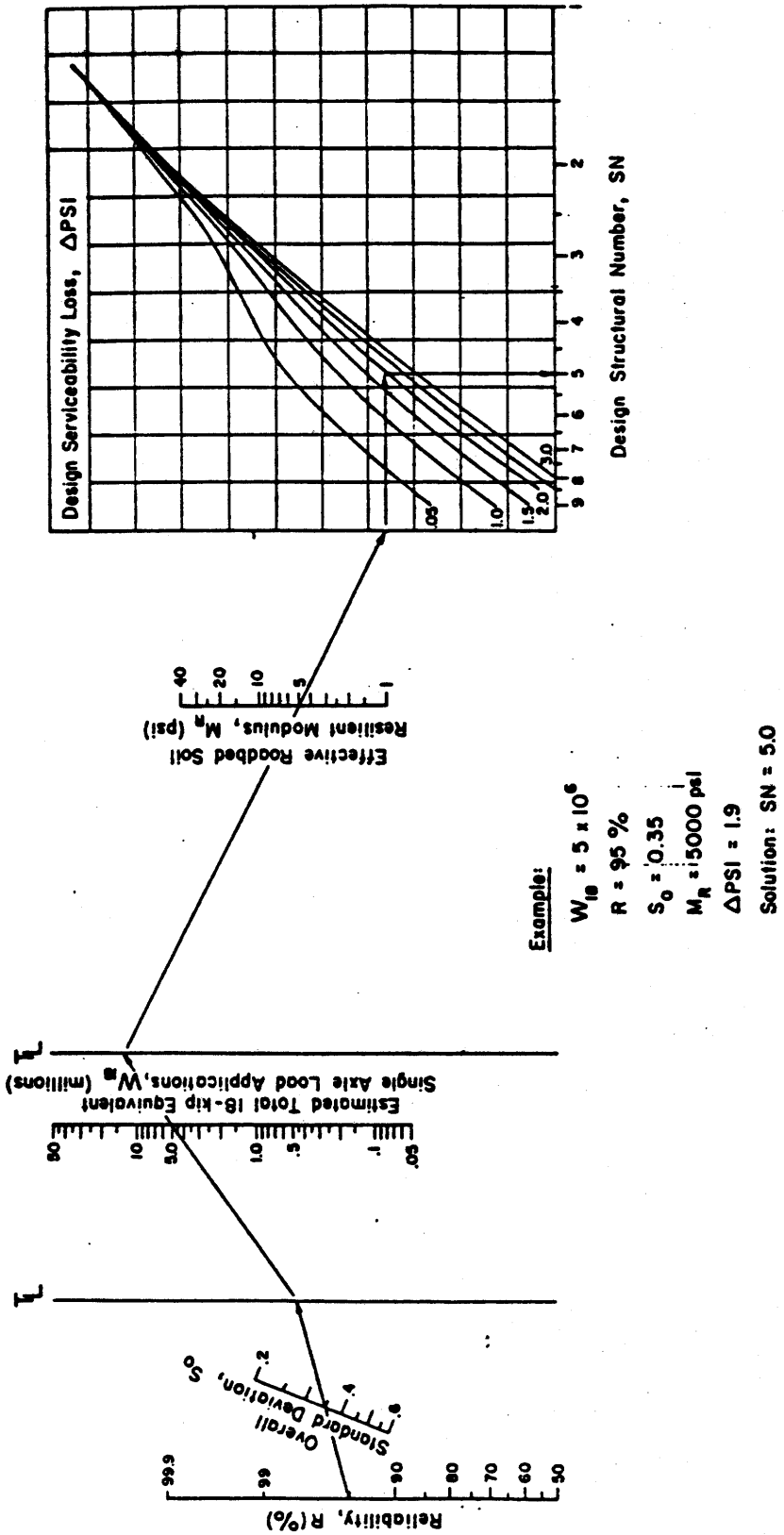


Figure 4. Design chart for flexible pavements based on using mean values for each input. [1]

considered acceptable. Transition zones between the two sections and between the sections and the existing pavement were also constructed.

Pavement construction began on May 15, 1989, with the removal of the existing wearing, base, and subbase courses to the top of the existing subgrade. After removing the pavement down to the subgrade, the existing subgrade was scarified to a depth of 4 in (100 mm). The scarified subgrade material was removed and compacted with a rubber tire roller. Following this, the subgrade was fine-graded to the planned elevations and recompacted.

For the thin section, there was no need to scarify and remove any portion of the subgrade. Therefore, after fine-grading the subgrade and applying a few passes of the vibratory roller for compaction, density and moisture were measured at several locations with a nuclear gauge to examine the adequacy of compaction.

The base material consisted of standard 2A crushed stone. Due to excessive moisture of the base material, the material was scarified and allowed to air-dry for 3 days, after which the base was compacted and cut to grade.

At this stage, construction activity was suspended for 10 days to permit installation of the instrumentation. The instrumentation installed at this stage consisted of soil strain gauges and geophones positioned at different depths in the subgrade layer; temperature sensors that were installed at different depths in the base and subgrade layers; and geophones, pressure cells, and different strain gauge transducers for measuring the strain at the bottom of asphalt concrete, which were located at the base-surface interface and the bottom of the base course, respectively. During the installation of the instrumentation, the exposed subbase was covered by plastic at the end of each working day.

After installation of the instrumentation, the bituminous concrete binder course (BCBC) for both thick and thin sections was placed. Two lifts of BCBC were required to meet the design specifications. Special precautions were taken to prevent damage to the gauges. The paver operator was instructed

to position the wheels of the paver and the dump truck delivering the hot mix approximately 2 ft (0.6 m) left of the outer wheel path where the gauges were installed. The rolling pattern for the first lift consisted of passes of the vibratory roller in the static mode in the direction of traffic only, as was specified by the gauge manufacturers. Adequacy of compaction was determined by nuclear density measurement at several stations. The second lift of BCBC was compacted using a vibratory roller in the vibrating mode in both directions in the inner wheel path and in the static mode in both directions in the outer wheel path. Both lifts of BCBC were placed on the same day.

The wearing course in both thick and thin sections consisted of two lifts that were constructed on the same day as BCBC construction. The rolling pattern for each lift consisted of one pass with the vibratory roller in the vibrating mode followed by several passes in the static mode with the rubber-tired roller. The finishing passes were made with the same vibratory roller in the static mode.

After each pavement layer was constructed, the road profile was surveyed using a rod and level. Profile measurements were taken every 2 ft (0.6 m) along the section at the centerline and the inner and outer wheel paths. By subtracting the measured profile of two successive layers, the layer thickness can be obtained at each of those points. Figure 5 shows the thickness of the asphalt concrete layer for the thick section. Figure 6 shows the thickness of the base layer and the asphalt concrete layer for the thin section. Note that the thickness shown for every station is the average thickness at the centerline and the inner and outer wheel path of the section.

INSTALLATION OF INSTRUMENTATION

After construction of the crushed aggregate base course, construction was suspended so that the transducers for the subbase and subgrade could be placed. These included:

- Soil strain gauges--in subgrade.
- Geophones--on top of subgrade and base course.

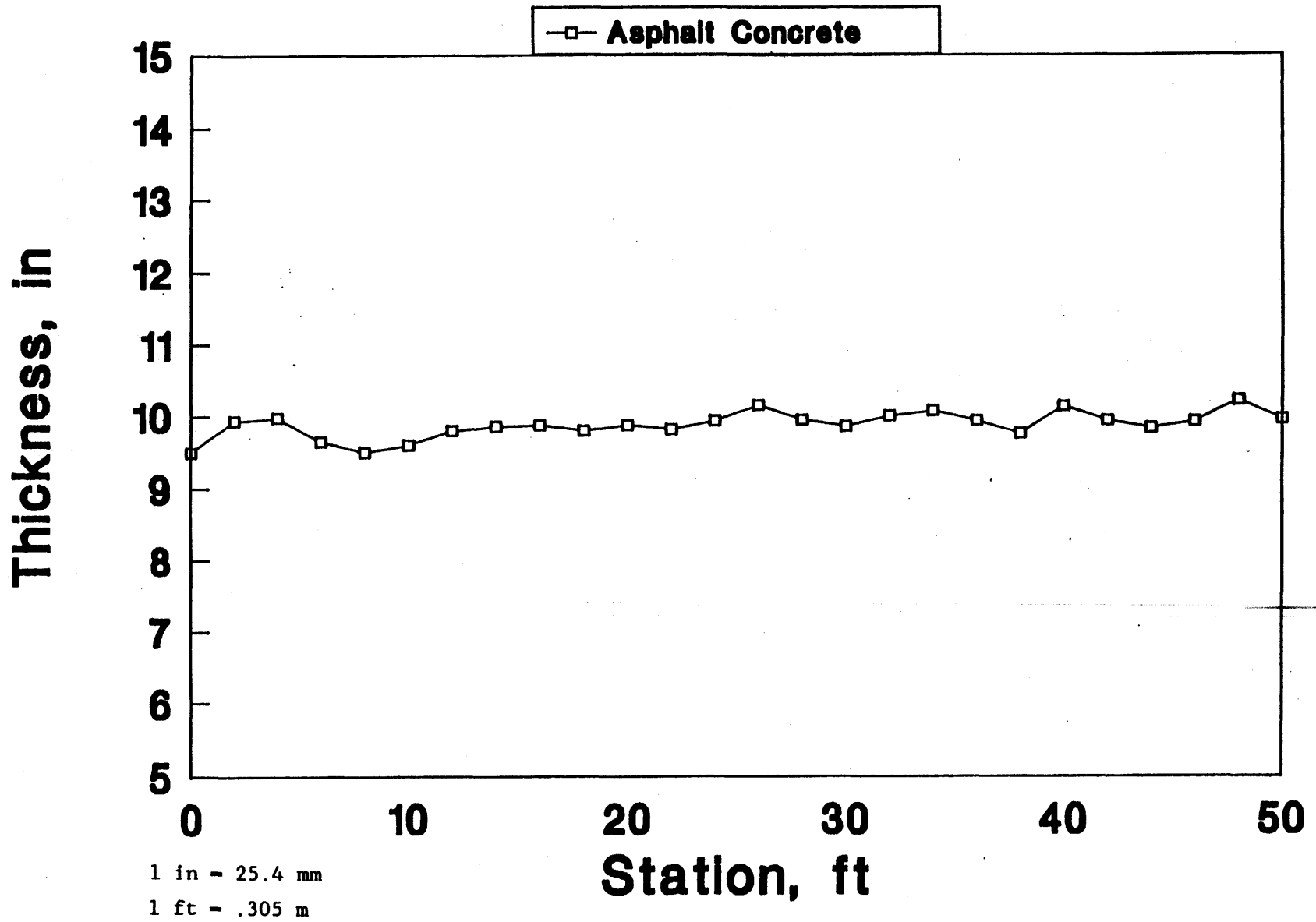


Figure 5.. Thickness of asphalt concrete layer of the thick section.

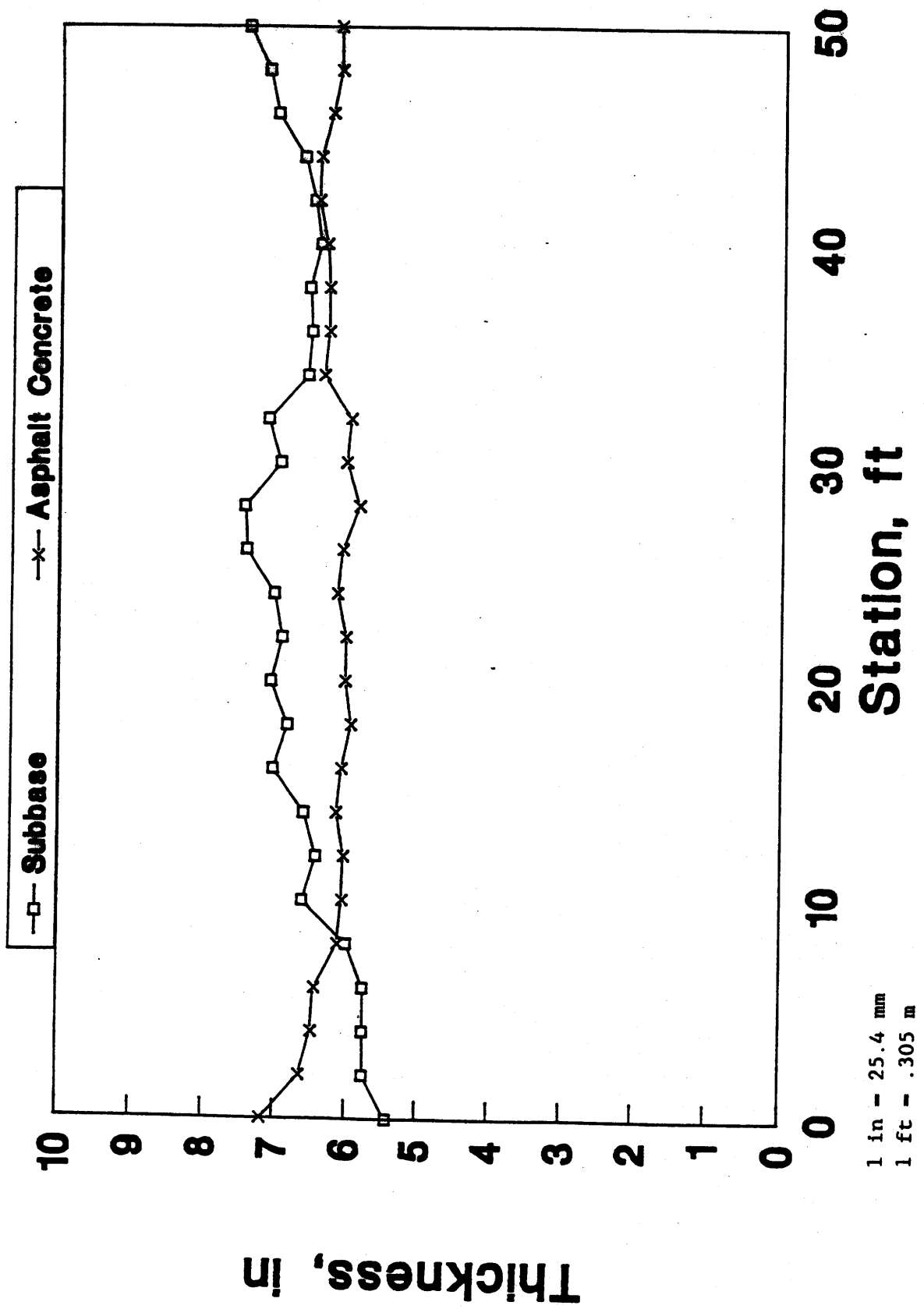


Figure 6. Thickness of asphalt concrete and crushed aggregate base layers of the thin section.

- Temperature sensors--in base course and subgrade.
- Asphalt concrete strain gauges--at bottom of BCBC layer.

After pavement construction, the following instruments were retrofitted at the specified location:

- Geophones--on top of asphalt concrete layer.
- Temperature sensors--in asphalt concrete layer.
- Single-layer deflectometer (SLD)--deep into subgrade.
- Multidepth deflectometer (MDD)--deep into subgrade.
- Moisture sensors--deep into subgrade.
- Loading plate--on top of asphalt concrete layer.

The installation of these instruments in pavements requires a great deal of care and should be performed by skilled technicians under the supervision of a pavement engineer. Detailed installation techniques and precautions for the installation of these instruments were reported in *Instrumentation for Flexible Pavements*.^[2] The following describes the techniques as employed for this particular job.

SOIL STRAIN GAUGES

Installation of Transport and Road Research Laboratory (TRRL) soil strain gauges took place after completion of placement and compaction of the crushed aggregate base layer. First, the locations selected for the strain gauges were surveyed. Then for each gauge, a hole was dug in the base course to the desired depth at the subgrade. During excavation, extra care was taken to minimize disturbance of the soil and keep the size of the hole to a minimum. The excavated materials were placed in plastic bags to preserve their moisture. The soil strain gauge was placed in the hole in the longitudinal direction and the excavated subgrade material was placed in small layers and carefully compacted. It is very important to monitor the gauge during compaction of the soil because the gauge can easily go out of range. To avoid

this problem, the compaction around the gauge was performed using a small hand tamper, and the level of effort was gradually increased until the desired level of compaction was achieved. The level of compaction was estimated by comparing the quantity of soil compacted into the hole with the excavated quantity. Subgrade buildup continued to the as-constructed level. Then the above procedure was repeated using crushed aggregate to fill the hole to the top of the base course.

H-GAUGES

H-gauge strain transducers were installed after completion of placement and compaction of the base course. First, the locations of the strain gauges were surveyed, and the sharp and large aggregates underlying them were removed. The H-gauges were then placed in the designated locations in the longitudinal direction. The lead wires were placed in 4-in (100-mm) deep preformed grooves in the base course for protection against heat of paving mix and relocation. Then, a slurry mixture of hot asphalt cement and fine sand was carefully poured over the gauges to keep them in place. The output from the H-gauges was monitored before, during, and after pavement construction. The resistance across the strain gauge bridges was also monitored during installation.

To avoid possible shifting of the H-gauges during construction, some hot-mix asphalt was placed over the gauges using a shovel before the paver approached. Care was taken to avoid contact of large aggregates in the mix with the gauges.

PRESSURE CELLS

The pressure cells were installed at the interface of the base course and the asphalt concrete layer. After completion of the base course, small depressions were made at the points of installation by removing some of the material from the subbase layer. The depressions were just large enough to permit placement of the pressure cells inside. A thin layer of fine sand was placed at the bottom of each depression. Each pressure cell was then placed on the sand, faceplate up and flush with the top surface layer. Extra care

was taken to place the pressure cell in a horizontal position. A slurry mixture of hot asphalt cement and fine sand was carefully poured over the pressure cell to keep it in place. To protect the cables, they were placed in trenches dug in the base course and covered with sand. The resistance across the pressure cell bridges was monitored during installation.

The same procedure as that applied to the H-gauges was used to avoid shifting of pressure cells during construction.

GEOPHONES

Geophones should be installed firmly on a mounting surface that is flat and leveled. The installation techniques for unbonded and bonded layers are outlined in the following sections.

Unbonded Layers

Before installation, the geophones were mounted on 4-by-4-by-1/8-in (100-by-100-by-3-mm) metal plates. Installation of geophones at the top of the subgrade and the crushed aggregate base course took place after completion of placement and compaction of the crushed aggregate base course.

After the location of the geophone was surveyed, a hole was dug into the crushed aggregate base, all the way to the top of the subgrade. During excavation, extra care was taken to minimize disturbance of the soil and keep the size of the hole to a minimum. The excavated material was placed in a plastic bag to preserve its moisture. Then a small hole was carefully dug in the subgrade so that the geophone could snugly fit inside the hole. The geophone was then placed in the hole with the base plate in a horizontal position. A small amount of excavated subgrade material was placed around the geophones and carefully compacted using a small hand tamper. Excavated crushed aggregate was then placed into the hole in small layers and compacted. This process continued until the hole was filled to the top of the base course.

The geophones at the top of the base course were installed by digging a small hole to fit the geophone. Due to lack of cohesion of crushed aggregate, it was not possible to place the geophone snugly. Therefore, an epoxy mix was placed into the hole to ensure secure installation of the geophone.

Bonded Layers

Installation of geophones at the top of asphalt concrete layer was relatively simple. There was no need to mount the geophones on flat plates because leveling the geophones at the surface is not difficult. A 1.5-in-deep-by-1-in-diameter (38-mm-deep-by-25-mm-diameter) hole was drilled at the desired location to accommodate the geophone. A groove was also cut from the hole to the edge of the pavement for placement of the lead wire. After the bottom of the hole was leveled and smoothed, the geophone was secured in the hole using a pasty epoxy compound. The remaining 1/4 in (6 mm) of the hole was also filled with epoxy.

INSTRUMENTED CORES

The installation of instrumented cores began after completion of pavement construction with the drilling of a hole in the pavement at the desired location, along the outer wheel path, using a 6-in (150-mm) barrel bit. The asphalt concrete cores that were used for instrumentation were obtained by drilling holes at parallel locations along the inner wheel path using a 6.25-in (159-mm) barrel bit. The combination of the 6- and 6.25-in barrels provides a 1/16-in (1.6-mm) clearance between the instrumented core and the existing pavement, which is filled with epoxy. A small trench was cut from each hole to the edge of the pavement for placement of the cables. As it was expected, the drilling water washed away some of the finer particles of unbonded base course. This problem was remedied by replacing the coarse particles in the hole with a mixture of sand and bitumen and leveling and compacting it with a plate the diameter of the hole.

Epoxy glue was spread on the side surface of the cores and the holes. The instrumented cores were then placed and the lead wires guided into the

trench. Finally, a surcharge weight of about 20 lb (90 N) was placed on the core until the epoxy glue hardened. All of the installed instrumented cores were slightly shorter than the depth of the drilled hole. Therefore, a mixture of sand and epoxy was used to fill and level the holes.

SINGLE-LAYER DEFLECTOMETER

Installation of the single-layer deflectometers was also performed after completion of paving. The installation began with coring of the pavement to the desired depth using a 6-in (152-mm) barrel bit. One SLD was installed at the top of the subgrade and the other at the top of the crushed aggregate base. From that level, a 1-in (25.4-mm) diameter hole was bored to a depth of about 8 ft (2.4 m). Then approximately 1/2 gal (2 l) of liquid sealant (elastomer) was poured into the hole. The SLD housing, base plate, and the guide tube were inserted into the hole until the plate was flush with the surface. (The amount of liquid sealant in the hole should be sufficient to allow some of it to be extruded around the housing onto the surface whose displacement is to be measured.) A surcharge weight was then placed on the base plate. The installation was resumed after 16 h when the sealant was completely cured. The following day, the reference rod was driven through the frangible bottom cap for 2 ft (0.6 m). The installation proceeded with insertion of the Linear Variable Differential Transformer (LVDT) housing assembly and zeroing of the LVDT output. After satisfactory zeroing of the LVDT, the housing was fastened to and flush with the collar nut and the top cap was glued in place. The excavated unbound materials were then placed over the cap and carefully compacted. The LVDT output was monitored during compaction to avoid driving the LVDT out of its linear range. The removed asphalt concrete core was then glued into the hole using an epoxy compound.

MULTIDEPATH DEFLECTOMETER

Multidepth deflectometers were retrofitted into the constructed pavement (see figure 7). The installation started with drilling a 1.5-in (38-mm) diameter hole to a depth of 7.1 ft (2.2 m) and lining the hole with a thin rubber liner to prevent moisture and loose material from damaging the transducers. An anchor was then placed at the bottom of the hole and fixed in

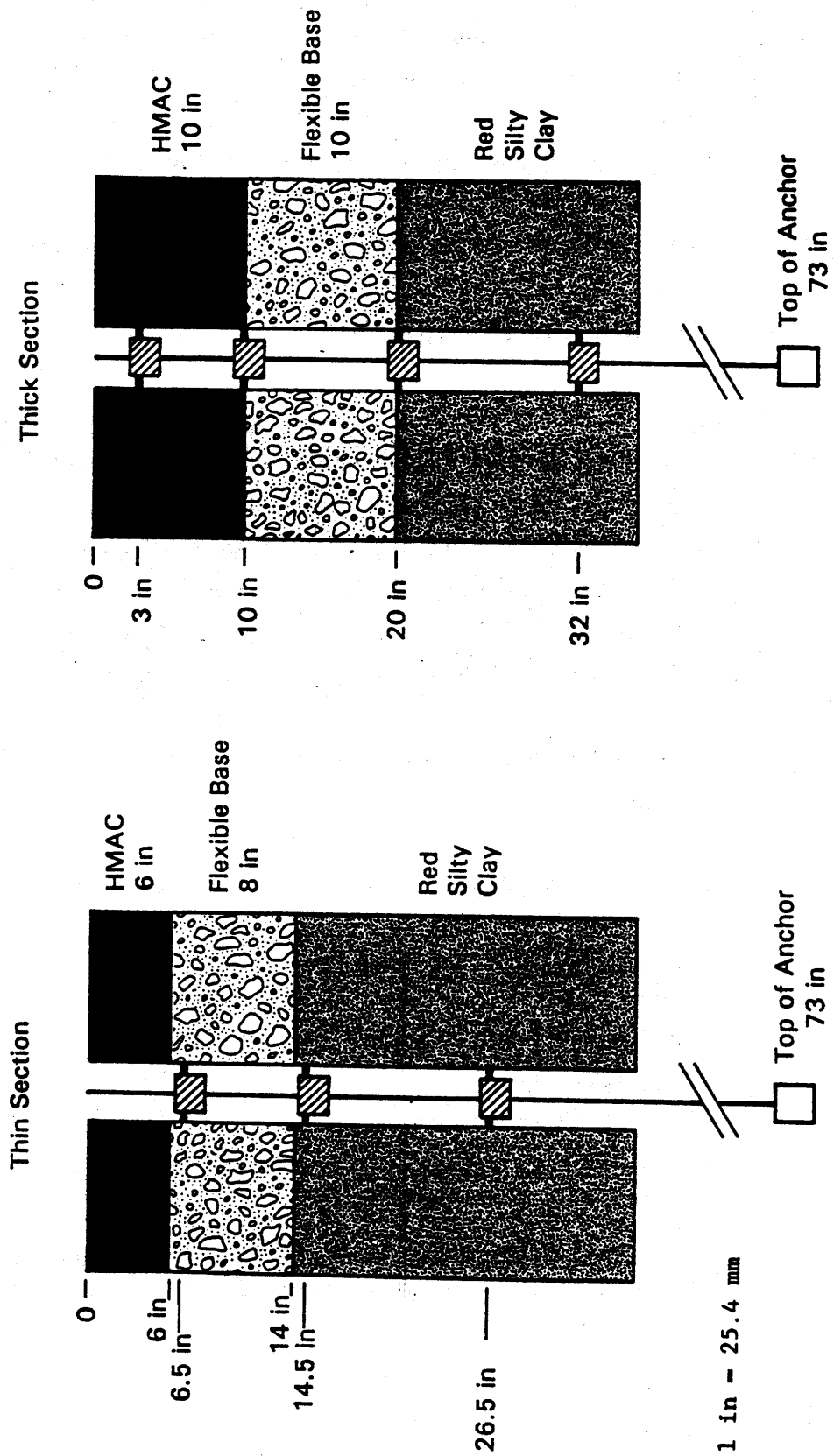


Figure 7. Multi-depth deflectometers installed in the test track.

place with cement grout. At this time the installation was stopped to allow the grout to cure. On the following day, an interconnecting rod was lowered and fixed into the snap connector. The MDD modules were slid over the interconnecting rod to the desired depth and locked in place. The interconnecting rod was then replaced with a rod containing the LVDT cores. (The locations of the cores can be adjusted to facilitate zeroing of the LVDT's prior to the completion of installation.) As the final step, down-hole calibration was performed using a specially designed calibration unit.

DATA ACQUISITION AND REDUCTION

The key to obtaining meaningful data for any instrumentation scheme is a data acquisition system that allows each designated transducer to be monitored for a given period of time at the designated sampling rate. In this section, the components of two data acquisition systems developed for this study are described. One system was used to collect data from the strain gauges, pressure cells, and single-layer deflectometers. The other system was used to collect data from the multidepth deflectometers.

The essential hardware required to perform the data acquisition consists of the following:

- Computers: Two portable Compaq II computers with the following specifications were used:
 - 80286 processor.
 - 12-MHz clock.
 - 640 KB of memory.
 - 80287 math coprocessor.
 - 20-MB fixed disk.
 - Serial/parallel port.

Each computer was equipped with a DT2801-A data acquisition board manufactured by Data Translation.

- Signal conditioners: Two types of Daytronic signal conditioners were used, a system 10 unit and a model 3270 strain gauge conditioner.

The following ancillary equipment was used:

- Infrared sensors: One transmitter and one receiver were used to trigger the data acquisition system when the ray between the transmitter and the receiver was broken by a truck.
- Ultrasonic sensor: This sensor was combined with a frequency counter to determine the time required for an acoustic signal to leave the source, reflect from the side of the truck, and return to the source. This assembly was used to measure the transverse position of the tractor trailer with respect to the pavement edge.

The software used to control the hardware for the first data acquisition system was the ASYST Scientific System. This package incorporates both an environment and a programming language. The language is based on FORTH. The ASYST environment has a variety of subroutines that can be called by a program.

An elaborate program was developed in the ASYST environment to control various parameters of the data acquisition system and convert the acquired analog signal to a digital signal through a data acquisition board. The board is configured for a maximum of 16 channels of single-ended bipolar inputs in direct memory access (DMA) mode. The number of active input channels and the board gain are software-controlled. One limitation of the system is that the data acquisition board does not have an independent control of gain for each input channel. This shortcoming can be handled through the proper choice of transducers or the introduction of a hardware amplifier into the circuitry. The data acquisition may be triggered manually (by hitting the carriage return) or automatically (upon receiving a signal from the triggering system).

In the DMA mode, the sampling rate depends on the number of input channels and the conversion delay, or the elapsed time needed for the board to acquire data from two successive channels. A conversion delay of 0.11 ms was used during the field testing. In addition to the sampling frequency, the duration of the data acquisition process (i.e., the total number of data points) was also controlled. This task was performed by dynamic sizing of the arrays. The required dimensions of the arrays were calculated from the

nominal speed of the truck, the specified conversion delay, the number of input channels, and the length of the instrumented section of the pavement.

Immediately after acquiring a signal from the gauges, the acquired signal can be displayed on the computer screen for visual verification. The captured data are then saved on the hard disk for future analysis. In every saved file along with the digital data, pertinent information regarding the measurement is also recorded, including date, time, site information, software gain, tire type, tire pressure, axle configuration, axle load, and truck speed.

A data reduction program was developed for use with the ASYST programming environment. After the stored data are retrieved, the digital signal (integer values from -2,048 to 2,048) is then converted back to voltage based on the gain value of the data acquisition board at the time of data collection. To convert the voltage signal into engineering units, the data arrays (in volts) from each channel were multiplied by the channel's corresponding calibration factor.

The software then plots the data from each channel for visual inspection. The program can focus on any range of data array by magnifying the signal for a close-up inspection and providing the coordinates of any point on the plot. Because data must be in ASCII format for some program applications, the program also allows downloading of the data arrays into ASCII files.

After the measured strain signal was plotted, points of maximum strain under axles were located and the corresponding values were recorded. For geophone signals, the beginning of the signal for a specific axle was located. The corresponding data arrays were then downloaded into ASCII format. The geophone data that represent velocity were then integrated to determine peak deflection under the axle.

Reduction of the data collected in this study was a very time-consuming process. Because engineering judgment is needed at various stages of the process, it is not feasible to completely automate the reduction process. After completing this process, the data can be fully analyzed and the effects of various variables and their significance can be studied.

The second data acquisition system, used to collect data from the multidepth deflectometers, consists of a Compaq 386 portable computer, a Data Translation DT2814 board, and data collection software. The data collection and analysis software consists of the following programs:

- ADFWD.EXE--captures signals under falling weight deflectometer (FWD) loading and builds a LOTUS 1-2-3 data file.
- ADTRUCK.EXE--captures signals under truck loading and builds a LOTUS file.
- FILTRUCK.EXE--filters high frequency noise from the signal (if required) and calculates peak deflections for each axle for each MDD.

At the maximum data acquisition speed, 10,000 sets of MDD data (up to 6 channels) are collected per second. The maximum speed is used under FWD testing: 600 samples are recorded over a 60-ms time interval. The FWD load pulse is approximately 30 ms. Under truck loadings, the truck length, speed, and number of required data points are entered, and the computer calculates a delay cycle between each set of data. Both the ADFWD and ADTRUCK programs are self-triggering; that is, a signal on any MDD channel will activate the data acquisition system. The output file also includes 100 pre-trigger data points. Calibration factors are entered in the data acquisition programs so that the outputs are in engineering units.

FIELD TESTING

Field testing of the existing instrumentation was carried out in two stages. Stage I was an exploratory experiment to debug the entire system and check the validity of data. It began on July 23, 1989, and ended on July 27, 1989. Stage II was a complete experiment; it began on August 16, 1989, and ended on August 22, 1989. In the first stage of testing, pavement response data under a variety of test conditions (as described in the data collection plan), measured by different instruments installed in the pavement, were collected. Tables 3 and 4 summarize the test conditions and the actual axle loads, respectively.

Table 3. Experimental plan for field testing in phase I.

Variable	Levels
Pavement Section	Thin and Thick
Load	Empty, Intermediate, Fully Loaded
Tire Pressure	120 and 125 psi (828 and 863 kPa)
Speed	20, 35, and 50 mi/h (32, 56, and 80 km/h)
Replicates	3 (stage I), 4 (stage II)

1 mi = 1.61 km

Table 4. Static load levels for the test track in pounds.

Test Period	Load Level	Axle			
		Steering	Single Drive	Front Tandem Trailer	Rear Tandem Trailer
Stage I	Empty (E)	7,550	17,640	5,010	3,760
	Intermediate (I)	7,550	17,640	16,740	14,690
	Fully loaded (L)	7,550	20,230	20,520	17,170
Stage II	Empty (E)	7,550	8,450	5,010	3,760
	Intermediate (I)	7,550	12,360	11,660	9,160
	Fully loaded (L)	7,550	19,640	20,820	16,790

1 lb = 4.5 N

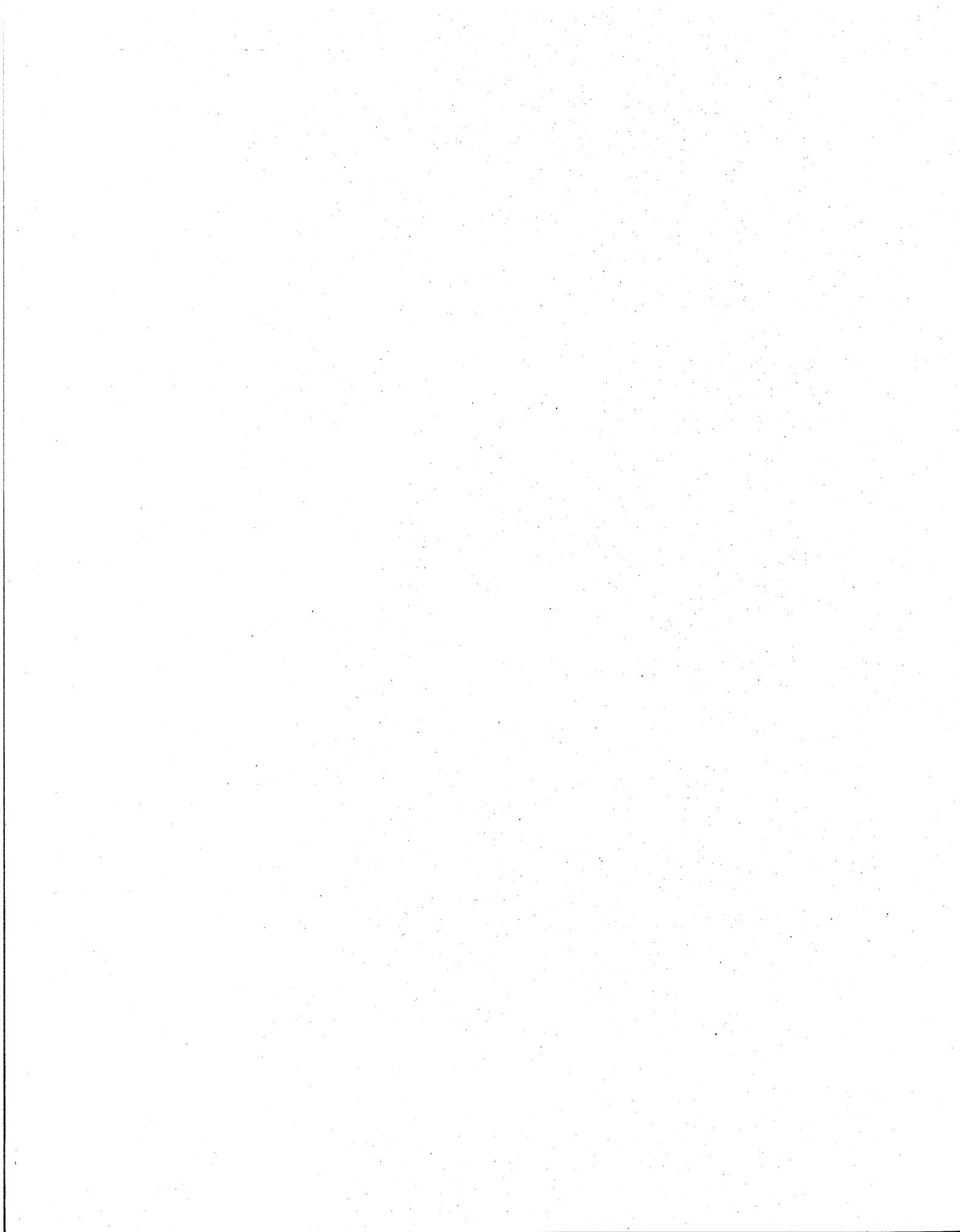
Since stage I was an exploratory experiment, only three replicate measurements were collected for any combination of variables during this stage of testing. Because hardware was not readily available, it was not feasible to perform testing on both thick and thin pavement sections at the same time.

During stage I of field testing, some of the instruments malfunctioned. Therefore, it was impossible to collect data from all the instruments. After the malfunctioning instruments were repaired and after a preliminary analysis of stage I results, a second stage of testing was conducted.

The second stage testing was conducted under the same combination of variables but with different axle weights for the three load levels; furthermore, the load on both drive and trailer axle was changed for each level, as shown in table 4.

Field testing for both stages I and II usually began in early morning hours and continued until mid-morning to minimize the temperature variation among the various tests. Throughout the testing, pavement temperature at various depths was measured on an hourly basis.

The test vehicle consisted of a single-axle tractor and a tandem-axle semi-trailer. The suspension for all axles was a conventional leaf-spring system. The 11R24.5 and 11R22.5 dual radial tires were mounted on the drive and trailer axles, respectively.



3. DATA ANALYSIS: PHASE I

As mentioned earlier in this report, one of the main objectives of this research was to evaluate the performance of the existing flexible pavement instrumentations under actual truck loading. The test variables, discussed in chapter 2, were selected to provide a wide range of measured responses under which the instrumentation could be evaluated. This chapter presents the results of data analyses performed on the measured data in order to evaluate the performance of the individual gauges.

STRAIN MEASUREMENTS IN THE ASPHALT CONCRETE LAYER

After the strain data were collected in the field, they were stored on floppy disks for conversion to engineering units and further analysis. The recorded strain signals were multiplied by calibration factors, which convert the volts into microstrains. The calibration factors used in this research were determined from the strain gauge properties supplied by the manufacturers of the individual gauges. After the measured data were converted into engineering units, the responses of the individual gauges under each pass of the test truck were plotted. The initial reference point was selected on the plots along with the maximum strain under the single drive axle and the maximum strain under the tandem trailer axle (see figure 8). The actual strains were then obtained by subtracting the initial reference point from the maximum strains.

SURVIVABILITY

As expected, not all the gauges survived the construction and installation activities. The following gauges survived in the thick section:

- One Dynatest gauge at station 9 and one at station 19 (two gauges were installed).
- One ARC gauge at station 21 (one gauge was installed).
- One Kyowa gauge at station 6; one at station 10; and one at station 18 (four gauges were installed).

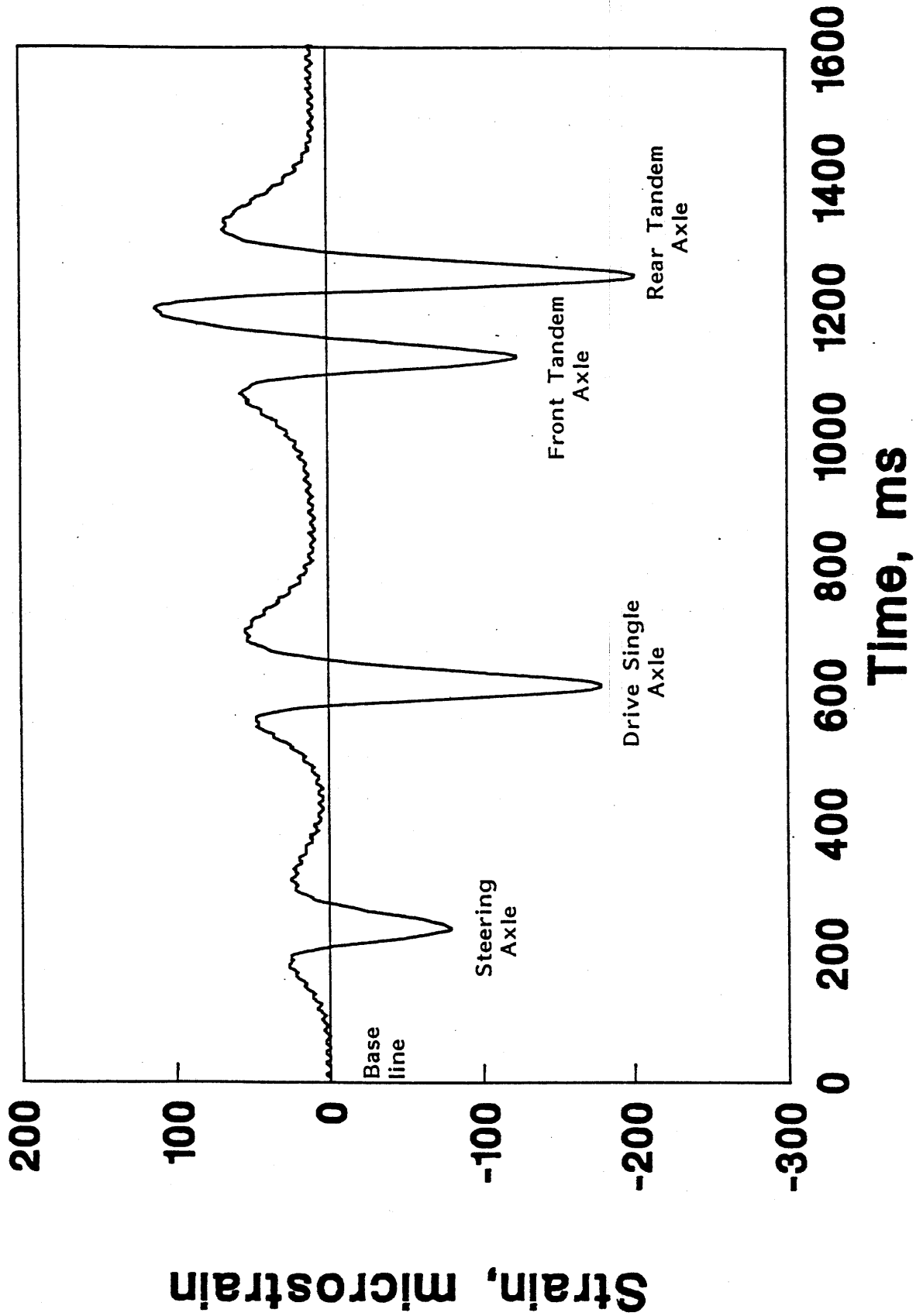


Figure 8. Typical response of asphalt concrete longitudinal strain gauge (thick section).

- One three-directional core gauge at station 8 (two gauges were installed).
- One longitudinal core gauge at station 12 and one at station 16 (four gauges were installed).

All gauges were installed in the longitudinal direction at the outer wheel track of the section. Two of the gauges in the thick section were unoperational shortly after construction: one Kyowa gauge at station 10 and one three-directional core gauge at station 8 (all three gauges failed on this core). Two additional gauges were unoperational during stage II: one Dynatest gauge at station 9 and one at station 19.

Overall, nine strain gauges were installed to measure strains in the asphalt concrete layer of the thick section. Two gauges failed during construction and two failed after construction. Two Dynatest gauges failed during the period between stage I and stage II. A post-failure examination of the Dynatest gauges indicated excessive permanent strains on both gauges.

The total number of gauges that survived the construction and installation activities in the thin section were as follows:

- One Dynatest gauge at station 9 and one at station 30 (two gauges were installed).
- One ARC gauge at station 34 (one gauge was installed).
- One Kyowa gauge at station 6; one at station 10; one at station 29; and one at station 33 (four gauges were installed).
- One three-directional core gauge at station 12 and one at station 27 (two gauges were installed).
- One transverse core gauge at station 32 (one gauge was installed).

Three of the gauges in the thin section were unoperational shortly after construction: one Kyowa gauge at station 6, one longitudinal core gauge at station 28, and one three-directional core gauge at station 27. (Again, all three gauges on this core were unoperational.) The Kyowa gauge at station 33 failed during the period between stage I and stage II testing.

The survivability of the asphalt concrete strain gauges was very inconsistent within groups of the same type of gauge and also from one pavement structure to another. The survivability of the Dynatest gauges varied the most. These gauges survived the construction activities in both sections, but the two gauges installed in the thick section failed due to excessive permanent strains during the early part of the stage II testing. On the other hand, the survivability of the Dynatest gauges installed in the thin section was perfect throughout the entire testing program. After the Dynatest gauges failed, some unsuccessful attempts were made to balance them into an operational range. It is interesting to note that both Dynatest gauges in the thick section failed within half an hour. In addition, both Dynatest gauges in the thin section survived the entire testing program even though they were subjected to higher strains than the gauges in the thick section. The survivability of the ARC gauges was perfect in both sections for the entire testing program. The survivability of the Kyowa gauges varied from one section to another and for various stages of the testing program. All failed Kyowa gauges showed out-of-scale responses and could not be electrically balanced. An interesting observation regarding the instrumented cores is that all three gauges on the three directional cores failed at once. The sudden failure of the three gauges may be due to failure of bondings between cores and old pavement. Overall, an average survivability of 70 percent for all types of gauges was better than the expected failure rate of 50 percent except for the Dynatest gauges installed in the thick section.

REPEATABILITY

The repeatability of the gauges is studied in terms of the means, standard deviations, and coefficients of variation of the four replicate measurements for each combination of the test variables. The data from the stage I and II testing programs will be used to evaluate all of the gauges, including those that failed at various times during testing.

In volume II of this report, appendix C shows the results of the four replicates and their corresponding means, standard deviations, and coefficients of variation. The coefficient of variation (COV) is defined as the ratio of the standard deviation to the mean, expressed as a percentage.

The lower the COV, the better the repeatability of the measuring device. In general, COV values below 10 percent are considered good, and COV values below 5 percent are considered excellent. Tables 5 and 6 show typical repeatability data from the thick and thin sections, respectively. As these tables indicate, most of the COV values are in the range of 2 to 6 percent. In general, the COV values are smaller for higher load levels under both the single-drive axle and tandem trailer axles. Based on the COV values, all the gauges showed good to excellent within-gauge repeatability except for the ARC and core gauges under the empty load level.

Because there are only four replicates, the data were pooled across certain test variable combinations, and the new standard deviations of the pooled observations were determined. This exercise increased the number of observations and reduced the effect of potential random error in the collected data. For every gauge, the following pooling patterns were used:

1. Pool the data from the two levels of tire pressure (eight replicates).
2. Pool the data for the fully loaded level across the speeds of 35 and 50 mi/h (56 and 80 km/h) (16 replicates).
3. Pool the data for the speed of 20 mi/h (32 km/h) across the intermediate and empty load levels (16 replicates).
4. Pool the data across the speeds of 35 and 50 mi/h (56 and 80 km/h) and across the load levels of intermediate and empty load levels (32 replicates).

The pooling process increased the number of observations from 4 replicates of each combination to 8, 16, or 32 replicates for different pooling patterns as shown by the number of replicates in parentheses.

The overall standard deviation of measured strain for each pooling pattern was calculated. The pooled standard deviations are summarized in tables 7 through 10. All the pooling activities concentrated on the data from the stage II testing program because a better vehicle alignment scheme was used, and the four replicates were selected based on the transverse vehicle location as measured by the ultrasonic distance-measuring device. It can be seen from the data in tables 7 through 10 that the pooling of these

Table 5. Strain values under drive axle with 20 kips/axle, tire pressure of 125 psi (863 kPa), thick section.

Speed (mi/h)	Dynatest Sta 9	Dynatest Sta 19	Kyowa Sta 6	Kyowa Sta 18	ARC Sta 21	Core Sta 12	Core Sta 16
20	193	208	237	161	344	218	234
20	208	235	211	179	358	216	246
20	223	228	233	176	379	211	222
Mean	208	224	227	172	360	215	234
STDV	12	11	12	8	14	3	10
COV	5.8	5.1	5.2	4.6	4.0	1.4	4.1
35	174	142	191	97	229	145	156
35	174	132	NA	95	224	135	152
35	176	127	193	96	210	130	131
Mean	175	134	192	96	221	137	146
STDV	1	6	1	1	8	6	11
COV	.7	4.6	.6	.7	3.6	4.3	7.4
50	122	98	108	78	152	107	135
50	120	98	103	87	154	100	136
50	118	98	103	83	154	97	134
Mean	120	98	104	83	153	101	135
STDV	2	NA	2	3	1	4	1
COV	1.7	NA	2.2	4.2	.7	4.0	.7

1 mi = 1.61 km

Table 6. Strain values under drive axle with 20 kips/axle, tire pressure of 105 psi (725 kPa), thick section.

Speed (mi/h)	Dynatest Sta 9	Dynatest Sta 30	Kyowa Sta 10	Kyowa Sta 29	Kyowa Sta 33	ARC Sta 34	Core Sta 12
20	362	375	448	436	448	745	270
20	362	402	439	482	384	686	282
20	375	414	464	487	460	837	322
Mean	366	397	450	468	431	756	292
STDV	6	16	10	23	33	62	22
COV	1.6	4.1	2.3	4.9	7.7	8.2	7.7
35	211	282	280	345	301	489	187
35	122	289	272	348	335	503	178
35	105	296	296	382	294	456	121
Mean	146	289	283	358	310	483	162
STDV	46	6	10	17	18	19	29
COV	31.6	2.1	3.5	4.7	5.8	4.0	18.1
50	140	184	166	228	260	448	135
50	140	211	167	225	269	464	140
50	149	220	174	228	262	424	140
Mean	143	205	169	227	264	445	138
STDV	5	16	3	1	4	17	2
COV	3.2	7.6	2.0	.5	1.6	3.7	1.6

1 mi = 1.61 km

Table 7. Summary of the pooled standard deviations of the strain measurements under the single drive axle, thin section.

Gauge	Pooling Pattern			
	1	2	3	4
Kyowa, Sta 10	19	6	5	3
Kyowa, Sta 29	10	6	12	4
Dynatest, Sta 9	17	5	3	2
Dynatest, Sta 30	14	7	4	3
Core, Sta 12	6	6	4	3
ARC, Sta 34	22	9	17	9

Table 8. Summary of the pooled standard deviations of the strain measurements under the tandem trailer axle, thin section.

Gauge	Pooling Pattern			
	1	2	3	4
Kyowa, Sta 10	6	7	3	3
Kyowa, Sta 29	15	5	5	3
Dynatest, Sta 9	9	6	2	3
Dynatest, Sta 30	15	5	5	3
Core, Sta 12	10	6	3	2
ARC, Sta 34	28	5	17	11

Table 9. Summary of the pooled standard deviations of the strain measurements under the single drive axle, thick section.

Gauge	Pooling Pattern			
	1	2	3	4
Kyowa, Sta 6	10	2	5	2
Kyowa, Sta 18	7	3	5	1
Core, Sta 12	13	3	6	3
Core, Sta 16	32	19	24	12
ARC, Sta 21	14	7	8	4

Table 10. Summary of the pooled standard deviations of the strain measurements under the tandem trailer axle, thick section.

Gauge	Pooling Pattern			
	1	2	3	4
Kyowa, Sta 6	9	3	8	5
Kyowa, Sta 18	10	2	3	2
Core, Sta 12	14	4	11	3
Core, Sta 16	34	15	22	10
ARC, Sta 21	12	10	7	2

combinations helped identify the most critical conditions under which the gauges produced the highest standard deviation. All of the gauge types were consistent; the highest measured standard deviation was encountered under the combination of the fully loaded level and the speed of 20 mi/h (32 km/h). This observation was also consistent under both axle configurations (i.e., single drive axle and tandem trailer axles) and at both test sections (i.e., thick and thin). This observation does not indicate poor repeatability of the gauges under the fully loaded level at 20 mi/h (32 km/h) because the measured strain values under this pattern are the highest; therefore, the standard deviation is expected to increase, and, as a result, the coefficient of variation will not be affected.

The most encouraging observation from this pooling exercise is that all of the gauges were very consistent (except the ARC gauge in the thin section and one core gauge in the thick section) and had low standard deviations under speeds of 35 and 50 mi/h (56 and 80 km/h), which is the normal range of speed for most truck traffic.

Based on the analysis of the collected data, it can be concluded that the repeatability of the Dynatest, Kyowa, ARC, and core gauges is very good even under the conditions that created relatively high standard deviations. The gauges will be further evaluated based on the other criteria.

EFFECTS OF TEST VARIABLES ON THE RESPONSE OF GAUGES

Axle load, tire pressure, and truck speed were selected as the variables for the field testing program. The first part of the analysis deals with the selection of those variables that significantly affect the values of the measured strains. If the effect of a variable (e.g., tire pressure, speed, or load) is proven insignificant, this variable was omitted from further evaluation.

The measured strain data from thin and thick structures under the various combinations of load, tire pressure, and speed were plotted for both single- and tandem-axle configurations (see appendix C in volume II of this report). From these plots it is obvious that the effect of tire pressure on

strain at the bottom of the asphalt concrete layer is insignificant compared to the effects of axle load and truck speed for all types of strain gauges. Therefore, tire pressure was held at one level (i.e., 125 psi [863 kPa]) while the effect of other variables (i.e., speed and axle load) was studied.

Effect of Axle Load on the Response of Strain Gauges

It has been shown in various research studies that the load level has a great effect on the measured strains at the bottom of the asphalt concrete layer.^[3,4] Therefore, the response of the different strain gauges under various load levels is of interest because it will indicate how the individual gauges perform when subjected to various levels of the strains. If one strain gauge is very stiff compared to the others, then the slopes of the strain-versus-load curve for this gauge will be smaller than the slopes of the other gauges. To study this effect, the strain-versus-load curves for the various types of strain gauges were developed. Figures 9 and 10 show typical strain-versus-load curves for the single drive axle at speeds of 20, 35, and 50 mi/h (32, 56, and 80 km/h) on the thick and thin pavement sections. Figures 11 and 12 show typical strain-versus-load curves for the tandem trailer axle at speeds of 20, 35, and 50 mi/h (32, 56, and 80 km/h) on the thick and thin pavement sections. The strain-versus-load curves for all gauges are shown in appendix C of volume II. The data show that the effect of increasing load level from the intermediate to the fully loaded level on the measured strains was consistent among all types of gauges under both the single- and tandem-axle configurations. However, the effect of increasing the load level from empty to the intermediate level on the measured strain was less consistent.

Effect of Truck Speed on the Response of Strain Gauges

The measurements from all of the types of strain gauges indicated that the speed of the test vehicle has a significant effect on the measured strains. Reductions in the measured strains on the order of 50 and 70 percent were observed for speeds of 35 and 50 mi/h (56 and 80 km/h) when compared to strains observed at 20 mi/h (32 km/h), respectively. Figures 9 through 12 also show the effect of speed on the measured strain from selected gauges.

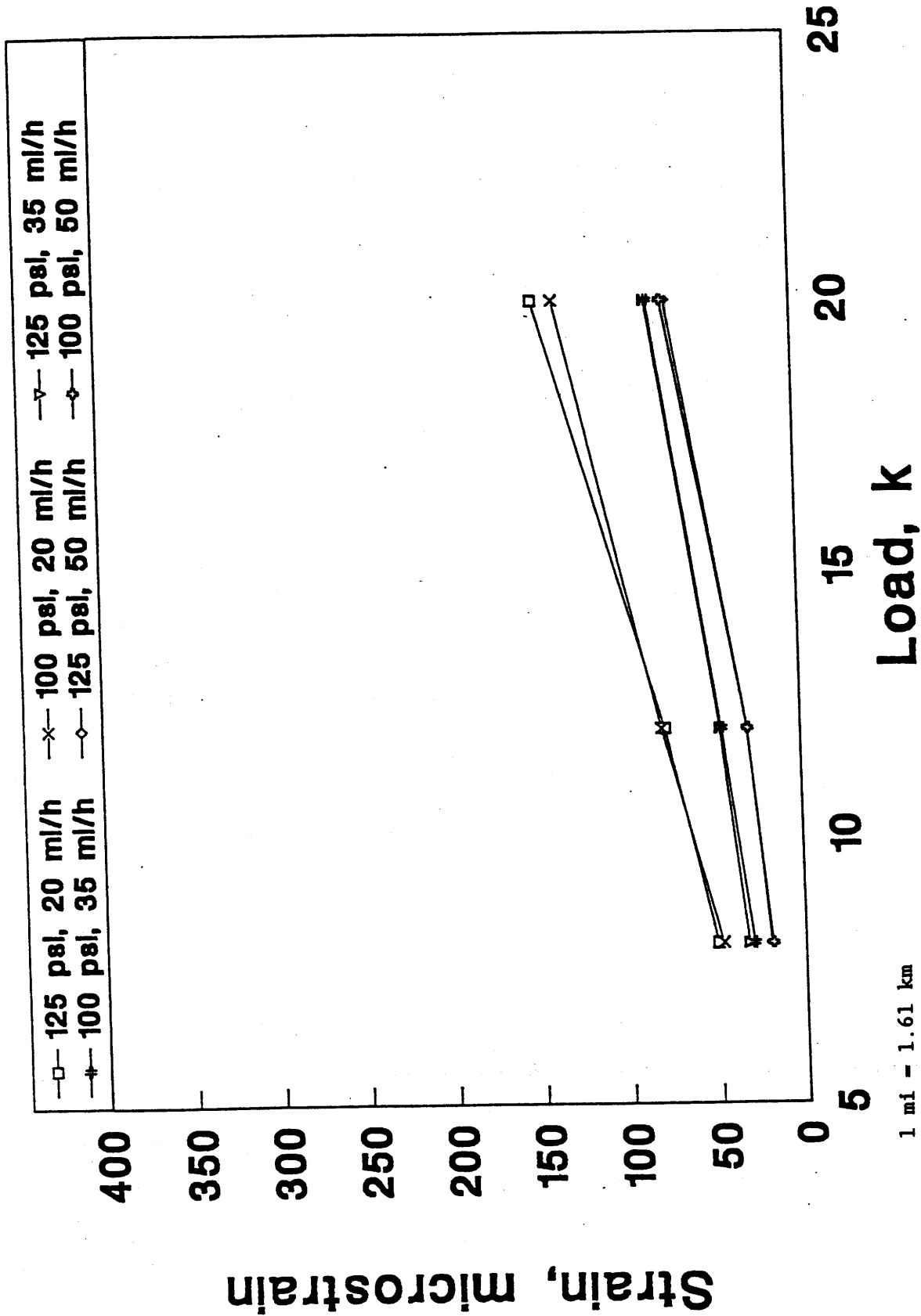
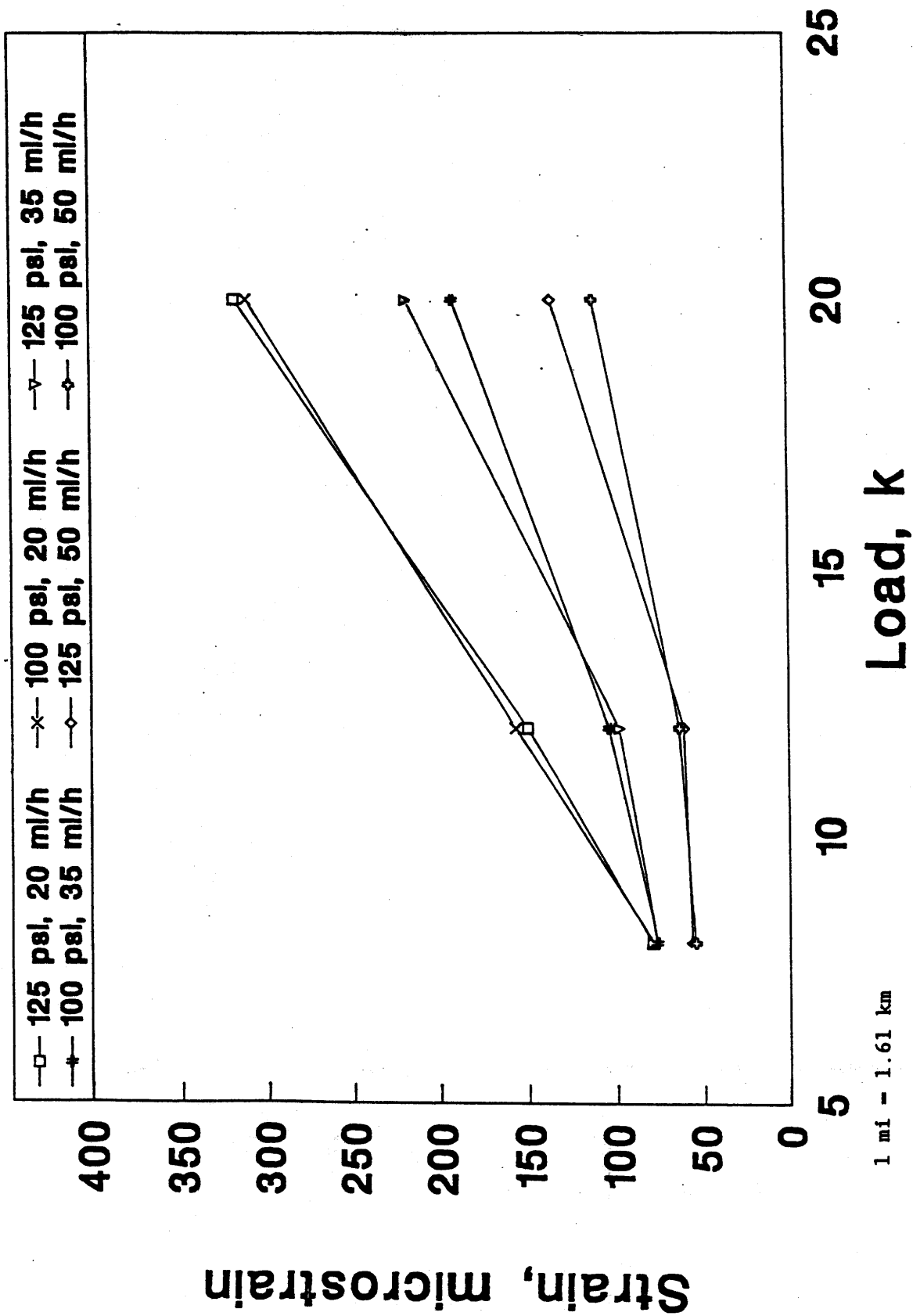
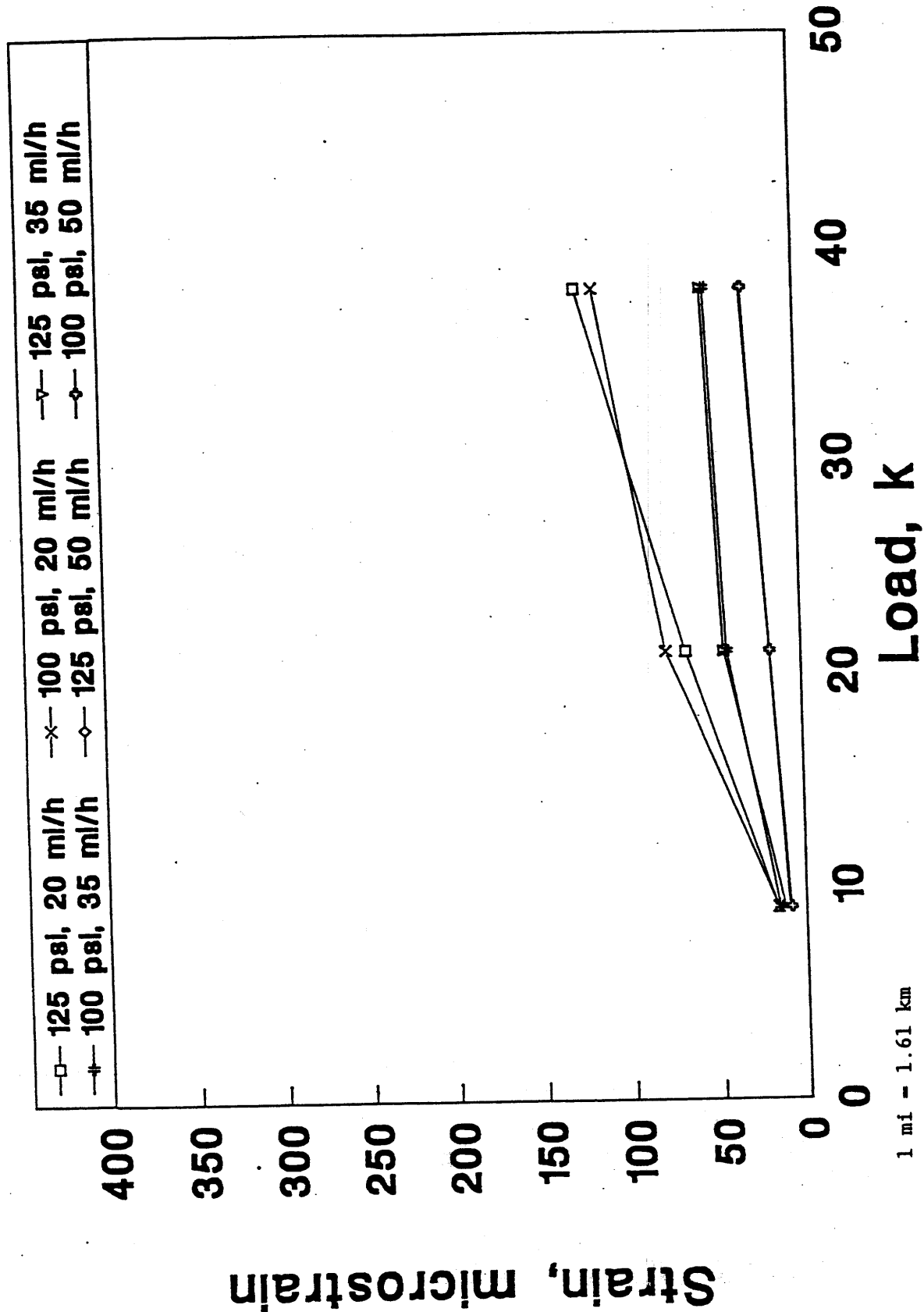


Figure 9. Effects of load, tire pressure, and speed on the response of the Kyowa gauge at station 18 of the thick section, drive single axle.



1 mi - 1.61 km

Figure 10. Effects of load, tire pressure, and speed on the response of the Kyowa gauge at station 10 of the thin section, drive single axle.



1 mi - 1.61 km

Figure 11. Effects of load, tire pressure, and speed on the response of the Kyowa gauge at station 18 of the thick section, trailer tandem axles.

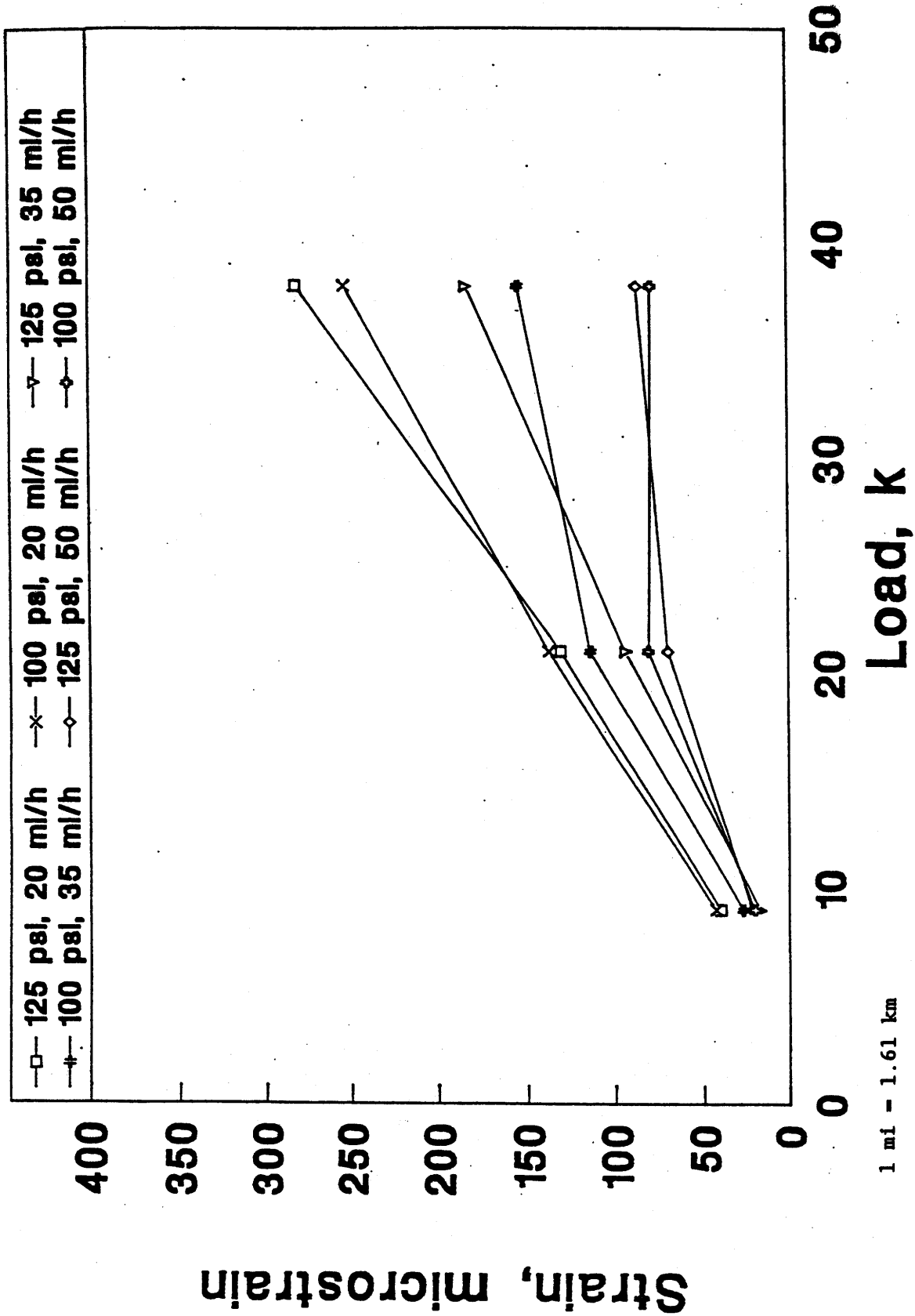


Figure 12. Effects of load, tire pressure, and speed on the response of the Kyowa gauge at station 10 of the thin section, trailer tandem axles.

An attempt was made to correlate the effect of speed with the individual gauge types: if speed has little effect on a certain type of gauge, a stiffer gauge may be indicated. This relationship was not consistent, and even though all gauges showed a reduction of measured strains under the higher speeds, the degree of reduction was not consistent for units of the same gauge type. This inconsistency made it impossible to correlate the speed effect to specific gauge types.

Theoretically, there are two reasons for the reduction in the measured strains as a function of speed: (1) the effect of viscoelasticity of the asphalt concrete layer and (2) the effect of pavement inertia. Due to the viscoelastic nature of the asphalt concrete material, the material will show stiffer behavior under shorter loading times. The shorter loading times occur at higher speeds, which explains the observed large reductions in the strains under higher speeds. The effect of the pavement inertia can be investigated by comparing the effect of speed on the strains from the thin and thick sections. Because the thick section has greater inertia, the effect of speed on the reduction of strains in the thick section should be more pronounced than that of the thin section. Table 11 shows a comparison between the percent reductions in the measured strains as a function of vehicle speed for the thin and thick sections. The data indicate that there is no significant difference between the average percent reductions from the thin and thick sections. Therefore, it can be concluded that effect of the inertia of the pavement is insignificant.

UNCERTAINTY

To study the uncertainty of the measurements from the various types of strain gauges, several factors must be taken into consideration. First, the gauges are installed at different stations along the longitudinal axis of the test section; therefore, the nonuniformity of the pavement material from one station to another must be taken into account. For this purpose, the FWD testing was conducted at 2-ft (.6-m) intervals and the layer moduli were backcalculated at each test point. Second, the layer thicknesses vary along the length of the test section. It is expected that the variation in the

Table 11. Percent reductions in the measured strains (with respect to strain measured at 20 mi/h [32 km/h]) as a function of vehicle speed.

Section	Axle Type	Speed (mi/h)	Gauge Type				Average
			Dynatest	Kyowa	ARC	Core	
Thin	Single	35	44	30	36	45	39
		50	54	48	41	53	49
	Tandem	35	38	32	35	42	37
		50	68	60	52	72	63
Thick	Single	35	35	35	34	43	37
		50	58	58	58	43	54
	Tandem	35	42	36	40	51	42
		50	63	62	67	58	63

1 mi - 1.61 km

thickness of the asphalt concrete layer is the major factor affecting the measured strains at the bottom of the asphalt concrete layer. It was shown in chapter 2 that the variation in the thickness of the asphalt concrete layer was controlled to ± 0.5 in (± 13 mm). Third, the dynamic load profile of the truck axles varies along the length of the section. The factors that affect the dynamic load profile include: roughness of the pavement surface, load level, truck suspension type, axle configuration, and truck speed.

One way of checking the uncertainty of measured strains is to compare them to theoretical strains. The solution of an elastic multilayer pavement model can be used to predict the theoretical strains. The variations in the previously mentioned factors may be considered as follows:

1. Nonuniformity of pavement material. The nonuniformity in the pavement material properties can be handled using the FWD backcalculated moduli at the corresponding stations where the strain gauges are installed. The effect of pavement temperature can be accounted for by adjusting the moduli of the asphalt concrete layer

to the average pavement temperature at the time of testing. The temperature adjustment procedure recommended in the AASHTO *Design Guide* was used.^[1]

2. Layer thickness variability. The variability in the thickness of the asphalt concrete layer can be handled by assuming that the thickness of the asphalt concrete layer at any point may vary from the design thickness by ± 0.5 in (± 13 mm). This variation will lead to the evaluation of a range of theoretical strains for each station. The mean value of the measured strains and the mean ± 1 standard deviation can then be compared to the range of the theoretical strains.
3. Dynamic load profile. Pavement response is affected not only by the static (or very low frequency) wheel load but also by a dynamic component of the load. That dynamic load component, commonly represented by a dynamic load coefficient (DLC), is induced by an interaction of pavement roughness and vehicle dynamics, mainly tire and suspension characteristics. The pavement profile for the entire length of the test track, including the test sections, was measured and is shown in figure 13. The International Roughness Index (IRI) for this profile was calculated to be 5 m/km (317 IPM). This level of roughness may cause significant variation in the measured strain. However, to estimate the magnitude of the strain variation, the parameters of the truck dynamics would have to be determined, in addition to the pavement profile data. Therefore, even though the effect of pavement roughness on measured strain was expected to be significant, it could not be estimated quantitatively within the scope of this study.

Using the first two factors, researchers determined the range of the theoretical strains from the elastic multilayer solution and compared them to the measured strains at 20 mi/h (32 km/h) as shown in figures 14 through 17. The layer moduli used in the theoretical analysis were backcalculated from the FWD deflection data. The data in these figures show that the measured strains are in the range of the calculated strains except for the ARC gauge, which is always measuring higher strains than the calculated values. It is important to recognize that the layer moduli used in this analysis were evaluated independent of the measured strains and adjusted based on the measured temperature throughout the asphalt concrete layer. The variation in the calculated envelope represents the variation of the material properties from one point of the test section to another. The fact that the measured strains are higher than calculated values for some stations and lower than the calculated values at other stations further emphasizes the effect of the dynamic load profile. Overall, the uncertainty of the strain gauges is very

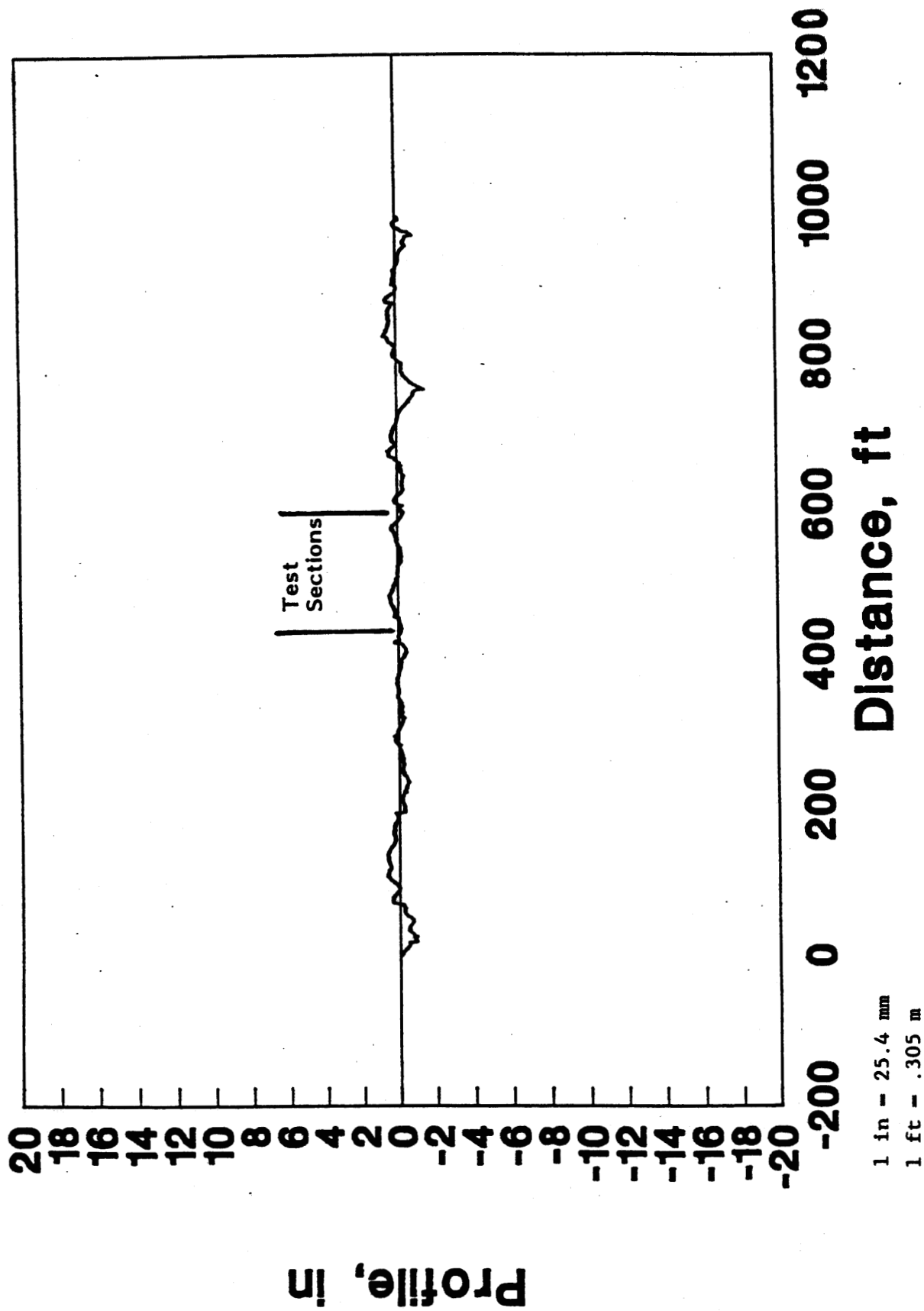


Figure 13. Profile of the test track.

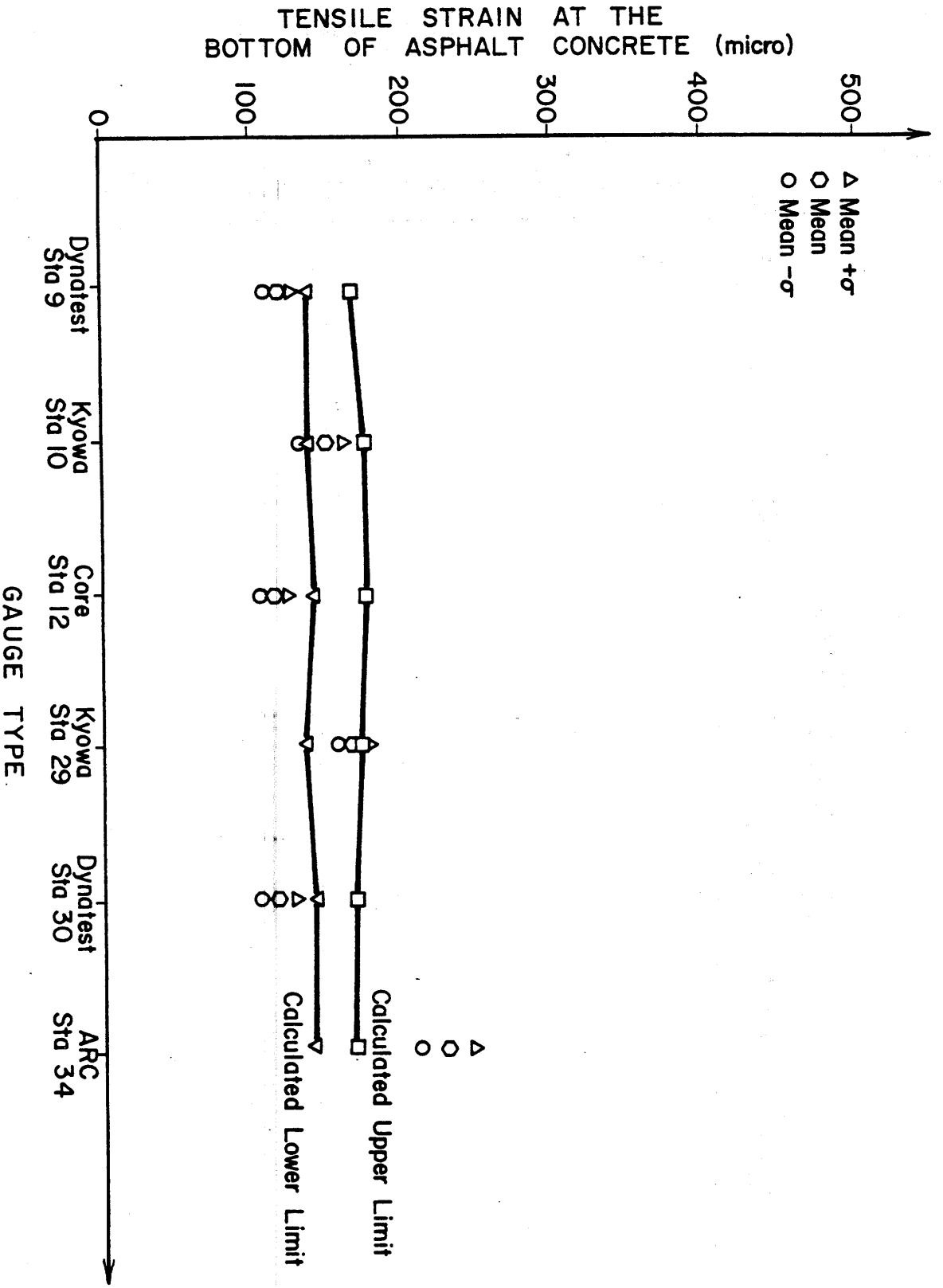


Figure 14. Comparison of measured and calculated strains under a drive single axle load of 20,000 lb (9 080 kg) for the thin section.

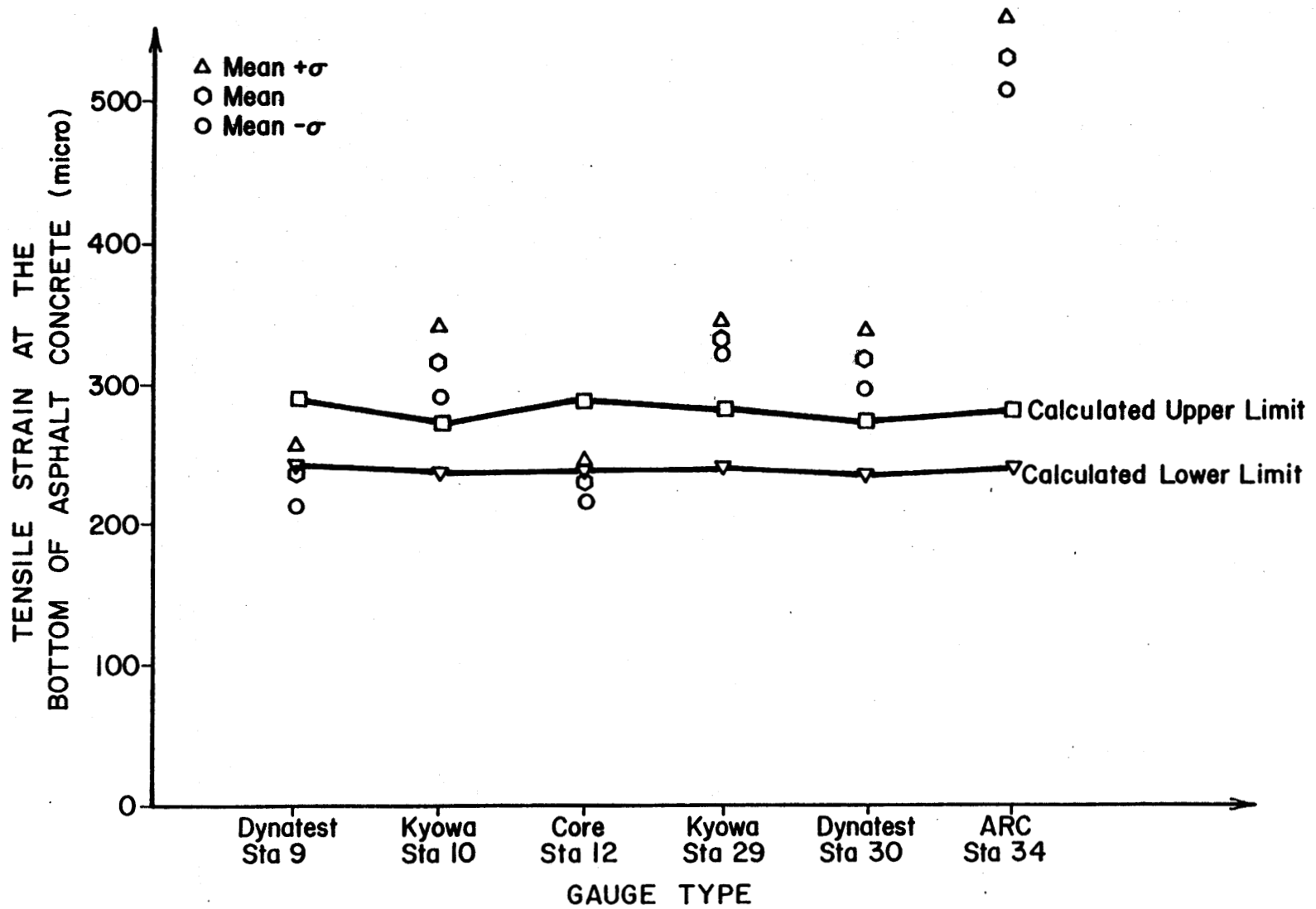


Figure 15. Comparison of measured and calculated strains under a drive single axle load of 12,000 lb (5 448 kg) for the thin section.

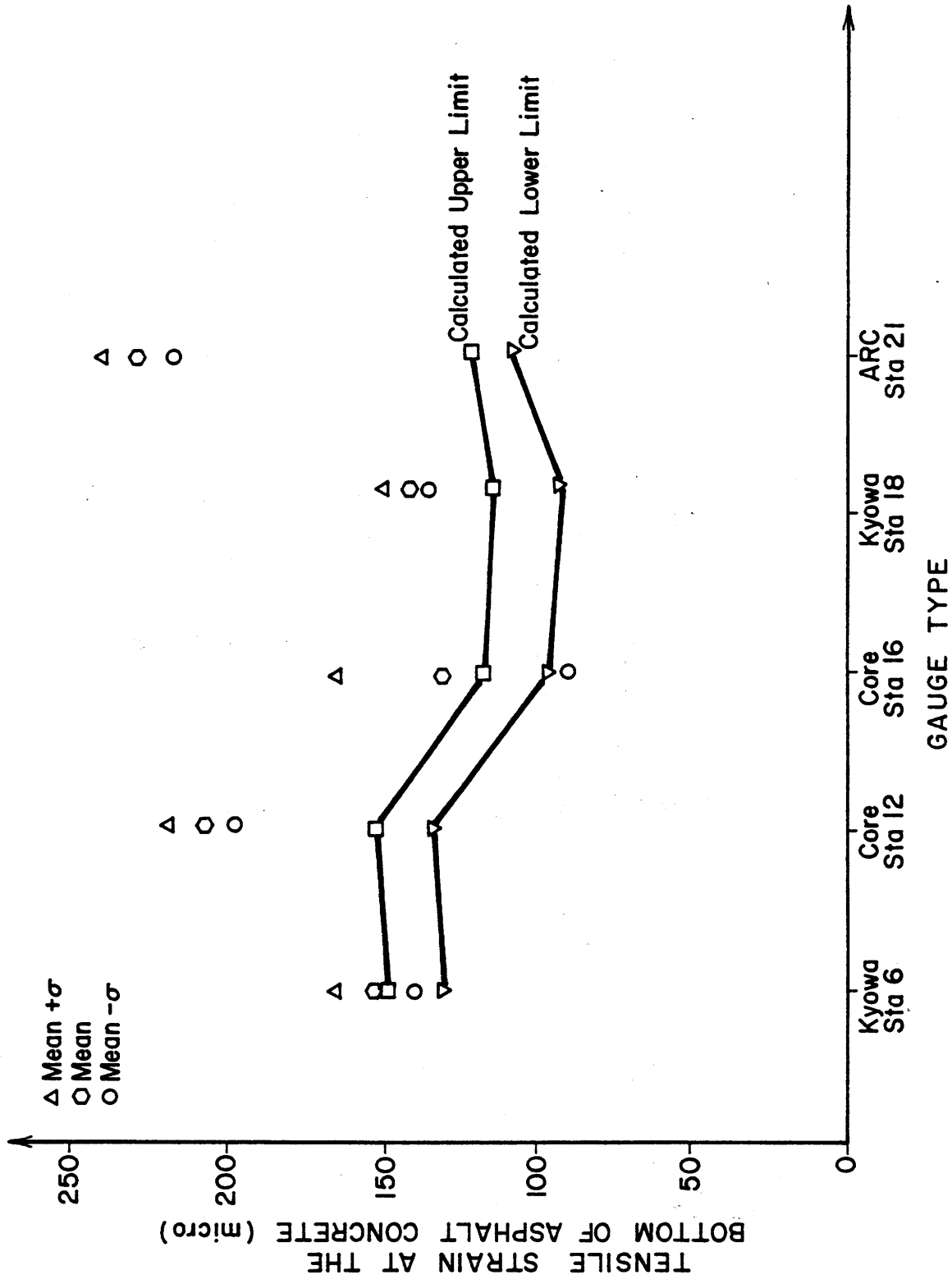


Figure 16. Comparison of measured and calculated strains under a drive single axle load of 20,000 lb (9 080 kg) for the thick section.

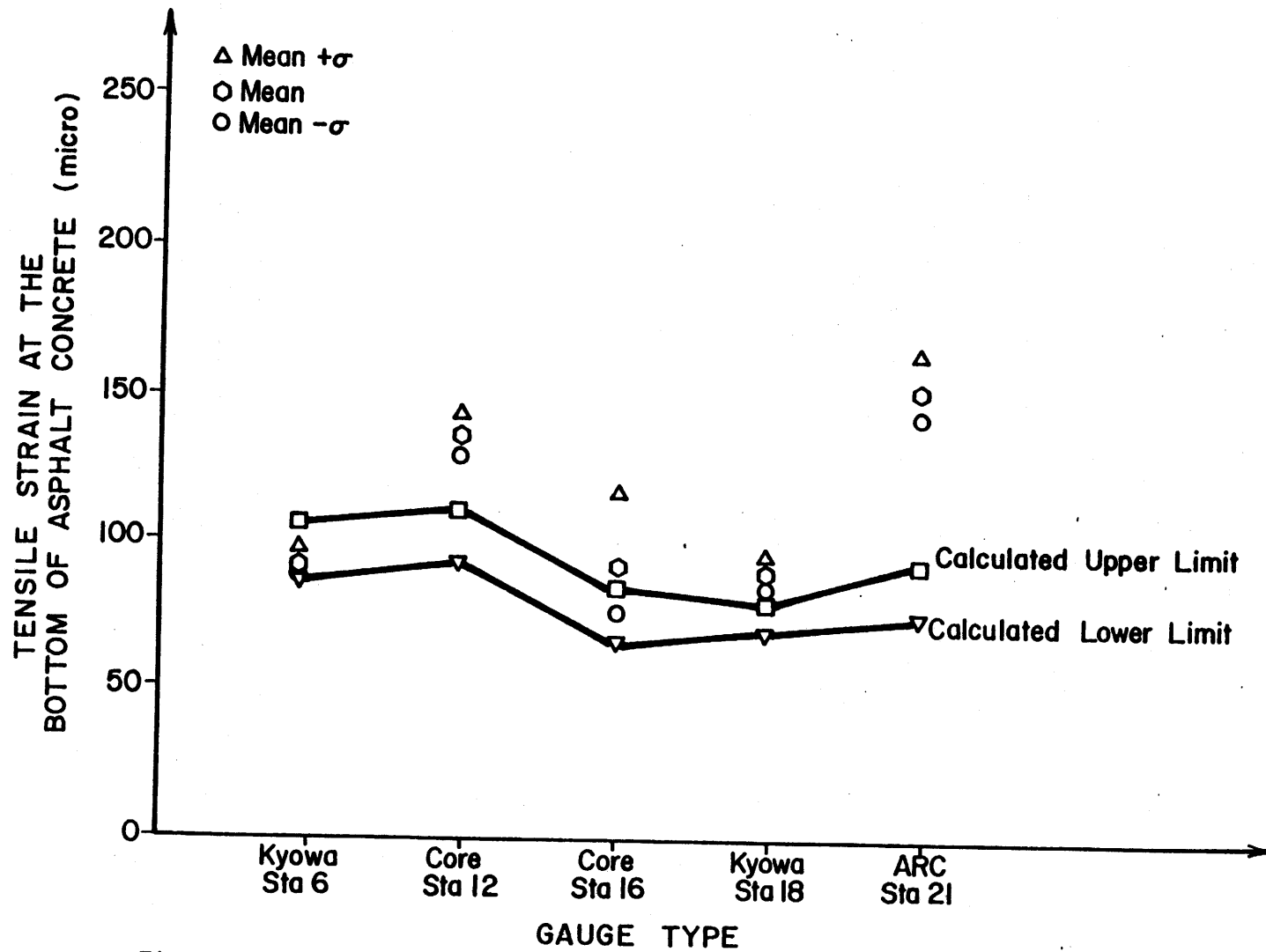


Figure 17. Comparison of measured and calculated strains under a drive single axle load of 12,000 lb (5 448 kg) for the thick section.

small except for the ARC gauge, which measured higher strains for both sections and under different load levels.

REGRESSION ANALYSIS OF STRAIN MEASUREMENTS

Because all strain gauges were installed at the same level and in the same direction at the bottom of the asphalt concrete layer, the relationship between the measurements from the individual gauges and the average measurements of the entire groups of gauges was investigated. Various linear regression analyses were conducted, in which the response of the individual gauges was considered as the dependent variable, and the overall mean of all types of gauges was considered as the independent variable. Throughout the entire testing program, the ARC gauges showed extremely high strain measurements compared to the other three groups of gauges. This trend was present in the data collected from both the thin and the thick sections. Therefore, the ARC gauge measurements were dropped from the regression analysis. The mathematical expression for the linear regression model is:

$$y = a + bx + \epsilon \quad (2)$$

where

- y - dependent variable
- a - intercept
- b - slope
- x - independent variable
- ϵ - error

To evaluate the performance of the individual gauges compared to the entire group of gauges, the intercept (a), the slope (b), the coefficient of correlation, and the standard error of parameter estimates should be examined. A good regression model has a low intercept, a slope close to unity, a high coefficient of correlation, and a low standard error of estimates.

The overall regression analysis included the development of the linear models for each combination of test variables, for stage I and II, and for

both test sections.^[3] Table 12 shows the summary of the statistical analysis for the various types of gauges. Figures 18, 19, and 20 show the actual data for the Dynatest, Kyowa, and core gauges, respectively.

The data show that the intercepts of the regression models are very small, especially for the Dynatest and Kyowa gauges, and the slopes are very close to unity. Considering the Dynatest gauges, it is clear that an intercept of -5.58 microstrains, a slope of 1.017, an R-squared value of 98.7 percent, and an error of estimates of 13.32 microstrains indicate a very good fit between this type of gauge and the overall mean of all gauges. The Kyowa gauges also indicated very good correlation with an intercept of -3.18 microstrains, a slope of 1.108, an R-squared value of 97.94 percent, and an error of estimates of 17.33 microstrains. Even though the standard errors of estimates are larger than the minimum measured strains, this should not be considered a bad performance because in actual field measurements, these low strain values would not be of any interest. Therefore, if the specific gauge did not accurately measure the extremely low strains, this would not be of serious concern to the pavement engineers.

The comparison of the performances of the Dynatest and Kyowa gauges is a very interesting step at this stage because the two gauges are identical in design concept and physical structure (both are H-gauges), but the Kyowa gauges are about 10 times less expensive than the Dynatest gauges. Based on the regression analyses, the performance of the Kyowa gauges is as good as that of the Dynatest gauges in all aspects (i.e., low intercepts, good slopes, high R-squared values, and low standard error of estimates) and under all combinations of loading conditions.

The core gauges performed somewhat inconsistently. The slopes of the regression lines were lower than the slopes of the two other types of gauges. Based on the combined data from all tests, the core gauges have the highest intercepts and standard error of estimates, the lowest R-squared value (93.15), and the lowest slope (.768). Apparent poor performance of the core gauges, compared to the other gauges, can be explained by the major differences in the strain-measuring concepts and the installation procedures. The core gauges consist of strain gauges glued to the bottom of extracted

Table 12. Statistical summary of the regression analysis for the thin and thick section, drive and trailer axles, stages I and II, phase I.

Independent Variable: Average value of all the gauges.

Dependent Variable	Intercept a	Slope b	Sample Size	R-squared %	Std. Error of Est.	Mean	Minimum	Maximum
Dynatest	-5.58	1.017	399	98.70	13.32	139.2	2	622
Kyowa	-3.18	1.108	480	97.94	17.33	141.3	5	632
Core	12.59	.768	478	93.15	22.31	112.2	11	462

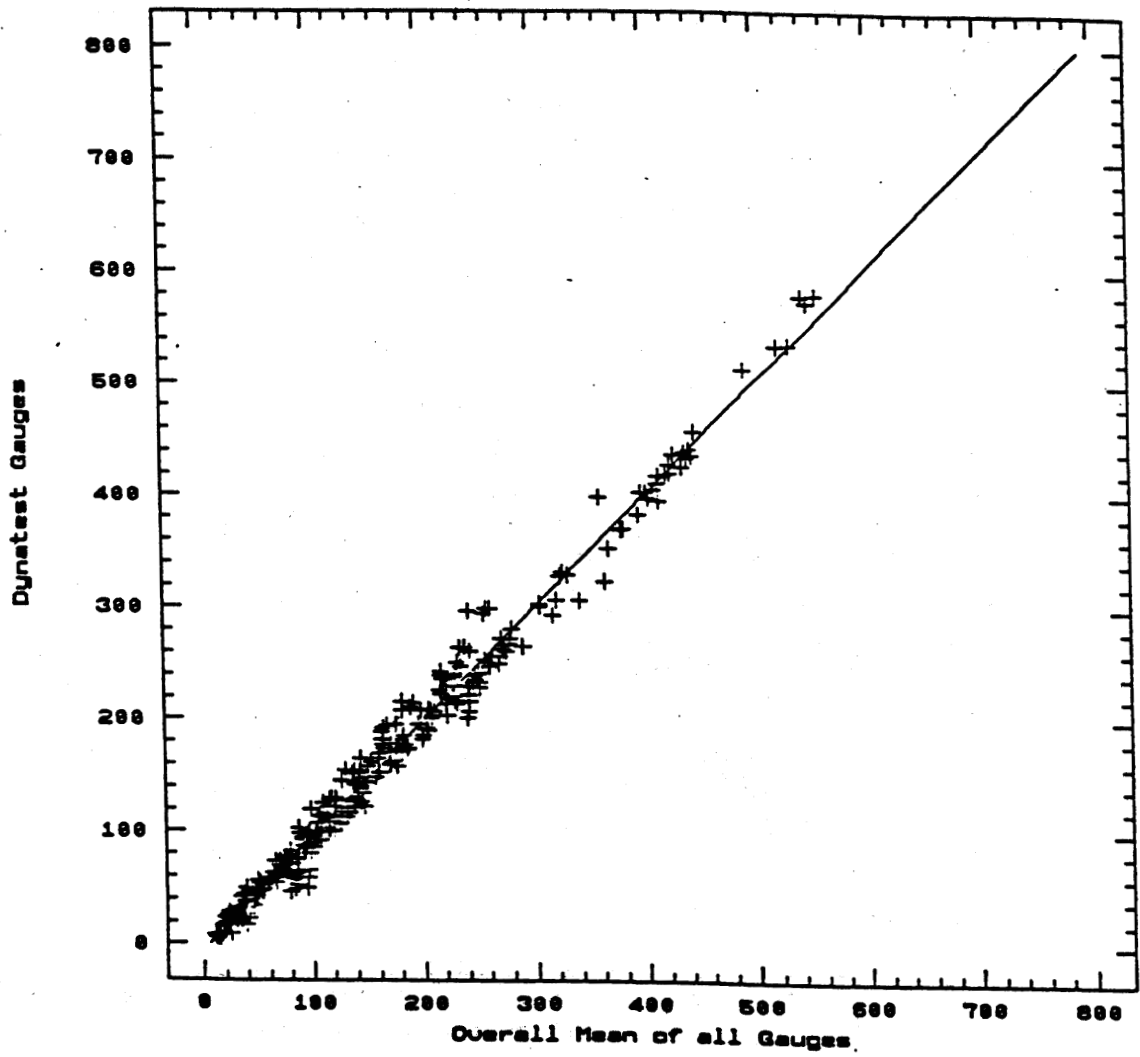


Figure 18. Correlation between Dynatest gauges and overall mean of all gauges--phase I.

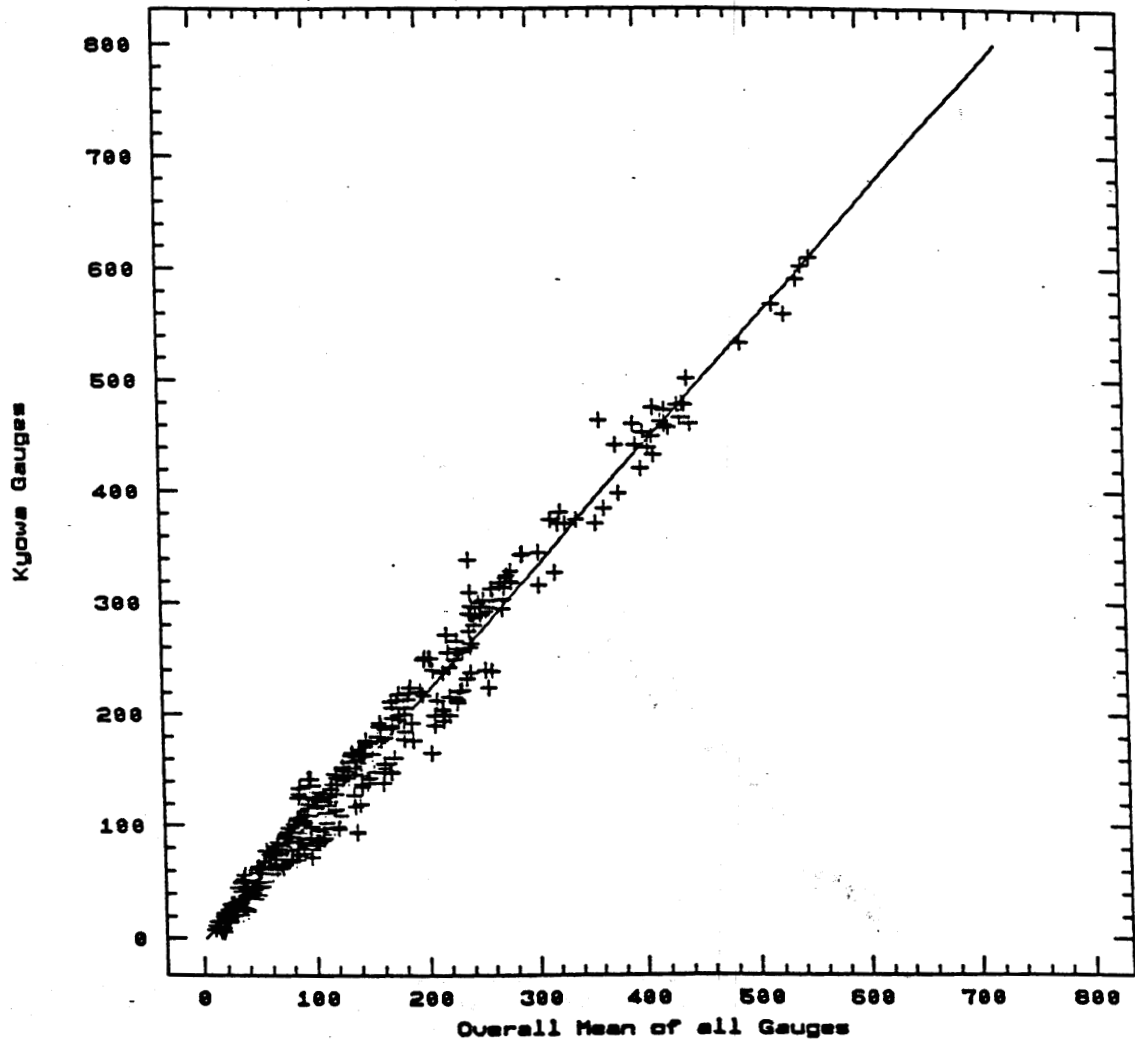


Figure 19. Correlation between Kyowa gauges and overall mean of all gauges--phase I.

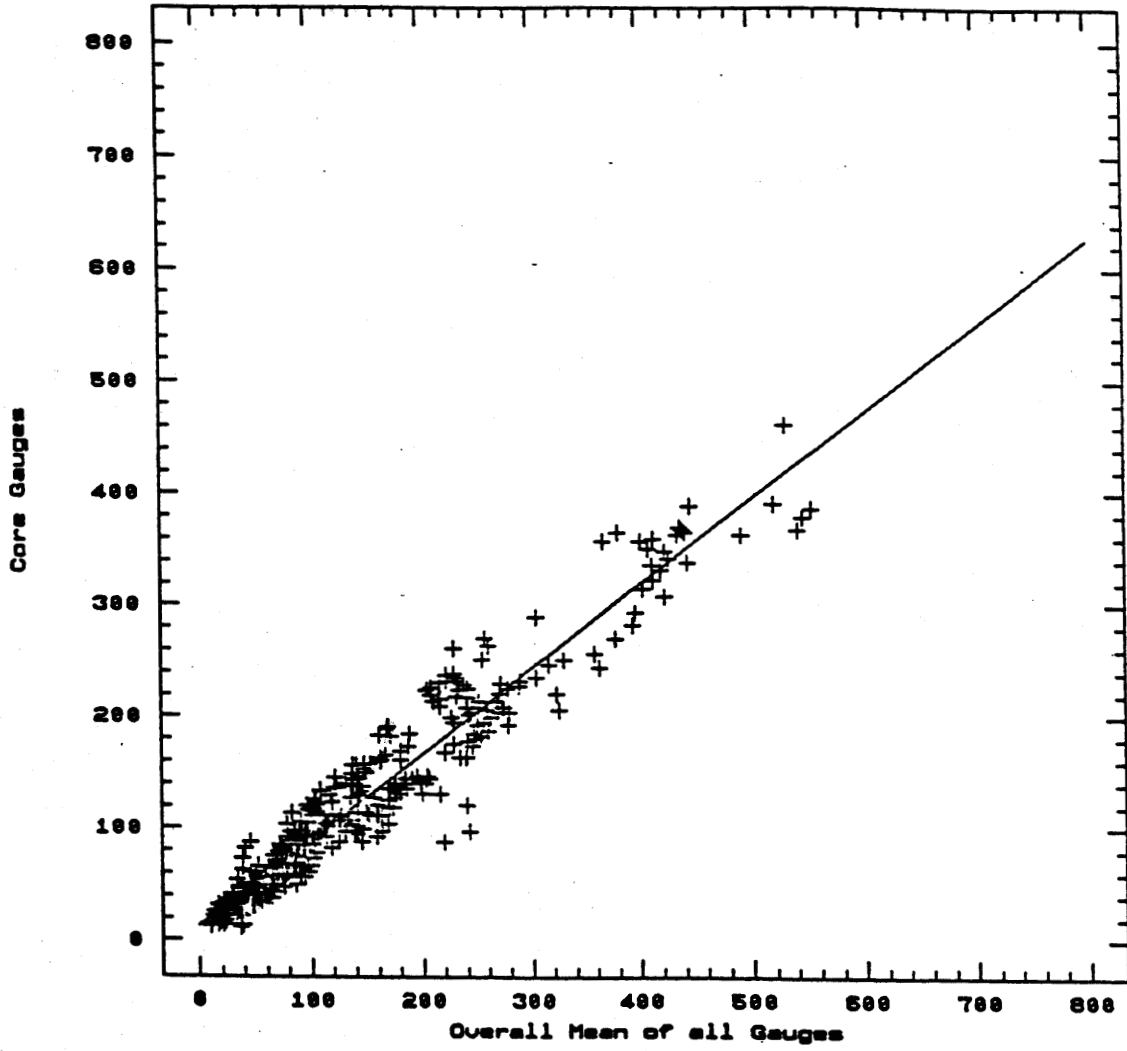


Figure 20. Correlation between core gauges and overall mean of all gauges--phase I.

cores using a certain type of epoxy, and the instrumented core is glued into the test section. One unique feature of the core gauges is that they can be retrofitted into new and old pavement sections, while the H-gauges must be installed during construction of new sections. The use of epoxy to glue the gauges to the cores may have been the major contributor to the different performance of the core gauges when compared with the other gauges. Another major contributor to the difference in the performance of the core gauges is the fact that the retrofitted core is not an integral part of the pavement. However, it is expected that if an appropriate calibration procedure can be developed to take into consideration the effect of the epoxy on the response of the core gauges, then the performance of the core gauges will be greatly improved. Therefore, the relatively poor performance of the core gauges compared to the other two types of H-gauges should not jeopardize their potential usefulness, but a better calibration procedure should be investigated.

STRAIN MEASUREMENT IN THE SUBGRADE LAYER

Two soil strain gauges were installed in each of the test sections. Both gauges are of the LVDT type, designed and manufactured by TRRL of England.^[4] Researchers intended to use the soil strain data to evaluate the in situ shear modulus of the subgrade material. Therefore, the gauges were installed in the longitudinal direction at depths of 2.5 and 6.5 in (64 and 165 mm) below the top of the subgrade in the outer wheel track of both sections.

The data from the soil strain gauges were collected along with the data from other gauges using the same data acquisition software. The measurements were converted into engineering units using the appropriate calibration factor and then divided by the total gauge length to obtain the strain value. The LVDT's used in the gauges have a maximum range of $\pm .12$ in (± 3 mm) and a total gauge length of 3.2 in (81 mm).

SURVIVABILITY

A special tool was designed to act as a spacer to hold the LVDT at or around its zero position during installation. Special care was taken during compaction of the surrounding soil to ensure that the LVDT stayed very close to its zero position. All four gauges were installed during an intermediate stage of the construction, after the base course was in place and before the placement of the asphalt concrete layer. All four gauges survived the installation activities. The gauge placed 2.5 in (64 mm) below the top of the subgrade of the thin section was unoperational after the placement and compaction of the asphalt concrete layer and after testing. Therefore, a 75-percent survival rate was attained with this type of soil strain gauge. This level of survivability is considered very good for this kind of application.

REPEATABILITY

Four replicate measurements were obtained for each combination of the test variables. Because these gauges were installed at great depths below the pavement surface (14.5 and 18.5 in [368 and 470 mm] for the thin section and 22.5 and 26.5 in [572 and 671 mm] for the thick section), the measuring signals were very weak and not all combinations of load and speed produced meaningful strain data. For example, the empty load level did not produce any measurable strains at these depths. Also, at 35 and 50 mi/h (56 and 80 km/h), a single peak was distinguished for the entire truck, which indicates that the strains from the steering, drive, and trailer axles at the depths where the gauges are installed overlap each other. On the other hand, at 20 mi/h (32 km/h), each axle group was represented by a distinguishing peak. Also for the intermediate load level, the deeper strain gauge in the thick section did not measure any strains at speeds of 35 and 50 mi/h (56 and 80 km/h).

A majority of the coefficients of variation obtained in the statistical analysis of the soil strain measurements are close to 10 percent, which indicates that the soil strain gauges have good repeatability. Under certain combinations of test variables, the strain level was approximately 6 microstrains and was still measured with good repeatability.

EFFECTS OF TEST VARIABLES ON THE RESPONSE OF SOIL STRAIN GAUGES

It was mentioned earlier that only certain combinations of the test variables produced measurable strains at the location where the soil strain gauges were installed in both the thin and thick sections.

The effects of load level and speed on the measurement of the soil gauge 6.5 in (165 mm) deep (from top of subgrade) in the thin section under the single drive axle are shown in figure 21. The data show that the load level has a significant effect on the values of the measured strains. Also, changing the speed from 20 to 35 mi/h (32 to 56 km/h) significantly affects the strains. Changing the speed from 35 to 50 mi/h (56 to 80 km/h) did not produce any significant change in the strains. The data show that reducing the load by 40 percent causes a 75-percent reduction in the strains. However, keeping the load constant and changing the speed from 20 to 35 mi/h (32 to 56 km/h) will also produce the same magnitude of reduction in the strains. Also note that these measurements have very good repeatability. Figure 22 shows the data from the tandem trailer axle, which are very similar to the data from the single drive axle.

In the case of the thick section, both the 2.5- and 6.5-in (64- and 165-mm) deep soil strain gauges were operational. However, the soil strain gauge 6.5 in (165 mm) deep (from top of subgrade and 26.5 in [673 mm] from pavement surface) did not register any strains under the intermediate load level at speeds of 35 and 50 mi/h (56 and 80 km/h).

Figures 23 and 24 show the strain measurements from the 6.5-in (165-mm) deep strain gauge for the fully loaded conditions as a function of speed for the single drive axle and tandem trailer axles, respectively. The effect of speed is very significant between 20 and 35 mi/h (32 and 56 km/h). This is very consistent with the data obtained from the thin section gauge. On the other hand, figure 25 shows the strain data from the 2.5-in (64-mm) deep strain gauge, which indicate an insignificant effect of speed for all three levels. This is a very interesting observation, but it cannot be verified against the data from the thin section because the 2.5-in (64-mm) deep gauge in the thin section was unoperational. This significant effect of speed on

Strain, microstrain

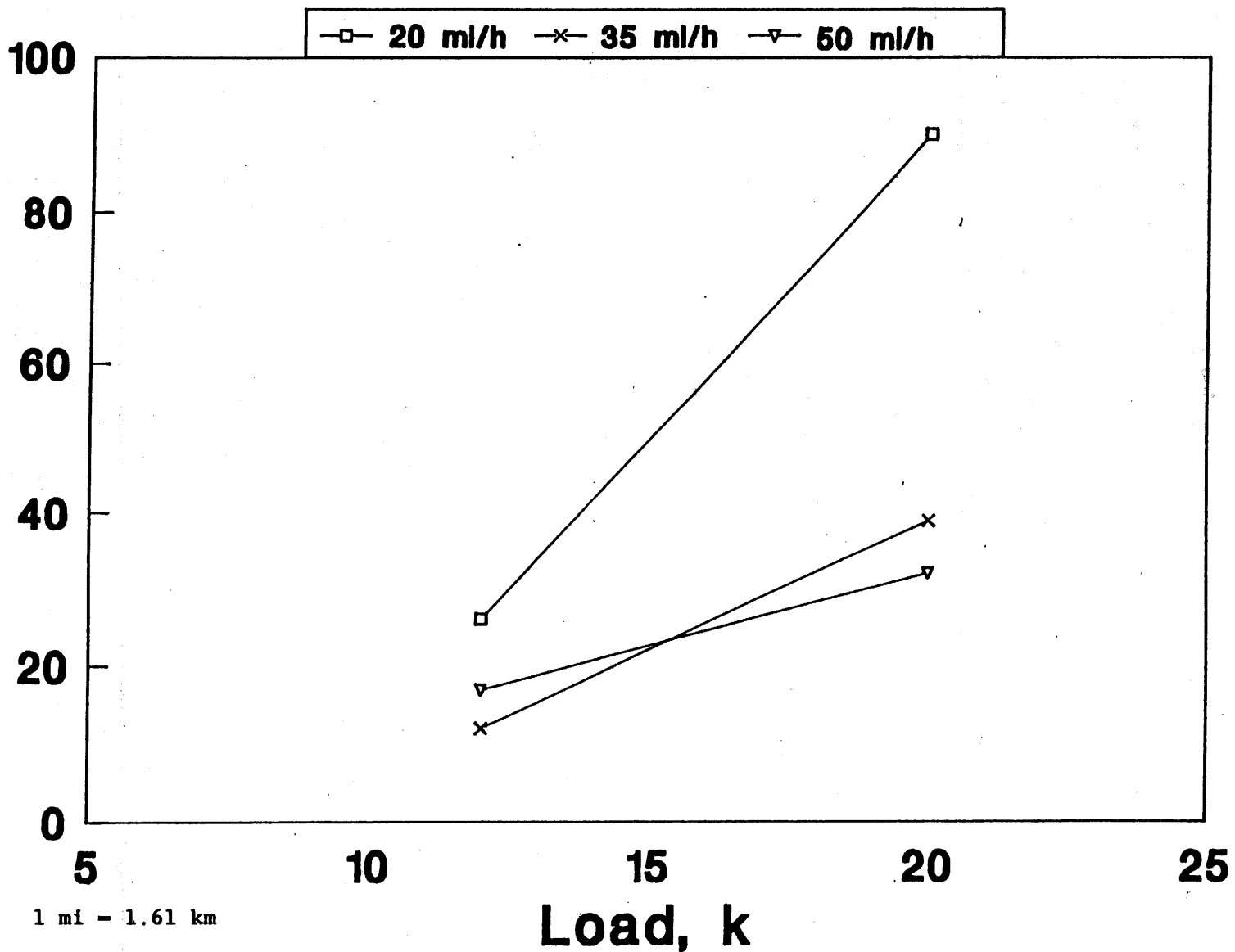


Figure 21. Effect of load and speed on the response of the soil strain gauge at 6.5 in (165 mm) from top of subgrade of the thin section, drive single axle.

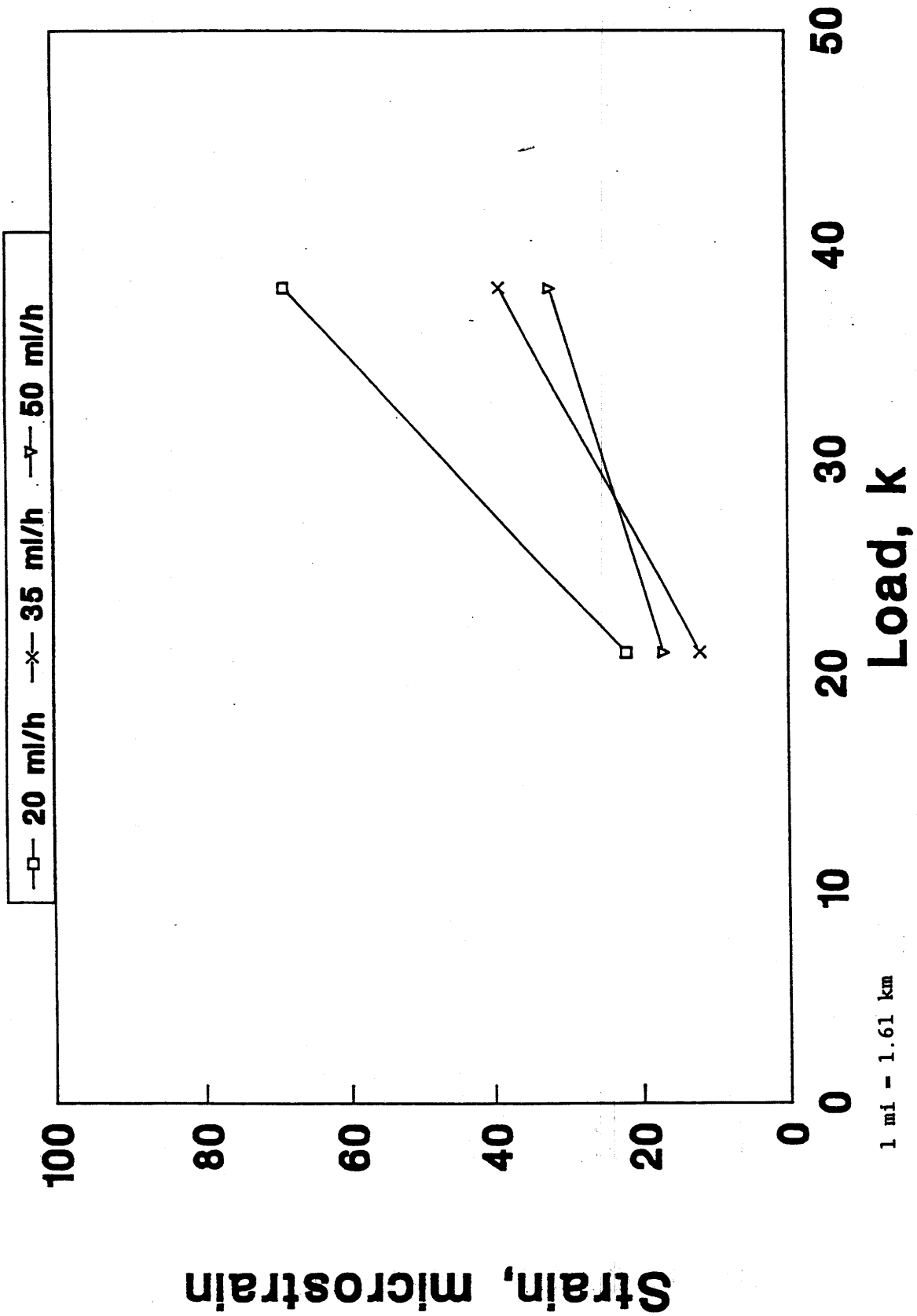


Figure 22. Effect of load and speed on the response of the soil strain gauge at 6.5 in (165 mm) from top of subgrade of the thin section, trailer tandem axles.

Strain, microstrain

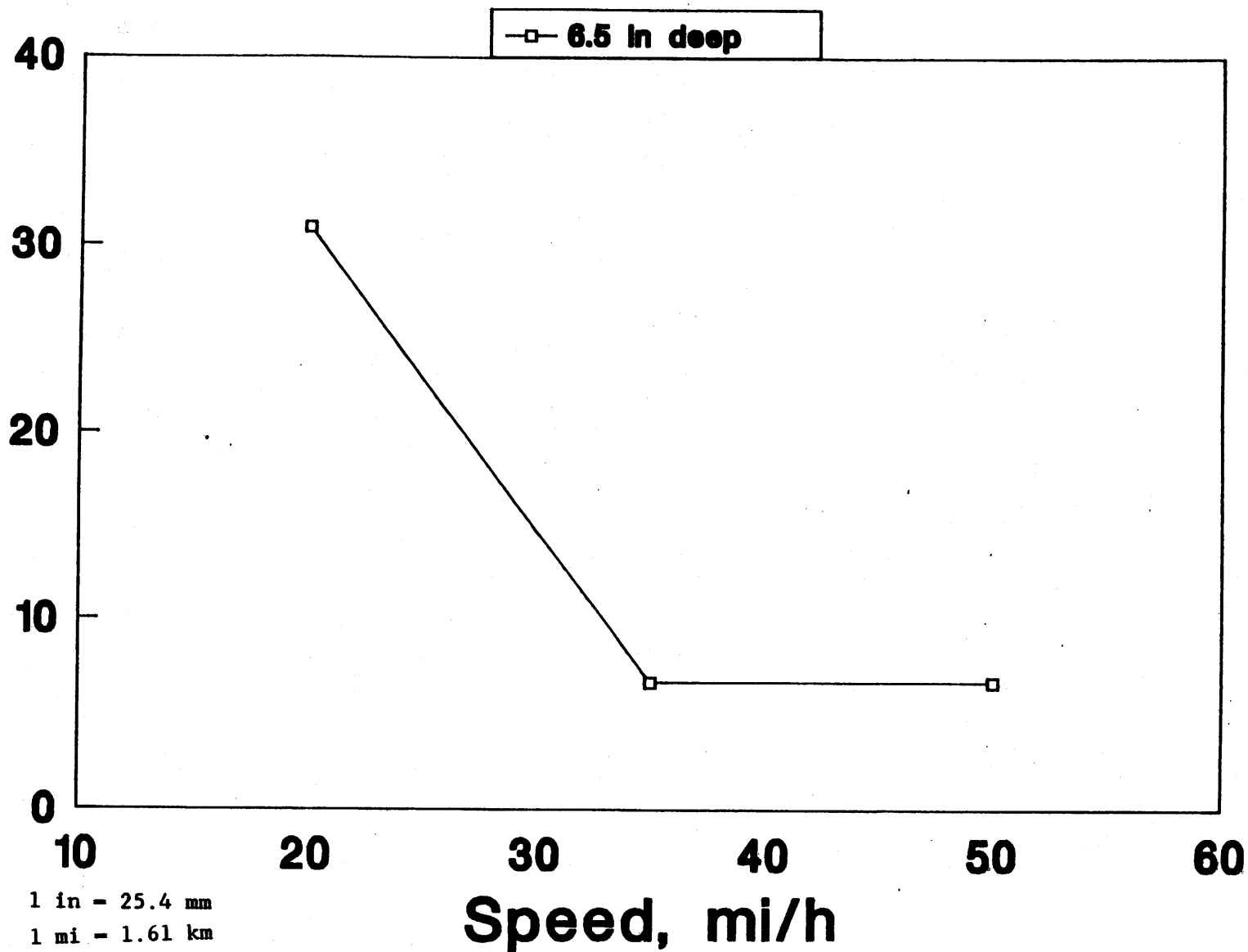


Figure 23. Effect of speed on the response of the soil strain gauge at 6.5 in (165 mm) from top of subgrade of the thick section, drive single axle, fully loaded.

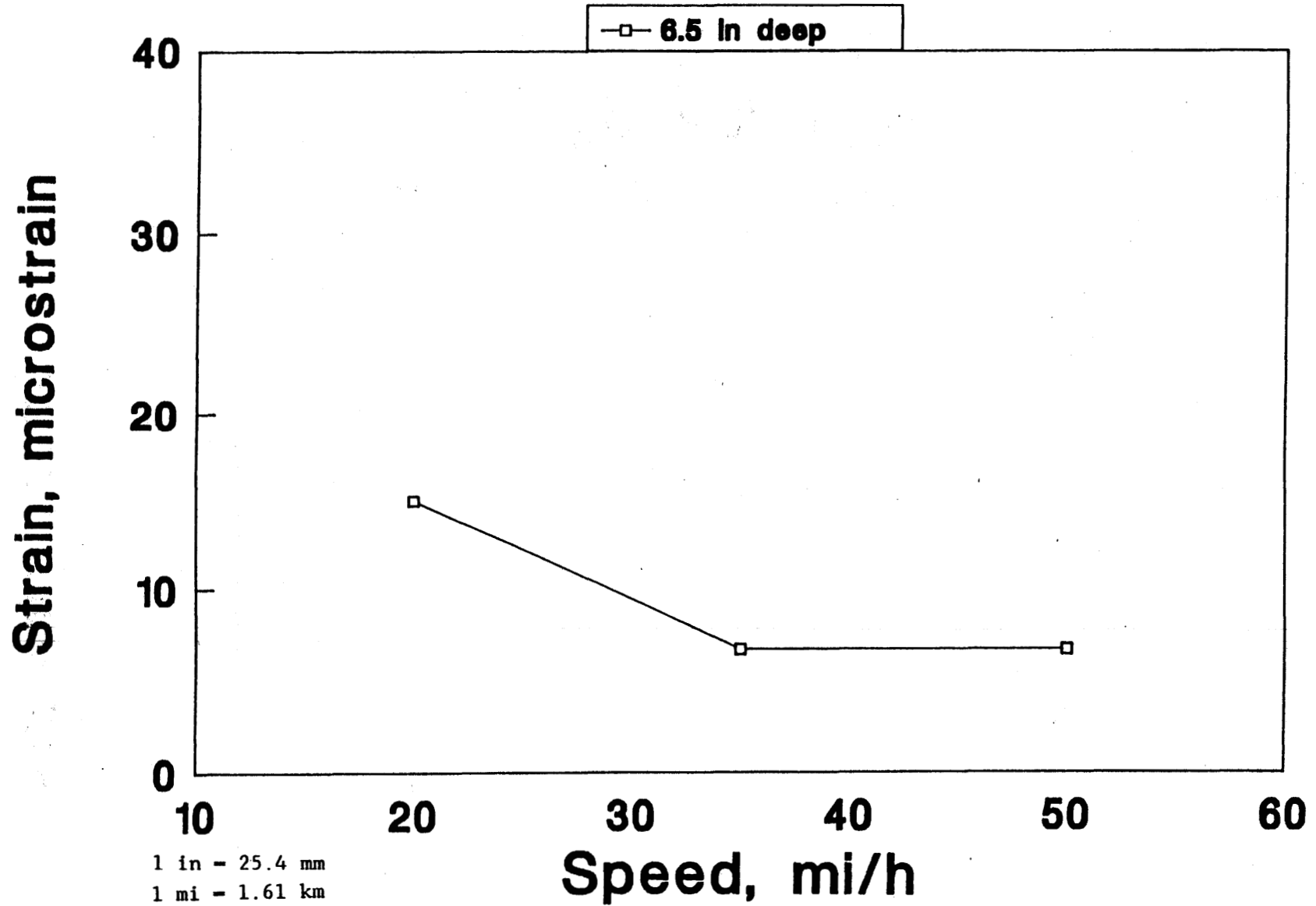
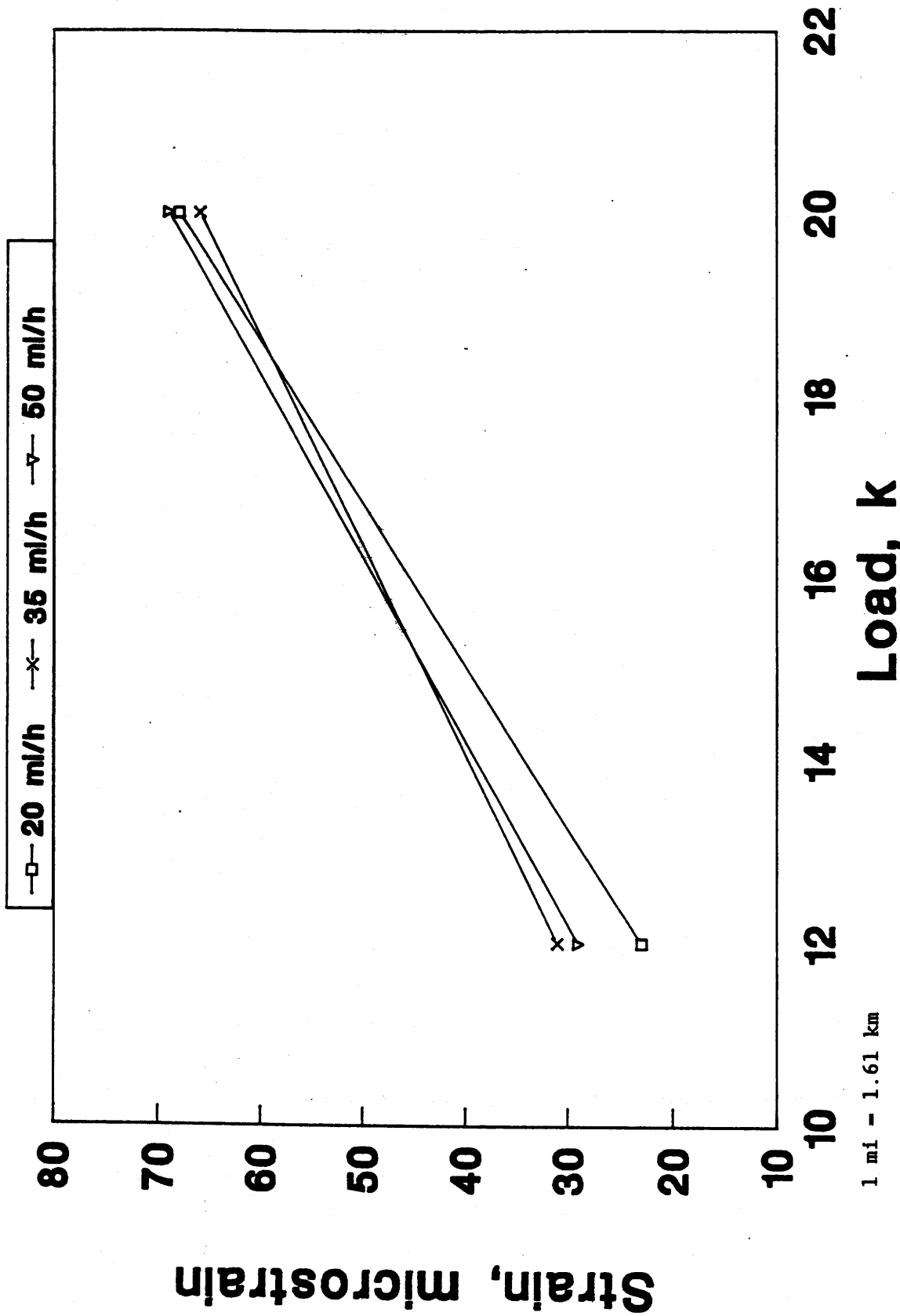


Figure 24. Effect of speed on the response of the soil strain gauge at 6.5 in (165 mm) from top of subgrade of the thick section, trailer tandem axles, fully loaded.



1 mi - 1.61 km

Figure 25. Effects of load and speed on the response of the soil strain gauge at 2.5 in (64 mm) from top of subgrade of the thick section, drive single axle.

the deeper strain gauge and the insignificant speed effect on the shallower strain gauge may be explained by the effect of the pore water pressure in the soil. The effective stress at any point within the soil is defined as the total stress minus the pore water pressure. Therefore, an increase in the pore water pressure would generate a reduction in the effective stress. In pervious soils, the magnitude of the pore water pressure is directly related to the length of drainage path--the longer the drainage path, the larger the pore water pressure would become. At the shallower gauge, the pore water pressure is reduced because it is close to the base-subgrade interface, which reduces the drainage time. Therefore, the water pore pressure does not affect the developed strains. On the other hand, at the deeper gauge, the drainage time is longer because the gauge is further below the base-subgrade interface; therefore, the pore water pressure affects the strains under various speeds.

Basically, the soil strain gauges operated very satisfactorily under the conditions where large enough strains were developed. As expected, the effect of load level was very noticeable in all the responses of the gauges. An interesting observation was made about the effect of speed on the strains at various levels in the subgrade. The measurements of the deep gauges (6.5 in [165 mm] below top of subgrade) were consistent in both sections. The measurements of the shallower gauge in the thick section could not be checked because the corresponding gauge in the thin section was unoperational.

UNCERTAINTY

The uncertainty of the soil strain measurements was investigated by comparing the measured values with the calculated values from the elastic multilayer solution. The range of calculated strains was obtained by allowing ± 0.5 in (± 13 mm) of variation in the asphalt concrete layer thickness. The measured soil strains at the speed of 20 mi/h (32 km/h) and the calculated upper and lower limits are plotted in figures 26 through 28. There are large variations between the measured and calculated values. The maximum variations existed at the deepest strain gauge location in the thick section. This variation was expected because the theory does not represent the actual nonlinear response of the subgrade and the maximum disagreement was expected at the lowest strain values as it appeared in the graphs.

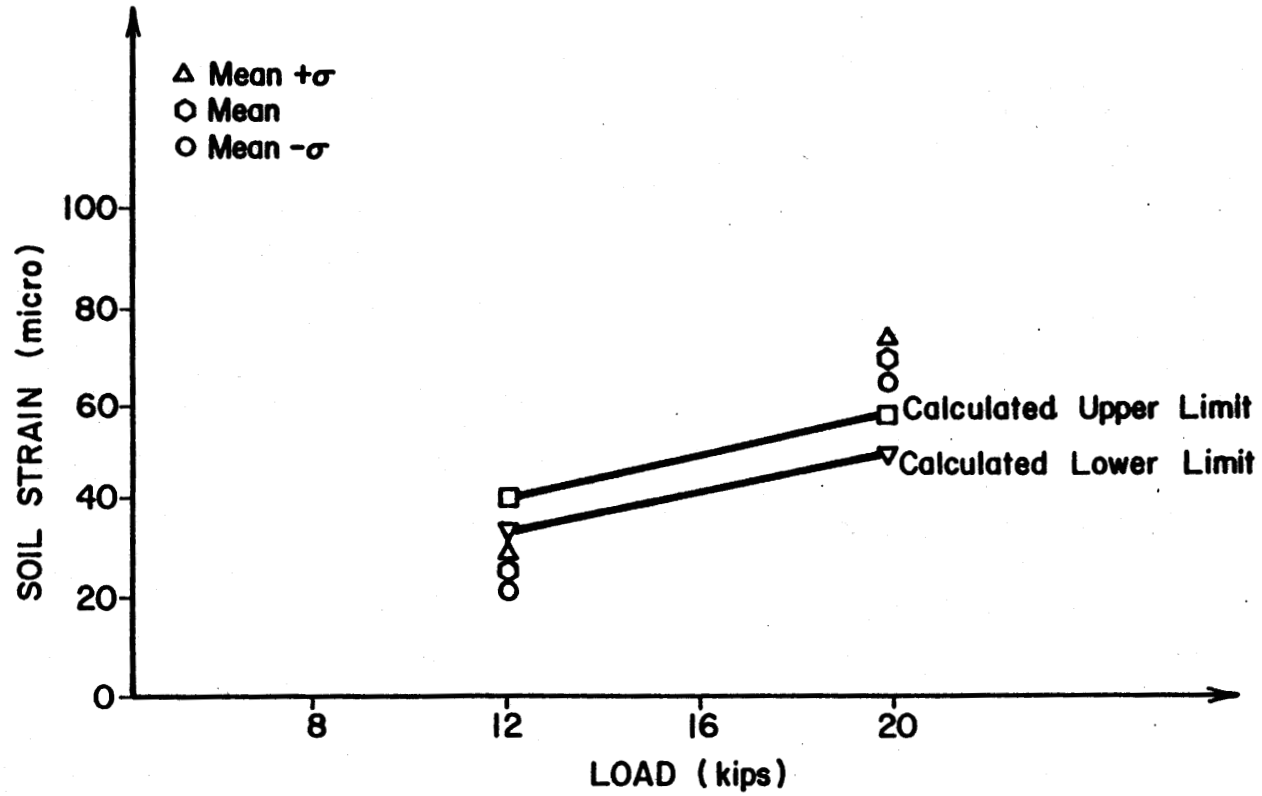


Figure 26. Comparison of the measured and calculated soil strains under the drive single axle of the thick section, 2.5 in (64 mm) from top of subgrade.

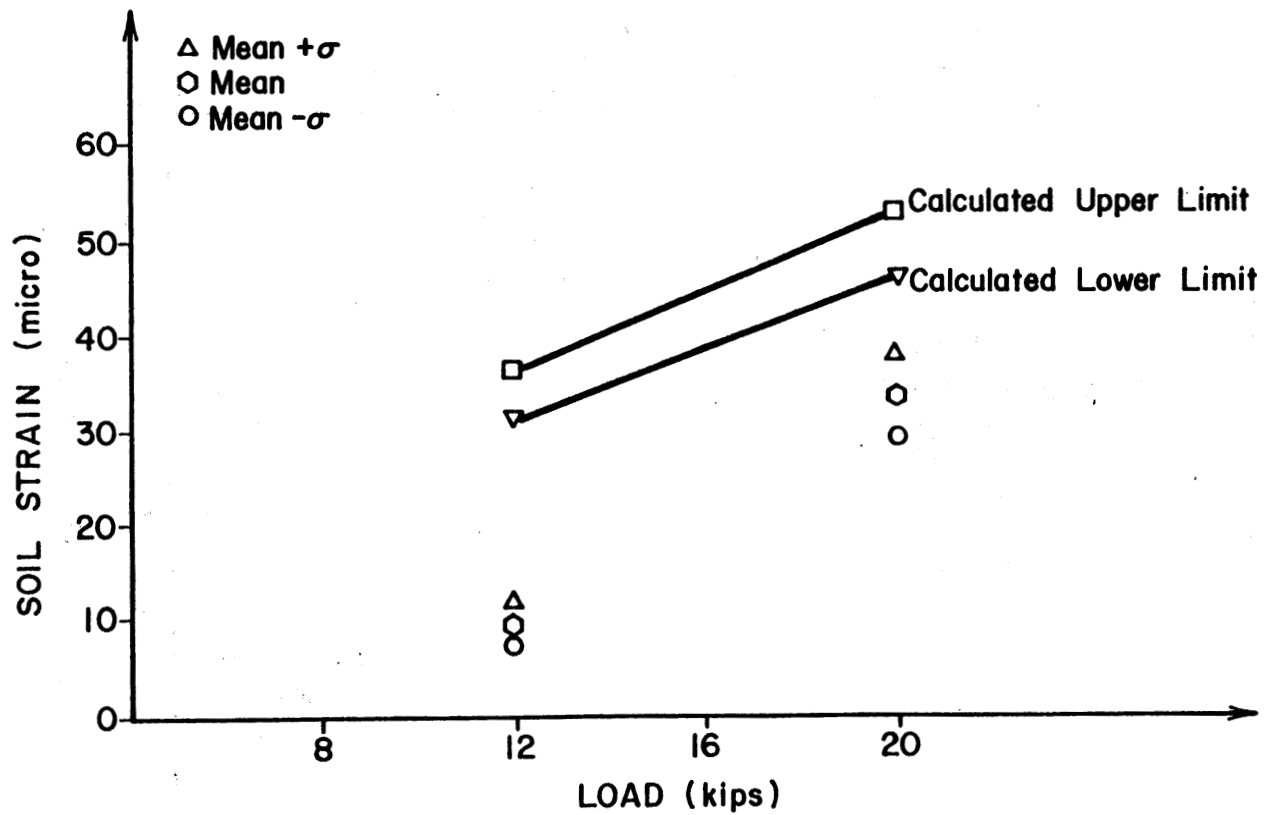


Figure 27. Comparison of the measured and calculated soil strains under the drive single axle of the thick section, 6.5 in (165 mm) from top of subgrade.

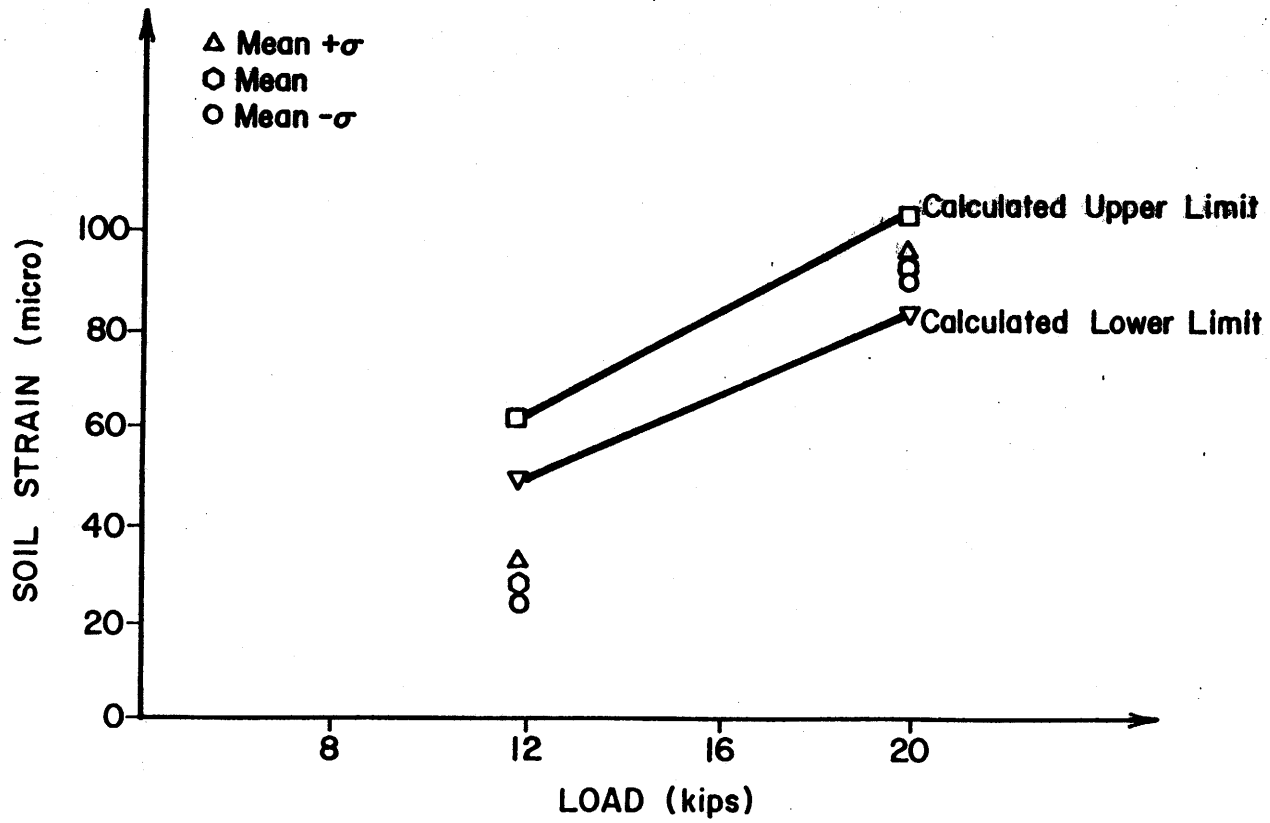


Figure 28. Comparison of the measured and calculated soil strains under the drive single axle of the thin section, 6.5 in (165 mm) from top of subgrade.

COMPRESSIVE STRESS MEASUREMENTS

SURVIVABILITY OF THE PRESSURE CELLS

Two diaphragm-type pressure cells were installed in the thin section as shown in figure 3. Methods of installation as described in chapter 2 were followed. Both cells were installed during construction of the test sections. One of the pressure cells failed during construction, leaving only one operational pressure cell. The cell failed because of an excessive permanent stress at the active face of the cell. This may have been due to the direct contact of a sharp aggregate with the active face of the cell. It also should be noted that, as a rule, this type of pressure cell was always used in fine-grained soils. This was the first application in which these cells were installed in contact with asphalt concrete and crushed aggregate bases. It is possible that the protection of the cells from sharp aggregates by a thin layer of sand was inadequate under dynamic loading conditions. Because only two pressure cells were installed, no firm conclusions can be drawn with respect to their survivability.

REPEATABILITY

The pressure cell measurements were collected along with the other gauge (i.e., strain gauge and deflection gauge) measurements. Four replicates were collected for each combination of the test variables. A typical response from the pressure cell is shown in figure 29. The mean, standard deviation, and coefficient of variation are summarized in table 13. The data show that all coefficients of variations are below 10 percent, which indicates good repeatability of the pressure cell.

EFFECT OF TEST VARIABLES ON THE PRESSURE CELL MEASUREMENTS

The response of the pressure cell under the various combinations of test variables is described in this section. The results of measurements for all combinations of test variables are plotted in figures 30 and 31. The data show that the load level is the most significant factor. The effects of truck

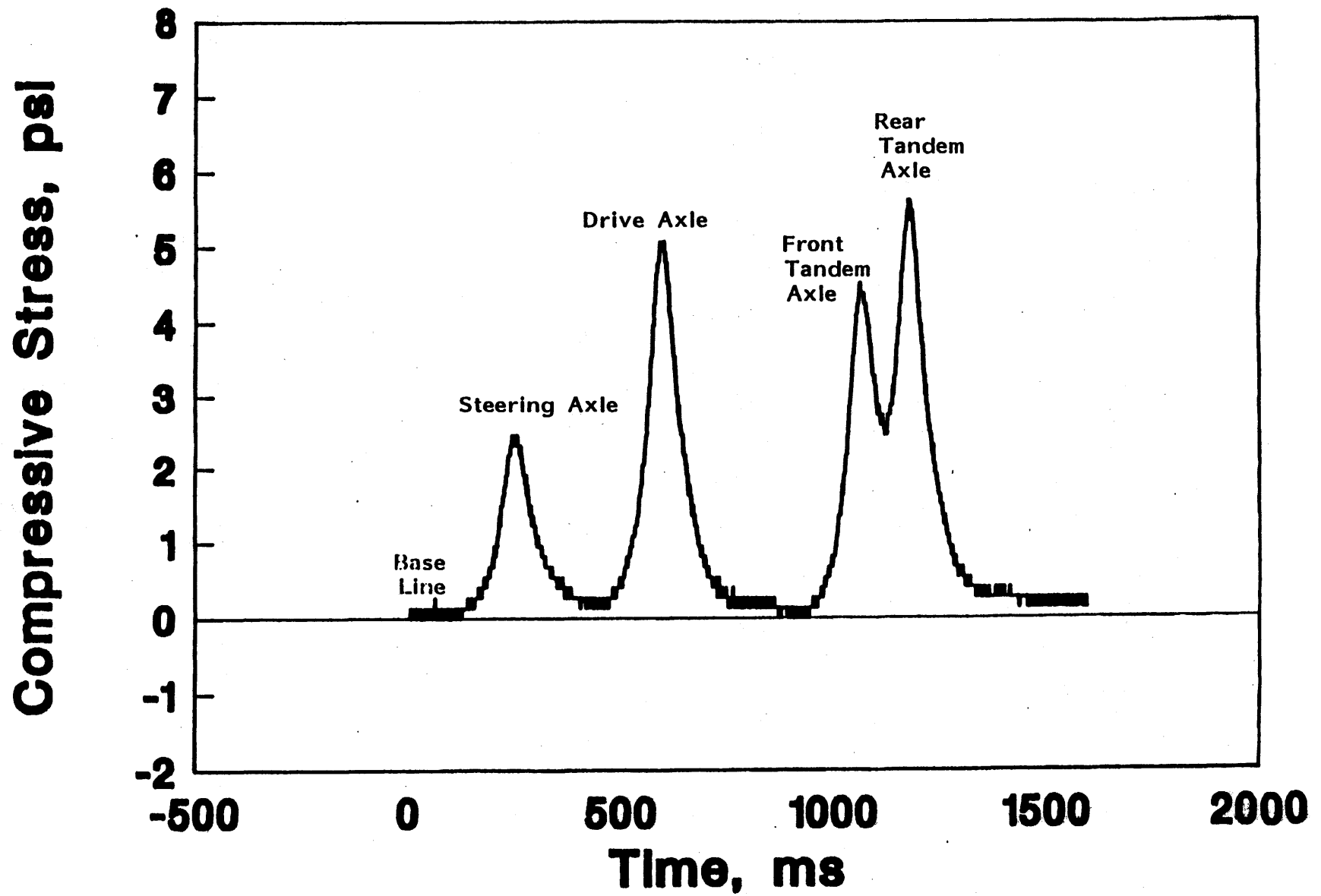


Figure 29. Typical response from the diaphragm pressure cell, thin section.

Table 13. Summary of the means, standard deviations, and coefficients of variation for the Nottingham-type pressure cell.

Axle Type	Axle Load (kips)	Speed (mi/h)	Mean*	Standard Deviation*	Coefficients of Variation (%)
Single Drive Axle	20	20	5.17	0.19	3.68
		35	4.96	0.21	4.23
		50	3.99	0.15	3.76
Tandem Trailer Axle (Rear Axle)	38	20	5.47	0.17	3.11
		35	5.37	0.17	3.17
		50	5.05	0.41	8.12
Single Drive Axle	12	20	2.60	0.15	5.77
		35	2.55	0.10	3.92
		50	2.25	0.07	3.11
Tandem Trailer Axle (Rear Axle)	21	20	3.94	0.22	5.58
		35	3.16	0.06	1.90
		50	3.36	0.16	4.76
Single Drive Axle	8	20	2.15	0.06	2.79
		35	1.40	0.07	5.00
		50	1.54	0.13	8.44
Tandem Trailer Axle (Rear Axle)	9	20	1.09	0.05	4.59
		35	0.94	0.04	4.26
		50	0.84	0.07	8.33

*All units are in psi.
1 mi = 1.61 km

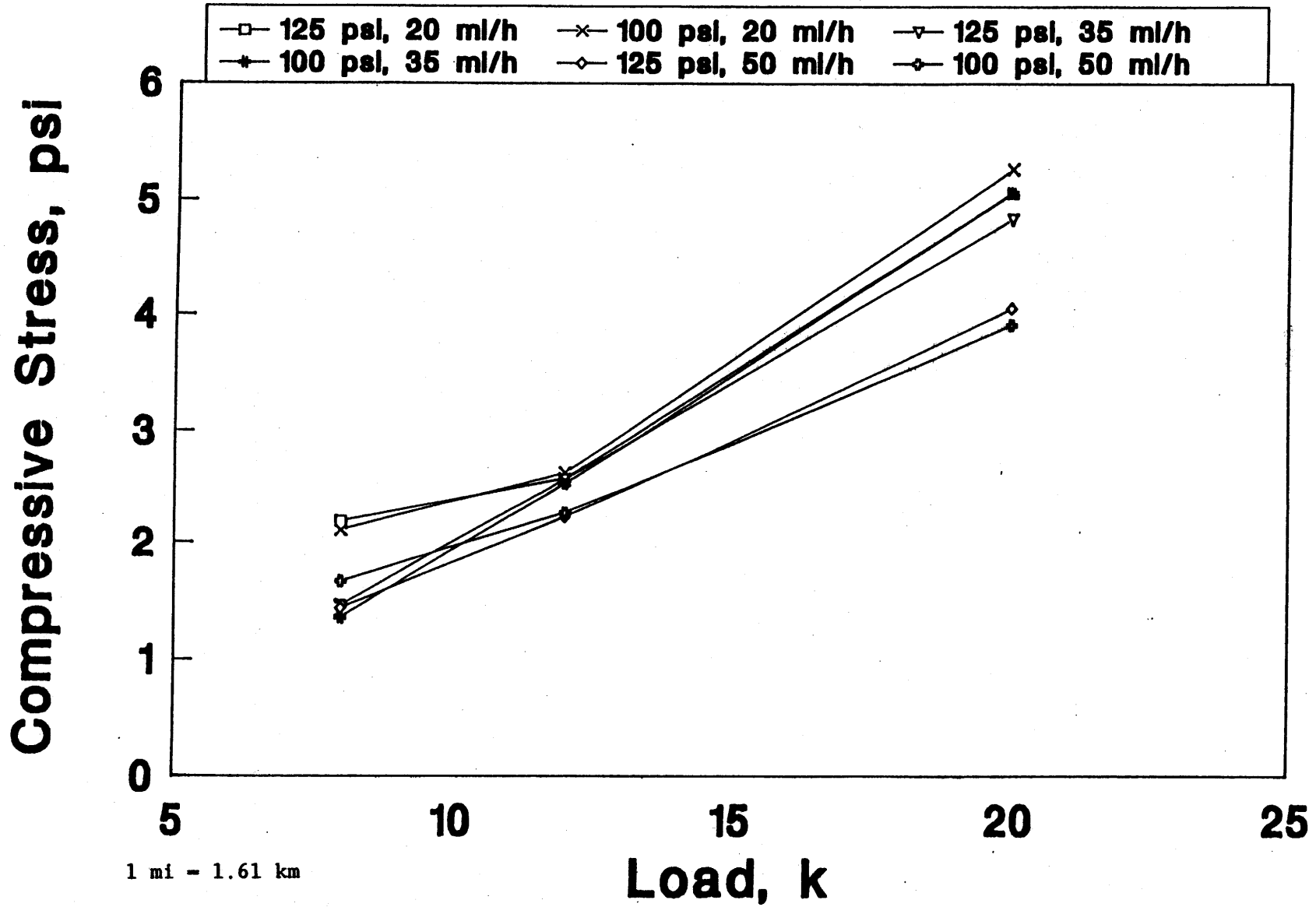


Figure 30. Effects of load, tire pressure, and speed on the response of the pressure cell, thin section, drive single axle.

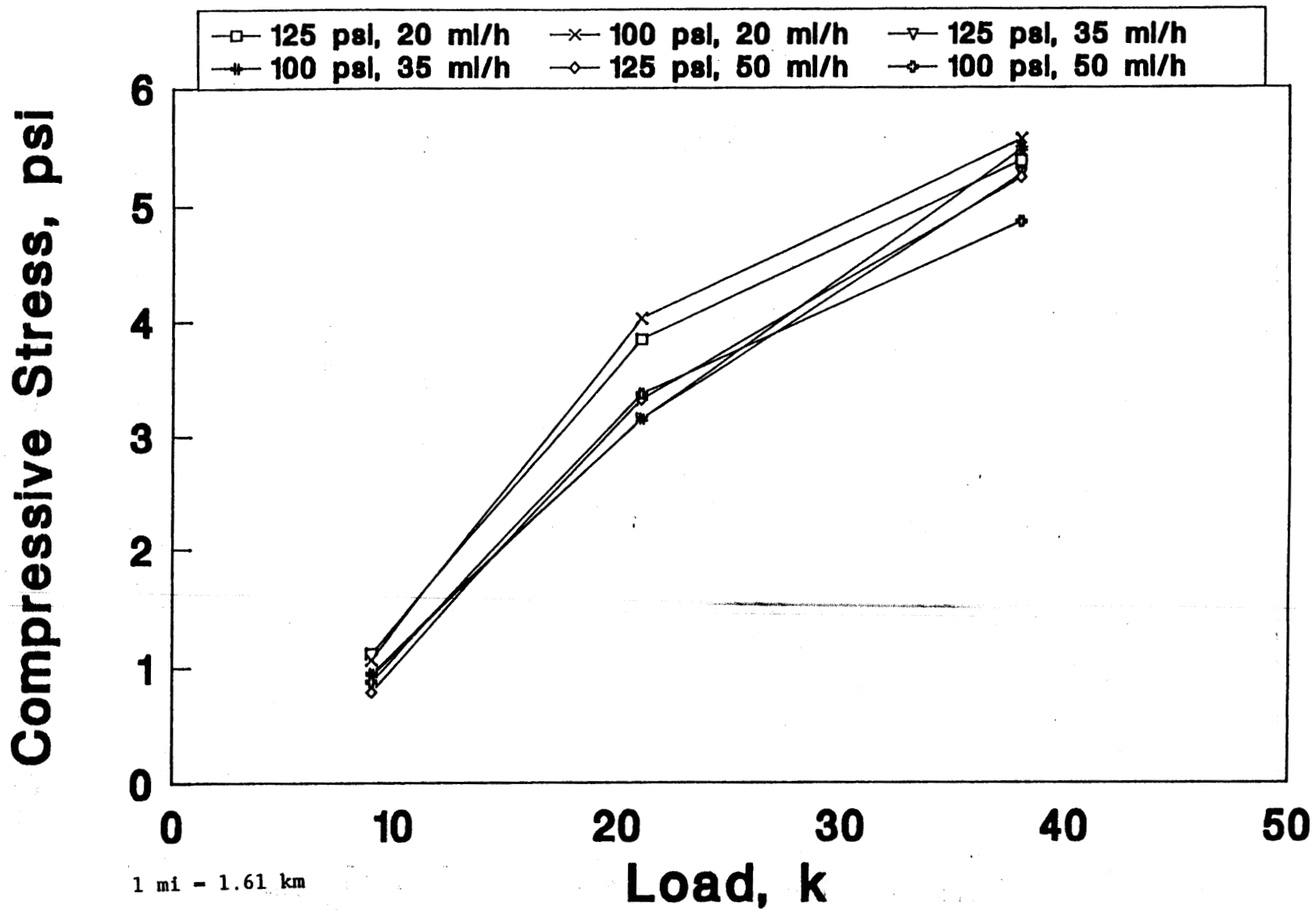


Figure 31. Effects of load, tire pressure, and speed on the response of the pressure cell, thin section, trailer tandem axles.

speed and tire pressure are insignificant for both single- and tandem-axle configurations.

Reducing the load level of the single drive axle from 20 to 12 kips (88 to 53 kN) decreased the measured stress for all combinations of speed and tire pressures by 45 to 50 percent. However, reducing the load level from 12 to 8 kips (53 to 35 kN) reduced the measured stress by 20, 47, and 30 percent for speeds of 20, 35, and 50 mi/h (32, 56, and 80 km/h), respectively.

In the case of the tandem trailer axles, reducing the load level from 38 to 21 kips (167 to 92 kN) decreased the measured stress by 28, 47, and 30 percent for speeds of 20, 35, and 50 mi/h (32, 56, and 80 km/h), respectively. Reducing the load from 21 to 9 kips (92 to 40 kN) resulted in an average decrease in the measured stress of 72 percent for all speeds and tire pressures.

Based on these observations, it can be concluded that the pressure at the asphalt concrete-base interface is strongly affected by the load level. However, the interactive effect of load level and axle configuration depends on the testing speed.

UNCERTAINTY

Note that only one pressure cell was operational during the test periods. The uncertainty of the measured pressures can be evaluated using an approach similar to the one used in the study of uncertainty of the strain measurements. The upper and lower limits of the calculated pressures were obtained by varying the thickness of the asphalt concrete layer by ± 0.5 in (± 13 mm). The measured pressures at 20 mi/h (32 km/h) and calculated static pressures are plotted in figure 32. The calculated pressure values are always higher than the measured ones and the difference becomes larger as the axle load increases. It is expected also that the dynamic load profile is a major factor on the measured pressures, but because only one pressure cell was operational, no solid conclusions can be made. Even though the measured pressures are different from the calculated ones, the pressure cell measurements were very stable and consistently had good repeatability.

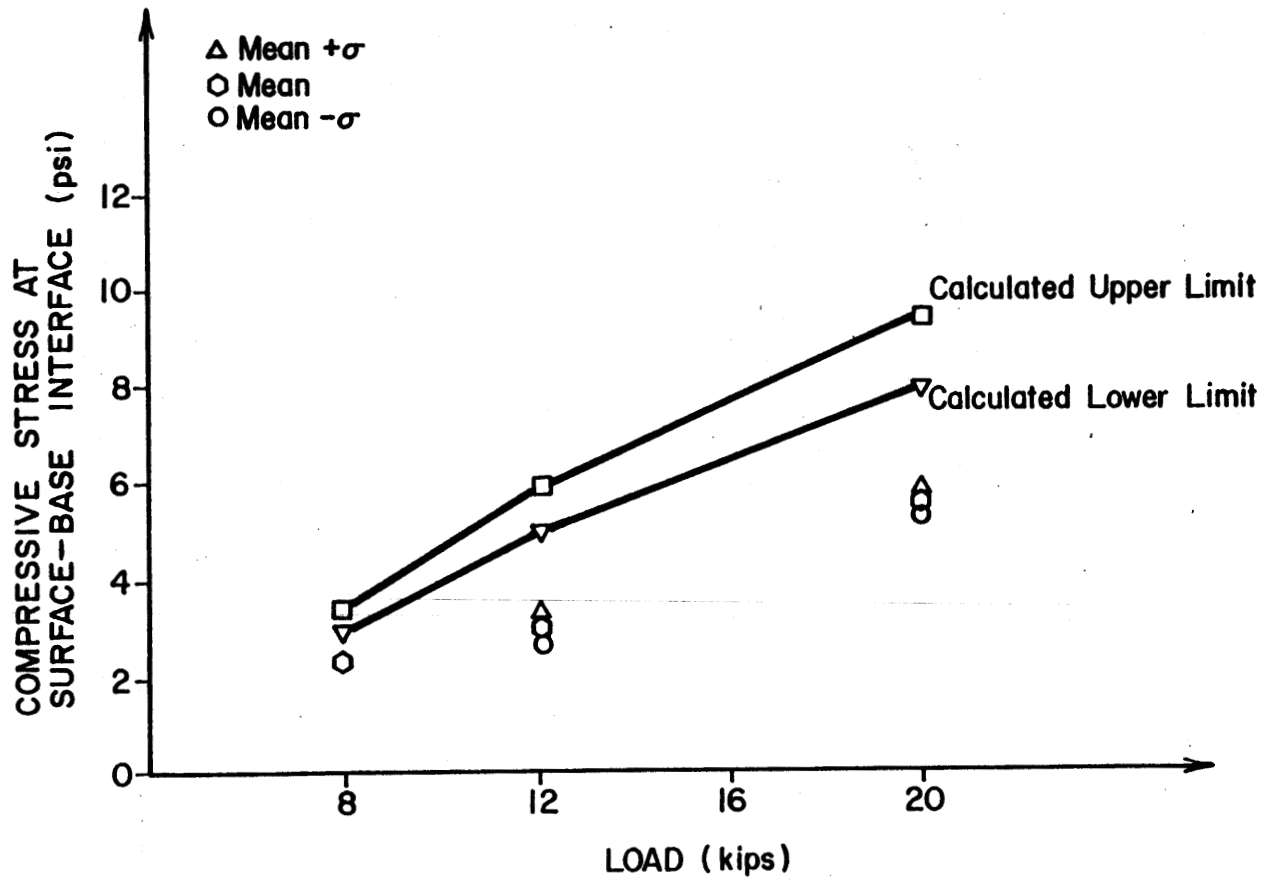


Figure 32. Comparison of measured and calculated pressures under the drive single axle at the thin section.

ANALYSIS OF DEFLECTION DATA

Three types of deflection-measuring devices were selected for the field testing experiment:

- Geophones.
- Single-layer deflectometer.
- Multidepth deflectometer.

The responses of the geophones and SLD devices under the various test combinations were collected using the main data acquisition software. The MDD responses were collected using a separate software and a separate computer (see chapter 2).

SURVIVABILITY

Nine geophones were installed at each section as shown in figures 2 and 3. After the construction of the sections was completed, one geophone at the base interface and one geophone at the subgrade interface in the thin section were unoperational. The rest of the geophones were operational for the entire testing period. The survivability rate of the geophones was very good for both sections: 78 and 100 percent for the thin and thick sections, respectively.

Two SLD's were installed in the outer wheel path of the thick section-- one at the subgrade level and one at the base course level. Both devices were retrofitted into the section after the construction was completed. The SLD installed at the subgrade level was driven out of range shortly after installation, and no data could be obtained from it. Because the sample size of the SLD's was very small, no true survivability rate could be obtained for evaluation.

The MDD's were installed after construction, precluding any operational losses during the construction process. Seven LVDT units were installed in the two experimental pavements. Three units were installed in the thin

section at the layer interfaces (6 and 14 in [152 and 356 mm]) and 12 in (305 mm) into the subgrade. Four units were installed in the thick sections at 3, 10, 20, and 32 in (76, 254, 508, and 813 mm), the top two of which were located in the asphalt surfacing. Schaevitz DC-E series LVDT's with a range of $\pm .1$ in (± 2.5 mm) were used. All seven LVDT's were working correctly after installation, and tests were made with the falling weight deflectometer.

Truck testing began about 1 month after installation, and problems were encountered with two LVDT's in the thick section. The LVDT at 32 in (813 mm) gave erratic readings due to a build-up of moisture at the bottom of the MDD hole, causing problems with the circuitry of the LVDT. This LVDT was not used during the tests; the only data obtained from this unit were the data collected immediately after installation. No additional data were collected from the MDD module at 10-in (254-mm) depth during this test due to misadjustment of the MDD central core. Under test traffic, MDD data were collected successfully on MDD modules 1 and 3 on the thick section. All of the three MDD's in the thin section worked, and a complete set of data was collected. It was learned that in order to ensure long-term durability of a DC LVDT, it is recommended that hermetically sealed units be used to minimize damage due to high humidity and moisture build-up. In general, two LVDT's were unoperational in the thick section, and all LVDT's were operational in the thin section during the testing period.

REPEATABILITY

The responses of the geophones were collected both under the FWD and truck loading. For the FWD case, the loading plate of the FWD was centered over the embedded surface geophone as closely as possible. The responses of the FWD geophones located at the center of the loading plate were collected and analyzed by the FWD machine. The responses of the embedded geophones were collected by the general data acquisition system. The results from the FWD deflections and the embedded geophones are shown in table 14. The data show a very close agreement between the FWD deflections and the embedded geophones measurements, which indicated that the geophones were operating properly.

Table 14. Geophone data under FWD.

Section	Station (ft)	Load (lb)	Peak Deflection (mils)	
			FWD Geophone	Embedded Geophone
Thin	36	8,236	19.11	17.02
	36	8,328	18.90	16.67
	40	8,143	22.20	23.10
	40	8,328	21.03	21.96
	40	8,421	21.44	21.60
	41	8,143	23.11	24.13
	41	8,421	22.03	20.96
	41	8,236	22.26	22.31
Thick	36	8,236	9.09	7.97
	36	8,328	9.06	7.90
	40	8,236	8.92	7.14
	40	8,236	8.90	7.15
	42.5	8,328	9.06	8.96
	42.5	8,328	9.00	8.65
	42.5	8,328	8.90	8.59

1 ft = .305 m

1 lb = 4.5 N

The geophone responses under truck loading were collected for all combinations of the test variables. The analysis of the data under the single drive axle showed that the measurements taken at 20 mi/h (32 km/h) are not good because the speed was too slow to provide good geophone signals. Therefore, the geophone data for 35 and 50 mi/h (56 and 80 km/h) were analyzed. The good geophone data are summarized in table 15 for the three surface geophones. The empty load level on the thick section did not produce good measurements. As mentioned earlier, the data in table 15 represent the best data obtained from the geophones. Even for the best data, the standard deviations and coefficients of variation are quite large, especially for the intermediate and empty load levels. Therefore, it is obvious that the 10-Hz geophones are not sensitive enough for this kind of application. The use of the 10-Hz geophones for measurement of pavement deflection is not recommended except when test conditions include a combination of heavy loads, high speeds, and thin pavement.

Attempts were made to integrate the geophone signals generated under the tandem axles. The resulting deflections were widely distributed, and no correlations existed between the various replicates. The reason for this bad performance is that the initial conditions of the geophone must always be at rest (i.e., at $t = 0$, $v = 0$, $x = 0$) in order to pick a clean peak velocity and to have meaningful deflections based on the integration of the velocity signals. This ideal case does not exist in a pavement section subjected to a moving truck load. The first blow of the FWD loading can be represented by the ideal case, which is why the embedded geophones worked well under the FWD loading.

The data from the operational SLD at the base course level were collected under all combinations of test variables. The measured deflections at the asphalt-base interface have shown that changing the tire pressure level from 100 to 125 psi (690 to 863 kPa) does not significantly affect the response of the SLD. Therefore, the data from the two levels of tire pressures were combined, and the means, standard deviations, and coefficients of variations of the combined data were evaluated and are summarized in table 16. All the coefficients of variations are below 10 percent, which indicates that the SLD is a very precise device. Combining the two levels of tire

Table 15. Summary of the means, standard deviations, and coefficients of variation for the surface geophones under the single drive axle.

Pavement Section	Single Axle Load (kips)	Speed (mi/h)	Geophone 1			Geophone 2			Geophone 3		
			Mean	STD*	COV(%)*	Mean	STD	COV(%)	Mean	STD	COV(%)
Thin	20	35	10.89	3.75	34.44	15.20	1.73	11.40	12.59	2.36	18.77
		50	9.87	1.25	12.64	9.83	0.84	8.56	9.12	1.29	14.13
	12	35	6.61	2.45	37.05	7.07	2.35	33.25	8.13	1.67	20.51
		50	3.50	1.30	37.02	4.54	0.89	19.66	3.87	0.91	23.39
	8	35	5.00	1.12	22.47	4.47	1.17	26.16	4.59	1.67	36.37
		50	2.85	0.78	27.44	2.68	0.38	14.01	2.97	0.68	22.78
Thick	20	35	9.79	1.29	13.90	8.63	0.96	11.12	8.31	2.24	27.02
		50	4.95	0.72	14.51	5.69	0.37	6.59	6.08	0.41	6.78
	12	35	5.23	1.06	20.17	3.87	1.35	34.95	4.72	1.15	24.45
		50	2.61	0.51	19.55	1.78	0.37	21.02	1.74	0.48	27.43

*STD - Standard Deviation

COV - Coefficient of Variation - STD/Mean

**All units are in mils.

1 mi = 1.61 km

Table 16. Summary of the means, standard deviations, and coefficients of variation for the single-layer deflectometer.

Axle Type	Axle Load (kips)	Speed (mi/h)	Mean*	Standard Deviation*	Coefficients of Variation (%)
Single Drive Axle	20	20	8.09	0.40	4.94
		35	7.04	0.34	4.83
		50	7.03	0.44	6.26
Tandem Trailer Axle (Rear Axle)	38	20	8.62	0.15	1.74
		35	8.51	0.24	2.82
		50	7.17	0.53	7.39
Single Drive Axle	12	20	4.82	0.36	7.47
		35	3.42	0.25	7.31
		50	3.28	0.18	5.49
Tandem Trailer Axle (Rear Axle)	21	20	5.78	0.41	7.09
		35	4.93	0.33	6.69
		50	3.34	0.26	7.78
Single Drive Axle	8	20	2.77	0.15	5.42
		35	2.67	0.23	8.61
		50	2.55	0.13	5.10
Tandem Trailer Axle (Rear Axle)	9	20	1.41	0.11	7.80
		35	1.30	0.09	6.92
		50	1.43	0.10	6.99

*All units are in psi.

1 mi = 1.61 km

pressures provides eight replicates for each combination of speed, axle, and axle type.

The data from the MDD's were also collected under all combinations of test variables. The measurements from the two levels of tire pressure were combined. The means, standard deviations, and coefficients of variations for all combinations of test variables on the thin section are shown in table 17. The summary data on the thick section include only the intermediate load level (see table 18). The data show that the MDD results are very repeatable.

As mentioned earlier, three surface geophones were installed in each section, and the top LVDT of the MDD was located 1 in (254 mm) below the surface of the pavement. Therefore, the data from the surface geophones and the top LVDT can be compared under various combinations of test variables. Table 19 shows the means of the measurements from the surface geophones and the first LVDT. The data indicate that the measurements obtained with the geophones and the MDD become close at a speed of 35 mi/h (56 km/h) and deviate at a speed of 50 mi/h (80 km/h). The truck speed did not significantly affect the MDD deflections, while the surface geophones data indicated the contrary. The geophones data under truck loading showed very large standard deviations and coefficients of variations for the very limited set of data for which the geophones have produced meaningful results. In summary, there are larger discrepancies between the surface geophones data and the first LVDT data, especially at the speed of 50 mi/h (80 km/h); however, the geophones data could not be trusted because they showed large variability.

EFFECTS OF TEST VARIABLES ON THE RESPONSE OF GAUGES

Based on the repeatability analysis of the geophones data, it was concluded that the majority of the geophones data are not good. Therefore, the effects of test variables and uncertainty analyses for the deflection gauges were evaluated only for the SLD and MDD measurements.

The effects of tire pressure, speed, and load level on the SLD measurements are shown in figures 33 and 34. As the figures illustrate, load level has the most significant effect for both the single drive axle and the

Table 17. Summary of the means, standard deviations, and coefficients of variation for the multidepth deflectometer on the thin section.

Axle Type	Axle Load (kips)	Speed (mi/h)	MDD1			MDD2			MDD3		
			Mean	STD*	COV(%)*	Mean	STD	COV(%)	Mean	STD	COV(%)
Single Drive Axle	20	20	14.51	1.42	9.79	8.28	0.95	11.47	2.26	0.26	11.50
		35	11.77	0.48	4.09	6.60	0.30	4.55	1.83	0.09	4.92
		50	14.82	0.95	6.41	8.61	0.54	6.27	2.31	0.10	4.33
Tandem Trailer Axle (Rear Axle)	38	20	16.17	1.21	7.48	9.41	0.86	9.14	2.70	0.29	10.74
		35	11.19	0.50	4.47	6.35	0.32	5.04	1.92	0.06	3.13
		50	16.65	1.19	7.15	9.91	0.65	6.56	3.00	0.16	5.33
Single Drive Axle	12	20	6.12	0.49	8.01	3.36	0.25	7.44	1.01	0.06	5.94
		35	5.09	0.37	7.27	2.78	0.19	6.83	0.86	0.06	6.98
		50	5.91	0.50	8.46	3.18	0.23	7.23	0.97	0.05	4.80
Tandem Trailer Axle (Rear Axle)	21	20	8.30	0.56	6.75	4.72	0.25	5.30	1.56	0.06	3.95
		35	7.20	0.32	4.44	4.07	0.17	4.18	1.34	0.06	4.48
		50	7.75	0.97	12.50	4.46	0.56	12.51	1.57	0.14	9.22
Single Drive Axle	8	20	3.23	0.24	7.38	1.69	0.10	6.03	0.63	0.02	3.82
		35	3.58	0.36	10.15	1.91	0.21	11.18	0.70	0.06	8.57
		50	2.64	0.28	10.54	1.42	0.15	10.78	0.54	1.05	8.61
Tandem Trailer Axle	9	20	1.77	0.17	9.60	0.91	0.08	8.79	0.39	0.03	7.69
		35	1.77	0.11	6.21	0.91	0.09	9.89	0.43	0.03	6.98
		50	1.36	0.26	19.12	0.65	0.11	16.92	0.34	0.04	11.76

*STD - Standard Deviation

COV - Coefficient of Variation - STD/Mean

**All units are in mils.

Table 18. Summary of the means, standard deviations, and coefficients of variation for the multidepth deflectometer on the thick section.

Axle Type	Axle Load (kips)	Speed (mi/h)	MDD1			MDD3		
			Mean	STD*	COV(%)*	Mean	STD*	COV(%)*
Single Drive Axle	12	20	4.56	0.30	6.58	1.54	0.10	6.49
		35	4.27	0.28	6.56	1.47	0.10	6.80
		50	4.13	0.16	3.87	1.40	0.05	3.57
Tandem Trailer Axle (Rear Axle)	21	20	5.59	0.19	3.40	2.03	0.09	4.43
		35	5.47	0.28	5.12	2.04	0.10	4.90
		50	5.70	0.23	4.04	2.13	0.13	6.10

*STD - Standard Deviation

COV - Coefficient of Variation - STD/Mean

**All units are in mils.

1 mi - 1.61 km

Table 19. Summary of the means of the surface geophones and the first LVDT of the MDD.

Pavement Section	Single Axle Load (kips)	Speed (mi/h)	Geophone 1 (mils)	Geophone 2 (mils)	Geophone 3 (mils)	MDD1
Thin	20	35	10.89	15.20	12.59	11.77
		50	9.87	9.83	9.12	14.82
	12	35	6.61	7.07	8.13	6.12
		50	3.50	4.54	3.87	5.91
	8	35	5.00	4.47	4.59	3.58
		50	2.85	2.68	2.97	2.64
Thick	12	35	5.23	3.87	4.72	4.27
		50	2.61	1.78	1.74	4.13

1 mi - 1.61 km

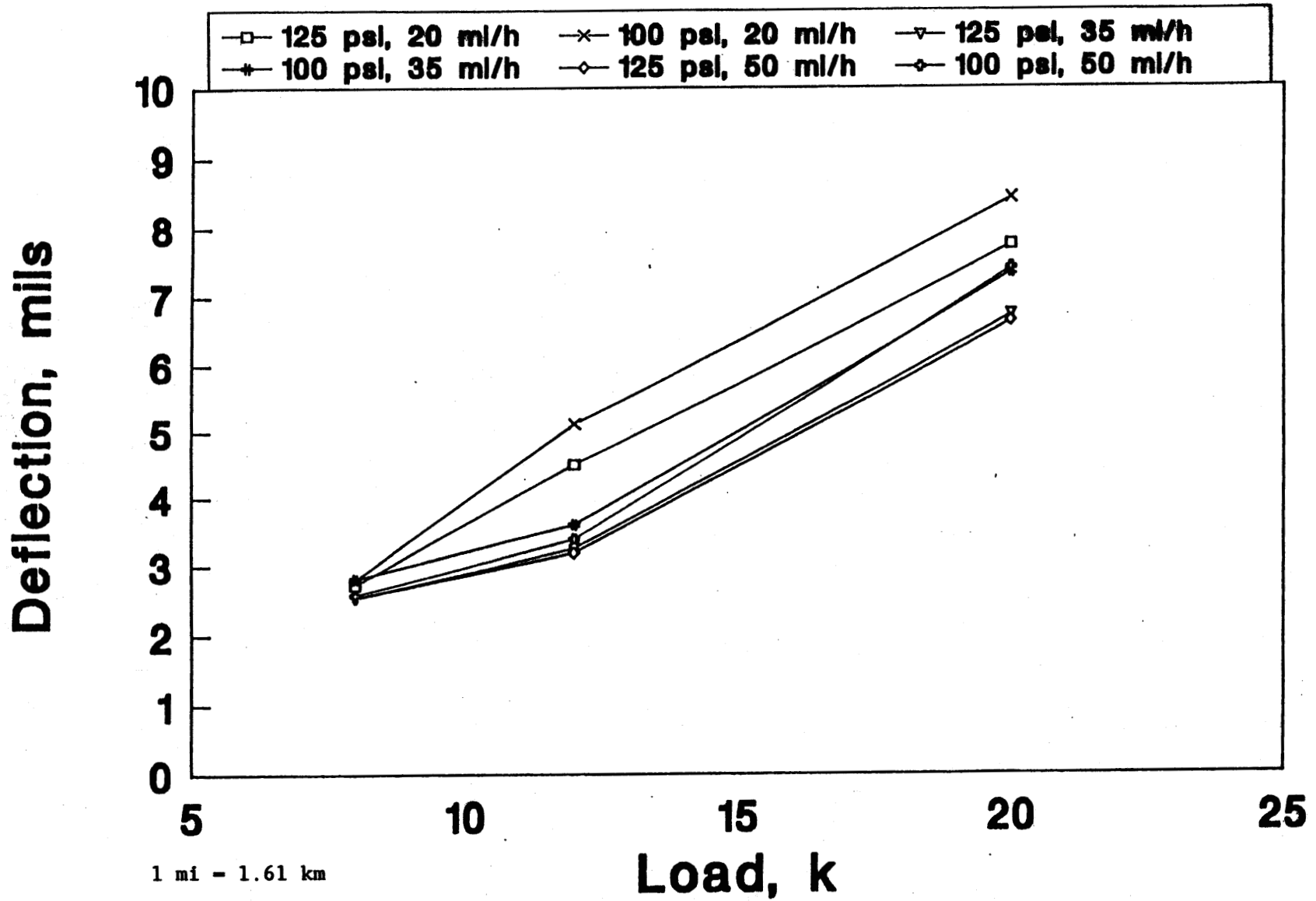


Figure 33. Effects of load, tire pressure, and speed on the response of the SLD at the surface/base interface of the thick section, drive single axle.

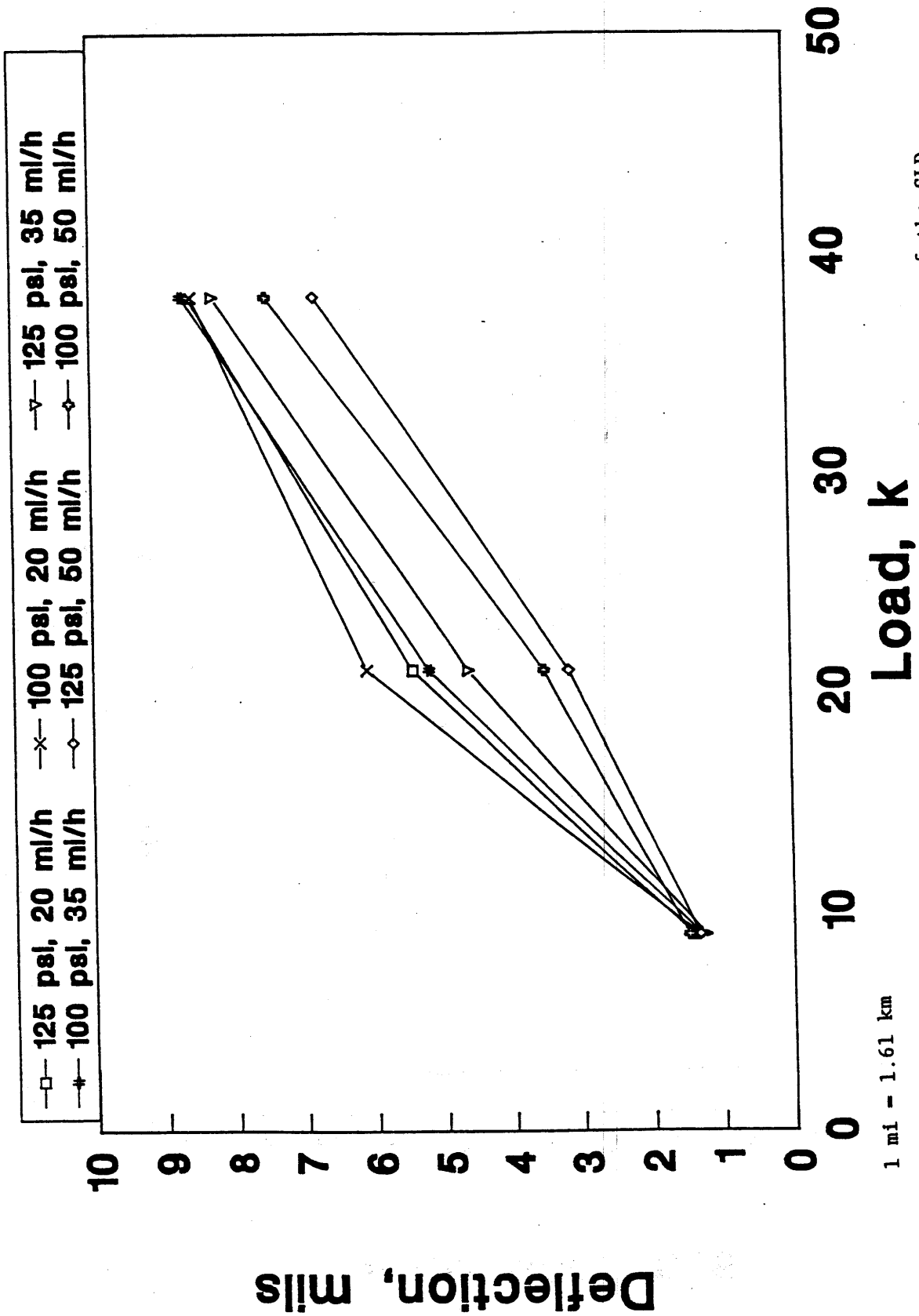


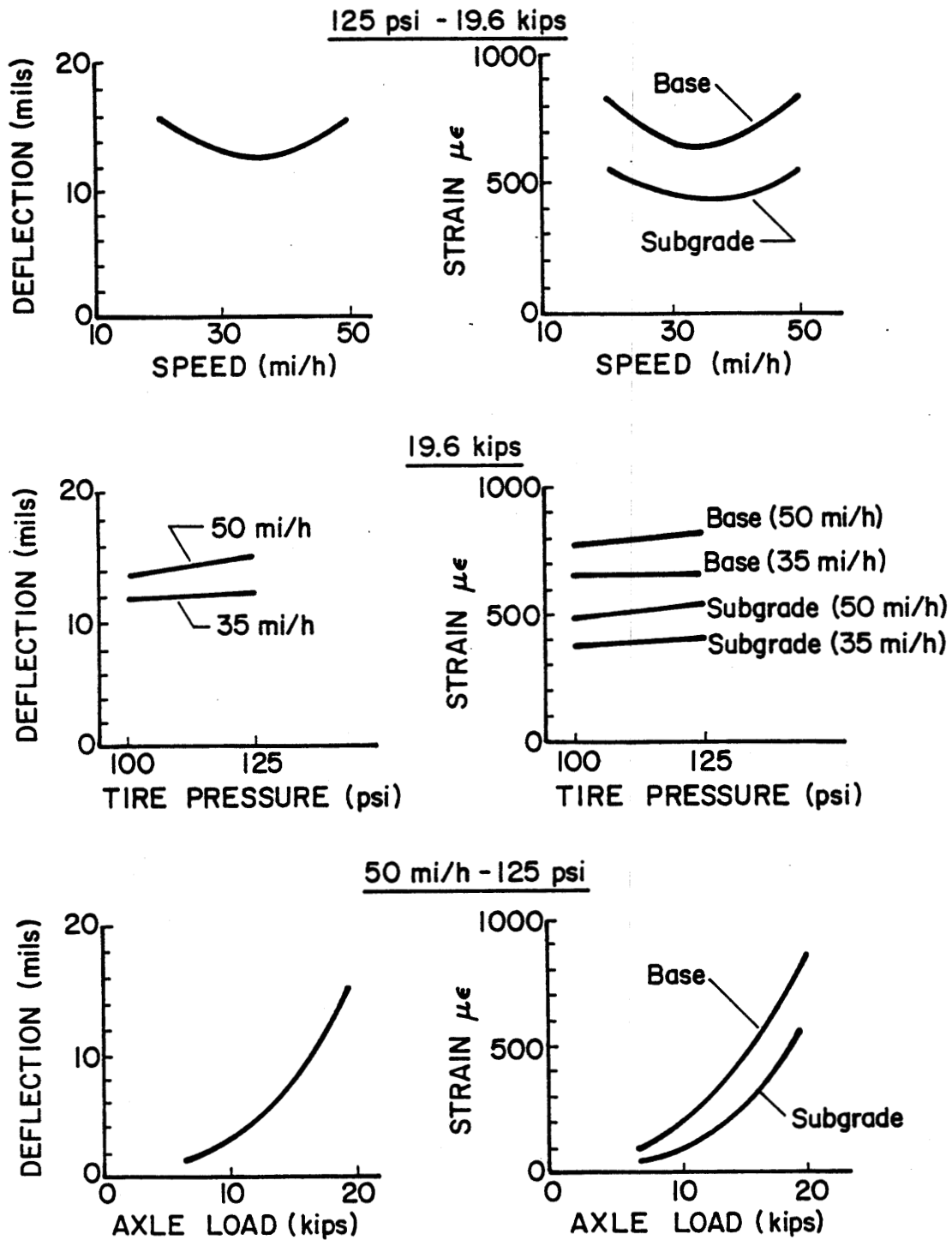
Figure 34. Effect of load, tire pressure, and speed on the response of the SLD at the surface/base interface of the thick section, trailer tandem axles.

tandem trailer axle. For the single drive axle, the deflection for the fully loaded case is 65 percent higher than the deflection for the intermediate load level for a speed of 20 mi/h (32 km/h); it is 100 percent higher for speeds of 35 and 50 mi/h (56 and 80 km/h). Under the empty load level, the effects of speed and tire pressure are insignificant. For the tandem axles, the load level is also the most significant factor. The deflections for the fully loaded case are 65 percent higher than deflections for the intermediate load level at speeds of 20 and 35 mi/h (32 and 56 km/h); it is 100 percent higher for a speed of 50 mi/h (80 km/h). For the empty load level under the tandem axles, the tire pressure and speed effects are both insignificant.

Finally, it can be concluded that the operational SLD performed excellently under all test combinations. The effect of speed on SLD measurements differs from the single drive axle to the tandem axles. In the case of the drive axle, the effect of speed was pronounced between 20 and 35 mi/h (32 and 56 km/h); for the tandem-axle case, the effect of speed was pronounced between 35 and 50 mi/h (56 and 80 km/h).

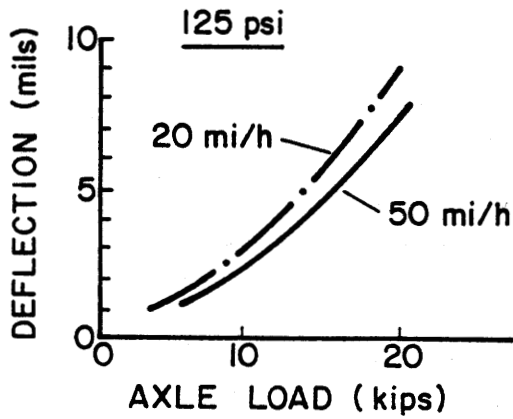
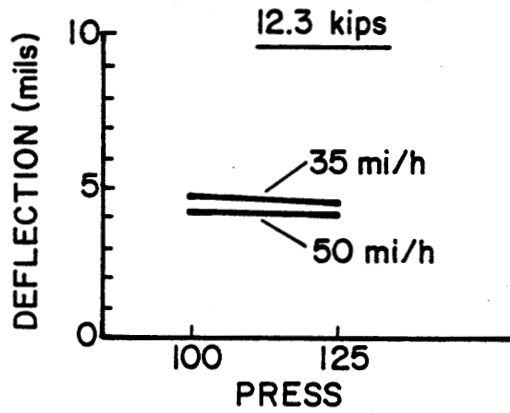
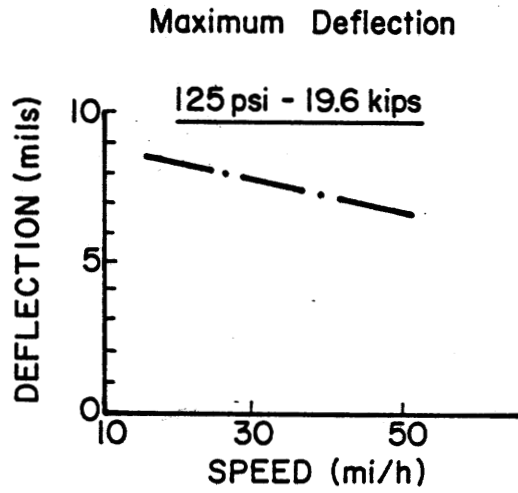
To demonstrate the effect of the test variables on the response of the MDD's, figures 35 and 36 have been drawn from the collected data. These figures show the pavement response for the single axle on the thick and thin pavements. The vertical strain is calculated by dividing the relative vertical deflections at consecutive MDD locations by the corresponding distance. Unexpected results for deflection (and vertical strain) versus speed were obtained on the thin pavement section. The minimum deflections under the fully loaded single axle were measured at 35 mi/h (56 km/h). The results at 20 and 50 mi/h (32 and 80 km/h) were similar but higher than the 35 mi/h (56 km/h) results. It was expected that as speed increased, the pavement deflections would decrease as was observed on the thick pavement (figure 36).

As anticipated, axle loads have a major impact on pavement response. This response is distinctly nonlinear: a 59-percent increase in axle load (12 to 20 kips [53 to 89 kN]) resulted in a 173-percent increase in deflection. This nonlinear response contradicts the strain gauge and FWD measurements. Tire pressures did not appear to have any major impact on the measured pavement responses (figures 35 and 36).



1 mi - 1.61 km

Figure 35. Effect of test variables on multidepth deflectometer output (thin pavement/single axle).



1 mi - 1.61 km

Figure 36. Effects of test variables on multidepth deflectometer output (thick pavement/single axle).

UNCERTAINTY OF THE MEASURED DEFLECTIONS

The uncertainty of the SLD measurements was investigated using the same approach as in the strain and pressure measurement cases. The FWD backcalculated moduli at the station where the SLD was installed were used in the multilayer elastic solution and the upper and lower limit values were calculated based on thickness variation of ± 0.5 in (± 13 mm). The data of the SLD at 20 mi/h (32 km/h) are plotted in figure 37. A very good agreement is found at all load levels. This indicates that the SLD is a very stable, repeatable, and low-uncertainty piece of instrumentation.

In order to evaluate the uncertainty of the MDD measurements, the FWD backcalculated moduli were used to conduct a sensitivity analysis to evaluate the effect of parameters on the expected response of the MDD's. For each case of the analysis, a single parameter, layer thickness or modulus, was varied about the mean value, and the effects on the predicted MDD measurement were evaluated. The results are tabulated in tables 20 and 21. From these tables, given all of the assumptions involved, it can be concluded that the measured MDD deflections closely matched those theoretically predicted using the linear elastic theory.

AUXILIARY MEASUREMENTS

MOISTURE MEASUREMENTS

Suction and temperature readings for the thick and thin instrumented borings were made on June 16, 1989, and on October 25, 1989. Readings for all sensors are shown in table 22.

The results of the two sets of data for the thin section are generally consistent. Positive suction values were obtained at a depth of 5.5 ft (1.7 m) for both dates, indicating wet conditions in the soil surrounding the sensor. Dry conditions were observed for both dates at a depth of 3.5 ft (1.1 m), and approximately neutral conditions were obtained for the base course.

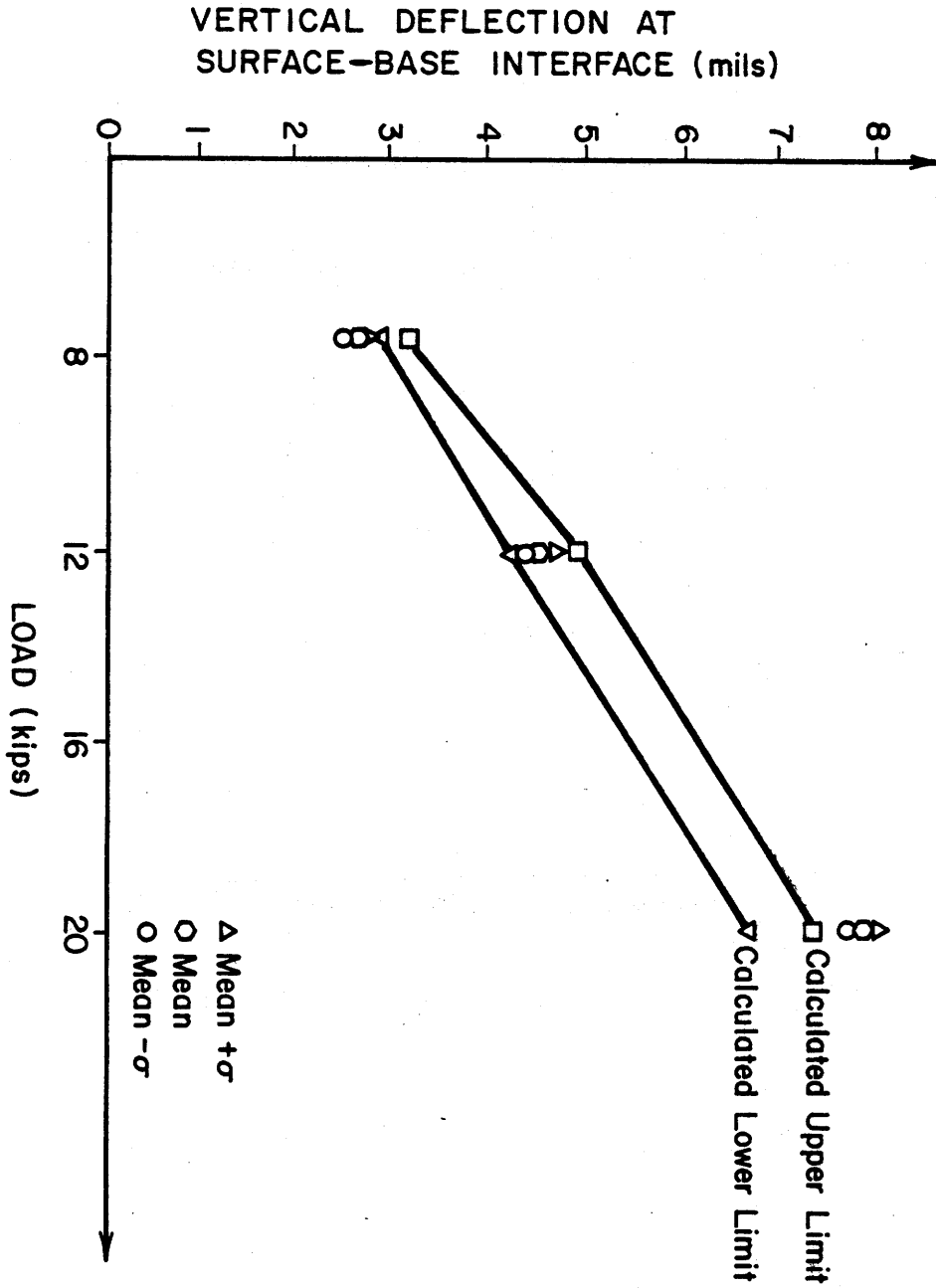


Figure 37. Comparison of calculated and measured deflections under the drive single axle at the thick section.

Table 20. Sensitivity analysis on thin pavement--predicted MDD values versus measured MDD values.

Variable	Range	Calculated Values	Measured Value
Surface Thickness	5.5 to 6.0 in	15.46 to 16.82	15.36
Base Thickness	7 to 9 in	15.55 to 16.70	15.36
Base Modulus	4.0 to 6.6 ksi	15.10 to 17.10	15.36
Subgrade Modulus	15.5 to 25.5 ksi	15.04 to 17.22	15.36

1 in = 25.4 mm

Table 21. Sensitivity analysis on thick pavement--predicted MDD values versus measured MDD values.

Variable	Range	Calculated Values	Measured Value
Surface Thickness	9 to 11 in	6.93 to 8.25	6.80
Base Thickness	9 to 11 in	7.43 to 7.77	6.80
Base Modulus	7.8 to 17.8 ksi	6.90 to 8.30	6.80
Subgrade Modulus	22.7 to 32.7 ksi	7.27 to 7.93	6.80

1 in = 25.4 mm

Table 22. Suction and temperature readings from the thin and thick test sections.

Pavement Thickness	Depth (ft)	June 16, 1989		October 25, 1989	
		Suction	Temperature* (°C)	Suction	Temperature (°C)
Thick	Base	-0.254	21.05	-1.648	11.42
	3.5	0.063	19.24	-4.494	10.06
	5.5	-0.586	16.31	0.059	15.25
Thin	Base	-0.118	19.55	-0.003	11.92
	3.5	-2.234	17.40	-2.546	13.02
	5.5	0.177	15.80	0.226	14.24

*Temperature-measuring device measures in °C.
1 ft = .305 m

Temperature conditions for the thin section sensors were observed to be reasonable for the two dates. Readings obtained in June decreased from 67 to 60 °F (20 to 16 °C) as the depth decreased from the base course to 5.5 ft (1.7 m) below the surface. Readings taken in late October increased from 54 to 57 °F (12 to 14 °C) over the same change in elevation. Seasonal variations and the effect of ambient temperature were clear for the base course sensor, and reduced influence was observed in the lower sensors until the lowest sensors approach (but do not reach) constant temperature with time.

Less consistent results were observed for the thick section. Dry conditions were indicated by the base course sensor (suction = -1.648) for the October reading. To achieve this, the base course must have been draining any water that entered it and experiencing significant moisture deficiency as well. The sensor located at 3.5 ft (1.1 m) was apparently failing because the suction reading indicated excessively dry conditions. When the sensor "completely fails," a reading of 99.99 or a "no reading" will be obtained, but unreasonable readings often occur prior to outright failure.

Similar temperature trends were observed for both the thick and thin sections. A condition of constant temperature was approached but not reached at a depth of 5.5 ft (1.7 m).

Two unsuccessful attempts were made to collect data from the nuclear dual tubes--one in June (immediately after installation) and one in October. Unfortunately, the equipment did not operate properly. It appeared that the data collection process was very complex and sensitive and required considerable previous experience for a successful experiment. Therefore, no data were obtained, and no recommendations or conclusions could be drawn concerning this system.

TEMPERATURE MEASUREMENTS

Knowing the temperature distribution throughout the asphalt concrete, base course, and subgrade layers is very important because temperature affects the in situ properties of these layers and, most significantly, the properties of the asphalt concrete layer. As discussed earlier, thermocouples and solid

state sensors were selected for this experiment. Both sensors were installed side by side on a temperature tree that ran from the surface through the base course and into the subgrade. The actual locations of the sensors in each layer are shown in figures 2 and 3. The purpose of this test was to monitor the temperature variation throughout the pavement layers during testing and to check the measured values from the different types of sensors.

Eight thermocouples and eight solid state sensors were installed in each temperature tree. One temperature tree was installed in each of the test sections. All of the sensors survived the construction and installation activities, and they remained operational throughout the entire testing period.

Test operators manually collected the temperature measurements and entered the values into prepared forms. The data were collected at 30- to 45-min intervals during testing periods. The top four sensors were located within the asphalt concrete layer; therefore, the average of these four sensors represents the average temperature of the asphalt concrete layer. Upon evaluation, the measurements from the solid state and thermocouples often did not agree. The thermocouples sometimes showed higher or lower temperatures than the solid state sensors. The maximum discrepancy between the two types of sensors was approximately 5 to 6 °F (2.8 to 3.3 °C). For a temperature in the range of 65 to 72 °F (18 to 22 °C), the maximum discrepancy was in the order of 2 °F (1 °C).

Because the ultimate goal is to evaluate the average temperature of the asphalt concrete layer, the differences in this value as measured by the thermocouples and solid state sensors should be examined. An examination of the overall data indicates that for average asphalt layer temperatures in the range of 68 to 77 °F (20 to 25 °C), the thermocouples and solid state measurements were very close to each other, with a maximum difference of 1 °F (0.6 °C). For average asphalt layer temperatures above 80 °F (27 °C), the solid state sensor measurements were 2 to 5 °F (1 to 3 °C) higher than the thermocouple measurements most of the time. A small laboratory experiment was conducted to explain the discrepancy. In the experiment, a calibrated mercury thermometer, a solid state sensor, and a thermocouple were all placed in a

bucket of water. The water temperature was reduced to 32 °F (0 °C) and then brought up to two other levels. The readings from the three sensors were taken simultaneously. The data, shown in table 23, indicate that the thermocouples always measured 2 to 5 °F (1 to 3 °C) lower than the solid state sensors. Thermocouples are known to have a slow and nonlinear response to temperature variation, which may have contributed to the discrepancy. Even though a discrepancy exists between the two sensors, both of them were very consistent throughout the entire testing period.

Table 23. Temperature measurements from the controlled laboratory experiment.

Calibrated Mercury Thermometer (°F)	Solid State Sensor (°F)	Thermocouple Sensor (°F)
32	32	30
93	93	90
121	120	115

$$^{\circ}\text{F} = 5(\text{F}-32)/9^{\circ}\text{C}$$

4. EVALUATION OF IN SITU RESILIENT MODULI FROM SENSORS DATA

One objective of this study was to develop a methodology that would allow measurements obtained from pavement instrumentation under known loading conditions to be converted into appropriate layers moduli. The instrumentation to be used includes strain gauges, pressure cells, and multidepth deflectometers. In this chapter, a procedure is presented for calculating layers moduli from sensors data. A computer model is described that uses strain, stress, or deflection data as input to evaluate the layers moduli. This method effectively minimizes error between the measured and theoretically computed pavement responses. The linear elastic computer program BISAR was used to perform the theoretical stress, strain, and deflection predictions.

A growing body of knowledge already exists in this area with regard to backcalculation of layers moduli under nondestructive testing methods such as the falling weight deflectometer measurement. The aim is to match measured pavement responses with those calculated using assumed layers moduli. For more than 2 decades, the matching process has been conducted by trial and error, with few rules to guide the analyst. In recent years, several automatic search routines have been developed that minimize error between measured and calculated deflection bowls. One such routine is the CHEVDEF routine developed by Bush; another is the generalized backcalculation procedure developed by Uzan.⁽⁵⁻⁸⁾ Uzan's generalized procedure is the one used in this project, and it is presented in this chapter. A users manual for the general purpose modulus backcalculation program, called PENMOD, is included in appendix A.

DESCRIPTION OF THE GENERALIZED MODULUS BACKCALCULATION PROCEDURE

The PENMOD computer model handles two-, three-, and four-layer systems under single or dual tire loading. Stress, strain, or multidepth deflectometer readings can be used as input, and the user can specify a rigid layer at any depth in the system.

The ultimate goal of the backcalculation process is to estimate pavement material properties. The procedure is designed to find the set of parameters that correspond to the best fit of the measured deflection data. The best fit is achieved by minimizing the error between the measured and calculated deflection bowls. The objective function can therefore be written as:

$$\text{minimize } \sum_{i=1}^s e_i^2 = \sum_{i=1}^s \left[\frac{W_i^m - W_i^c}{W_i^m} \right]^2 W_{e_i} \quad (3)$$

where

- e_i^2 - relative squared error of sensor i
- W_i^m - measured deflection at sensor i
- W_i^c - computed deflection at sensor i
- s - number of sensors
- W_{e_i} - user-supplied weighing factor for sensor i

Equation 3 can be rewritten simply as:

$$\text{minimize } \sum_{i=1}^s e_i^2 = \sum_{i=1}^s \left[1 - \frac{W_i^c}{W_i^m} \right]^2 W_{e_i} \quad (4)$$

Different techniques are available for minimizing the objective function expressed in equation 4. The unknown variables are those required to compute the surface deflection W_c^i , that is:

$$W_c^i = F_i(X_j) \quad (5)$$

where

- X_j - unknown variables
- j - 1 to n unknowns

Any solution to equation 4 calls for a solution of equation 5, obtained numerically in most cases by running a separate program (such as the BISAR or CHEVRON computer program in the case of linear elasticity and ILLI-PAVE in the case of nonlinear elasticity). The number of calls depends on the minimization algorithm used. For example, the CHEVDEF program calls the deflection computation program $(N_{\text{LAYER}} + 1) * \text{ITER} + 1$ times for each bowl to be analyzed, where N_{LAYER} is the total number of layers for which moduli are to be determined and ITER is the number of iterations. Generally, the pattern search technique requires numerous calls of the deflection computation program for each measured bowl; this can be inefficient in the case where a large number of bowls are to be analyzed. This drawback is overcome in the Uzan system by generating ahead of time a data base containing deflection bowls for the expected range of moduli and using a three-point LaGrange interpolation technique to compute the deflection bowl for any set of unknown values within the expected range. It is worth mentioning that, after the generation of the data base, the deflection computer program is no longer required.

The above discussion relates strictly to a deflection-based backcalculation procedure. To create a truly general-purpose system, the following additions were made:

- W_1^m , the measured surface deflection, was generalized to a measured response (i.e., deflection, stress, or strain).
- The loading conditions were changed from a single load (e.g., FWD load plate or single tire) to dual loads representing the dual tires at one side of a single axle.

Although the approach is conceptually simple, generating a data base for a range of acceptable moduli values and interpolating within it to minimize errors, it offers several distinct advantages. First, after the data base has been built, fitting measured bowls to calculated bowls is very rapid. Second, it is possible to replace the linear elastic approach with a nonlinear approach. Rather than varying E values and running a linear elastic program such as BISAR to generate theoretical bowls, it is possible to vary K_1 values ($E = K_1 \theta **K_2$) and run a finite element program such as ILLI-PAVE to generate the required bowls. The pattern search procedure would then find the best set

of K_1 values for the base and subgrade to minimize error between measured and theoretical bowls.

INPUTS TO THE GENERALIZED BACKCALCULATION PROCEDURE

The procedures developed in this project permit flexible inputs of measured pavement responses. Measured values can be taken from different sensors, which is the case with surface or depth deflection sensors, or from multiple loading positions on a single sensor. For example, the readings on a single strain gauge as a wheel approaches the gauge can be used. Additionally, it is possible to combine these by inputting, for example, the maximum deflection responses on MDD gauges as the wheel is directly over the gauges, together with the deflections when the wheel is some distance away.

Strain Gauge

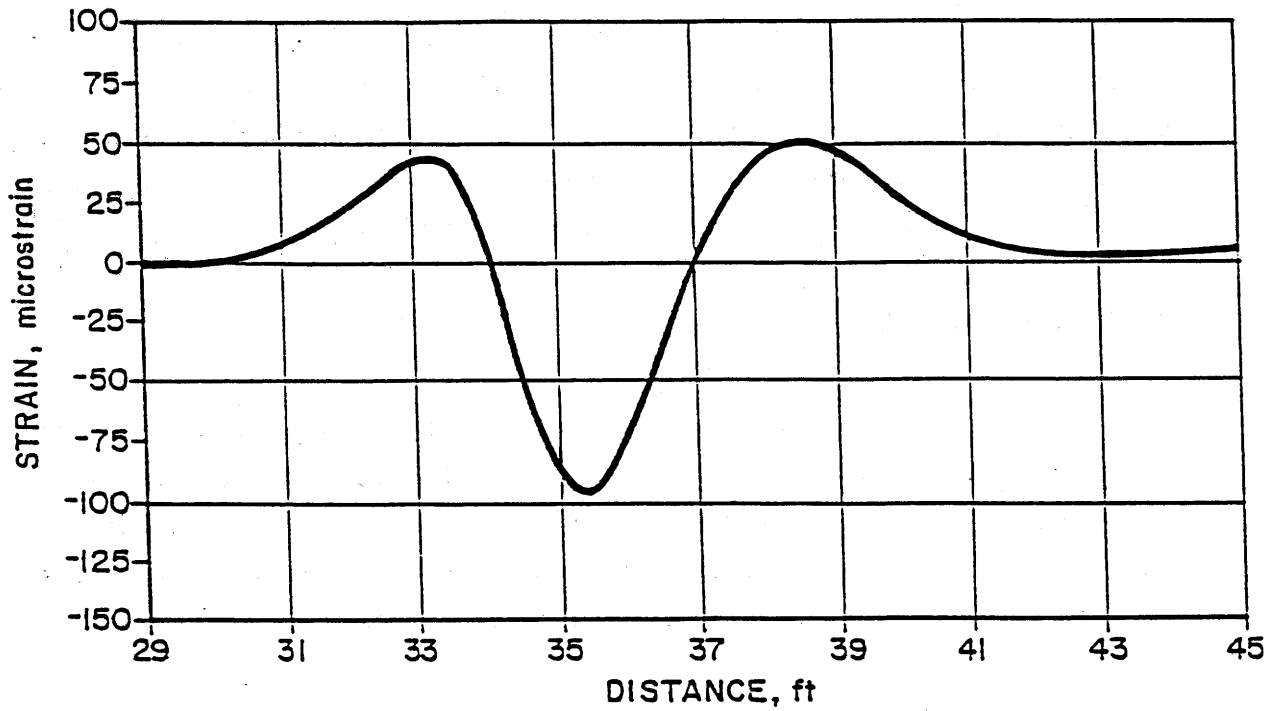
The ideal setup for modulus backcalculation from pavement instrumentation would include sensors positioned at various depths within the pavement. Strain gauges are typically installed at the bottom of the asphalt layer and it is difficult to measure strains in unbound materials. Therefore, to analyze strain gauge data, it is necessary to use the strains induced as the wheel approaches the single gauge. An example of this can be seen in figure 38; the tensile strains at offsets of 0, 6, 12, 18, 24, and 30 in (0, 152, 305, 457, 610, and 762 mm) are extracted from the strain pulse. Using these offsets and the relevant gauge depth (6 in [152 mm]), a data base of strain values will be generated for the user-supplied range of acceptable moduli (an example of this data base is given later in this chapter). The measured tensile strains as shown in figure 38 are then compared with the calculated strains in the data base.

Stress Sensor

Stress sensors may be installed at various depths within the pavement layers. In theory, it should be feasible to simply take the maximum stresses from several stress sensors located at various depths and use these in the backcalculation procedure. However, the performance of current stress sensors

Thin Section
Dynatest, Station 9
50 mi/h

Distance from peak strain (in)	0	6	12	18	24	30
Tensile strain (microstrain)	-95	-82	-40	10	40	40



1 mi = 1.61 km
1 in = 25.4 mm
1 ft = .305 m

Figure 38. Typical strain response under a fully loaded single axle.
The table shows the measured strains at various offsets.

within pavements is open to question. Clearly, representative moduli will only be calculated from accurately measured pavement responses.

Multidepth Deflectometer

These deflection-based sensors can be located at various depths within each layer of the pavement. However, these devices present an added complication because they measure the relative movement between the sensor location and an anchor buried at some depth (in this project, 73 in [1 854 mm]) below the surface. The movement of the anchor must also be taken into account. This is accomplished within the generalized backcalculation procedure by calculating the theoretical anchor movement for each combination of layer moduli within the data base. Then, on entering the pattern search, the theoretical relative deflection (theoretical deflection at depth minus theoretical anchor movement) can be compared with the MDD readings.

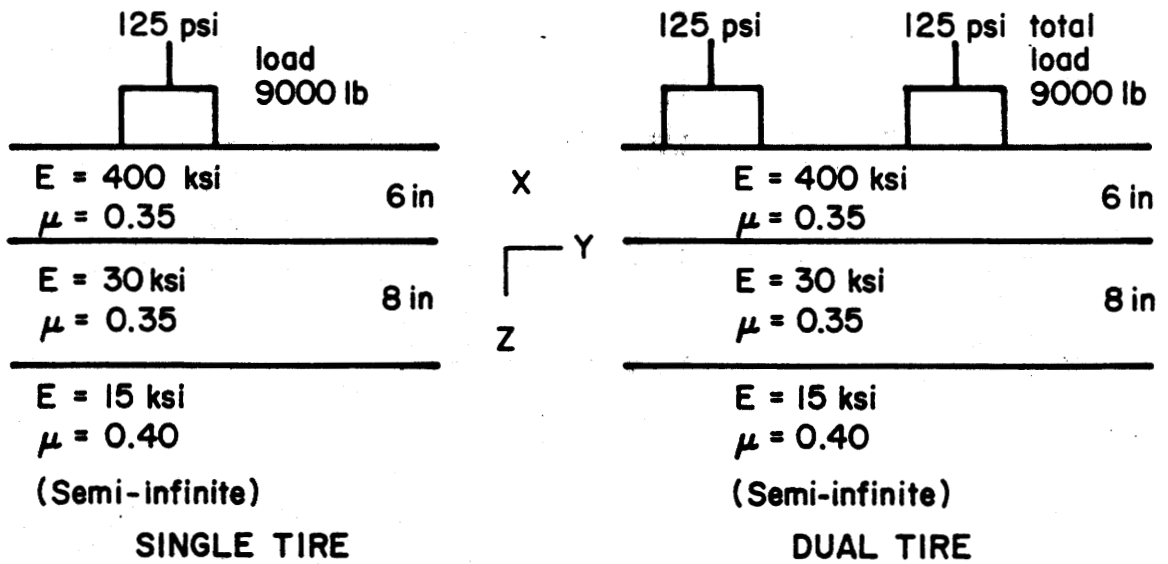
SENSITIVITY ANALYSIS

The PENMOD generalized layer backcalculation procedure uses stress, strain, or deflection measurements as input. Other inputs include layer thicknesses, wheel loads, and the radial offsets of the wheel to the gauges. The output is the set of layers moduli that minimizes error between measured and theoretically calculated strains or deflections.

In such a procedure, valid concerns exist regarding the effects of uncertainties in measuring several of the key input parameters, such as wheel position, on the backcalculation process. A sensitivity analysis was performed to quantify the impact of variations in each of the key variables.

The BISAR computer program was used to calculate interface tensile strains and depth deflections for the two test configurations shown in figure 39. The calculated strains and deflections for the single tire loading are shown in table 24.

In each sensitivity run, a single parameter was changed and all other parameters were held constant. For example, to study the effect of a 3-in



1 in = 25.4 mm

Figure 39. Test configurations for single and dual tire wheels.

Table 24. Calculated strains and deflections for the single tire loading configuration.

CALCULATED STRAINS (+TENSION)						
Offset from Center of Load (in)						
	0	6	12	18	24	30
x	0	6	12	18	24	30
y	0	0	0	0	0	0
z	6	6	6	6	6	6
E_t	272.6	67.8	-38.9	-44.2	-35.9	-26.6

CALCULATED DEPTH DEFLECTIONS						
Offset from Center of Load (in)						
	0	0	14	20	26	78
x	0	0	0	0	0	0
y	0	0	0	0	0	0
z	6	0	14	20	26	78
W_i	16.34	13.99	12.39	10.00	8.38	3.44
MDD*	12.93	10.58	8.98	6.59	4.97	

*The MDD measures the deflection relative to the anchor located at a depth of 78 in (1 981 mm).
1 in = 25.4 mm

(76-mm) offset in wheel position, the BISAR program was rerun with the wheel positioned 3 in (76 mm) from the strain gauge or MDD. The calculated strains for such a run are shown in table 25. These should be compared with those produced when the wheel ran directly over the gauge (see table 24). These values were then input into the modulus backcalculation scheme; it was assumed that the wheel ran directly over the gauge and that the best set of moduli had been calculated. Comparing these backcalculated values with the known input values ($E_1 = 400$, $E_2 = 30$, $E_3 = 15$) permits an estimation of the error associated with a measurement error of 3 in (76 mm) in lateral positioning.

Table 25. Calculated strains for the 3-in (76-mm) lateral offset.

	Offset from Center of Load (in)					
	0	6	12	18	24	30
x	0	6	12	18	24	30
y	3	3	3	3	3	3
z	6	6	6	6	6	6
E_t	250.0	68.6	-32.6	-41.5	-34.6	-25.9

1 in = 25.4 mm

The computations performed in the sensitivity analysis are described in table 26. The results of the sensitivity analysis are shown in tables 27 through 30.

SYSTEMATIC ERROR ANALYSIS

Based on the results presented in tables 27 through 30, the following conclusions can be drawn:

- In order of decreasing significance, the most important test parameters are:
 1. Surface Thickness.
 2. Wheel Positioning.
 3. Load.
 4. Error in Readings.

Table 26. Descriptions of sensitivity analysis runs.

Run	Description
1	Input calculated values and correct layer thicknesses to establish accuracy of backcalculation scheme.
2	Increase calculated response by 1% (one-directional error); all other parameters remain fixed to simulate a measurement error.
3	Increase calculated response by 5% (one-directional error).
4	Increase calculated response by 10% (one-directional error).
5	Increase wheel offset by 1 in. Rather than running directly over the gauge, assume the center of the tire missed the center of the gauge by 1 in. In the case of dual tires, the center point of the duals missed the center of the gauge by 1 in.
6	Increase wheel offset to 3 in.
7	Increase surface thickness by 10% from 6 to 6.6 in.
8	Decrease surface thickness by 10% from 6 to 5.4 in.
9	Increase base thickness by 10% from 8 to 8.8 in.
10	Decrease base thickness by 10% from 8 to 7.2 in.
11	Increase wheel loads by 10%, simulating problems with dynamic loading.
12	Decrease load by 10%.
13	Use fewer sensor readings. Use only three strain and deflection readings as input to calculation process (use strains at 0, 12, and 24 in and deflections at 6, 14, and 26 in only).

1 in = 25.4 mm

Table 27. Sensitivity analysis on strain data/single tire used to backcalculate layer moduli (known: $E_1 = 400$ ksi, $E_2 = 30$ ksi, $E_3 = 15$ ksi).

Backcalculation Results								
Test	Parameter	E_1	% Error	E_2	% Error	E_3	% Error	Absolute Average Error %
1	Calculated strains	406	+1.5	30.6	+2.0	14.8	-1.3	1.6
2	Strains +1%	404	+1	30.1	+0.3	14.8	-1.3	0.9
3	Strains +5%	385	-3.7	29.1	-3.0	14.1	-6.0	4.2
4	Strains +10%	365	-8.7	27.7	-7.6	13.2	-12.0	9.4
5	Offset +1 in	414	+3.5	30.4	+1.3	15.0	0.0	1.6
6	Offset +3 in	481	20.2	28.0	-6.6	16.5	+10.0	12.2
7	Surfacing thickness +10%	653	63.2	32.8	+9.3	18.8	+25.3	32.6
8	Surfacing thickness -10%	383	-4.2	27.7	-7.6	15.0	+0.0	3.9
9	Base thickness +10%	403	+0.7	31.4	+4.7	15.2	+1.3	2.2
10	Base thickness -10%	402	+0.5	32.2	+7.3	15.0	+0.0	2.6
11	Load 10%	384	-4.0	26.1	-12.9	14.1	-6.0	7.6
12	Load -10%	432	+8.0	36.6	+22.0	15.6	+4.0	11.3
13	Use only three	406	+1.5	30.4	+1.3	14.7	-2.0	1.6

1 in = 25.4 mm

Table 28. Sensitivity analysis on multidepth deflectometer data/single tire used to backcalculate layer moduli (known: $E_1 = 400$ ksi, $E_2 = 30$ ksi, $E_3 = 15$ ksi).

Test	Parameter	Backcalculation Results						Absolute Average Error %
		E_1	% Error	E_2	% Error	E_3	% Error	
1	Calculated deflections	387	-3.2	31.5	+5.0	15.1	+0.6	2.9
2	Deflections +1%	385	-3.7	31.1	+3.7	14.9	-0.6	2.7
3	Deflections +5%	368	-8.0	30.0	+0.0	14.4	-4.0	4.0
4	Deflections +10%	349	-12.7	28.8	-4.0	13.7	-8.7	8.5
5	Offset +1 in	412	+3.0	30.3	+0.7	14.9	-0.6	1.4
6	Offset +3 in	453	+13.2	32.6	+8.6	14.6	-2.7	8.2
7	Surfacing thickness +10%	515	+28.7	31.2	+4.0	14.9	-0.6	11.1
8	Surface thickness -10%	308	-23.0	31.6	+5.3	15.0	+0.0	9.4
9	Base thickness 10%	442	+10.5	28.4	-5.3	15.0	+0.0	5.3
10	Base thickness -10%	438	+9.5	33.0	+10.0	16.7	+11.3	10.2
11	Load +10%	360	-10.0	28.8	-4.0	13.6	-9.3	7.8
12	Load -10%	439	+9.7	33.0	+10.0	16.7	+11.3	10.3
13	Use only three MDD's (6, 14, 26 in)	384	-4.0	31.7	+5.7	15.1	+0.6	3.4

1 in = 25.4 mm

Table 29. Sensitivity analysis on strain data/dual tires used to backcalculate layer moduli (known: $E_1 = 400$ ksi, $E_2 = 30$ ksi, $E_3 = 15$ ksi).

Backcalculation Results								
Test	Parameter	E_1	% Error	E_2	% Error	E_3	% Error	Absolute Average Error %
1	Calculated strains	412	+3.0	32.1	+7.0	15.0	+0.0	3.3
2	Strains +1%	409	+2.2	29.8	-0.7	14.8	-1.3	3.3
3	Strains +5%	390	-2.5	28.7	-4.3	14.3	-4.7	3.8
4	Strains +10%	371	-7.2	27.3	-9.0	13.7	-8.7	8.3
5	Offset +1 in	405	+1.2	30.8	+2.7	14.6	+4.0	2.6
6	Offset +3 in	342	-14.5	36.4	-21.3	12.2	-18.7	18.2
7	Surfacing thickness +10%	660	+65.0	32.5	+8.3	19.6	+30.6	34.6
8	Surfacing thickness -10%	376	-6.0	28.0	-6.7	14.8	-1.3	4.7
9	Base thickness 10%	402	+0.5	31.0	3.3	15.4	-2.7	2.2
10	Base thickness -10%	418	+4.5	28.9	-3.7	14.8	-1.3	3.2
11	Load +10%	376	-6.0	26.9	-10.3	13.9	-7.3	7.9
12	Load -10%	458	+14.5	33.9	+13.0	16.4	+16.0	14.5
13	Use only three MDD's (6, 14, 26 in)	411	+2.7	30.0	+0.0	14.9	-0.6	1.1

1 in = 25.4 mm

Table 30. Sensitivity analysis on multidepth deflectometer data/dual tires used to backcalculate layer moduli (known: $E_1 = 400$ ksi, $E_2 = 30$ ksi, $E_3 = 15$ ksi).

Test	Parameter	Backcalculation Results						Absolute Average Error %
		E_1	% Error	E_2	% Error	E_3	% Error	
1	Calculated deflections	391	-2.2	30.7	+2.3	15.1	+0.7	1.7
2	Deflections +1%	379	-5.2	30.8	+2.7	15.0	+0.0	2.6
3	Deflections +5%	363	-9.2	29.6	-1.3	14.4	-4.0	4.8
4	Deflections +10%	348	-13.0	28.3	-5.7	13.8	-8.0	8.9
5	Offset +1 in	400	+0.0	30.2	+0.7	15.0	+0.0	0.2
6	Offset +3 in	409	+2.2	28.3	-5.7	15.3	+2.0	3.3
7	Surfacing thickness +10%	517	-29.2	32.6	+8.6	14.8	-1.3	13.0
8	Surface thickness -10%	300	-25.0	29.5	-1.7	15.2	+1.3	9.3
9	Base thickness 10%	462	+15.5	29.3	-2.3	14.8	-1.3	6.3
10	Base thickness -10%	380	-5.0	29.1	-3.0	15.2	+1.3	3.1
11	Load +10%	348	-13.0	28.6	-4.7	13.7	-8.7	8.8
12	Load -10%	430	+7.5	34.2	+14.0	16.8	+12.0	11.2
13	Use only three MDD's (6, 14, 26 in)	394	-1.5	30.5	+1.7	15.1	+0.6	1.3

1 in = 25.4 mm

The surface thickness is relatively easy to measure accurately. However, wheel position, load, and any errors in the readings are often difficult to measure.

- The results of computation were better with the deflection data than with the strain data in that they were stable under both single and dual tire loads. The performance under a wheel positioning error of 3 in (76 mm) for the strain values resulted in average single and dual tire errors of 12.2 and 18.2 percent, respectively, and the corresponding deflection errors were 8.2 and 3.3 percent. This implies that to obtain repeatable modulus values from strain measurements, the lateral offset should be measured with a margin of error of less than 3 in (76 mm). The 1-in (25-mm) offset did not cause significant errors in all cases.
- A variation in load of 10 percent produced a similar variation (8 to 12 percent) in the average backcalculated modulus values.
- When fewer sensor values (three) were used, the error percentages were similar to those obtained using the full set. In two cases, the error was reduced when fewer sensor values were used.

RANDOM ERROR ANALYSIS

The first part of the sensitivity analysis dealt with the systematic type errors that were introduced into the measurements of the strain and deflection gauges. This section deals with the effect of random errors on the backcalculated modulus values. Four sets of six random numbers were generated based on a mean of 0.0 and a standard deviation of 1.0. The random numbers were then transformed into random errors for the levels of 1, 5, and 10 percent of the strain values. In order to clearly identify the effect of error percentage, the same set of random numbers was used for all three levels. The sensitivity analysis was conducted using the same approach as for the systematic error case. The original moduli were used to calculate the strain basins under single and dual tires for the same pavement structure used with the systematic error analysis. Table 31 shows the strain basins corresponding to random errors levels of 1, 5, and 10 percent under single tire loading. Table 32 shows the effect of random error on the backcalculated moduli under single tire loading. Tables 33 and 34 show the strain basins for random error levels of 1, 5, and 10 percent and the backcalculated moduli under dual tire loading, respectively.

Table 31. Strain basins generated from random errors for single tire load.

	Offset from Center of Load (in)					
	0	6	12	18	24	30
X	0	6	12	18	24	30
Y	0	0	0	0	0	0
Z	6	6	6	6	6	6
Original Strain Basin	273	68	-39	-44	-36	-27
1% random error	276	67	-39	-44	-36	-27
	273	68	-39	-43	-36	-27
	275	68	-39	-45	-36	-27
	274	67	-39	-45	-36	-27
5% random error	289	66	-40	-42	-35	-27
	276	70	-39	-39	-35	-29
	286	68	-37	-47	-36	-26
	277	65	-37	-46	-34	-27
10% random error	305	63	-42	-40	-34	-28
	280	72	-39	-34	-34	-31
	299	69	-36	-50	-36	-25
	281	62	-44	-49	-32	-26

1 in - 25.4 mm

Table 32. Effect of random errors on the backcalculated moduli for single tire load (known moduli: $E_1 = 40$ ksi, $E_2 = 30$ ksi, $E_3 = 15$ ksi).

Backcalculation Moduli							
Random Error Level	E_1	% Error	E_2	% Error	E_3	% Error	Absolute Average Error %
1%	398	-0.5	29.3	-2.3	16.0	+6.7	3.2
	398	-0.5	29.5	-1.7	15.2	+1.3	1.2
	406	+1.5	28.3	-5.7	16.4	+4.7	4.0
	400	0.0	29.2	-2.7	16.4	+4.7	2.5
5%	358	-10.5	33.2	+10.7	12.5	-16.7	12.6
	371	-7.3	32.9	+9.7	11.3	-24.7	13.9
	400	0.0	29.0	-3.3	15.6	+4.0	2.4
	423	+5.75	27.9	-7.0	18.1	+20.7	11.2
10%	319	-20.3	37.1	+23.7	9.8	-34.7	26.2
	333	-16.8	37.7	+25.7	7.5	-50.0	30.8
	398	-0.5	29.3	-2.3	14.9	-0.7	1.2
	350	-12.5	34.0	+13.3	15.2	+1.3	9.0

Table 33. Strain basins generated from random errors for dual tire load.

	Offset from Center of Load (in)					
	0	6	12	18	24	30
X	0	6	12	18	24	30
Y	0	0	0	0	0	0
Z	6	6	6	6	6	6
Original Strain Basin	177	67	-14	-32	-30	-23
1% random error	179	67	-14	-32	-30	-23
	178	68	-14	-31	-29	-24
	179	67	-14	-32	-30	-23
	178	67	-14	-32	-29	-23
5% random error	189	65	-15	-30	-29	-24
	179	69	-14	-28	-29	-25
	186	68	-14	-34	-30	-22
	180	64	-15	-33	-28	-23
10% random error	198	63	-15	-29	-29	-24
	181	71	-14	-24	-28	-27
	194	68	-13	-36	-30	-21
	183	61	-16	-35	-27	-23

1 in = 25.4 mm

Table 34. Effect of random errors on the backcalculated moduli for dual tire load (known moduli: $E_1 = 40$ ksi, $E_2 = 30$ ksi, $E_3 = 15$ ksi).

Random Error Level	Backcalculation Moduli						Absolute Average Error %
	E_1	% Error	E_2	% Error	E_3	% Error	
1%	391	-2.3	32.5	8.3	13.6	-9.3	6.6
	389	-2.8	32.6	8.7	13.4	-10.7	7.4
	402	0.5	31.6	5.3	14.2	-5.3	3.7
	399	-0.3	31.9	6.3	14.3	-4.7	3.8
5%	344	-14.0	35.9	19.7	11.1	-26.0	19.9
	336	-16.0	36.9	23.0	10.0	-33.3	24.1
	396	-1.0	31.7	5.7	13.7	-8.7	5.1
	385	-3.75	33.2	11.0	14.3	-4.7	6.5
10%	294	-15.0	39.2	30.7	8.8	-41.3	29.0
	270	-32.5	41.7	39.0	6.6	-56.0	42.5
	390	-2.5	32.0	6.7	13.0	-13.3	7.5
	360	-10.0	35.5	18.3	13.7	-8.7	12.3

The data shown in tables 32 and 34 show that the effect of 1-percent random error is negligible at all levels of layers moduli (i.e, surface, base, and subgrade). On the other hand, the effects of the 5-percent and 10-percent random error are significant at all levels of layers moduli. In deciding whether this type of error is important or not, one must evaluate the source of the random error. In this respect, the only source of random error can be from the rounding off of the A/D board data when the data were collected in the field. The 12-bit boards used in this project have 4,096 levels within a range of ± 5 V. The typical strain gauge calibration factor was around 500 microstrains/V. This indicates that each mid-level represents 0.6 microstrains, or less than 1 percent of the measured values. Based on this analysis, one can conclude that the effects of random error on the backcalculated moduli are insignificant.

MODULUS BACKCALCULATION USING MDD DATA COLLECTED UNDER A FALLING WEIGHT DEFLECTOMETER

In order to evaluate the layer moduli for the thick and thin pavement sections, deflections were measured using a falling weight deflectometer. Later in this report, analysis will focus on determining layer moduli from tensile strain and deflections measured under truck loads. While it is acknowledged that it will not be possible to directly compare these layer moduli, a comparison of moduli calculated under FWD and truck analyses should show similar trends. For example, if a weak base is detected using the FWD, then a weak base should also be evident in the truck analysis.

The FWD was positioned directly over the multidepth deflectometers and drops were made at three different load levels. Deflections were simultaneously measured on the surface and at the MDD locations; the results are shown in tables 35 and 36. A review of the normalized deflections indicates very little evidence of nonlinear behavior.

Traditional analysis of the surface deflection of the entire pavement using a layer modulus backcalculation program resulted in the average layer moduli shown in table 37. These results showed extremely low values for the base course of both sections, particularly in the thin pavement. In order to

Table 35. FWD and MDD test results from the thin pavement section.

Drop #	Load (lb)	FWD Deflections (mils)						MDD (mils)		
		0	12	24	32.5	48	-12	6.5	14.5	26.5
1	7,310	12.68	8.46	4.74	3.03	1.26	8.54	11.19	7.64	2.57
2	8,606	15.47	10.51	5.94	3.74	1.52	10.59	13.68	9.78	3.18
3	10,271	18.54	12.64	7.21	4.53	1.85	12.79	16.67	12.04	3.81

Drop #	Load (lb)	Normalized Deflections (mils/kip)						mils/kip		
		0	12	24	32.5	48	-12	6.5	14.5	26.5
1	7,310	1.73	1.16	0.65	0.41	0.17	1.17	1.53	1.04	0.35
2	8,606	1.80	1.22	0.69	0.43	0.18	1.23	1.59	1.13	0.37
3	10,271	1.83	1.23	0.70	0.44	0.18	1.24	1.62	1.17	0.37

1 lb - 4.5 N

Table 36. FWD and MDD test results from the thick pavement section.

Drop #	Load (lb)	FWD Deflections (mils)						MDD (mils)			
		0	12	24	32.5	48	-12	3	10	20	32
1	7,495	5.51	3.15	1.97	1.34	1.26	3.38	4.74	3.71	2.05	1.09
2	8,698	6.85	3.98	2.44	1.65	1.52	4.33	5.81	4.58	2.56	1.36
3	10,271	8.07	4.84	2.95	2.01	1.10	5.24	6.91	5.54	3.02	1.59

Drop #	Load (lb)	Normalized Deflections (mils/kip)						mils/kip			
		0	12	24	32.5	48	-12	3	10	20	32
1	7,495	0.73	0.42	0.26	0.18	0.09	0.45	0.63	0.49	0.35	0.14
2	8,698	0.78	0.46	0.28	0.19	0.10	0.49	0.67	0.53	0.37	0.16
3	10,271	0.78	0.47	0.29	0.19	0.11	0.51	0.67	0.54	0.37	0.15

1 lb = 4.5 N

validate these moduli values, it was decided that the analysis should be expanded to include the depth deflections as well as the surface deflections in the analysis scheme. This modification is discussed in the following paragraphs.

Table 37. Layer moduli backcalculated using surface deflections only.

Pavement	AC Modulus (ksi)	Base Modulus (ksi)	Subgrade Modulus (ksi)
Thin	409	5.3	20.3
Thick	427	11.9	26.7

The thin section surface and depth deflections shown in table 35 were used to backcalculate the layer moduli, and the results are shown in tables 38 and 39. Table 38 shows the consequences of using only the surface deflections to backcalculate the layer moduli values. The base modulus is very low and there is a large discrepancy between the measured and predicted depth deflections. The LVDT-measured deflection at the bottom of the base (14.5 in [368 mm]) was underpredicted, while the LVDT-measured deflection in the subgrade (26.5 in [673 mm]) was overpredicted. To correct this situation, the pavement was remodeled as a four-layer system with the introduction of a 12-in (305-mm) subbase layer. The analysis was repeated and the results are shown in table 39. This shows a much better agreement between measured and computed bowls for both the surface and at various depths. Table 39 shows the modulus of the asphalt layer to decrease slightly as load increases; the moduli of the base and subgrade are fairly constant. The modulus of the base (23,000 psi [158,621 kPa]) is representative of a fair-to-good base under wet conditions.

This analysis was repeated for the thick section and the results are shown in tables 40 and 41. In this case, the inclusion of the 12-in (305-mm) subbase reduced the error-per-sensor value but did not have a major impact on the backcalculated layer moduli.

Table 38. Layer moduli backcalculated using a three-layer system and surface deflections only (thin pavement).

Load (lb)		Deflections (mils)									Elastic Moduli (ksi)			
		FWD					MDD			E ₁	E ₂	E ₃	E ₄	
		0	12	24	32.5	48	6.5	14.5	26.5					
7,310	M	12.68	8.50	4.74	3.03	1.26	11.19	7.64	2.57	474.7	8.0	-	22.2	
	C	13.24	8.63	4.47	2.78	1.33	10.74	5.18	3.13					
	E%	-4.43	-1.55	5.65	8.21	-5.29	4.04	32.15	-21.97					
8,606	M	15.47	10.55	5.94	3.74	1.53	13.68	9.78	3.18	453.3	7.6	-	21.2	
	C	16.32	10.64	5.51	3.43	1.64	13.24	6.39	3.86					
	E%	-5.51	-.85	7.20	8.34	-6.87	3.24	34.66	-21.50					
10,271	M	18.54	12.72	7.21	4.53	1.85	16.67	12.04	3.81	452.7	7.4	-	21.0	
	C	19.68	12.86	6.67	4.15	1.98	15.96	7.68	4.65					
	E%	-6.14	-1.07	7.46	8.40	-6.77	4.24	36.24	-22.08					

M - Measured deflection in mils
 C - Computed deflection in mils
 1 lb = 4.5 N

Table 39. Layer moduli backcalculated using a four-layer system and both surface and depth deflections (thin pavement).

Load (lb)	Deflections (mils)									Elastic Moduli (ksi)			
	FWD					MDD							
	0	12	24	32.5	48	6.5	14.5	26.5	E ₁	E ₂	E ₃	E ₄	
7,310	M	12.68	8.50	4.74	3.03	1.26	11.19	7.64	2.57	488.6	27.7	6.1	26.0
	C	12.89	8.70	4.76	2.98	1.26	10.77	7.68	2.57				
	EX	-1.65	-2.32	-.48	1.62	-.25	3.71	-.54	.17				
8,606	M	15.47	10.55	5.94	3.74	1.53	13.68	9.78	3.18	446.8	23.3	5.6	25.1
	C	16.01	10.75	5.88	3.68	1.56	13.39	9.64	3.13				
	EX	-3.50	-1.93	.96	1.56	-1.72	2.10	1.43	1.42				
10,271	M	18.54	12.72	7.21	4.53	1.85	16.67	12.04	3.81	428.8	24.7	5.4	25.0
	C	19.39	12.99	7.12	4.46	1.89	16.23	11.79	3.75				
	EX	-4.16	-2.16	1.26	1.50	-1.95	2.64	2.11	1.70				

M - Measured deflection in mils
 C - Computed deflection in mils
 1 lb = 4.5 N

Table 40. Layer moduli backcalculated using a three-layer system and surface deflections only (thick pavement).

Load (lb)		Deflections (mils)										Elastic Moduli (ksi)			
		FWD					MDD					E ₁	E ₂	E ₃	E ₄
		0	12	24	32.5	48	3	10	20	32					
7,310	M	5.51	3.26	1.97	1.34	.71	4.74	3.71	2.05	1.09	396.6	29.2	-	45.7	
	C	5.47	3.30	1.93	1.32	.71	4.50	3.88	1.97	1.16					
	EX	.64	-1.33	2.21	1.46	.34	5.02	-4.55	4.07	-6.70					
8,606	M	6.85	4.15	2.44	1.65	.91	5.81	4.58	2.56	1.36	374.4	27.7	-	42.0	
	C	6.78	4.11	2.41	1.66	.89	5.56	4.80	2.46	1.46					
	EX	1.07	1.03	1.32	-.42	1.82	4.25	-4.77	3.85	-7.04					
10,271	M	8.07	5.04	2.95	2.01	1.10	6.91	5.54	3.02	1.59	396.0	24.3	-	41.7	
	C	8.03	4.97	2.94	2.02	1.08	6.62	5.76	2.87	1.72					
	EX	.47	1.33	.48	-.39	2.14	4.19	-4.05	5.01	-7.90					

1 lb = 4.5 N

Table 41. Layer moduli backcalculated using a four-layer system and both surface and depth deflections (thick pavement).

Load (lb)		Deflections (mils)										Elastic Moduli (ksi)			
		FWD					MDD					E ₁	E ₂	E ₃	E ₄
		0	12	24	32.5	48	3	10	20	32					
7,310	M	5.51	3.26	1.97	1.34	.71	4.74	3.71	2.05	1.09	409.6	30.9	35.7	48.3	
	C	5.44	3.32	1.95	1.33	.70	4.49	3.88	2.06	1.11					
	E _X	1.32	-1.77	1.13	.55	1.17	5.35	-4.61	-.73	-1.80					
8,606	M	6.85	4.15	2.44	1.65	.91	5.81	4.58	2.56	1.36	384.6	29.4	33.4	44.2	
	C	6.74	4.12	2.43	1.67	.89	5.55	4.80	2.58	1.39					
	E _X	1.65	.69	.39	-1.22	2.54	4.55	-4.79	-.65	-2.49					
10,271	M	8.07	5.04	2.95	2.01	1.10	6.91	5.54	3.02	1.59	411.1	25.8	31.5	44.3	
	C	7.97	5.00	2.97	2.04	1.07	6.60	5.77	3.03	1.63					
	E _X	1.23	.88	-.70	-1.40	3.01	4.53	-4.14	-.46	-2.37					

1 lb = 4.5 N

The above results demonstrate the benefit of having sensors in the pavement while attempting to characterize the layer's properties. Using surface deflections alone, the thin pavement would have been incorrectly characterized as having extremely low base values when in fact the weak layer was at the top of the subgrade. A very important conclusion, drawn from these results, is therefore that both pavement surface and interior deflection measurements are necessary for accurate calculation of pavement layer moduli.

In the analysis of strain and deflection data that follows, both pavements will be modeled as four-layer systems and the results obtained will be compared with those obtained under the FWD analysis.

MODULUS BACKCALCULATION USING SENSOR DATA COLLECTED UNDER TRUCK LOADING

In this section the PENMOD program is used to process the strain basins and multidepth deflections in order to backcalculate in situ resilient moduli. The overall analysis is broken into the following three steps:

1. Backcalculation of in situ moduli from the measured strain basins.
2. Backcalculation of in situ moduli from the measured MDD deflections.
3. Backcalculation of in situ moduli from the combination of the measured strain basins and MDD deflections.

All the backcalculation analyses are conducted based on measurements under the single drive axle. The following represents a brief discussion of each analysis.

BACKCALCULATION OF IN SITU MODULI FROM THE MEASURED STRAIN BASINS

The strains at the bottom of the asphalt concrete layer were collected from three different types of gauges, namely, Kyowa gauges, Dynatest gauges, and instrumented core gauges. The Dynatest gauges installed in the thick section were unoperational during the stage II testing; therefore, the backcalculated moduli of the thick section are based only on the measurements of the Kyowa and core gauges. In the case of the thick section, the

measurements from the Kyowa gauge installed at station 6 and the core gauge installed at station 12 were selected for the backcalculation process. Tables 42 and 43 summarize the values of the backcalculated moduli as a function of the truck speed and load for the thick and thin sections. The data show good agreement between the two types of gauges (i.e., Kyowa and core gauges). The effect of speed on the moduli of the asphalt concrete layer (E_1) is very noticeable under all load levels. The effect of load magnitude on the backcalculated moduli is insignificant, which implies a linear response.

Tables 44 and 45 summarize the backcalculation results of the thick and thin sections based on the measurements from all three types of gauges. In this case, less agreement is evident in the results obtained from the various gauges in the thin section than that demonstrated by the thick section data. The effect of truck speed on the backcalculated moduli of the asphalt concrete layer is very significant, while the effect of load level is insignificant. The data in table 43 have consistently shown that the highest moduli values were calculated from the core gauge measurements. While the Dynatest gauge produced the second highest moduli, the Kyowa gauge produced the lowest moduli values for all combinations of truck speed and load level.

BACKCALCULATION OF IN SITU MODULI FROM THE MEASURED MDD DEFLECTIONS

As discussed earlier in the report, one MDD was installed in each test section (thick and thin). The MDD in the thick section had four modules at depths of 3, 10, 20, and 32 in (76, 254, 508, and 813 mm), and the MDD in the thin section had three modules at depths of 6.5, 14.5, and 26.5 in (165, 368, and 673 mm). In the case of the MDD, the peak deflections at each level were used to backcalculate the in situ moduli. Tables 44 and 45 summarize the in situ moduli for the thick and thin sections, respectively.

BACKCALCULATION OF IN SITU MODULI FROM THE COMBINATION OF THE MEASURED STRAIN BASINS AND MDD DEFLECTIONS

The results discussed above indicated that neither the multidepth deflectometer nor strain gauges alone provided sufficient information to characterize the layer properties of the instrumented section. Consequently,

Table 42. Backcalculated moduli for the thick section under the single drive axle, based on the strain measurements.

Speed (mi/h)	Load (kips)	Station (strain gauge)	E_1 (ksi)	E_2 (ksi)	E_3 (ksi)	E_4 (ksi)
50	20	6 (k)	545	10	7	60.0
		12 (c)	461	10	5	60.0
	12	6 (k)	556	10	6.6	60.0
		12 (c)	640	10	12.8	60.0
	8	6 (k)	534	10	6.9	60.0
		12 (c)	641	10	12.9	60.0
35	20	6 (k)	350	10	5	43.9
		12 (c)	366	10	5	60.0
	12	6 (k)	347	10	5	39.0
		12 (c)	349	10	5	41.0
	8	6 (k)	393	10	11	60.0
		12 (c)	361	10	5	60.0
20	10	6 (k)	258	10	16	60.0
		12 (c)	230	10	11.1	60.0
	12	6 (k)	214	18	40	60.0
		12 (c)	200	22	40	60.0
	8	6 (k)	200	21	40	60.0

k - Kyowa gauge
c - core gauge
1 mi - 1.61 km

Table 43. Backcalculated moduli for the thin section under the single drive axle, based on the strain measurements.

Speed (mi/h)	Load (kips)	Station (strain gauge)	E ₁ (ksi)	E ₂ (ksi)	E ₃ (ksi)	E ₄ (ksi)
50	20	30 (d)	758	10.0	5.0	10.0
		29 (k)	675	10.0	5.0	10.0
		12 (c)	1170	10.0	5.0	18.0
	12	30 (d)	900	12.0	5.0	10.0
		29 (k)	896	10.0	5.0	10.0
		12 (c)	1500	44.0	5.0	34.6
	8	30 (d)	900	14.8	5.0	10.0
		29 (k)	764	10.0	5.0	10.0
		12 (c)	1500	23.1	5.0	37.8
35	20	30 (d)	511	10.0	5.0	10.0
		29 (k)	425	10.0	5.0	10.0
		12 (c)	828	10.0	5.0	10.0
	12	30 (d)	700	10.0	5.0	10.0
		29 (k)	568	10.0	5.0	10.0
		12 (c)	1368	10.0	7.7	60.0
	8	30 (d)	855	10.0	5.0	10.0
		29 (k)	703	10.0	5.0	10.0
		12 (c)	1339	10.0	5.5	60.0
20	20	30 (d)	329	10.0	10.0	60.0
		29 (k)	298	10.0	8.0	60.0
		12 (c)	368	10.0	12.2	60.0
	12	30 (d)	329	13.5	40.0	60.0
		29 (k)	302	10.0	10.7	59.7
		12 (c)	420	19.7	40.0	60.0
	8	30 (d)	---	----	----	----
		29 (k)	233	18.6	14.7	10.0
		12 (c)	431	10.0	14.8	50.1

d - Dynatest gauge
k - Kyowa gauge
c - core gauge
1 mi - 1.61 km

Table 44. Backcalculated moduli for the thick section under the single drive axle, based on the MDD measurements.

Speed (mi/h)	Load (kips)	E ₁ (ksi)	E ₂ (ksi)	E ₃ (ksi)	E ₄ (ksi)
50	20	363	10.3	23.9	50.0
35	20	340	10.0	22.7	50.0
20	20	200	12.2	23.4	50.0

1 mi - 1.61 km

Table 45. Backcalculated moduli for the thin section under the single drive axle, based on the MDD measurements.

Speed (mi/h)	Load (kips)	E ₁ (ksi)	E ₂ (ksi)	E ₃ (ksi)	E ₄ (ksi)
50	20	200	11.8	9.1	47.1
	12	900	10.0	13.4	41.0
	8	900	25.4	25.0	50.0
35	20	551	10.0	8.5	50.0
	12	900	11.8	19.2	41.0
	8	900	11.4	17.8	50.0
20	20	201	11.2	8.8	44.1
	12	900	10.0	11.4	41.0
	8	900	12.7	22.0	50.0

1 mi - 1.61 km

it was decided to investigate if by combining strain and deflection data an iterative scheme could be developed by which more accurate layer moduli could be determined. The data set chosen for evaluation is shown in table 46. These data were measured on the thick pavement section using a fully loaded truck with single drive axle and 125 psi (863 kPa) tire pressure. The data represent the peak depth deflections and strain bowls measured under the single axle (19.6 kips [86.2 kN] on dual tires). The strains were measured with the Kyowa gauge and were thought to be representative of the entire section.

Table 46. Strain and deflection data used in analysis.

Speed (mi/h)	MDD Deflections (mils)			Strain Gauge (microstrain)			
	Depths (in)			Offset (in)			
	3	20	31	0	6	12	24
20	8.46	3.36	1.56	155.4	100.7	10.7	-45.4
35	7.50	2.81	1.34	120.8	99.6	38.7	-41.5
50	6.98	2.74	1.37	79.9	69.1	40.9	-23.5

1 in = 25.4 mm
1 mi = 1.61 km

The plot of the MDD deflection bowl as the wheel approaches is shown in figure 40. An initial concern was that with this and other collected data sets the relationship between deflection and speed was relatively constant (or decreasing slightly), whereas the relationship with the strain was very different. As the speed increased from 20 mi/h (32 km/h) to 50 mi/h (80 km/h), the measured tensile strains at the bottom of the asphalt would decrease by a factor of two or more. This is similar to the findings of other researchers.^[9] This apparent discrepancy is explained by measuring the radius of curvature of the deflection basin. A useful indicator of curvature is the "surface curvature index," which is defined as the difference between

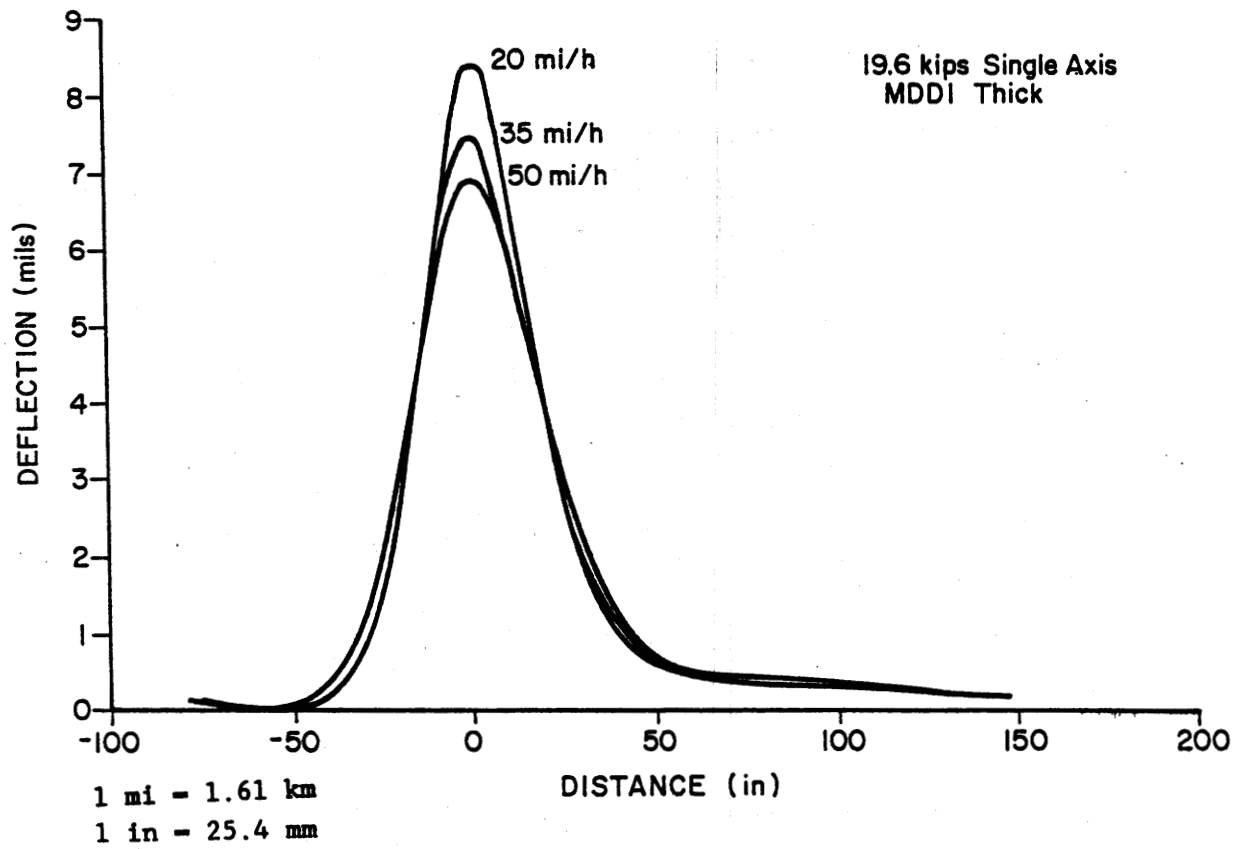


Figure 40. Typical responses of the top MDD for different truck speeds.

the maximum deflection (when the wheel is directly over the sensor) and the deflection present when the wheel is 1 ft (0.3 m) away from the sensor. At 50 mi/h (80 km/h) the surface curvature index was 1.8, whereas at 20 mi/h (32 km/h) it was 3.0. This indicates that the radius of curvature would be much smaller under the 20 mi/h (32 km/h) speed and the measured strains would be much higher.

The analysis procedure consists of using the PENMOD program in an iterative mode. Basically, the strain gauge data are used to obtain the modulus value for the surface layer, and the multidepth deflections are used for determining E values for the base, subbase, and subgrade layer. A four-layer structure was assumed, as shown in figure 41.

The procedure consists of using PENMOD as follows:

- Step 1: Fix the E_1 value calculated from the strain bowl; use the MDD data to calculate E_2 , E_3 , and E_4 values.
- Step 2: Fix the E_2 , E_3 , and E_4 values calculated in step 1; use the strain data to calculate an E_1 value.

Steps 1 and 2 are repeated until the error between measured and computed deflection and strain values is reduced to an acceptable level. The results of this analysis are shown in table 47. At each speed level, two iterations were used. The surface modulus showed some distinct speed effects; the base and subbase were weak, and the subgrade was relatively strong.

CONCLUSIONS AND RECOMMENDATIONS

Based on the backcalculation analyses from the strains, deflections, and combinations of strains and deflections data, the following conclusions can be drawn:

1. The backcalculation program is stable and produces repeatable results. This was demonstrated by the sensitivity analysis, which showed that the original strain and deflection basins were reproduced with an average error of less than 2 percent.

LOAD 9,820 lb
PRESSURE 125 psi

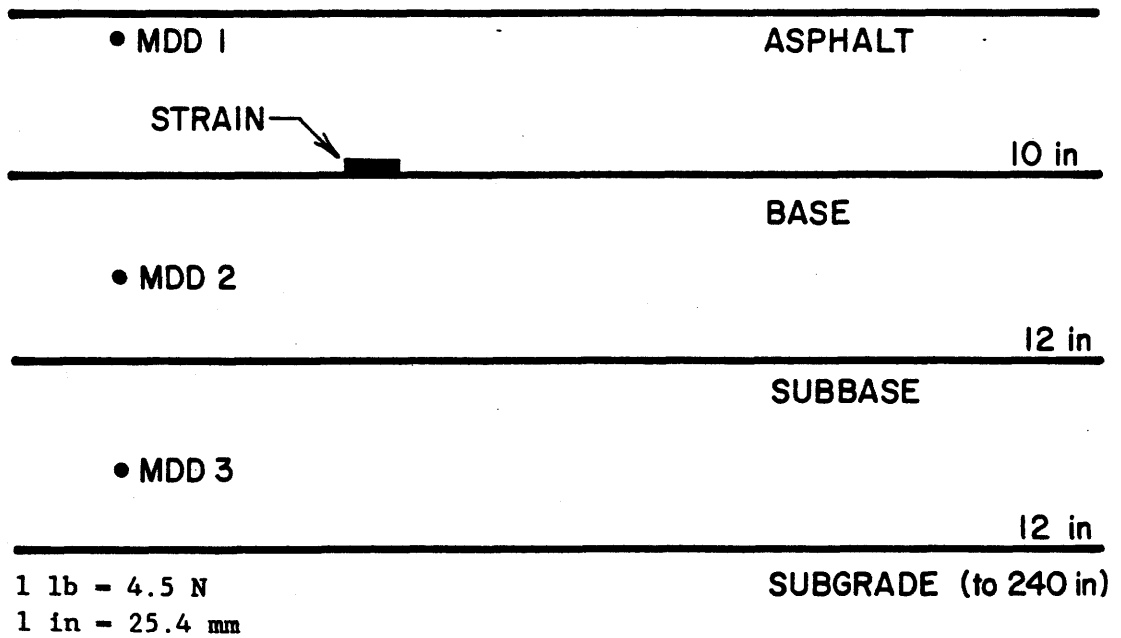


Figure 41. Setup of MDD and strain gauge for pavement layers moduli evaluation.

Table 47. Layer moduli values backcalculated using both deflection and strain data.

Speed (mi/h)	Description	MDD (mils) Depths			Max. Strain (microstrain)	Moduli (ksi)				No. Iteration
		3 in	20 in	32 in		E ₁	E ₂	E ₃	E ₄	
20	Measured	8.46	3.36	1.56	155.4	291	8.9	18.7	44.2	2
	Calculated	8.46	3.36	1.56	171.0					
	% Error	0.0	0.0	0.0	-10.0					
35	Measured	7.50	2.81	1.34	120.8	414	8.0	20.7	48.1	2
	Calculated	7.31	2.74	1.34	132.5					
	% Error	2.6	2.4	0.0	-9.7					
50	Measured	6.98	2.74	1.37	79.9	751	5.3	13.9	36.0	2
	Calculated	6.79	2.69	1.36	88.8					
	% Error	2.7	1.7	0.6	-11.2					

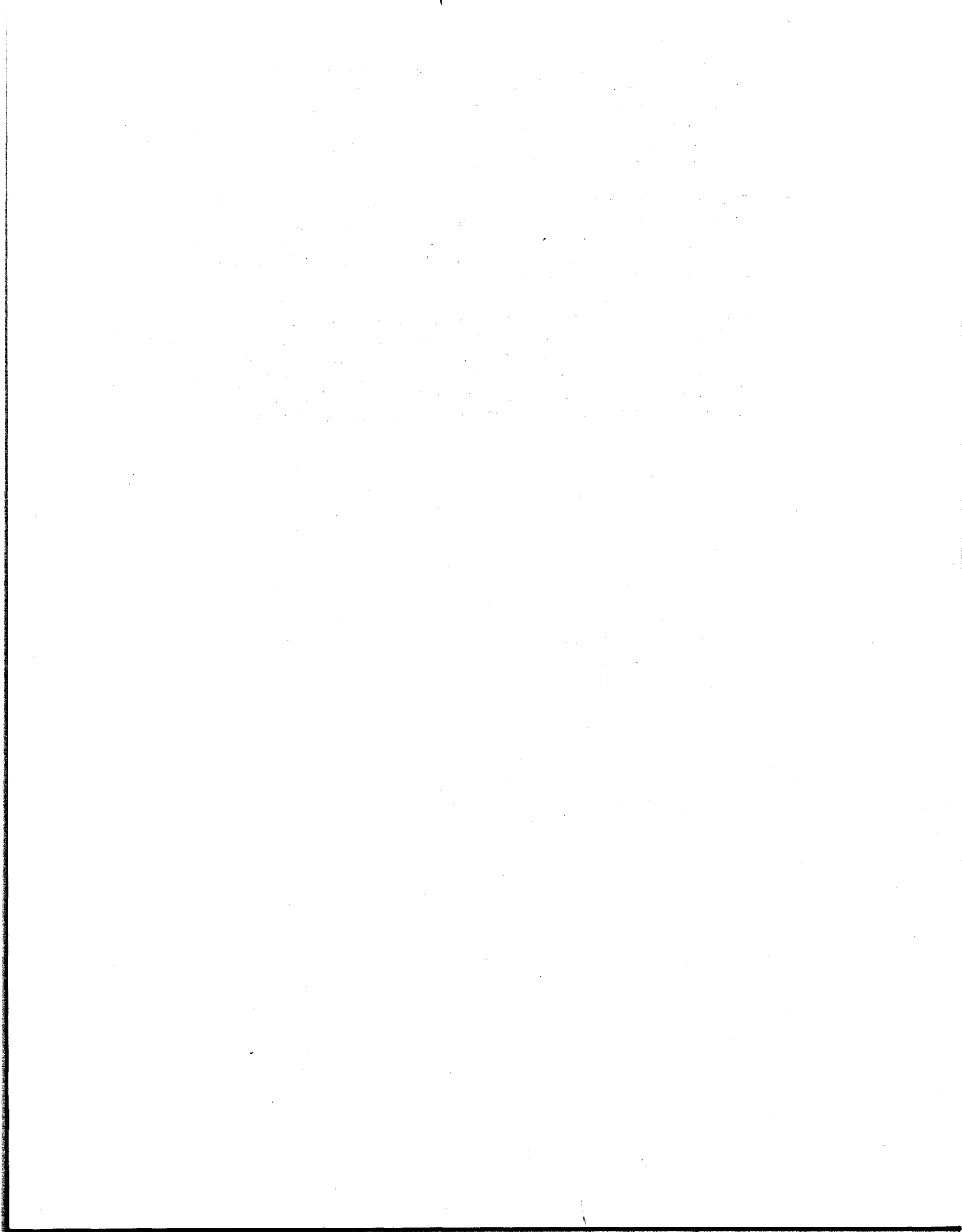
1 mi = 1.61 km

1 in = 25.4 mm

2. A 10-percent error in estimating the thickness of the asphalt concrete layer has a large impact on the backcalculated moduli. However, the thickness of the asphalt concrete layer can be measured in the field with a measurement error of much less than 10 percent.
3. The effects of wheel offsets of 1 in (25 mm) and 3 in (76 mm) were investigated. It was shown that the 3-in (76-mm) offset may produce errors as high as 18 percent in the backcalculated moduli. The errors produced from a 1-in (25-mm) offset were usually lower than 2 percent for both strains and deflection measurements. Therefore, the lateral position of the test vehicle should be measured to the nearest 1 in (25 mm) in order to limit the error in the backcalculated moduli. The 1-in (25-mm) accuracy can usually be achieved, since any truck locating system will be capable of providing this resolution. The ultrasonic system used in this study has a 1-in (25-mm) resolution.
4. A \pm 10-percent error in estimating the load produced an average error in the backcalculated moduli of 8 percent for both the strains and deflection measurements.
5. The effects of three levels of systematic error on the strains and deflections were investigated. The 1-percent and 5-percent levels were insignificant. The 10-percent level produced an average of 8.5-percent error on the backcalculated moduli. Although the 8.5-percent error is not very large, the 10-percent level of systematic error is not very likely to occur in field testing.
6. The effects of three levels of random error on the strains were investigated. The errors introduced in the backcalculated moduli increased with increasing the magnitude of the random errors. The effect of the 1-percent random error was insignificant, while the 5- and 10-percent random errors produced significant errors in the backcalculated moduli. By examining the possible sources of the random errors, it was concluded that only random errors of 1 percent or less are likely to occur in field testing.
7. The pavement layer moduli were backcalculated from the FWD load deformation measurements. Both the FWD surface sensors and MDD sensors were used independently to backcalculate the layers moduli. The results of the independent FWD and MDD analyses did not agree with each other. However, when the FWD surface deflections and the MDD deflections were combined, the analysis showed that good estimates of the layers moduli were produced that satisfy both the FWD and MDD deflections with a small percentage of error.
8. The pavement layer moduli were backcalculated from the measurements of different types of strain gauges. The backcalculation analyses were conducted for three levels of speed and three levels of axle load. The responses from the Kyowa, Dynatest, and core gauges were used in the analyses. In both sections, the effect of speed was significant on the backcalculated moduli of the asphalt concrete layer and insignificant on the moduli of the other layers. The effect of axle load was insignificant on the backcalculated moduli

of all layers. The moduli from the Kyowa and core gauges of the thick section were in good agreement. Those moduli from the thin section followed a pattern where the moduli from the core gauges were the highest, while the Dynatest gauges produced the second highest and the Kyowa gauges produced the lowest results for all combinations of truck speed and load level.

9. The pavement layer moduli were backcalculated from the MDD measurements. The effect of speed on the backcalculated moduli of all layers was insignificant, which is inconsistent with the strain gauge results. The effect of load level was also insignificant on the moduli of all layers.
10. Finally, the pavement layer moduli were backcalculated from the combination of measured strains and MDD deflections. The results showed that this combination analysis is the most promising, since the strains data are very effective in backcalculating the moduli of the asphalt concrete layer, while the MDD deflections are effective in the determination of the base and subgrade moduli.



5. INVESTIGATION OF NEW INSTRUMENTATION IDEAS

The main objective of phase II of the research was to investigate new methods for measuring flexible pavement response variables such as strains, stresses, and deflections. The investigation included gauges currently used in other areas, such as portland cement concrete, as well as new instrumentation ideas. Based on this investigation, the most promising gauges were evaluated in a laboratory. The results of the laboratory experiments provided the basis for further recommendations for field installation and testing under actual truck loading. This chapter discusses the findings of the initial investigation of the new instrumentation methods for flexible pavements.

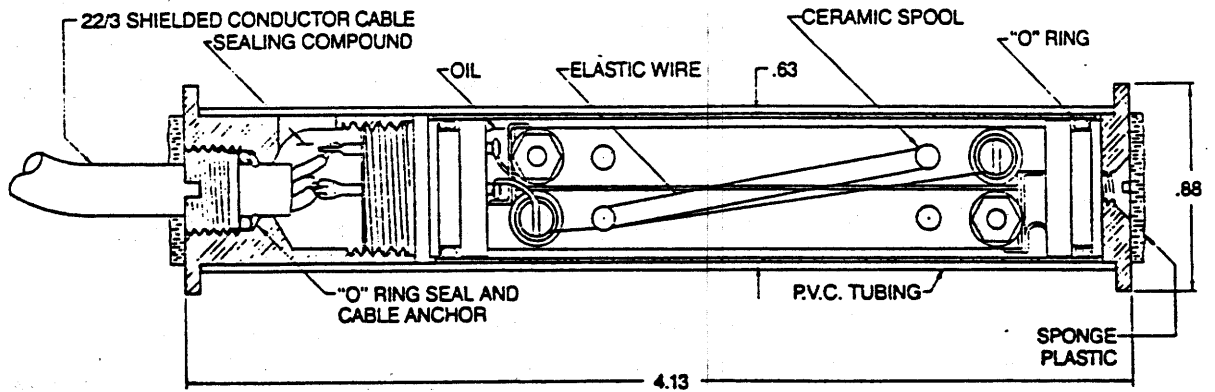
INVESTIGATION OF GAUGES USED IN PORTLAND CEMENT CONCRETE

Two types of gauges that are most commonly used in instrumenting portland cement concrete are the Carlson strain gauge and the TML embedment strain gauge. Each of these gauges was evaluated in terms of principles of measurement, cost, availability, operating temperature, moisture effects, linearity, and applications. Finally, specific recommendations were given regarding the potential applications of each gauge.

CARLSON GAUGE

Principles of Measurement

This gauge (model CM-4) consists of two coils of highly elastic steel wire, one of which increases in length and electrical resistance when a strain occurs, while the other decreases. The ratio of the two resistances is independent of temperature and the change in the ratio of the coil resistances is a measure of strain. The sum of resistances is a measure of temperature. The overall length of the gauge is 4.13 in (105 mm), which is very close to the overall length of the Kyowa and Dynatest gauges. The other physical dimensions of the gauge are shown in figure 42.



SPECIFICATIONS - M SERIES

Slope Indicator Co. Model Number	CM-4	CM-8	CM-10
Carlson Model Number	M4	M8	M10
Range (micro-strain)*	3900	2000	1600
Least reading (micro-strain)	5.8	2.9	2.3
Least reading temperature (°F)	.1	.1	.1
Gauge length (inches)	4.062	8	10
Weight (lbs)	.19	.32	.37

* Normally set at factory for 2/3 to 3/4 of range in compression
 If specified, range may be divided equally between compression and expansion

$^{\circ}\text{F} = 5(\text{F}-32)/9^{\circ}\text{C}$

1 in = 25.4 mm

1 lb = 4.5 N

Figure 42. Physical characteristics of the Carlson gauge.

The Carlson gauge has been used successfully in portland cement concrete pavements with a very good long-term stability. Its construction is flexible enough to be used in asphalt concrete, base courses, and subgrade materials. However, the gauge must be modified to resist bending stresses during the construction of asphalt pavements because the polyvinyl chloride (PVC) tubing will soften under the high paving temperature (275 to 300 °F [135 to 148 °C]).

End anchors will also have to be installed in order to provide enough anchoring force between the gauge and the asphalt concrete.

Cost and Availability

The total cost of this gauge is \$114 based on the manufacturer's quote as of September 1, 1989. In addition to the unit price, it is estimated that \$30 per gauge will be needed to provide anchors and protection against bending. The gauge is available in the United States through Carlson/RST Instruments, Inc. in Campbell, California, and Slope Indicator Co. in Seattle, Washington.

Operating Temperature

This investigation has revealed some potential problems in using this gauge in asphalt concrete pavements because of the high paving temperature during construction. The Carlson gauge has an all-steel frame with a coefficient of thermal expansion of 6.7 microstrains/°F (12.1 microstrains/°C). This type of gauge will have to be installed during the construction of asphalt concrete pavement where temperatures as high as 300 °F (148 °C) will be encountered. Using the coefficient of thermal expansion of the Carlson gauge and a temperature of 230 °F (128 °C) above room temperature, the expected permanent strain in the Carlson gauge will be 1,380 microstrains. This amount of strain represents 71 percent of the gauge's full linear range of $\pm 1,950$ microstrains. This is a very serious limitation of the Carlson gauge and makes it inappropriate for use in asphaltic concrete materials. However, it may still be used in soils and base course materials.

Moisture Effects

Because the primary use of the Carlson gauge is in portland cement concrete slabs, and it is usually installed during the concrete's plastic stage, the structure of the gauge is watertight. No additional moisture protection is required for its application in asphalt concrete, base course, or subgrade materials.

Linearity and Range

The Carlson gauge's linear range (see figure 42) of $\pm 1,950$ microstrains yields an overall range of 3900 microstrains. This range is normally set at the factory for .67- or .75-in (17- or 19-mm) compression. However, if specified, the range may be divided equally between compression and tension.

Applications

This gauge can be used to measure static and dynamic strains. However, due to the problem of high thermal strains at high temperatures, the Carlson gauge is not appropriate for use in asphaltic concrete layers.

Recommendations

As discussed earlier, the major disadvantage of the Carlson gauge is its high thermal strains at high temperatures. Therefore, it can only be used in base courses and subgrade materials. In the case of base courses and subgrade materials, this problem is not present. Another limitation of the Carlson gauge (model CM-4) is that the gauge can only register strains higher than 5.8 microstrains; this could cause a problem if the gauge were installed deep into the subgrade. It was recommended that the Carlson gauge be considered for possible use in the base course materials because none of the gauges already tested were appropriate for this application.

TML EMBEDMENT STRAIN GAUGE

Principles of Measurement

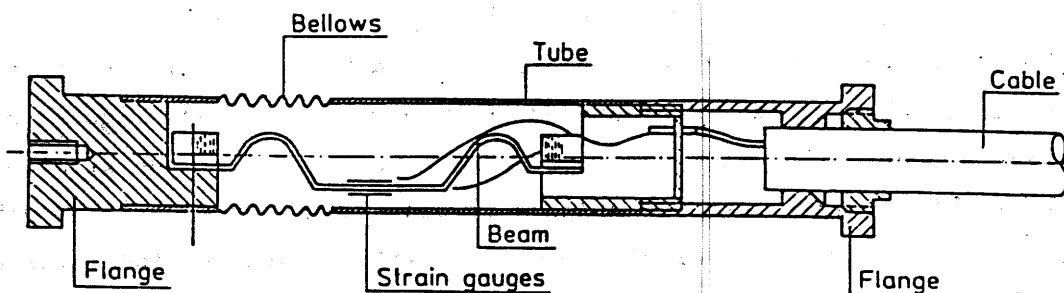
The TML gauge (model KM-100HB) consists of a bonded strain gauge that is connected to an elastic beam and covered by rubber bellows (see figure 43). It has been successfully used in concrete structures. One of the greatest features of this gauge is its low modulus of elasticity, 5,700 psi (39.3 MPa), which eliminates the problem of differential stiffness between the gauge and the asphalt concrete at high temperatures or between the gauge and the base course and subgrade materials. The sensing element is enclosed in a rubber bellows, which gives it its low modulus. The gauge's present structure would not withstand the bending forces during compaction of flexible pavements. Therefore, the gauge has to be modified to provide protection against bending. Detailed characteristics of the TML gauge are shown in figure 43.

Cost and Availability

The total cost of the gauge is \$245 based on the distributor's quote as of September 1, 1989. An additional \$30 will be required to provide bending protection and anchors for each gauge. The TML embedment gauge is manufactured by the Tokyo Sokki Kenkyujo Co. of Japan and distributed in the United States through Texas Measurements, Inc. in College Station, Texas.

Operating Temperature

The range of operating temperature for this gauge is -4 to 356 °F (-20 to 180 °C), which is well above the paving temperature of asphaltic concrete (300 °F [148 °C]). The gauge material has a coefficient of thermal expansion of 6.1 microstrains/°F (11 microstrains/°C). Using the coefficient of thermal expansion of the gauge and a temperature of 230 °F (128 °C) above room temperature, the expected permanent strain in the gauge will be 1,400 microstrains. The overall range of the TML gauge is 10,000 microstrains, which is well above the expected permanent thermal strain.



Capacity : $\pm 5000 \times 10^{-6}$ strain
 Non-linearity : 1% RO
 Apparent Elastic Modulus : Approx. 400 kgf/cm²
 : Approx. 10000 kgf/cm²
 (for KM-A)
 Input/output : 350Ω Full bridge (strain)
 : Quarter bridge 3-wire
 : (temperature)
 : 120Ω Half bridge (for KM-30)

Type	Dimensions (mm)			Rated output (mV/V)	Gauge length (mm)	Temperature range (°C)	Lead Wires
	A	B	C				
KM-30	34	12	10	2.5	31	-20 to +60	2.4 mm dia. 0.04 mm ² 3-wire shielded vinyl cord 2 meters long
KM-50F	54	20	17	4.0	50	-20 to +80	6.0 mm dia. 0.3 mm ² 4-wire chloroprene cord 2 meters long
KM-100A	104	20	17	2.5	100	-20 to +80	8.0 mm dia. 0.3 mm ² 5-wire chloroprene cord 2 meters long
KM-100B	104	20	17	2.5	100	-20 to +80	8.0 mm dia. 0.3 mm ² 5-wire chloroprene cord 2 meters long
KM-200A	205	28	17	5.0	200	-20 to +80	11.5 mm dia. 0.5 mm ² 5-wire shielded chloroprene cord 2 meters long
KM-100HB	104	20	17	2.5	100	-20 to +180	6.0 mm dia. 0.3 mm ² 5-wire shielded fluoroplastic cord 2 meters long

* The gauge is temperature-compensated for the material having a linear expansion coefficient of $11 \times 10^{-6} / ^\circ\text{C}$.

Figure 43. Physical characteristics of the TML gauge.

Moisture Effects

The gauge was designed specifically for long-term strain measurements in wet concrete; therefore, it is totally sealed against moisture penetration.

Linearity and Range

The linear range of the TML gauge is $\pm 5,000$ microstrains, which is well above the expected strain level in asphalt concrete pavements (see figure 43). The nonlinearity of the gauge is 1 percent of the rated output, which is 2.5 mV/V.

Applications

With the TML gauge's low modulus, it is expected that the gauge will be used to measure strains in asphaltic concrete, base course, and subgrade materials. It will measure both static and dynamic strains.

Recommendations

The feasibility study on the TML embedment gauge indicated that the gauge has a great potential for usage in measuring strains in all layers of flexible pavements (surface, base, and subgrade). This conclusion is supported by the TML gauge's low modulus of elasticity, wide range of strain and operation temperature, and waterproof construction. Research has not uncovered any technical disadvantages associated with this gauge. However, the expected unit cost of approximately \$300 may be a limitation. It was recommended that three TML gauges be obtained and tested in the laboratory for possible installation in the asphalt concrete, base course, and subgrade layers.

NEW INSTRUMENTATION CONCEPTS

This part of the investigation covers the methods for measuring pavement response that are not currently in practice or are used in areas other than pavement instrumentation. The main objective was to identify those concepts

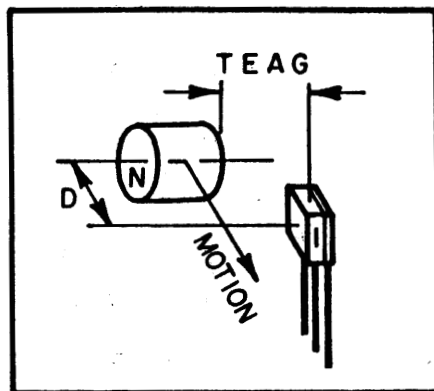
and, through modification, redesign, or invention, develop a new design that makes them applicable for flexible pavement instrumentation. New concepts identified under this part of the research include (1) the Hall effect sensor, (2) piezoelectric film, and (3) an inductive displacement sensor. Each of these concepts was evaluated in terms of its principles of measurement, projected cost and availability, operating temperature, moisture effects, linearity and range, and applications. Finally, specific recommendations were given regarding the potential applications of each concept.

HALL EFFECT SENSOR

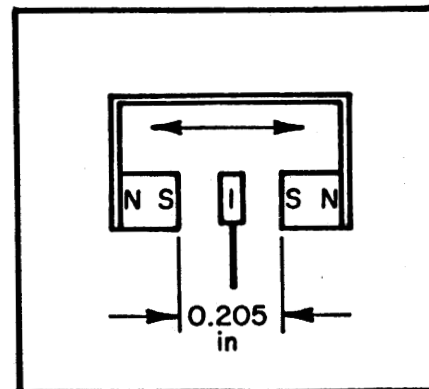
Principles of Measurement

The Hall effect principle states that when a current-carrying conductor is exposed to a magnetic field, a voltage will be generated perpendicular to both the current and the magnetic field. The Hall device develops an output voltage that is proportional to the intensity of the applied perpendicular magnetic field. Typically, this is 30 mV/gauss. An internal amplifier is normally provided to boost the output voltage and lower the impedance. Typical output signal swings are ± 5 V for a 12-V device. In operation, both the magnets and the Hall effect sensor will be anchored to the material. As the material expands or contracts under loads or temperature, a relative movement between the magnets and the Hall effect sensor will occur. This relative movement generates a voltage related to the direction and magnitude of the strain.

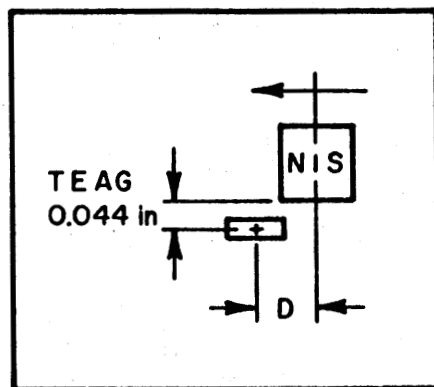
The actual application of the Hall effect sensor can be achieved in four different configurations as shown in figure 44. A feasibility study on the applicability of the Hall effect sensor to strain- and deflection-measuring gauges for asphalt concrete pavements was conducted. All four configurations were tested in the laboratory. The evaluation criteria selected were linear range, gain, and ease of implementation. Table 4B summarizes the laboratory testing results. Based on these results, the push-pull slide-by mode was considered the most favorable configuration for field applications.



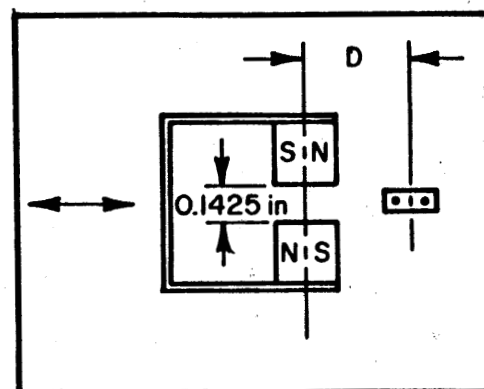
Slide-By Mode



Push-Push Head-On Mode



Edgewise Slide-By Mode



Push-Pull Slide-By Mode

1 in = 25.4 mm

Figure 44. Configurations of the Hall effect sensor.

Table 48. Laboratory-measured data on the Hall effect sensor.

Configuration	Linear Range (in)	Gain (MV/in)	Ease of Implementation
Slide-By Mode	0.2	2,700	Moderate
Push-Push Head-On Mode	0.1	12,800	Very Difficult
Edgewise Slide-By Mode	0.2	2,700	Moderate
Push-Pull Slide-By Mode	0.125	7,750	Very Easy

1 in = 25.4 mm

Cost and Availability

The Hall effect sensor compares favorably with other measuring devices. A complete transducer costs about \$32, or approximately \$12 in hardware and \$20 (1 h) in assembly labor. The regulator cost is about \$.90. Alnico 5 magnets cost about \$2.50. Several manufacturers, including Honeywell and Sprague, produce stabilized linear sensors. Numerous retail and wholesale electronics vendors carry these sensors as a stock item. Alnico 5 magnets are available from the same sources; all other materials are readily available.

Operating Temperature

It is expected that during construction of asphalt concrete layer, the gauge will be subjected to a temperature as high as 300 °F (148 °C). To evaluate the effect of high temperature on the sensor, the sensor with a magnet was tested before and after being heated at 300 °F (148 °C) for a 24-h period. The data from this experiment, shown in figure 45, indicate that the effect of high construction temperature is negligible.

The inservice temperature of asphalt concrete pavements may range from 0 to 120 °F (-32 to 49 °C). Therefore, the linear range and gain of the sensor were additionally evaluated under five levels of temperatures: 3, 30, 70, 90,

Effect of Heat on the Magnet Push-push Mode

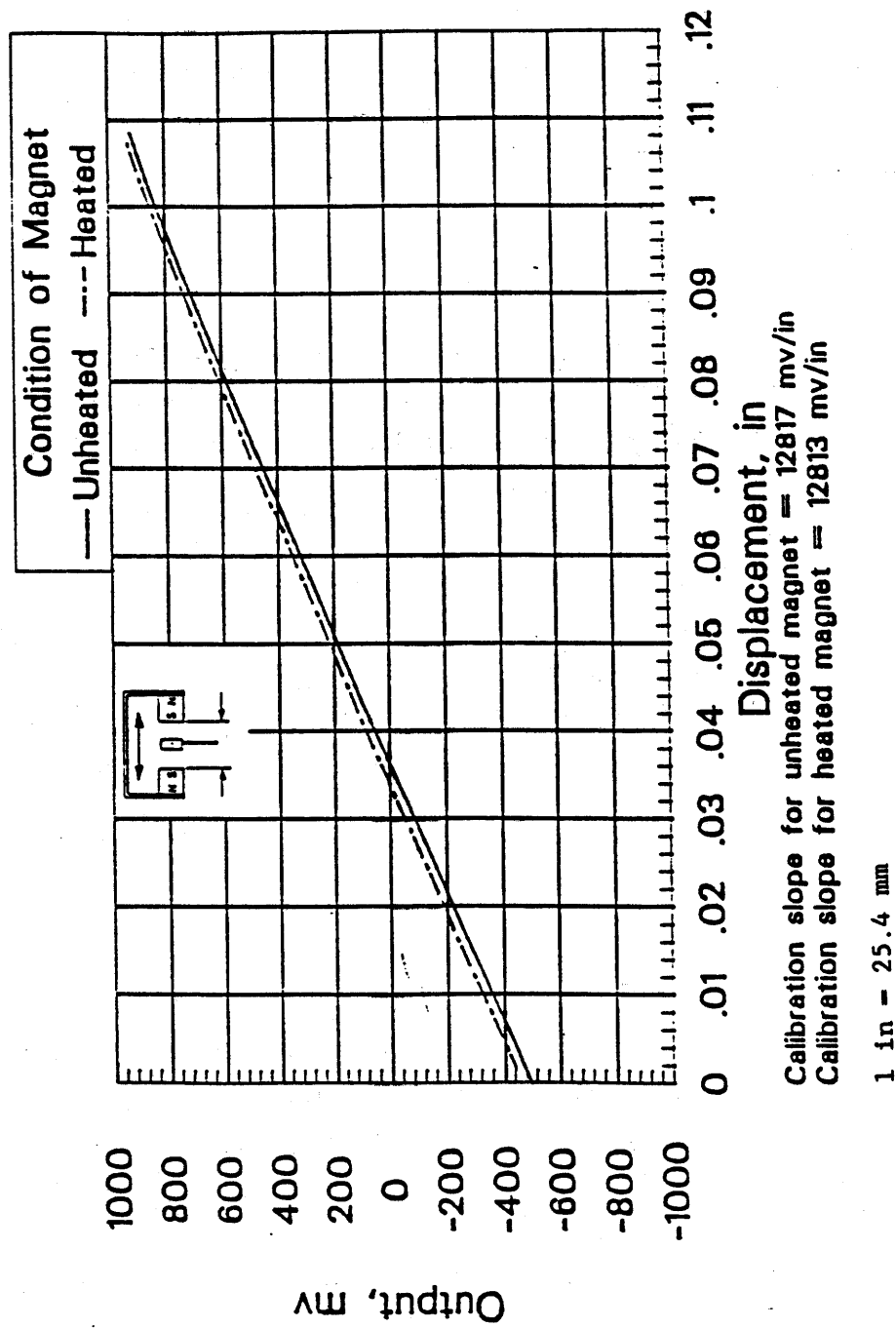


Figure 45. Effect of high construction temperature on the Hall effect sensor.
 Magnet was heated at 300° F for 24 hours.

and 120 °F (-16, -1, 21, 32, and 49 °C). Figure 46 shows the effect of inservice pavement temperatures on the sensor response to be negligible.

Moisture Effects

It is expected that moisture will damage the Hall effect sensor; therefore, the magnets and the Hall effect sensor will both be coated with epoxy.

Linearity and Range

To maximize the signal-to-noise ratio of the sensor, two alternatives were tested: placement of the amplifier inside the gauge and use of triaxial cables. These alternatives will be examined in the discussion of laboratory testing of new instrumentation (chapter 6).

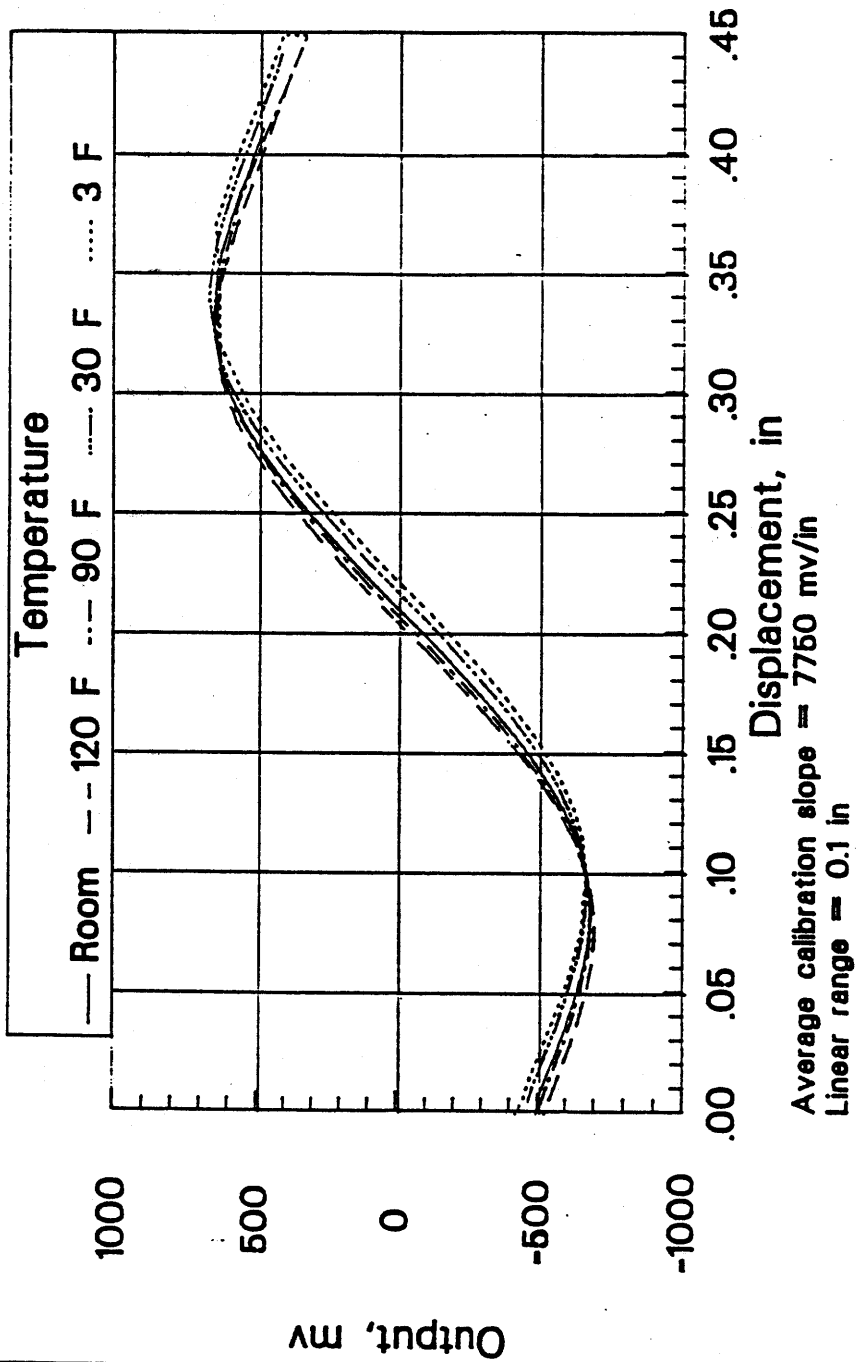
Applications

The feasibility study indicated that the gauges built with the Hall effect sensor will have a very low modulus of elasticity in the direction of the measured strains. Therefore, the gauges can be used to measure strain and deflections under both static and dynamic loads in the asphalt concrete, base course, and subgrade materials.

Recommendations

The investigation did not uncover any technical disadvantages for the Hall effect gauge. However, some field installation problems may be encountered. For instance, the gauge may be driven out of range during construction and field installation activities. Several methods of protecting the gauge components from dislocation, including the use of a release pin, chemically degradable link, and electrical release, were investigated. A prototype release pin mechanism was tested in the laboratory and performed well. The release pin mechanism was subsequently selected for field applications.

Effect of Temperature Slide-Through Mode



1 in = 25.4 mm

Figure 46. Effect of in-service temperature on the Hall effect sensor.

Based on the feasibility study and laboratory tests that have been conducted on the Hall effect sensor, it was concluded that the sensor has a very high potential for success as a strain and displacement gauge. The tests indicated that the performance of the gauge is not affected by any external factors, such as the high construction temperature, range of service temperature, and moisture. Therefore, it was recommended that asphalt concrete gauges, soil strain gauges, and deflection gauges be built and tested. The schematic and circuit diagrams of these gauges are presented in appendix B.

PIEZOELECTRIC FILM

Principles of Measurement

Piezoelectricity means "pressure electricity." When certain crystals are subjected to mechanical stress, electrical charges proportional to the mechanical stress appear on their surfaces. This effect is called piezoelectricity.

Polyvinylidene fluoride (PVDF) is a polymer that exhibits the properties of piezoelectricity. This polymer is manufactured with most of its molecular dipoles oriented in the same direction by the simultaneous application of a strong electric field and heat. This yields a permanently poled device on the order of 5 to 1,000 μm thick with electrodes attached to the film faces.

PVDF films develop an electrical charge proportional to the change in mechanical stress or strain. This charge diminishes with time due to internal resistance and the electrical impedance of the attached circuit. Unconditioned output voltages can be as high as several hundred volts, depending on the applied stress.

Cost and Availability

A complete prototype transducer costs about \$37, or approximately \$17 in hardware and \$20 (1 h) in labor. The piezoelectric film is available in standard sample sizes and configurations for about \$6 per sensor. A standard

sample worked fine for the prototype phase, but to improve the signal characteristics, a custom sensor should be ordered; this will undoubtedly involve a relatively large charge because of the small sensor quantities required.

Several manufacturers, including Pennwalt and Solvay, manufacture piezoelectric films. Due to the custom nature of the film's applications, orders must be placed directly with the manufacturers.

Operating Temperature

The manufacturer's literature specified a maximum operating/storage temperature of 212 °F (100 °C). Not knowing what safety factor was used in the manufacturer's calculations or whether it can withstand high paving temperatures, a piezoelectric sample film was exposed to a temperature of 275 °F (135 °C) for 10 s, which represents typical upper-end installation temperature in asphaltic concrete. The sample showed signs of severe wrinkling and discoloration and shrunk in length by 16 percent. This eliminated the film as a potential sensor in the asphaltic concrete layer. It may still have possibilities for use in the base and subgrade, as the temperature in these layers is much lower. However, the manufacturer's literature also indicates that the film's gain is temperature-dependent (see figure 47).

Linearity and Range

The large signal level generated by this sensor makes the resolution of small strains practical. An on-sensor amplifier can be provided by the manufacturer, which facilitates transmission of the signal over long distances.

To properly evaluate the signal characteristics of this film, a software algorithm needs to be developed and tested to compensate for the effects of all the variables that affect the output wave form, including temperature, rate of force application, and aging characteristics, to name only a few.

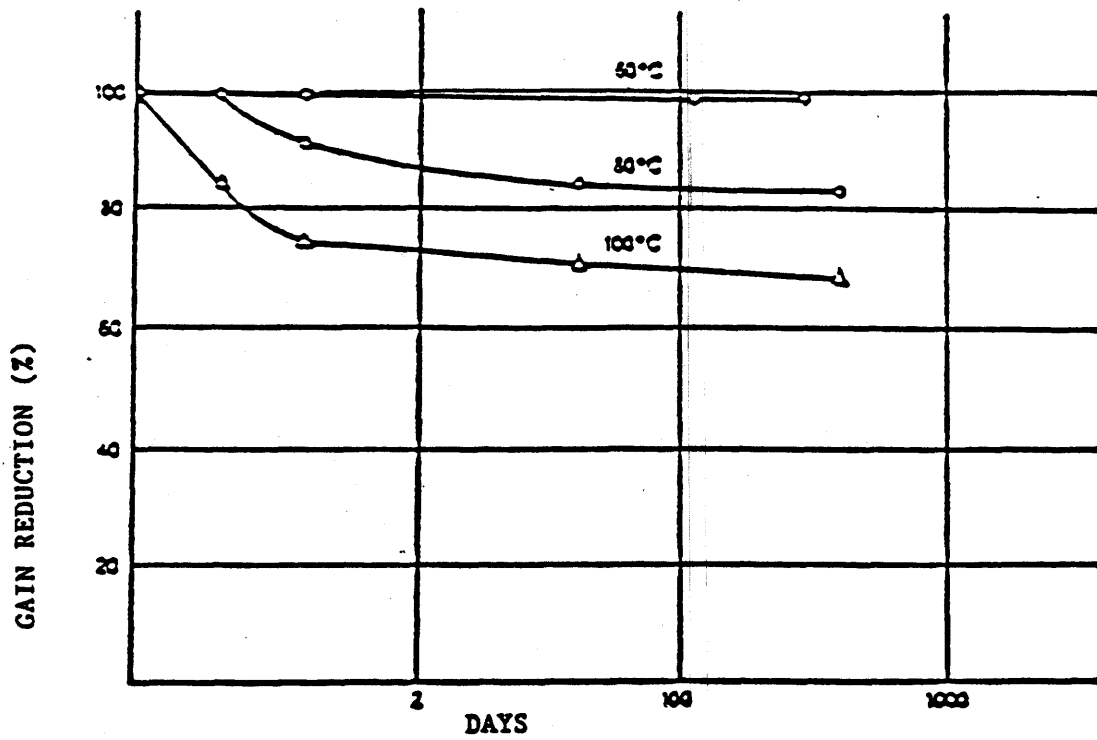


Figure 47. Relationship between gain and sensor life at different temperatures for the piezoelectric film.

This software is not commercially available and must therefore be custom-developed.

Applications

Due to the nature of the film, only dynamic signals can be measured practically. Static measurements could theoretically be made with additional hardware and sensor redesign, which would make the gauge prohibitively expensive.

Recommendations

Based on the above discussion, the piezoelectric film clearly has several disadvantages relative to this specific application. The effects of high paving temperature on the gauge and inservice temperature on the gain are the most serious limitations. In addition, a special data acquisition software must be developed to properly evaluate the signal.

Based on the observations in the feasibility study, it was decided that the piezoelectric film will not be a successful sensor to measure strains and deflections of the flexible pavement layers. Therefore, it was not recommended for any further laboratory or field testing.

INDUCTIVE DISPLACEMENT TRANSDUCER

Principles of Measurement

An inductive displacement gauge uses an adjustable inductive coil as the sensing element rather than the traditional resistive gauge or linear variable differential transformer. It works by varying its resonant frequency (in conjunction with a fixed capacitor) by moving a loading slug in and out of the coil. This inductance-capacitance (LC) circuit is part of an oscillator, which is tuned by the slug movement relative to the coil. In operation, the coil and the slug will be anchored to the surrounding material. As the material expands or contracts under loads or temperature, a relative movement between the coil and the slug will occur. This relative movement will

generate a shift in the oscillation frequency related to the direction and magnitude of the strain. This variation in frequency will then be read directly by either an inexpensive computer data acquisition board or a frequency counter, or it can be converted into an analog voltage signal for plotting and/or computer acquisition. A telescoping containment housing (sensor shell) with anchors has been designed to facilitate mounting and alignment in the field.

Cost and Availability

It is estimated that a completed transducer would cost about \$60, or approximately \$20 in hardware and \$40 (2 h) in assembly labor. The inductive sensor element is hand-wound in a drill press or lathe.

Operating Environment

If properly assembled, this sensor will not be affected by either temperature or moisture. Components can be selected to cancel out any temperature effects. Moisture is sealed out by an epoxy coating. The possibility of any magnetic interference from the test vehicles should be investigated.

Linearity and Range

The natural frequency of the coil circuit, given by equation 6, is inversely proportional to the coil inductance, which is proportional to the position of a slug in a coil:

$$N_f = \frac{1}{2\pi} \frac{1}{\sqrt{LC}} \quad (6)$$

where

L = inductance (H)

C = capacitance (F)

The range is only limited by the length of the coil and the resolution required. A practical range would be ± 0.050 in (1.27 mm) or $\pm 50,000$ microstrains. If a displacement of 0.100 in (2.54 mm) were to correspond to the frequency output from 0 to 100,000 Hz, then the calibration factor would be 1 Hz per microstrain. This frequency could be read directly by inexpensive acquisition boards commercially available without A/D conversion, or it could be easily converted into an analog voltage for plotting and/or recording.

Applications

The basic exterior shell of this transducer is the same as the Hall effect transducer shell, and therefore it can be used to measure strains and deflections in asphalt concrete, base course, and subgrade materials.

Recommendations

This sensor is a custom-designed element; off-the-shelf components are limited to the oscillator electronics. Assembly requires the assistance of an electronics technician. It was recommended that this sensor design be pursued based on the advantages listed above. The schematics and circuit diagrams of this gauge are presented in appendix B.

INVESTIGATION OF WIRELESS GAUGES

The protection of gauge wires during instrument installation, pavement construction, and field testing is a major problem for all types of pavement instrumentation. Large and sharp stones in the asphalt concrete material and in the crushed aggregates base can easily cut through the wires, especially under the high stresses associated with dynamic loading. As the pavement deteriorates, its deflection under truck loading becomes larger, which in turn imposes large strains on the wires and eventually causes failure. In addition to the stress and strain problems on the wires, high quality and expensive shielded wires must always be used to reduce the noise interference in the measured signals.

Because of all the above problems that may be encountered with the wires connecting the sensors to the signal conditioning units, the possibility of using wireless gauges was investigated. Wireless sensors are commonly used on rotating shafts where contacting devices are not feasible. A wireless system transmits the measuring signal from the sensor location impressed on a radio frequency carrier, normally by frequency modulation (FM). A typical carrier frequency would be 100 MHz, or approximately the center of the commercial FM radio band. This carrier frequency is recommended because of the availability of inexpensive receivers (FM radios). Both the gauge and the transmitter are powered by a long-life battery that can be disconnected remotely.

The sensor signal is converted into a variable frequency at the site of collection. This drastically reduces the amount of electrical interference (noise) impressed upon the signal during transmission to the acquisition system because most noise components are very short in duration but high in amplitude. Analog signals are very susceptible to this type of interference, but FM signals are not.

A self-contained gauge would be placed in the ground and would be self-supporting, whereas traditional gauges require transmission lines (wires) leading to the gauge to supply power and extract the signal. The elimination of wire placement requirements would greatly simplify the installation process.

The wireless gauge is comparable to other strain measurement systems in per-channel cost. A completed transducer would cost about \$300, with most of the cost applied to physical hardware. The prospect of failure makes this overall transducer more expensive. If this gauge fails, both the transducer and the transmitter are lost because both are underground in an inaccessible location. If a more traditional gauge fails, only the gauge is lost, not the above-ground conditioning system. The cost of failure is thus considerable. Currently, pavement instrumentation is still at an experimental stage, where high failure rates are always expected. Therefore, wireless gauges may not be used successfully until more experience with in situ instrumentation of pavements is obtained and the possibility of sensors failure is reduced.

RECOMMENDATIONS

Based on the findings of the feasibility studies conducted in this part of the research, the following recommendations were made:

1. The Carlson strain gauge (model CM-4) should be tested for possible use in base course materials.
2. The TML embedment strain gauge (model KM-100HB) should be tested for potential use in asphaltic concrete, base course, and subgrade materials.
3. The Hall effect sensor should be further investigated through the manufacture of prototype gauges and laboratory testing. The Hall effect sensor should be tested for possible applications in asphalt concrete strain gauges, soil strain gauges, single-layer deflectometers, and multidepth deflectometers.
4. The research has uncovered several serious problems with the piezoelectric film with regard to pavement instrumentation applications. Therefore, it was recommended that no further investigations or evaluations of piezoelectric film be conducted.
5. The inductive displacement sensor was recommended for investigation through the manufacture and laboratory testing of prototype gauges. It was recommended that the inductive sensor be tested for possible applications on the single-layer deflectometer.
6. The risk of failure of the wireless gauge makes it very costly because both the gauge and the transmitter will be lost at once. Therefore, the wireless gauge was not recommended for any further investigations.

1948

1949

1950

1951

1952

1953

1954

1955

1956

1957

1958

1959

1960

1961

1962

1963

1964

1965

6. TESTING OF NEW INSTRUMENTATION: PHASE II

LABORATORY TESTING OF NEW INSTRUMENTATION

As was discussed in chapter 5, the new instrumentation investigation addressed two categories of sensors: (1) gauges used in portland cement concrete and (2) new instrumentation concepts. In this section, the laboratory testing of the selected gauges will be discussed. It was decided that different sets of tests would be conducted on each category of gauge. The gauges from the portland cement concrete category were only subjected to a single laboratory test to determine their modulus of elasticity in the direction of applied strain (i.e., tensile strains). This test was considered adequate because this category of gauge already exists in the market and the temperature, moisture, and dynamic characteristics of these gauges are well documented in the literature and various instrumentation catalogs.

The gauges under the new instrumentation concepts category were subjected to several laboratory tests to evaluate the various characteristics of the new gauges. Based on the results of these tests, two types of gauges--the Hall effect sensor and the inductive displacement gauge--were recommended for further evaluation. The inductive displacement gauge requires the use of iron powder cores (slug). Several unsuccessful attempts were made to locate a quantity of this type of core through commercial sources. An alternative was to manufacture the cores in the laboratory. The manufactured cores had unit weights several times lower than the required level. This decrease in the core's unit weight produced a much shorter linear range than the range obtained from the original cores. Ultimately, three inductive displacement gauges were built using available 2-in (51-mm) cores and subjected to laboratory calibration tests.

MEASUREMENT OF THE MODULUS OF ELASTICITY OF EXISTING GAUGES

The test for the measurement of the modulus of elasticity consisted of subjecting the gauge to a given tensile force and measuring the corresponding tensile strain. From the cross-sectional area of the gauge, the tensile

stress can be calculated. The modulus of elasticity of the gauge is then calculated as the ratio of the tensile stress to the tensile strain. The modulus of elasticity was measured for the following gauges:

- TML embedment gauge (model KM-100HB).
- TML embedment gauge (model KM-100B).
- TML embedment gauge (model PML).
- Kyowa gauge (model KM-120-H2-11 L100-3).
- Carlson gauge (model CM-4).

Table 49 summarizes the modulus of elasticity values for the various types of gauges.

Table 49. Modulus of elasticity values for various types of gauges.

Type of Gauge	Modulus of Elasticity (psi)
TML Model KM-100HB	270,000*
TML Model KM-100B	270,000*
TML Model PML	223,000
Kyowa Model	240,000
Carlson Model CM-4	N/A

* From manufacturer-supplied information.

The modulus of elasticity is a very important characteristic because the force required to generate a given level of strain in the gauge is directly related to its modulus. Another important factor is the relationship between the modulus of elasticity of the gauge and that of the surrounding material. The ideal situation would involve the use of a gauge that has the same modulus of elasticity as the surrounding material. However, this goal is difficult to achieve because the asphalt concrete material has a temperature-dependent

modulus. The majority of the asphalt concrete strain gauges are built from materials that have a constant modulus of elasticity. Therefore, a perfect match between the modulus of the asphalt concrete material and that of the gauge under the various temperature conditions is impossible. Another way to address the modulus of elasticity problem would be to ensure that the gauge material is always softer than the asphalt concrete material in order for the gauge to measure the applied strain without a potential bearing capacity problem.

It is well known that the modulus of the asphalt concrete material depends on many variables, such as aggregate gradation (dense or open), asphalt grade, asphalt concrete, air voids, etc. In addition, the temperature-modulus relationship is different for different asphalt concrete mixtures. In general, it can be assumed that the majority of asphalt concrete mixtures have moduli ranging from 100,000 to 1,200,000 psi (690 to 8,275 MPa) with the lower end being at the high temperature, around 100 °F (38 °C), and the upper end being at the freezing temperature. An average modulus for the majority of asphalt concrete mixtures at normal inservice pavement temperatures, around 70 °F (21 °C), would be approximately 400,000 psi (2,760 MPa). Therefore, any gauge having a modulus of 400,000 psi (2,760 MPa) or less would have a good possibility of success in measuring the strains in asphalt concrete materials.

The previous discussion covers the measurement of strains in the asphalt concrete materials. When the strains in the unstabilized base course and subgrade materials are measured, the situation is very similar, except that the modulus of the surrounding material is lower and is moisture-dependent. The range of the base and subgrade moduli is between 5,000 and 100,000 psi (34.5 and 690 MPa) for wet and dry conditions, respectively. In general, an average value of 20,000 psi (138 MPa) is usually assumed for normal inservice moisture conditions.

LABORATORY TESTING OF THE NEW INSTRUMENTATION CONCEPTS GAUGES

As mentioned earlier, the Hall effect gauge is the only type of gauge from this category that was subjected to laboratory testing. This section presents a brief discussion of the individual tests.

Effect of Temperature

The Hall effect gauges to be used in the asphalt concrete layer were subjected to high temperature testing, which consisted of subjecting each gauge to a temperature of 300 °F (148 °C) and measuring its linear range and gain before and after the high temperature treatment. The data from this test were shown in figure 45 (chapter 5) and indicated that the high construction temperature will have no effect on the linear range or the gain of the Hall effect gauge.

The second temperature testing series consisted of testing the Hall effect gauges under a range of pavement service temperatures (i.e., 3, 30, 77, 90, and 120 °F [-16, -1, 25, 32, and 49 °C]). Again, the test consisted of the effect of temperature on the linear range and the gain of the gauges. The data from this test, shown in figure 46 (chapter 5), indicated that the range of temperature will have no effect on the linear range or the gain of the Hall effect gauge.

Dynamic Characteristics

Because the gauges will be installed in inservice pavements subjected to high-speed moving loads, it would be beneficial to measure their dynamic characteristics. The dynamic testing was conducted on the MTS machine and consisted of two tests: (1) sinusoidal testing and (2) pulse testing. Under the sinusoidal testing series, the gauges were subjected to sinusoidal displacement functions with frequencies ranging between 1 and 10 Hz. This frequency range simulates the frequency range of the signals generated by a loaded truck moving at speeds between 20 and 60 mi/h (32 and 96 km/h). The data from the sinusoidal testing are shown in table 50, which indicates that

the gauge response is identical to the input sinusoidal function (MTS-generated function) as measured by its frequency and amplitude.

Under the pulse testing series, the Hall effect gauges were subjected to pulse displacement functions with various pulse durations. The MTS-generated pulse durations ranged from 70 to 150 ms. Table 51 shows the data obtained from the pulse testing. The data indicate that the impulse response of the Hall effect gauge is very similar to the expected input signal as measured by its pulse duration and amplitude.

Measurement of Modulus of Elasticity

As shown in the figures in appendix B, the structure of the Hall effect gauge consists of an outer and an inner tube separated by a layer of silicone grease. Therefore, the apparent modulus of elasticity of the Hall effect gauge is negligible.

Effect of Bending

As the Hall effect gauge is installed in the pavement layer to measure horizontal strains, it will be subjected to both tensile and bending stresses. Due to the structure of the Hall effect gauge, it was suspected that the bending stresses would increase the apparent modulus of elasticity of the gauge, which in turn might stiffen the gauge. The effect of bending was tested by applying an increasing lateral force to the gauge and measuring the required longitudinal force to produce a preset longitudinal displacement. Figure 48 shows the data from this test, which indicate that the effect of the lateral force is negligible for all levels. Therefore, the effect of bending on the Hall effect gauge is negligible.

THE USE OF HALL EFFECT SENSORS IN THE MULTIDDEPTH DEFLECTOMETER

PURPOSE OF TESTING

The Texas Transportation Institute (TTI) has evaluated the Hall effect sensor in a multidepth deflectometer environment. The replacement of the

Table 50. Response of the Hall effect gauges to sine input under MTS loading frame.

MTS Frequency (Hz)	Measured Frequency (Hz)	Frequency Difference (%)	Input Amplitude (in)	Measured Amplitude (in)	Amplitude Difference (%)
2	2.3	14	0.050	0.050	0.6
2	2.1	6	0.050	0.050	0.6
2	2.3	14	0.050	0.050	0.6
2	2.2	11	0.100	0.107	7.2
2	2.2	10	0.100	0.108	7.5
2	2.2	11	0.150	0.156	4.1
2	2.2	10	0.150	0.155	3.6
2	2.2	12	0.150	0.212	41.4
2	2.3	13	0.200	0.212	6.2
2	2.2	11	0.250	0.268	7.4
2	2.2	10	0.250	0.267	6.8
2	2.2	12	0.250	0.267	6.9
5	5.4	8	0.050	0.048	-4.7
5	5.4	8	0.050	0.047	-5.6
5	5.5	10	0.050	0.047	-5.3
5	5.5	10	0.100	0.101	1.4
5	5.5	10	0.100	0.102	1.5
5	5.5	10	0.150	0.157	4.8
5	5.7	14	0.150	0.155	3.6
5	5.5	10	0.150	0.155	3.5
5	5.5	10	0.200	0.208	3.9
5	5.5	10	0.200	0.208	4.0

1 in = 25.4 mm

Table 50. Response of the Hall effect gauges to sine input under MTS loading frame (continued).

MTS Frequency (Hz)	Measured Frequency (Hz)	Frequency Difference (%)	MTS Amplitude (in)	Measured Amplitude (in)	Amplitude Difference (%)
5	5.5	10	0.250	0.260	3.9
5	5.5	10	0.250	0.260	4.1
5	5.5	10	0.250	0.260	3.9
8	8.7	9	0.050	0.047	-5.3
8	8.3	3	0.050	0.048	-4.7
8	8.9	11	0.050	0.047	-5.3
8	9.2	15	0.100	0.099	-0.7
8	9.4	18	0.100	0.099	-0.7
8	8.9	11	0.150	0.151	0.4
8	8.9	11	0.150	0.150	0.0
8	8.9	11	0.150	0.150	-0.1
8	8.9	11	0.200	0.202	0.8
8	9.2	15	0.200	0.202	0.8
8	8.9	11	0.250	0.255	2.0
8	8.9	11	0.250	0.255	1.9
8	8.9	11	0.250	0.256	2.2
10	10.3	3	0.050	0.042	-16.4
10	11.4	14	0.050	0.042	-15.3
10	11.0	10	0.050	0.042	-16.1
10	11.0	10	0.150	0.148	-1.1
10	11.0	10	0.150	0.148	-1.2
10	11.0	10	0.150	0.148	-1.7
10	11.0	10	0.200	0.196	-2.2

1 in = 25.4 mm

Table 50. Response of the Hall effect gauges to sine input under MTS loading frame (continued).

MTS Frequency (Hz)	Measured Frequency (Hz)	Frequency Difference (%)	MTS Amplitude (in)	Measured Amplitude (in)	Amplitude Difference (%)
10	11.0	10	0.200	0.195	-2.4
10	11.0	10	0.250	0.249	-0.3
10	11.0	10	0.250	0.250	0.0
10	11.4	14	0.250	0.250	0.1
20	23.6	18	0.050	0.034	-31.4
20	23.6	18	0.050	0.034	-31.4
20	22.0	10	0.100	0.083	-16.9
20	22.0	10	0.100	0.083	-16.9
20	22.0	10	0.150	0.128	-14.6
20	22.0	10	0.150	0.128	-14.5
20	22.0	10	0.150	0.127	-15.1
20	22.0	10	0.200	0.172	-14.0
20	22.0	10	0.200	0.171	-14.4
20	22.0	10	0.250	0.220	-11.9
20	22.0	10	0.250	0.220	-11.9
20	22.0	10	0.250	0.219	-12.3

1 in = 25.4 mm

Table 51. Response of the Hall effect gauges to haversine input under MTS loading frame.

MTS Frequency (Hz)	Measured Frequency (Hz)	Frequency Difference (%)	Input Amplitude (in)	Measured Amplitude (in)	Amplitude Difference (%)
2	2.3	13	0.050	0.052	4.0
2	2.2	10	0.050	0.051	1.4
2	2.2	10	0.100	0.103	3.1
2	2.3	14	0.150	0.154	2.9
2	2.3	14	0.150	0.155	3.1
2	2.2	10	0.150	0.153	1.7
2	2.2	10	0.200	0.196	-1.9
2	2.2	10	0.200	0.197	-1.7
2	2.2	10	0.200	0.195	-2.5
2	2.2	10	0.250	0.248	-0.6
2	2.2	10	0.250	0.248	-0.6
2	2.3	15	0.250	0.249	-0.5
5	6.1	22	0.050	0.046	-8.3
5	6.2	25	0.050	0.046	-7.9
5	5.2	3	0.050	0.047	-6.1
5	6.0	20	0.100	0.098	-1.6
5	5.5	10	0.150	0.151	0.7
5	5.4	8	0.150	0.152	1.1
5	5.4	8	0.150	0.152	1.1
5	5.6	12	0.200	0.194	-2.9
5	5.5	10	0.250	0.243	-2.7
5	5.7	14	0.250	0.243	-2.8

1 in = 25.4 mm

Table 51. Response of the Hall effect gauges to haversine input under MTS loading frame (continued).

MTS Frequency (Hz)	Measured Frequency (Hz)	Frequency Difference (%)	MTS Amplitude (in)	Measured Amplitude (in)	Amplitude Difference (%)
5	5.5	10	0.250	0.246	-1.6
8	8.5	6	0.050	0.042	-16.2
8	8.7	9	0.050	0.042	-16.9
8	5.3	-33	0.050	0.041	-17.5
8	8.7	9	0.100	0.094	-6.1
8	9.2	15	0.100	0.093	-6.8
8	8.7	9	0.100	0.094	-6.4
8	8.5	6	0.150	0.147	-2.0
8	8.7	9	0.150	0.147	-2.1
8	9.2	15	0.150	0.146	-2.4
8	8.7	9	0.200	0.192	-4.2
8	8.7	9	0.200	0.192	-4.1
8	9.2	15	0.250	0.241	-3.5
8	9.4	18	0.250	0.241	-3.5
8	9.2	15	0.250	0.242	-3.1
10	11.4	14	0.050	0.044	-11.9
10	11.8	18	0.050	0.044	-12.8
10	11.8	18	0.050	0.254	407.2
10	11.0	10	0.100	0.094	-6.1
10	11.4	14	0.100	0.094	-6.0
10	11.0	10	0.150	0.140	-6.7
10	11.0	10	0.150	0.140	-6.6
10	11.0	10	0.200	0.140	-29.8

1 in = 25.4 mm

Table 51. Response of the Hall effect gauges to haversine input under MTS loading frame (continued).

MTS Frequency (Hz)	Measured Frequency (Hz)	Frequency Difference (%)	MTS Amplitude (in)	Measured Amplitude (in)	Amplitude Difference (%)
10	11.4	14	0.200	0.187	-6.3
10	11.0	10	0.200	0.187	-6.5
10	11.4	14	0.200	0.187	-6.3
10	11.4	14	0.250	0.235	-5.9
10	11.0	10	0.250	0.234	-6.4
10	11.0	10	0.250	0.233	-6.6
20	20.6	3	0.050	0.035	-30.8
20	66.0	230	0.050	0.034	-31.3
20	22.0	10	0.050	0.033	-34.7
20	22.0	10	0.100	0.077	-23.5
20	22.0	10	0.150	0.122	-19.0
20	22.0	10	0.150	0.122	-18.9
20	22.0	10	0.150	0.123	-18.2
20	22.0	10	0.200	0.164	-18.2
20	22.0	10	0.200	0.164	-18.2
20	22.0	10	0.250	0.206	-17.5
20	22.0	10	0.250	0.208	-16.8
20	22.0	10	0.250	0.208	-16.8

1 in = 25.4 mm

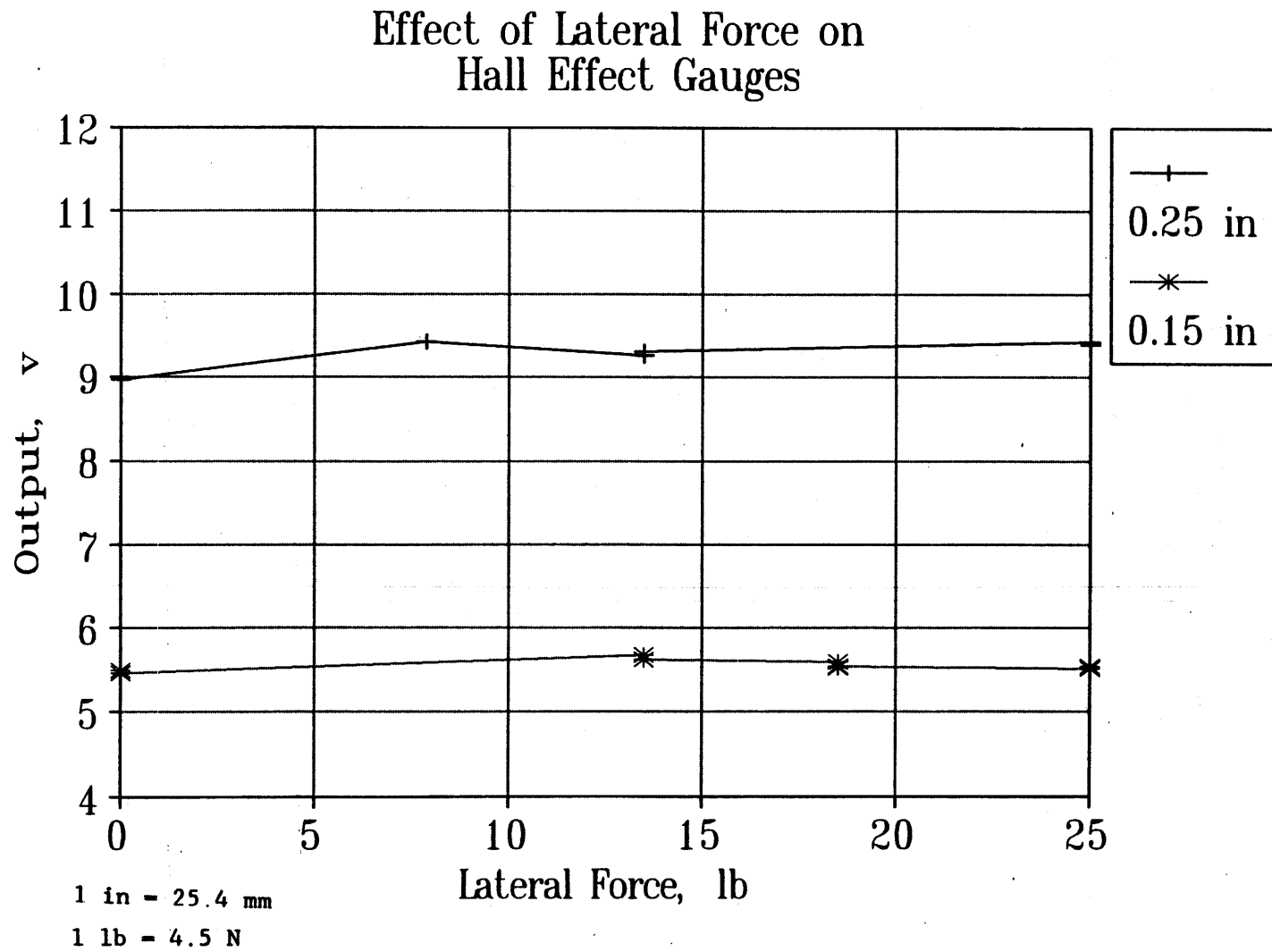


Figure 48. Effect of lateral force on Hall effect gauges.

current LVDT sensor in the MDD module was investigated, together with the response of the new system to both truck and FWD-type loading. Because the FWD is a high-frequency loading device (loading time 0.03 s), it can be used to determine if the Hall effect sensor has the frequency response that allows accurate measurement of relatively rapid loadings.

HARDWARE SETUP

The MDD module was modified to hold the Hall effect sensor. The cross sections of the current MDD and the modified MDD module are shown in figure 49. The Hall effect sensor was built into the center core and two magnets were installed in the modified MDD module. The MDD modules containing the Hall effect sensor magnets are shorter than the LVDT-based modules; this is an advantage because the units can be placed closer together. The LVDT and Hall effect sensor setups are shown in figure 50.

The LVDT was monitored using a microcomputer-based data acquisition system. The LVDT used was a ± 0.125 -in (3.175-mm) AC unit from Schaevitz; -0.125 in (-3.175 mm) is equivalent to 10 V. Because the voltage output from the Hall effect sensor is very small, in the millivolt range, a low-noise voltage amplifier system (capable of 10 times amplification) was built to aid in data acquisition. The output of the Hall effect sensor was monitored using a digital oscilloscope with manual triggering.

CALIBRATION OF SENSORS

Both the LVDT and the Hall effect sensors were calibrated in the laboratory and in the field. The laboratory calibration of the LVDT matched the manufacturer's calibration factor; the Hall effect calibration was similar to results discussed earlier in this chapter.

A unique feature of the MDD is that the sensors can be calibrated in the field prior to testing. This is achieved by decoupling the center core from the system anchor and then attaching an extension from the core to an accurate surface micrometer. The field calibration has been found to be important in the past in that the lab and field calibrations are frequently 2 to 3 percent

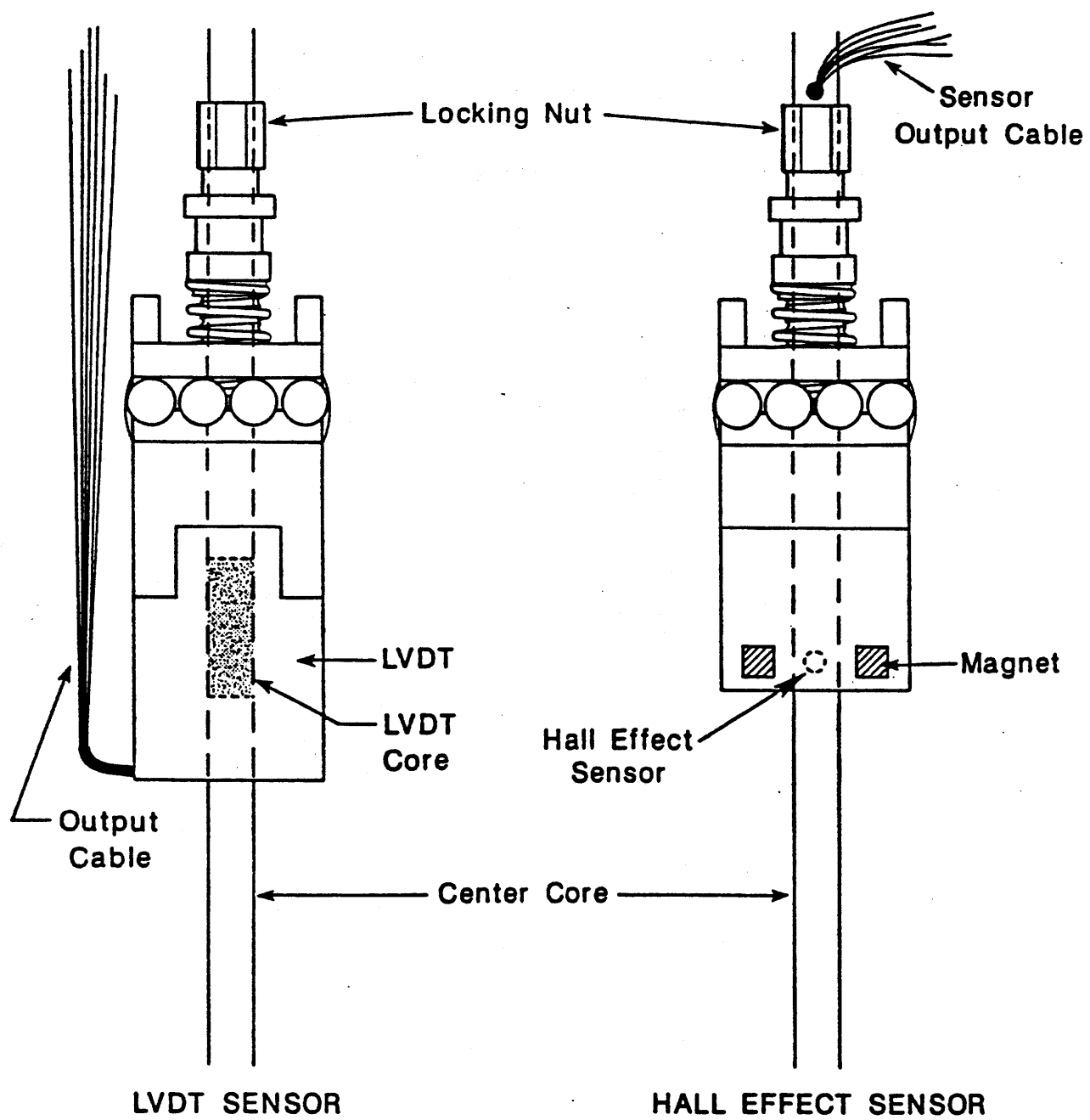
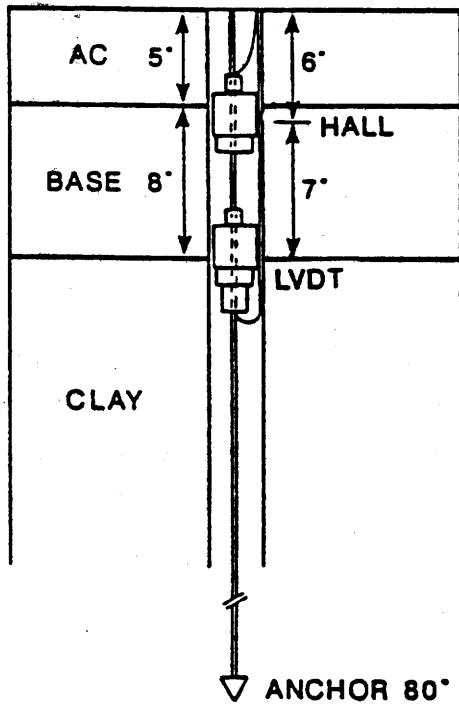
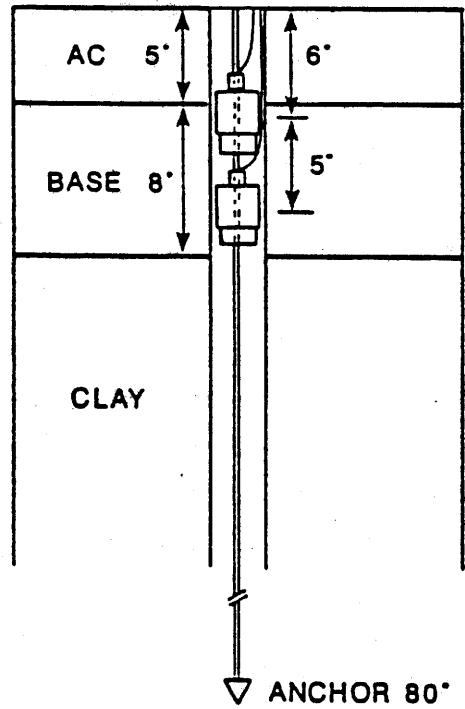


Figure 49. Multidepth deflectometer configurations.

1 LVDT SENSOR
1 HALL EFFECT



2 HALL EFFECT SENSORS



1 in - 25.4 mm

Figure 50. LVDT and Hall effect setups at TTI research annex.

off for LVDT's; however, the field calibration factors remain constant. The results of the field calibration are shown in figure 51. The Hall effect is linear over a range of ± 0.05 in (1.27 mm), whereas the LVDT is linear over the specified range of ± 0.125 in (3.175 mm).

The small range of the Hall effect sensor created a mechanical installation problem; it is critical to set the sensor in the center of its travel range to ensure that data are collected in the linear range. Furthermore, if data are collected over a period of time and the pavement layers deform, then the Hall effect sensor will need to be continually readjusted to the center of its linear range.

EXPERIMENTAL PLAN

PAVEMENT DESIGN

The test sections for phase II were designed following the same AASHTO procedure used in the design of the phase I test sections (see chapter 2). The layer thicknesses used in phase II consist of 6 in (152 mm) of asphalt concrete on top of 8 in (203 mm) of base for the thin section and 10 in (254 mm) of asphalt concrete on top of 10 in (254 mm) of base for the thick section.

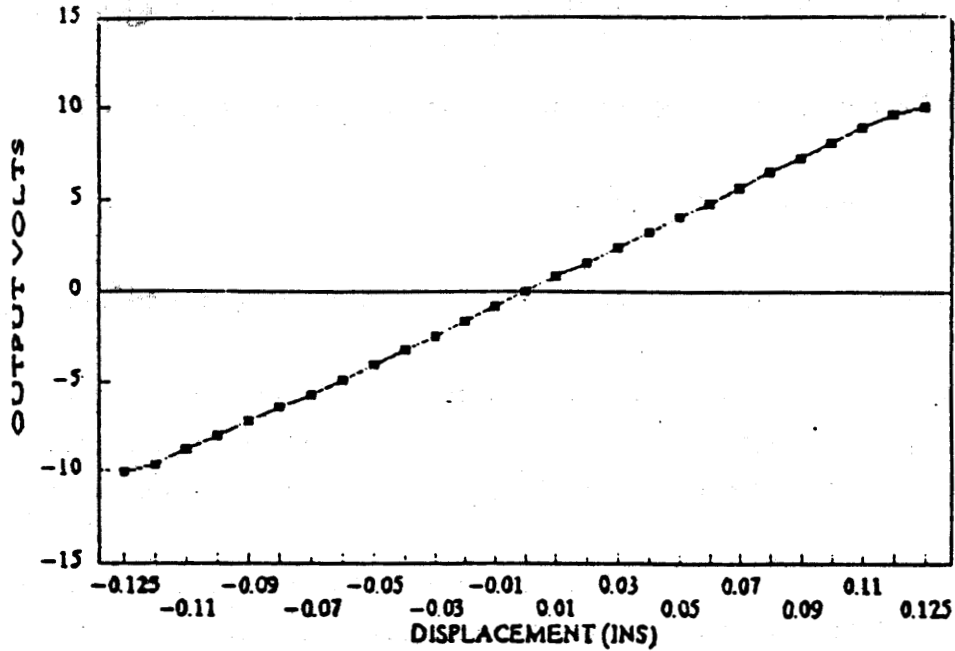
DATA COLLECTION PLAN

The data collection plan was similar to the plan implemented in phase I. The data from the instrumentation were collected under a single axle tractor and a tandem axle trailer with dual radial tires with the following combinations of load, tire pressure, and speed:

- Load levels: empty trailer, fully loaded trailer, and intermediate load level.
- Testing speeds: 20, 35, and 50 mi/h (32, 56, and 80 km/h).

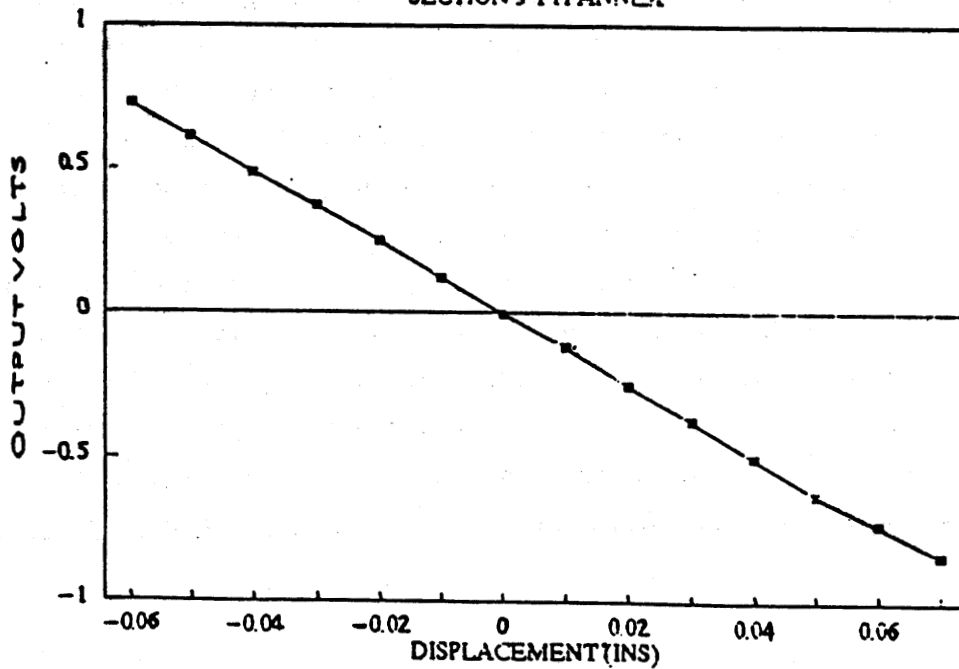
FIELD CALIBRATION LVDT SENSOR

SECTION 9 TTI ANNEX



FIELD CALIBRATION HALL-EFFECT SENSOR

SECTION 9 TTI ANNEX



1 in = 25.4 mm

Figure 51. Field calibration of Hall effect multidepth deflectometer.

- Tire pressures: manufacturer's suggested cold inflation and suggested inflation plus 35 psi (241 kPa).
- Replicates: Four replicates of each measurement were collected.

The above experiment provided a total of:

$$3(\text{load}) \times 3(\text{speed}) \times 2(\text{pressure}) \times 4(\text{replicates}) = 72 \text{ measurements/gauge}$$

All data were collected using the same data acquisition system used in the first phase of this project. In addition to the full-scale testing, PennDOT's falling weight deflectometer was used to test the instrumented sections.

PennDOT's portable WIM equipment was used to measure the dynamic loads. This portable WIM is the Golden River capacitance-mat type.

INSTRUMENTATION LAYOUT

The installation of the gauges within the existing test sections was accomplished through partial removal of the sections and retrofitting of the gauges in the pavement layers. Thirty ft (9.2 m) of the asphalt concrete layer of each section were removed. The base course material stayed in place; therefore, the installation of gauges into the subgrade was performed through partial excavation of the base course material at the instruments' locations. The instrumentation within the base course layer was installed at mid-depth level and required minimal excavation. After the instrumentation was installed in the base course and subgrade, the strain gauges at the bottom of the asphalt concrete layer were installed and the new asphalt concrete layer was constructed. Table 52 summarizes the gauges that were installed in both sections, and figures 52 and 53 show the distribution of gauges in the thin and thick sections, respectively.

In both sections, the Hall effect gauges have three replicates at all levels of installation (i.e., surface, base, and subgrade layers). The Kyowa gauges, installed in the asphalt concrete layer, served as a reference because they were tested in the first field testing experiment and showed very good performance. The TML embedment gauges (type PML) are very similar to the

Table 52. Summary of gauges for phase II field testing.

Gauge Type	Number of Gauges/Section	Orientation	Location
Kyowa gauges	4	Longitudinal	At the bottom of asphalt concrete
Core strain gauges	4	Longitudinal	At the bottom of asphalt concrete
Carlson strain gauge (CM-4)	1	Longitudinal	Within the base course layer
TML embedment gauge (PML type)	4	Longitudinal	At the bottom of asphalt concrete
TML strain gauge (KM-100HB)	1	Longitudinal	At the bottom of asphalt concrete
TML strain gauge (KM-100B)	1	Longitudinal	Within the base course layer
TML strain gauge (KM-100B)	1	Vertical	Within the subgrade
Hall effect strain gauge	3	Longitudinal	At the bottom of asphalt concrete
Hall effect strain gauge	3	Longitudinal	Within the base course
Hall effect strain gauge	3	Vertical	Within the subgrade
Hall effect deflection gauge	2	Vertical	At the surface of the pavement
Inductive deflection gauge	2	Vertical	At the surface of the pavement
Multidepth deflectometer	1	Vertical	Throughout the depth of pavement
Thermocouples	8	N/A	Throughout the depth of pavement
Solid state sensors	8	N/A	Throughout the depth of pavement
Transverse location device	1	N/A	At the side of the section
Infrared triggering device	1	N/A	At the beginning of the section

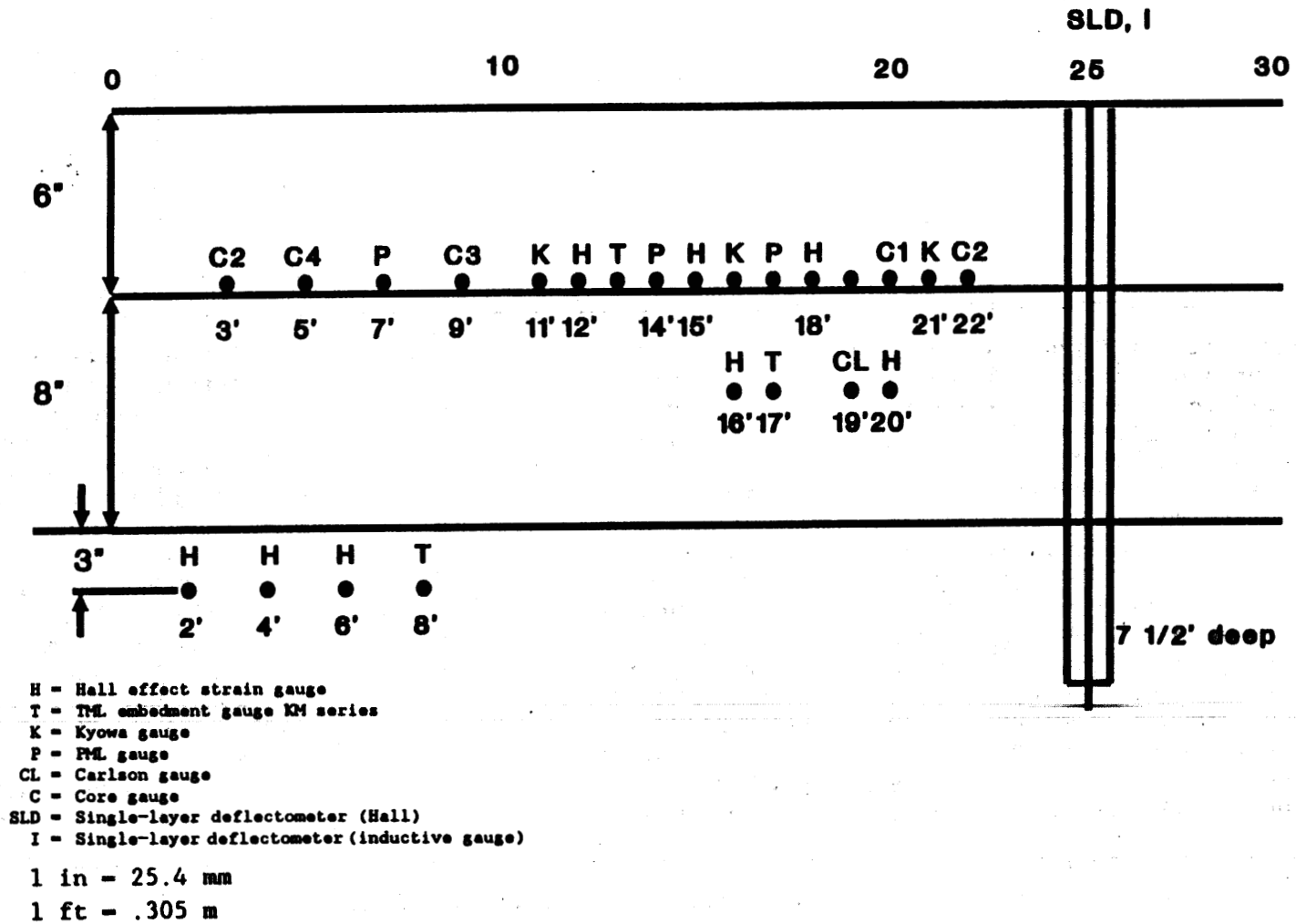


Figure 52. Layout of instrumentation for the thin section, outer wheel path.

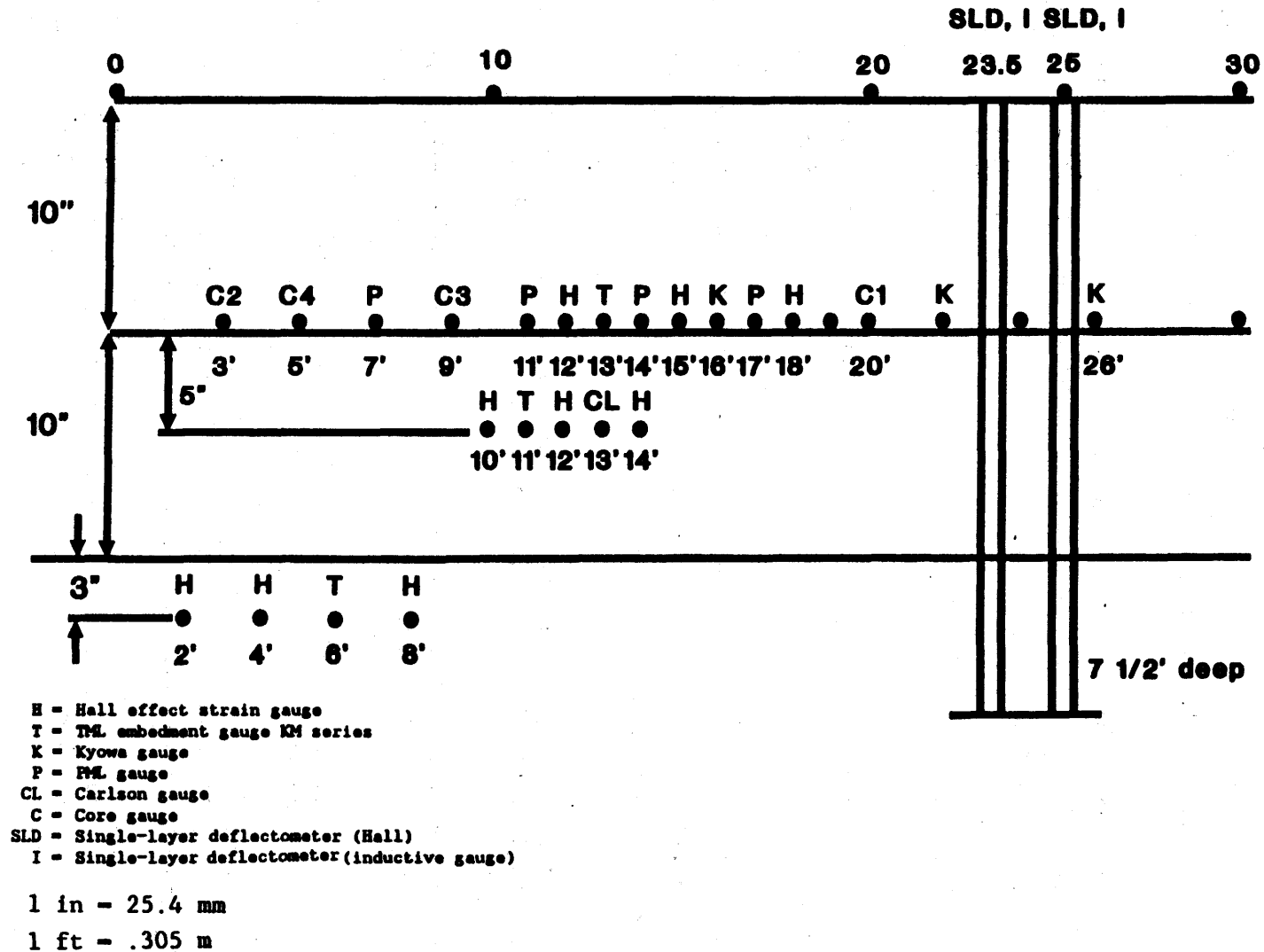


Figure 53. Layout of instrumentation for the thick section, outer wheel path.

Kyowa gauges; they were installed in both wheel tracks and their performance was compared with the performance of the Kyowa gauges.

Four different types of core gauges were installed in the inner wheel path of each section. The objective of this plan is to evaluate the effect of clearance and gauge size on the performance of the core gauges.

Two SLD's with Hall effect sensors and one inductive displacement sensor were installed in the outer wheel path of each section. The SLD's monitored the displacement of the surface layer:

DATA ANALYSIS PLAN

As discussed under the data collection plan, four replicates of each measurement were collected. In addition, the transverse location device was used to ensure that the wheel passes in replicate runs were within an acceptable distance from each other. After the transverse vehicle location and the dynamic load (from the WIM system) were known for each unit of data, the following analysis was performed:

- **Survivability of the sensors:** represents the number of gauges still operational after construction relative to the number of gauges initially installed.
- **Repeatability of the sensors:** dispersion of measurements for specific test conditions (i.e., mean, standard, deviation, and coefficient of variation).
- **Effect of test variables:** how the various test conditions affected the response of the sensors.
- **Uncertainty of the measurements:** difference between the sensor measurements and the theoretical value as predicted from the theory of elasticity solution.
- **Regression analysis:** In situations where different types of gauges are measuring the same response, a regression analysis will be conducted to correlate the measurements of each individual gauge with the measurements of other gauges.

A special data analysis was planned for the measurements from the core gauges. However, the core gauge failed, and, because no back-up gauges were

available for replacement, the experiment had to be abandoned. Additional reasons for not replacing the broken gauge were poor performance of core gauges in phase I and limited funds remaining in the project budget.

PAVEMENT CONSTRUCTION

The phase II test sections (thin and thick) were constructed at the test track within the same region of the phase I test sections. The construction process was as follows:

1. Cut a 30-ft-long-by-12-ft-wide (9.2-m-long-by-3.7-m-wide) section of the phase I thick and thin sections as far as possible from the existing gauges.
2. Remove the cut asphalt concrete layer.
3. Level and compact the existing base course to the desired density.
4. Leave the pavement section open for a period of 2 weeks to allow for the installation of gauges into the base course and subgrade.
5. After the base course and subgrade gauges are installed, install the asphalt concrete strain gauges.
6. After the asphalt concrete gauges are installed, proceed with the paving operation.
7. After the paving operation and compaction are completed, install the surface single-layer deflectometer.

INSTALLATION OF INSTRUMENTATION

The Kyowa, PML, and TML strain gauges in the asphalt concrete layer were installed following the same procedure used in the phase I testing program. The Hall effect strain gauges in the asphalt concrete and unbonded layers were installed using a special procedure due to the unique structure of the gauges. The structure of the Hall effect strain gauge consists of an outer and an inner tube separated by a layer of silicone grease. Therefore, the tensile strength of the Hall effect gauge is negligible. This was expected to present a problem in installation because the Hall effect gauge will be driven out of range by compaction stresses. Consequently, the Hall effect gauges were built with a mechanical release pin attached to the middle of the gauge. After

installation and final compaction of the pavement section, the release pin was removed by pulling it with a cable extended through the shoulder of the test section. Some difficulties were encountered in pulling the release pins from the Hall effect soil strain gauges.

All strain gauges were monitored during the installation and pavement compaction activities. Only static compaction was allowed over the gauges, which was very effective in reducing the failure rate of the gauges in the asphalt concrete layer.

The Hall effect and inductive displacement single-layer deflectometers were installed according to a procedure similar to the one used in the phase I testing program.

DATA ACQUISITION AND REDUCTION

The data acquisition and reduction system described in chapter 2 was also used to collect the data from all the gauges installed in phase II. The gain of the Hall effect sensors was relatively low, in the order of 1.30 mV/Gauss; therefore, a special magnification box was built to boost the output voltage to the range of ± 5 V.

7. DATA ANALYSIS: PHASE II

The second main objective of this research project was to investigate and test new concepts of pavement response measurements suitable for field installation. Various new concepts were investigated, including Carlson gauges, TML gauges, Hall effect sensors, piezoelectric film, inductive displacement, and wireless gauges. All new concepts were subjected to laboratory evaluation, and the most promising ones were selected for field testing. The test variables, discussed in chapter 6, were selected to provide a wide range of measured responses under which the new instrumentation concepts could be evaluated. This chapter presents the results of data analyses performed on the measured data in order to evaluate the performance of the individual new concepts.

STRAIN MEASUREMENTS IN THE ASPHALT CONCRETE LAYER

Strain data were collected under the various combinations of test variables using the data acquisition package developed in this project. The measurements from the individual gauges were converted into engineering units using calibration factors developed from laboratory testing as discussed in chapter 6. The full time history of strain data was collected from each gauge under each pass of the test vehicle. The strain time history included the response under the steering axle, single drive axle, and tandem trailer axles. Similar to the analysis of phase I data (chapter 3), the actual strains were obtained from the strain time history by subtracting the initial reference from the maximum strains (see figure 8).

The following strain gauges were installed in the asphalt concrete layer: Kyowa, Hall effect, PML, and TML. All gauges were installed during the construction of the test sections. The actual locations of these gauges in both sections were shown in figures 52 and 53.

SURVIVABILITY

The gauge tested under phase II were all new instrumentation concepts except for the Kyowa gauges. As expected, not all gauges survived the construction and installation activities. All gauges were installed in the longitudinal direction at the outer wheel track of the section. The following gauges survived in the thick section:

- Three Hall effect strain gauges at stations 12, 15, and 18.
- Four PML strain gauges at stations 8, 11, 14, and 17.
- Three Kyowa strain gauges at stations 16, 22, and 26.

The TML gauge installed at station 13 was unoperational after construction.

The following gauges survived in the thin section:

- Three Hall effect strain gauges at stations 12, 15, and 18.
- Three PML strain gauges at stations 7, 14, and 17.
- Three Kyowa strain gauges at stations 11, 16, and 22.

The TML gauge installed at station 13 was only operational under certain combinations of test variables. The Kyowa gauge at station 11 was unoperational toward the middle of the testing program.

The survivability of the asphalt concrete gauges was very good, in general, except for the TML-type strain gauge.

REPEATABILITY

The repeatability of the gauges is studied in terms of the means, standard deviations, and coefficients of variation of the four replicate measurements for each combination of test variables. The results of the four replicates and their corresponding means, standard deviations, and coefficients of variation are presented in appendix D of volume II of this report. The lower the COV, the better the repeatability of the measuring

device. In general, COV values less than 10 percent are considered good, and COV values less than 5 percent are considered excellent. Tables 53 and 54 show typical repeatability data from the thick and thin sections, respectively. As these tables and the data in appendix D of volume II indicate, most of the COV values are in the range of 1 to 6 percent. Based on the COV range, all the gauges showed good to excellent within-gauge repeatability.

EFFECT OF TEST VARIABLES ON THE RESPONSE OF GAUGES

As mentioned in the testing plan, the test variables included axle load, tire pressure, and truck speed. In addition, strain data were collected under both the single drive axle and the tandem trailer axles.

The measured strain data from thin and thick structures under the various combinations of load, tire pressure, and speed are tabulated in appendix D of volume II for both single- and tandem-axle configurations. From these tables, it is obvious that the effect of tire pressure on strain at the bottom of the asphalt concrete layer is insignificant compared to the effects of axle load and truck speed for all types of strain gauges. The conclusion is similar to the one drawn based on the data of phase I (see chapter 3). Therefore, the effect of axle load and vehicle speed on the response of all strain gauges was studied.

Effect of Axle Load on the Response of Strain Gauges

The data from the thick section were consistent among all gauges. The measured strains in the thick section increased as the load increased. The thin section data showed less consistency among the various gauges and with respect to the effect of load on the measured strains. The majority of the data showed a linear relationship between the strain and axle load. However, the slope of the stress versus load changes from one gauge to another within the same group of gauges.

Table 53. Strain values under drive axle with 18.5 kips/axle, tire pressure of 100 psi (690 kPa), thick section.

Truck Speed (mi/h)	ACH-12 DRV	ACH-15 DRV	ACH-18 DRV	K-16 DRV	K-22 DRV	K-26 DRV	PML-7 DRV	PML-11 DRV	PML-14 DRV	PML-17 DRV
20	131.10	119.95	115.68	27.35	28.05	117.66	124.74	81.06	35.89	79.53
20	129.55	115.40	114.75	28.05	27.91	115.55	121.15	80.64	35.48	79.32
20	132.62	118.00	110.00	26.65	27.97	119.71	126.89	81.22	35.74	78.46
20	129.09	120.80	119.00	27.60	28.11	118.39	123.09	81.02	35.73	78.75
Mean	130.59	118.54	114.86	27.41	28.01	117.83	123.97	80.98	35.71	79.01
STD	1.39	2.08	3.22	0.51	0.08	1.51	2.11	0.21	0.15	0.43
CV	1.06	1.75	2.80	1.86	0.27	1.28	1.70	0.26	0.42	0.55
35	130.75	75.12	73.60	16.44	21.74	103.13	92.94	74.25	25.19	51.60
35	131.90	80.20	73.13	15.88	21.24	103.93	93.64	76.99	25.65	52.64
35	131.60	81.50	72.65	15.86	21.19	103.62	93.84	77.51	25.95	50.74
35	129.10	75.30	72.00	15.75	21.37	103.41	93.06	76.31	25.07	51.69
Mean	130.84	78.03	72.85	15.98	21.38	103.52	93.37	76.27	25.46	51.67
STD	1.09	2.86	0.59	0.27	0.22	0.29	0.38	1.24	0.35	0.67
CV	0.83	3.66	0.81	1.67	1.01	0.28	0.41	1.62	1.38	1.30
50	122.76	85.25	66.05	16.02	14.59	63.78	65.01	51.23	24.13	46.82
50	115.11	78.51	63.09	16.03	14.00	57.60	60.97	56.55	24.00	43.23
50	101.60	73.90	68.84	17.53	15.44	62.68	58.29	54.95	22.56	41.17
50	99.29	76.65	66.00	16.56	14.83	58.05	64.76	56.47	22.61	45.37
Mean	109.69	78.58	66.00	16.54	14.72	60.53	62.26	54.80	23.32	44.15
STD	9.67	4.19	2.03	0.61	0.52	2.73	2.80	2.16	0.74	2.14
CV	8.81	5.33	3.08	3.72	3.51	4.52	4.49	3.94	3.17	4.85

1 mi = 1.61 km

Table 54. Strain values under drive axle with 18.5 kips/axle, tire pressure of 135 psi (932 kPa), thin section.

Truck Speed (mi/h)	K-11 DRV	K-16 DRV	K-22 DRV	PML-7 DRV	PML-14 DRV	PML-17 DRV	TML-13 DRV
20	107.14	186.24	248.83	63.02	75.23	57.47	100.03
20	97.65	192.64	221.74	64.41	77.65	59.99	100.13
20	96.40	177.99	221.88	58.93	76.00	58.49	96.31
20	94.12	180.98	240.23	58.60	75.26	57.06	97.03
Mean	98.83	184.46	233.17	61.24	76.04	58.25	98.37
STD	4.96	5.57	11.76	2.53	0.98	1.13	1.72
CV	5.02	3.02	5.04	4.13	1.29	1.94	1.75
35	70.44	182.13	134.28	41.84	59.03	48.72	87.38
35	83.60	184.35	147.34	41.06	61.49	50.92	79.44
35	86.04	182.30	146.99	38.36	60.07	50.47	83.80
35	76.42	177.16	143.44	44.56	56.39	49.28	79.75
Mean	79.13	181.48	143.01	41.46	59.25	49.85	82.59
STD	6.13	2.65	5.27	2.21	1.87	0.89	3.25
CV	7.75	1.46	3.68	5.33	3.15	1.78	3.94
50	39.47	126.74	126.84	25.73	37.77	39.54	70.16
50	43.87	125.81	122.58	25.69	38.80	39.67	69.54
50	46.35	128.80	126.73	25.85	37.17	39.72	71.92
50	47.41	129.01	129.02	26.36	37.17	39.07	68.14
Mean	44.27	127.59	126.29	25.91	37.73	39.50	69.94
STD	3.06	1.36	2.33	0.27	0.67	0.26	1.36
CV	6.91	1.06	1.85	1.03	1.76	0.65	1.94

1 mi = 1.61 km

Effect of Truck Speed on the Response of Strain Gauges

The measurements from all the strain gauges indicated that the speed of the test vehicle has a significant effect on the measured strains. This observation is consistent with the data collected under phase I of the project. Reductions in the measured strain in the order of 30 and 50 percent were observed for speeds of 35 and 50 mi/h (56 and 80 km/h) when compared to strains observed at 20 mi/h (32 km/h), respectively. Even though the effect of speed on the measured strains was consistent among all gauges, the absolute reductions in the measured strains were inconsistent. The analysis of phase I data indicated that the inertia of the pavement is insignificant and the effect of speed on the measured strains is mainly due to the viscoelastic behavior of the asphalt concrete material.

UNCERTAINTY

As discussed under the analysis of phase I data (chapter 3), several factors must be taken into consideration when evaluating the uncertainty of the measurements from the various types of strain gauges. The various means of handling these factors were also discussed. The phase II data were also subjected to the effects of the same factors; therefore, a similar approach was used to consider the effect of nonuniformity of pavement material and thickness variability. As far as dynamic loads are concerned, PennDOT's WIM system was used to evaluate the dynamic load variations at the test sections. The test track (tractor-trailer combination) was loaded at the three load levels of empty, intermediate, and loaded, and the individual axles were weighed statically and as they ran over the WIM pads. Table 55 shows the measurements of the WIM system for the gross weight, single drive axle, and front and rear tandem axles. The WIM data indicate that a variability in the dynamic loads exists among the various replicate measurements. The front tandem axle showed the highest variability.

The WIM data were used in the uncertainty analysis: the variability of WIM measurements for the various cases of axle type and load level was used to adjust the static loads. As a result, a range of static loads is obtained that is used in the theoretical analysis.

Table 55. Summary of the WIM measurements.

Type of Weight	Static Weight (lb)	Number of Observations	Mean	Standard Deviation	Coefficients of Variation (%)
Gross Weight	25,160	16	29,492	3,026	10
	43,391	17	42,692	1,591	4
	66,675	30	63,343	3,194	5
Drive Single Axle	7,935	16	10,164	1,095	11
	13,230	17	13,600	1,312	10
	18,220	30	17,019	1,013	6
Front Tandem	5,170	16	6,970	1,906	27
	12,655	17	12,686	2,250	18
	22,450	30	20,146	1,363	7
Rear Tandem	3,470	16	5,657	777	14
	9,165	17	10,080	1,878	19
	17,635	30	19,236	1,897	10

1 lb = 4.5 N

Using the variability in the layer thickness, material nonuniformity, and dynamic loads, researchers determined the range of the theoretical strains from the elastic multilayer solution and compared them to the measured strains at 70 mi/h (32 km/h) as shown in figures 54 through 57. The data in these figures show that the majority of the measured strains are in the range of the calculated strains for the thin section. The measured strains on the thick section showed higher variability among the various gauges and a larger range of calculated strains. It is important to recognize that the WIM data give an indication of the variability of dynamic loads. However, it does not provide any information regarding the dynamic load profile along the test section. The dynamic load profile is a major contributor to the fact that the measured strains are higher than calculated values for some stations and lower than calculated values at other stations. The variation in dynamic load profiles and the strain response along a highway section is represented by various degrees of roughness developed in inservice highway pavements.

REGRESSION ANALYSIS OF STRAIN MEASUREMENTS

A linear regression analysis was conducted to investigate the relationship between the measurements from the individual gauges and the average measurements of all gauges. The Hall effect, the Kyowa, and the PML strain gauges were all installed at the bottom of the asphalt concrete layer in the longitudinal direction. The general form of the regression equations and the evaluation procedure were presented in chapter 3 of this report. Therefore, the discussion here will be limited to the presentation of the intercept, slope, coefficient of correlation, and the standard error of parameter estimate for each group of gauges.

Table 56 shows the summary of the statistical analysis for the various types of gauges. Figures 58, 59, and 60 show the actual data for the Kyowa, Hall effect, and PML gauges, respectively. The data show that the intercepts of the regression models are very small for all types of gauges. However, the coefficients of correlation for the Kyowa and PML gauges are rather low, and the slopes of all types of gauges are far from unity.

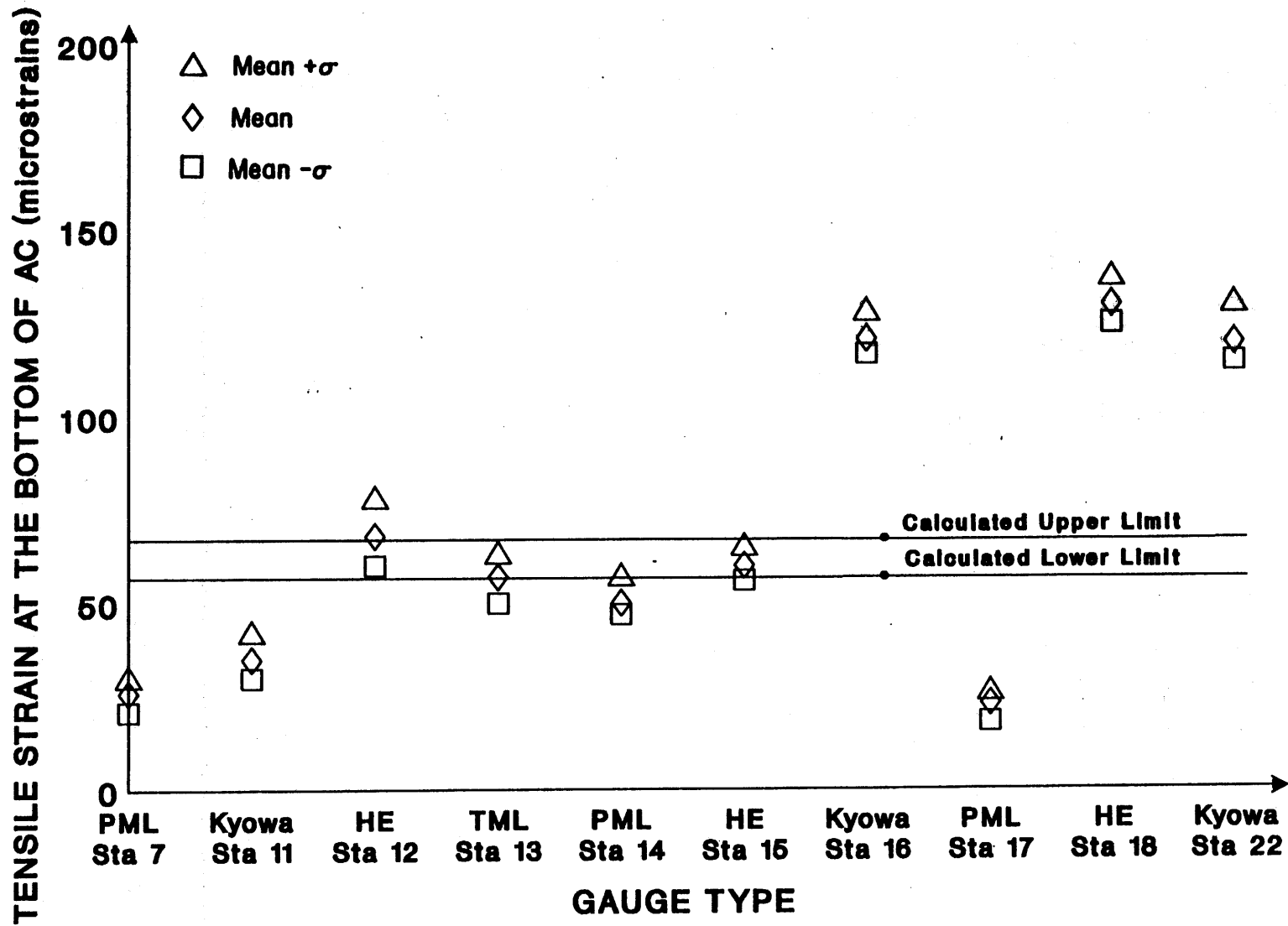


Figure 54. Comparison of measured and calculated strains under a single drive axle load of 13,500 lb (6 129 kg) for the thin section.

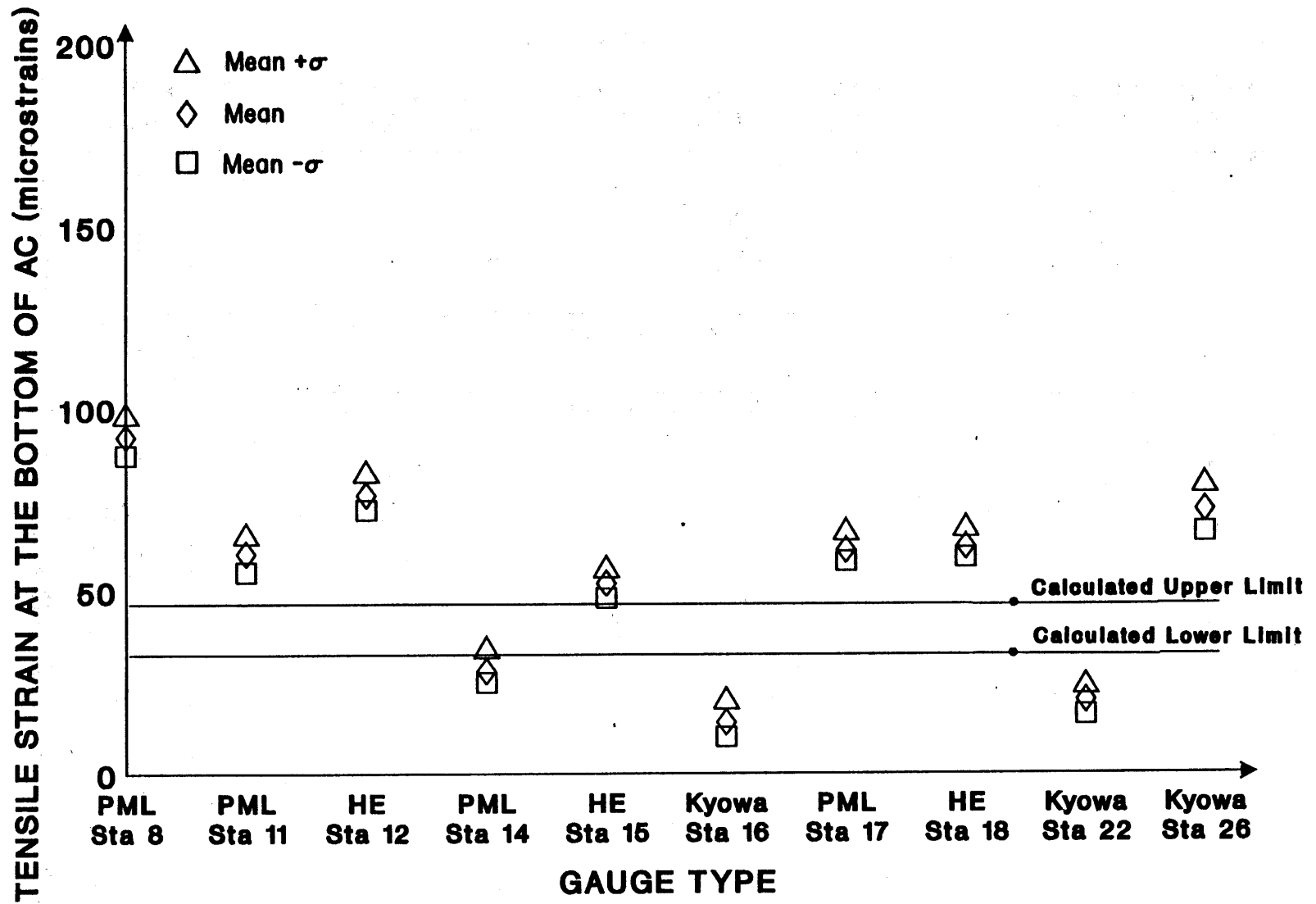


Figure 56. Comparison of measured and calculated strains under a single drive axle load of 13,500 lb (6 129 kg) for the thick section.

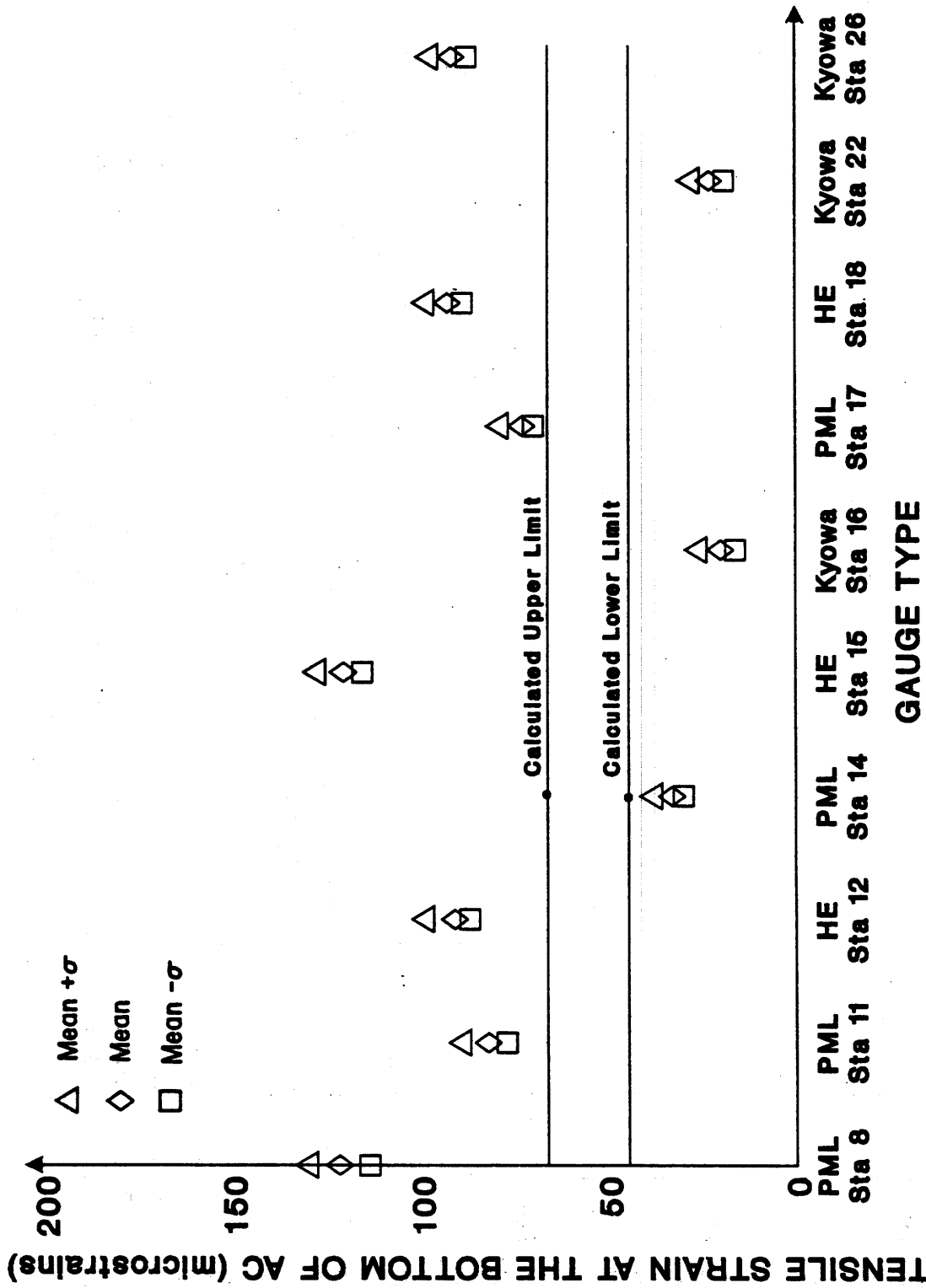


Figure 57. Comparison of measured and calculated strains under a single drive axle load of 18,500 lb (8 399 kg) for the thick section.

Table 56. Statistical summary of the regression analysis for the thin and thick section, drive and trailer axles, phase II.

Independent Variable: Average value of all the gauges.

Dependent Variable	Intercept a	Slope b	Sample Size	R-squared %	Std. Error of Est.	Mean	Minimum	Maximum
Kyowa	-6.91	1.055	864	66	16.3	44	7	96
Hall Effect	5.76	1.261	864	91	8.8	76	22	120
PML	1.39	0.68	864	64	11.1	34	9	84

K vs All Thin & Thick Sections

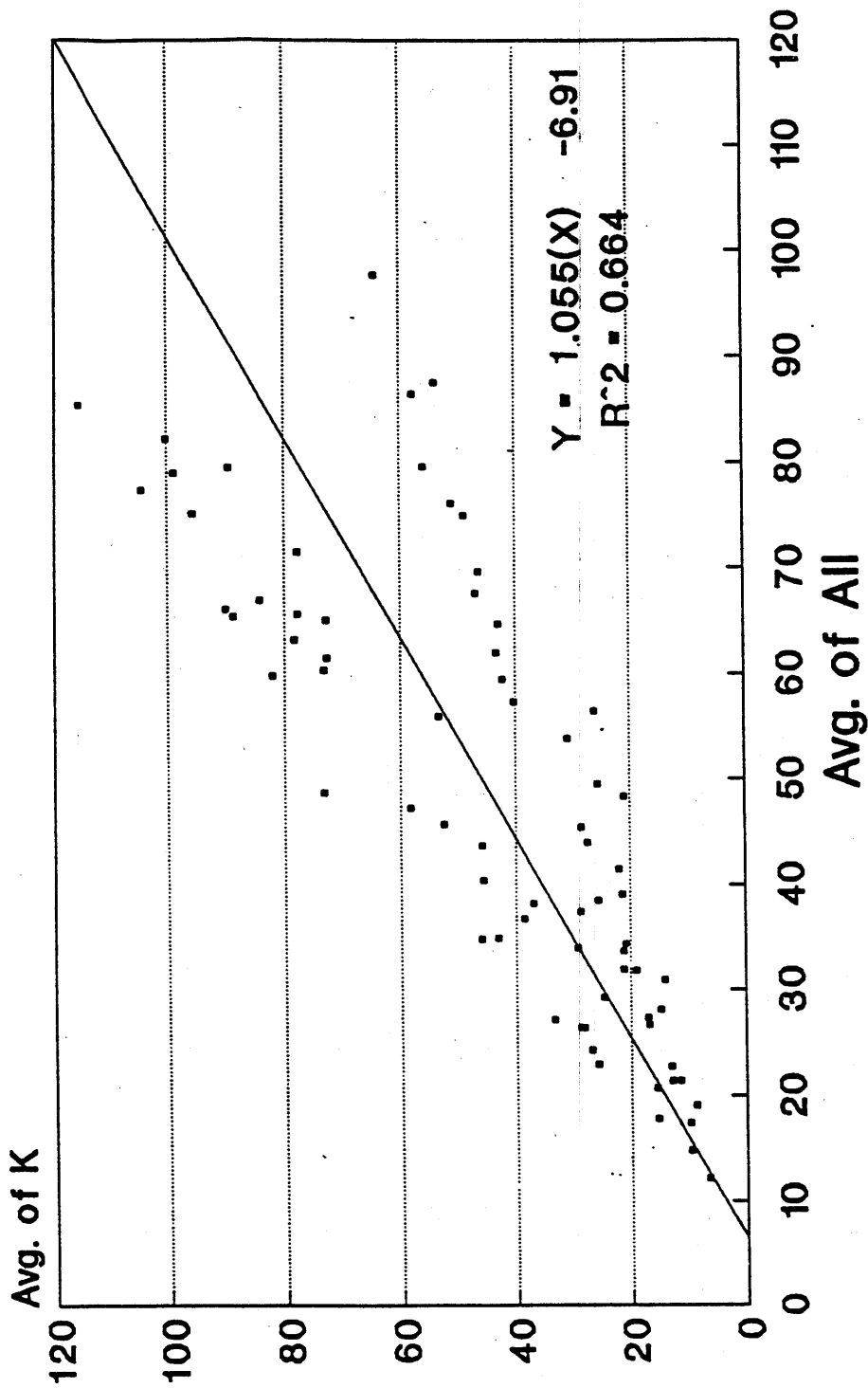


Figure 58. Correlation between the Kyowa gauges and the overall mean of all gauges--phase II.

ACH vs All Thin & Thick Sections

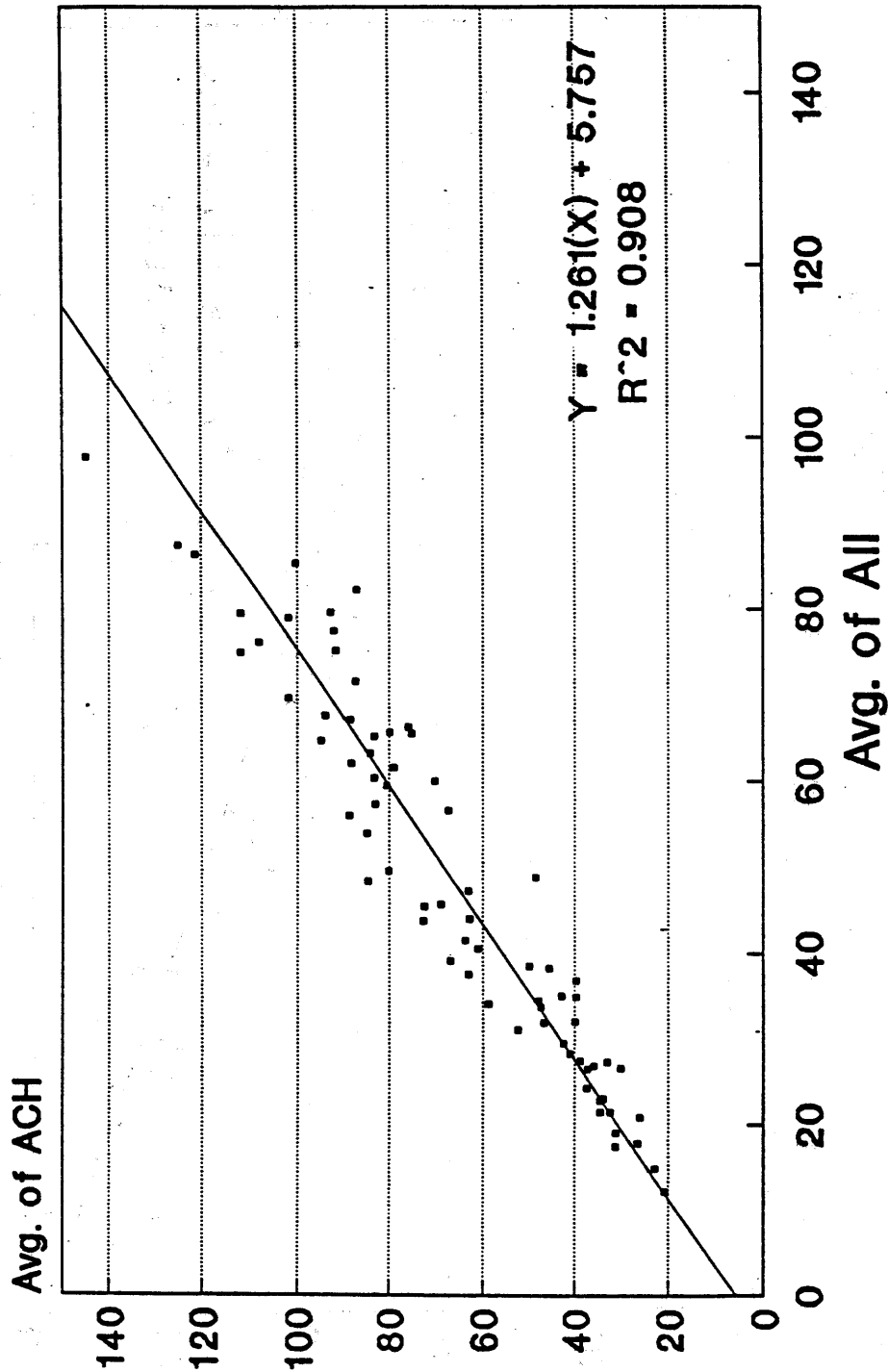


Figure 59. Correlation between the Hall effect gauges and the overall mean of all gauges--phase II.

PML vs All Thin & Thick Sections

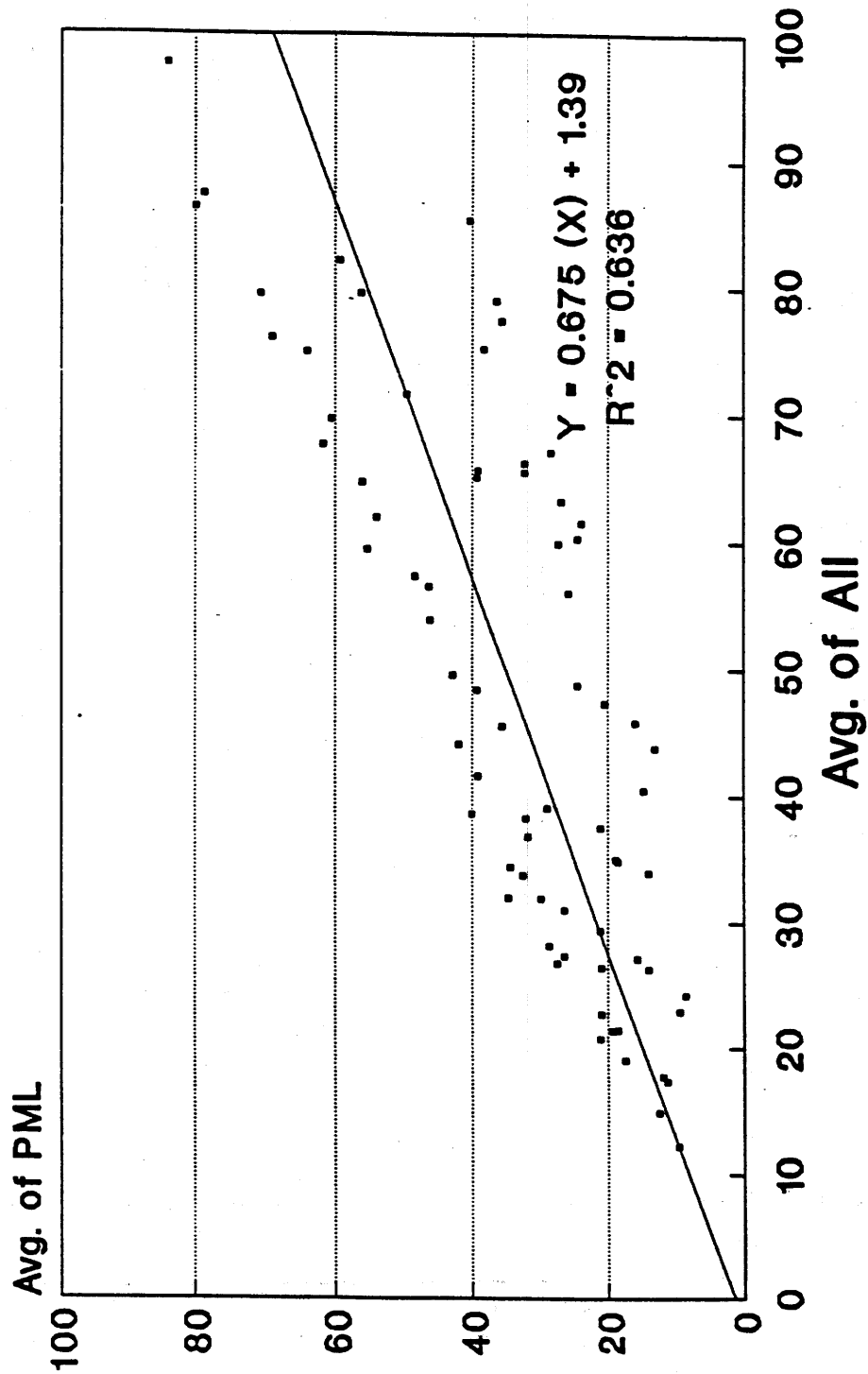


Figure 60. The correlation between the PML gauges and the overall mean of all gauges--phase II.

The results of the regression analysis indicate that there is not a good correlation between the various types of gauges. The Hall effect gauge has the highest R-squared value, while the Kyowa and PML gauges have low R-squared values. Note that the Kyowa gauges were evaluated in the first phase of the research and had performed extremely well compared to the other types of gauges.

Additional regression analyses were conducted to identify the source of the low R-squared values. These analyses separated the data from the two pavement sections. Figures 61, 62, and 63 show the actual data for the Kyowa, Hall effect, and PML gauges on the thick section. Note that the R-squared values are considerably higher than the ones generated from the combined analysis (i.e., thin and thick). Based on this data, it can be concluded that there is good agreement among the various types of gauges on the thick section and poor agreement among the various gauges on the thin section. In general, the strain values measured from the thin section are always 20 to 50 percent higher than the ones measured from the thick section. Finally, the regression analysis has supported the conclusions drawn based on the other evaluation criteria, which indicate that the Hall effect gauges can be used in pavement instrumentation. However, more research must be performed to investigate the design and methods of installation of those gauges, especially when they are subjected to high strains.

STRAIN MEASUREMENTS IN THE UNBONDED LAYERS

Strain gauges were installed in the crushed aggregate base course and the subgrade layers. The Hall effect, Carlson, and TML soil strain gauges were installed at mid-depth into the base course in the longitudinal direction. The Hall effect and TML soil strain gauges were installed 3 in (76 mm) into the subgrade in the vertical direction. The actual locations of these gauges in both sections were shown in figures 52 and 53.

SURVIVABILITY

The gauges in the base and subgrade layers of the thick section that survived the installation and construction process are listed below:

K vs All Thick Sections

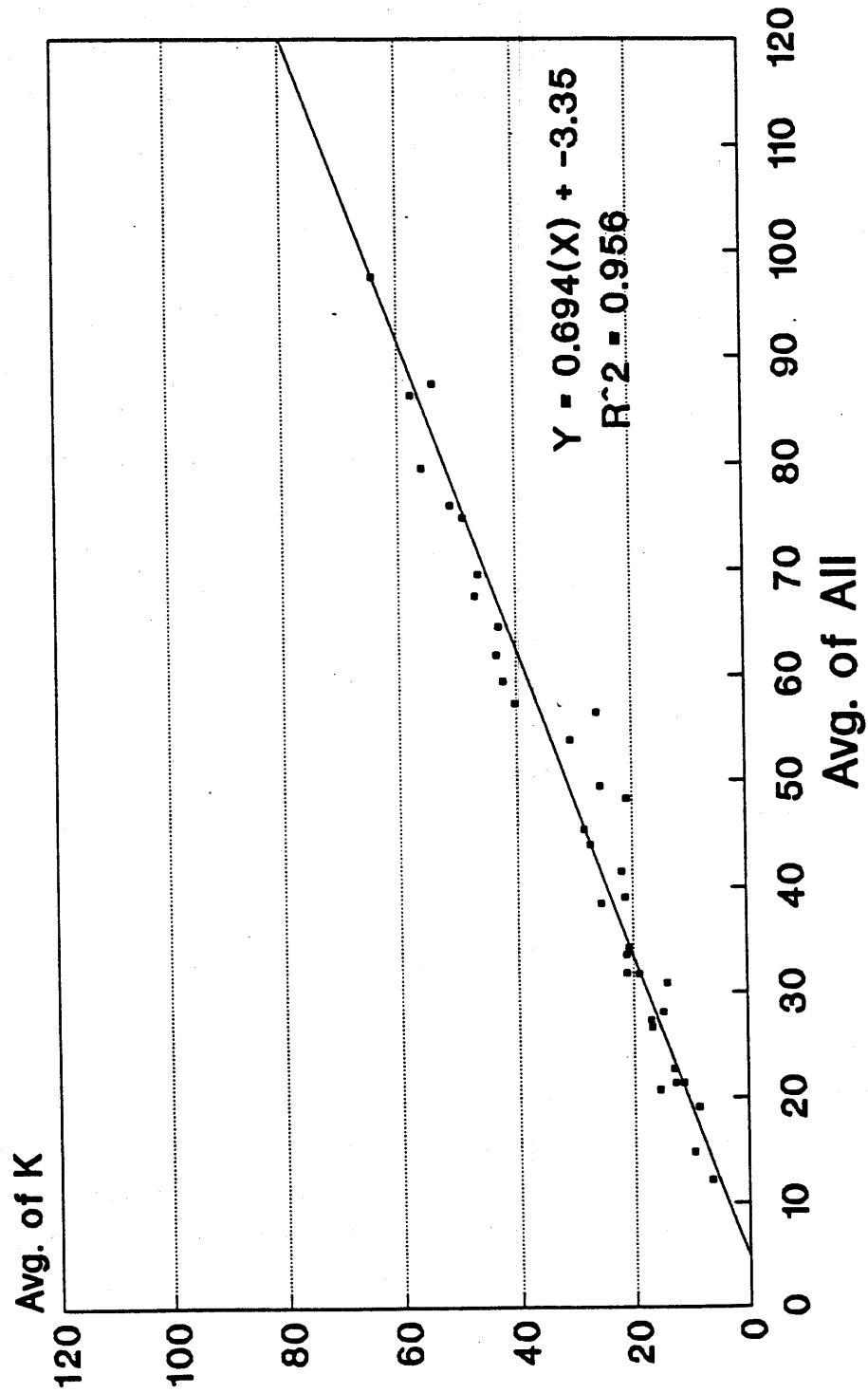


Figure 61. Correlation between the Kyowa gauges and the overall mean of all gauges, thick section.

ACH vs All Thick Sections

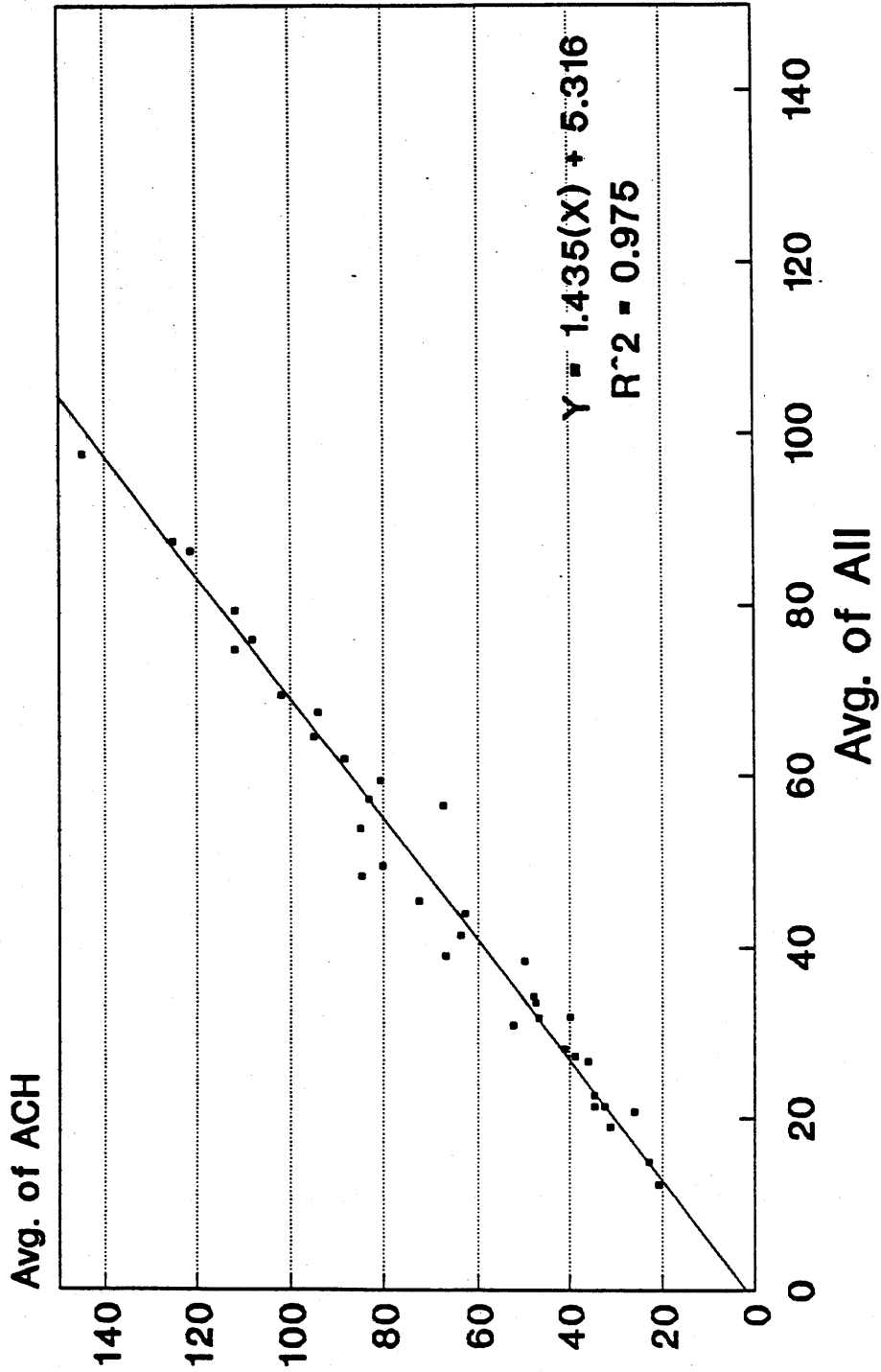


Figure 62. Correlation between the Hall effect gauges and the overall mean of all gauges, thick section.

PML vs All Thick Sections

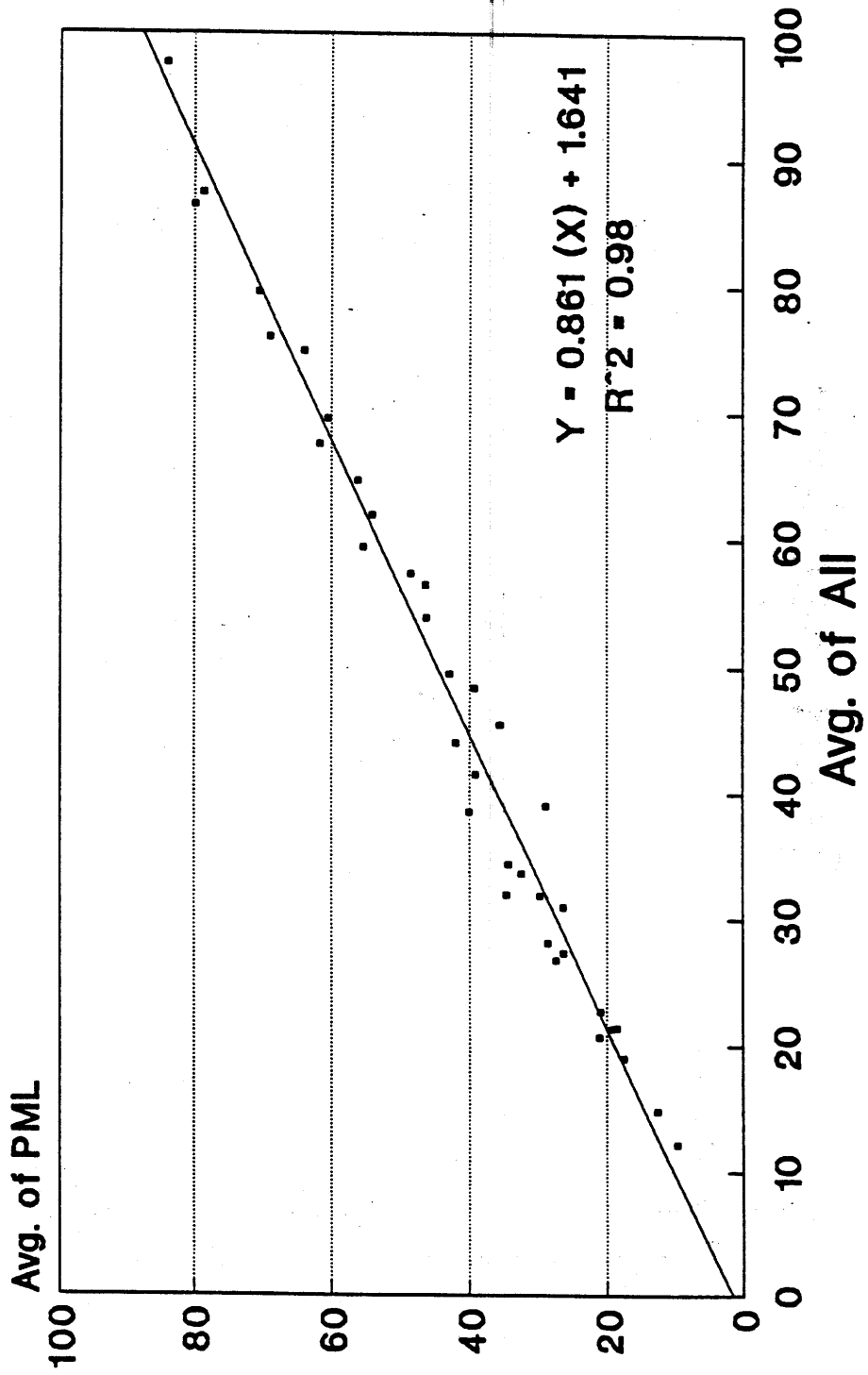


Figure 63. Correlation between the PML gauges and the overall mean of all gauges, thick section.

- One TML soil strain gauge in the base course at station 11.
- One Hall effect soil strain gauge in the base course at station 14.
- One Hall effect soil strain gauge in the subgrade at station 8.

Two Hall effect strain gauges and one Carlson gauge in the base course and two Hall effect gauges and one TML soil strain gauge in the subgrade were unoperational shortly after construction.

One gauge in the base and subgrade layers of the thin section survived the installation and construction process: one Hall effect strain gauge in the base course at station 20.

One TML soil strain gauge, one Hall effect strain gauge, and one Carlson gauge in the base course and three Hall effect soil strain gauges and one TML soil strain gauge in the subgrade were all unoperational shortly after construction. The above data indicate that the failure rate of the soil strain gauges is very high, which indicates that some major improvements must be made in the design and installation procedures of these new concept soil strain gauges.

REPEATABILITY

The data from the soil strain gauges were collected simultaneously with the data from the asphalt concrete strain gauges. Therefore, four replicates were obtained for each combination of the test variables. Again, the evaluation of the repeatability of the gauges will depend on their measured coefficients of variation. Tables 57 and 58 show typical data from the soil strain gauges for the thick and thin sections, respectively. The data show that a majority of COV's are less than 10 percent, which indicates that the survived soil strain gauges did actually have good repeatability. Appendix E in volume II shows the results of the four replicates and their corresponding means, standard deviations, and COV's.

Table 57. Strain values in unbonded layers under drive and tandem axles, heavy load level, tire pressure of 100 psi (690 kPa), thick section.

Truck Speed (mi/h)	CABH-14 DRV	TCAB-11 DRV	CABH-14 TAN1	TCAB-11 TAN1	CABH-14 TAN2	TCAB-11 TAN2	SGH-8 DRV	SGH-8 TAN1	SGH-8 TAN2
20	33.40	63.45	17.70	44.84	34.70	87.96	32.80	19.15	40.40
20	33.10	70.85	17.15	48.81	34.40	91.83	33.45	20.30	36.15
20	30.75	66.05	19.10	45.20	36.80	87.77	35.80	23.25	40.75
20	32.85	64.20	18.08	49.99	33.05	88.04	36.65	20.50	39.80
Mean	32.53	66.14	18.01	47.21	34.74	88.90	34.68	20.80	39.27
STD	1.04	2.88	0.71	2.23	1.34	1.69	1.60	1.51	1.84
CV	3.21	4.35	3.95	4.73	3.87	1.90	4.60	7.24	4.67
35	31.19	61.13	16.28	38.19	37.32	84.83	33.45	20.48	46.91
35	31.45	60.35	16.50	40.80	33.25	84.61	32.10	16.65	42.00
35	30.15	61.12	16.29	40.80	35.22	83.73	32.68	17.33	46.67
35	31.40	62.06	14.55	39.13	37.35	84.00	33.80	16.77	41.15
Mean	31.05	61.17	15.90	39.73	35.78	84.29	33.01	17.80	44.18
STD	0.53	0.61	0.79	1.12	1.70	0.44	0.66	1.56	2.62
CV	1.70	0.99	4.95	2.82	4.75	0.53	2.01	8.78	5.94
50	25.11	37.73	9.06	8.37	28.75	35.99	35.45	11.49	32.20
50	26.64	31.86	11.14	20.18	25.69	62.08	41.65	9.15	37.05
50	25.20	37.71	N/A	9.80	N/A	41.20	27.60	N/A	N/A
50	30.76	33.90	N/A	13.03	N/A	56.16	33.95	N/A	N/A
Mean	26.93	35.30	10.10	12.84	27.22	48.86	34.66	10.32	34.63
STD	2.30	2.53	1.04	4.56	1.53	10.63	5.00	1.17	2.42
CV	8.53	7.15	10.29	35.49	5.62	21.77	14.41	11.34	7.00

1 mi = 1.61 km

Table 58. Strain value in unbonded layers under drive and tandem axles, intermediate load level, tire pressure of 100 psi (690 kPa), thin section.

Truck Speed (mi/h)	CABH-20 DRV	CABH-20 TAN1	CABH-20 TAN2
20	72.50	65.25	60.17
20	59.15	73.20	48.45
20	59.96	73.51	60.10
20	81.67	73.65	63.60
Mean	68.32	71.40	58.08
STD	9.35	3.56	5.74
CV	13.69	4.98	9.88
35	81.05	47.25	91.22
35	81.49	55.65	93.03
35	87.25	50.80	87.19
35	81.45	66.95	90.45
Mean	82.81	55.16	90.47
STD	2.57	7.43	2.11
CV	3.10	13.47	2.33
50	49.75	31.37	79.31
50	35.69	28.08	65.15
50	35.38	29.53	64.77
50	50.05	31.20	64.50
Mean	42.72	30.04	68.43
STD	7.18	1.34	6.28
CV	16.82	4.48	9.18

1 mi = 1.61 km

EFFECTS OF TEST VARIABLES ON THE RESPONSE OF SOIL STRAIN GAUGES

As discussed earlier, very few soil strain gauges survived the installation and construction process. The collected data are scattered and do not support any recommendations or conclusions with respect to the performance of these gauges. In general, the new concept soil strain gauges require major improvements before they can be used in full-scale testing facilities.

ANALYSIS OF DEFLECTION DATA

Three types of deflection-measuring devices were selected for the field-testing experiment:

- Single-layer deflectometer with Hall effect sensor.
- Single-layer deflectometer with inductive displacement sensor.
- Multidepth deflectometer with Hall effect sensor.

The analyses of the data from the two single-layer deflectometers are combined, while the analysis of the MDD data is discussed separately.

SURVIVABILITY

Two types of single-layer deflectometers were installed at each section: one with the Hall effect sensor and one with the inductive displacement sensor. All SLD's were attached to the top of the asphalt concrete layer and measured surface deflections. The SLD with the Hall effect sensor in the thick section was unoperational after the installation and construction process. Considering that both SLD's were using the new measuring concepts, their survivability was good.

REPEATABILITY

The repeatability data of the SLD's are shown in tables 59, 60, and 61 for both thick and thin sections. The full data for all gauges are shown in

Table 59. Summary of the means, standard deviations, and coefficients of variation for the single-layer deflectometer with inductive displacement sensor, thick section.

Axle Type	Axle Load (kips)	Speed (mi/h)	Mean	Standard Deviation	Coefficients of Variation (%)
Single Drive Axle	18,000	20	5.53	0.56	10.07
		35	4.30	1.16	27.03
		50	5.32	2.09	39.38
Tandem Axle (Rear Axle)	41,000	20	5.73	0.23	4.05
		35	4.37	1.01	23.18
		50	5.20	1.70	32.67
Single Drive Axle	13,000	20	5.15	1.37	26.55
		35	3.37	1.17	34.61
		50	5.85	1.20	20.45
Tandem Axle (Rear Axle)	23,000	20	5.84	0.13	2.16
		35	1.41	0.11	7.65
		50	6.38	1.33	20.92
Single Drive Axle	8,000	20	1.52	0.17	11.01
		35	1.82	0.64	34.99
		50	2.85	0.26	9.14
Tandem Axle (Rear Axle)	9,000	20	0.52	0.08	15.02
		35	0.97	0.15	15.33
		50	0.71	0.23	32.22

1 mi = 1.61 km

Table 60. Summary of the means, standard deviations, and coefficients of variation for the single-layer deflectometer with Hall effect sensor, thin section.

Axle Type	Axle Load (kips)	Speed (mi/h)	Mean	Standard Deviation	Coefficients of Variation (%)
Single Drive Axle	13,000	20	4.55	0.09	2.03
		35	5.09	0.36	7.13
Tandem Axle (Rear Axle)	23,000	20	4.26	0.14	3.33
		35	4.61	0.20	4.34
Single Drive Axle	8,000	20	3.34	0.02	0.67
		35	3.51	0.23	6.52
Tandem Axle (Rear Axle)	9,000	20	3.28	1.35	40.99
		35	1.92	0.14	7.47

1 mi = 1.61 km

Table 61. Summary of the means, standard deviations, and coefficients of variation for the single-layer deflectometer with inductive displacement sensor, thin section.

Axle Type	Axle Load (kips)	Speed (mi/h)	Mean	Standard Deviation	Coefficients of Variation (%)
Single Drive Axle	18,000	20	5.45	0.14	2.49
		35	4.89	0.09	1.89
		50	4.58	0.83	18.07
Tandem Axle (Rear Axle)	41,000	20	5.61	0.02	0.31
		35	5.10	0.25	4.85
		50	3.82	1.07	27.96
Single Drive Axle	13,000	20	4.27	0.80	18.67
		35	4.68	0.25	5.32
		50	4.28	0.60	14.12
Tandem Axle (Rear Axle)	23,000	20	3.67	0.93	25.31
		35	4.16	0.37	8.80
		50	3.96	0.62	15.53

1 mi - 1.61 km

appendix F of volume II. The data indicate that the majority of COV values for the inductive displacement SLD on the thick section are more than 15 percent, and some of these are as high as 39 percent. The COV values for the SLD's on the thin section are in general less than 10 percent for the Hall effect sensor and somewhat more variable for the inductive displacement sensor (see table 61). In general, the repeatability of the SLD's on the thick section was poor, and the repeatability of the Hall effect SLD on the thin section is good. The repeatability of the inductive displacement SLD on the thin section was poor.

EFFECT OF TEST VARIABLES ON THE RESPONSE OF SLD

By examining the data in appendix F of volume II, it is obvious that the effect of tire pressure on the response of SLD's is negligible. The effect of axle load and speed on the response of SLD's can be investigated by examining the data in tables 59, 60, and 61. The effect of load is significant; however, the change in the measured deflection on the thick section (table 59) did not coincide well with the change in the magnitude of axle load. For example, the change in the deflection was on the order of 8 percent for a change in the single drive axle load of 27 percent, while the change in the deflection was in the order of 70 percent for a change in the single drive axle load of 55 percent. This inconsistency was also shown under the tandem axle load. The changes in the deflections on the thin section (tables 60 and 61) coincide closely with the changes in the axle load magnitudes. One major inconsistency in the inductive displacement SLD data is that the gauge measured the same magnitude of deflections on the thick and thin section for similar axle loads (tables 59 and 61). This indicates that there are some serious problems with the inductive displacement SLD. The effect of speed on the measured deflections can also be investigated by examining the data in tables 59, 60, and 61. The data showed highly inconsistent relationships between the measured deflection and vehicle speed.

UNCERTAINTY

The same approach used in the uncertainty study of strain gauges was used in this analysis. The researchers calculated a range of theoretical

deflections based on the variations in the various factors affecting the deflection response of the pavement (see chapter 3). The deflection data are plotted in figures 64, 65, and 66 for thick and thin sections. The figures show that there is not a good agreement between the measured and calculated surface deflections. However, the differences are not great, which is somewhat encouraging for the first application of these new concepts.

ANALYSIS OF MDD DATA

The modified MDD gauges were installed in section 9 of the Texas A&M Experiment Pavement test section. This pavement consists of 5 in (127 mm) of asphaltic concrete over an 8-in (203-mm) crushed limestone base. The MDD system was anchored at a constant depth as shown in figure 50.

Testing of the sensors was accomplished by a falling weight deflectometer and fully loaded dump truck. The FWD loading time was approximately 0.03 s; whereas the truck was traveling at creep speed with an axle loading time of approximately 3 s. Due to exposed wiring, neither the FWD nor the truck could be placed directly over the test hole. The FWD test plate was placed near the MDD hole so that the distance from the plate edge to center of MDD hole was 2.5 in (64 mm). In the truck test, the edge of the truck tire was approximately 4 to 6 in (102 to 152 mm) from the MDD hole.

During each test, data from both sensors were recorded simultaneously. The LVDT sensors were logged by computer; the Hall effect signals were captured on digital oscilloscope.

Figures 67 and 68 show typical raw deflection traces for the FWD and truck loads, respectively. The traces appear similar in overall shape; however, the main difference is that the Hall effect channel (6 in [152 mm] deep) has significantly more noise than the LVDT (13 in [330 mm] deep). Efforts described below were undertaken to identify the frequency of the noise and to eliminate it from the signal. The source of the noise was not determined. It was thought to be from the sensor rather than from the amplification system, which had been tested in the laboratory.

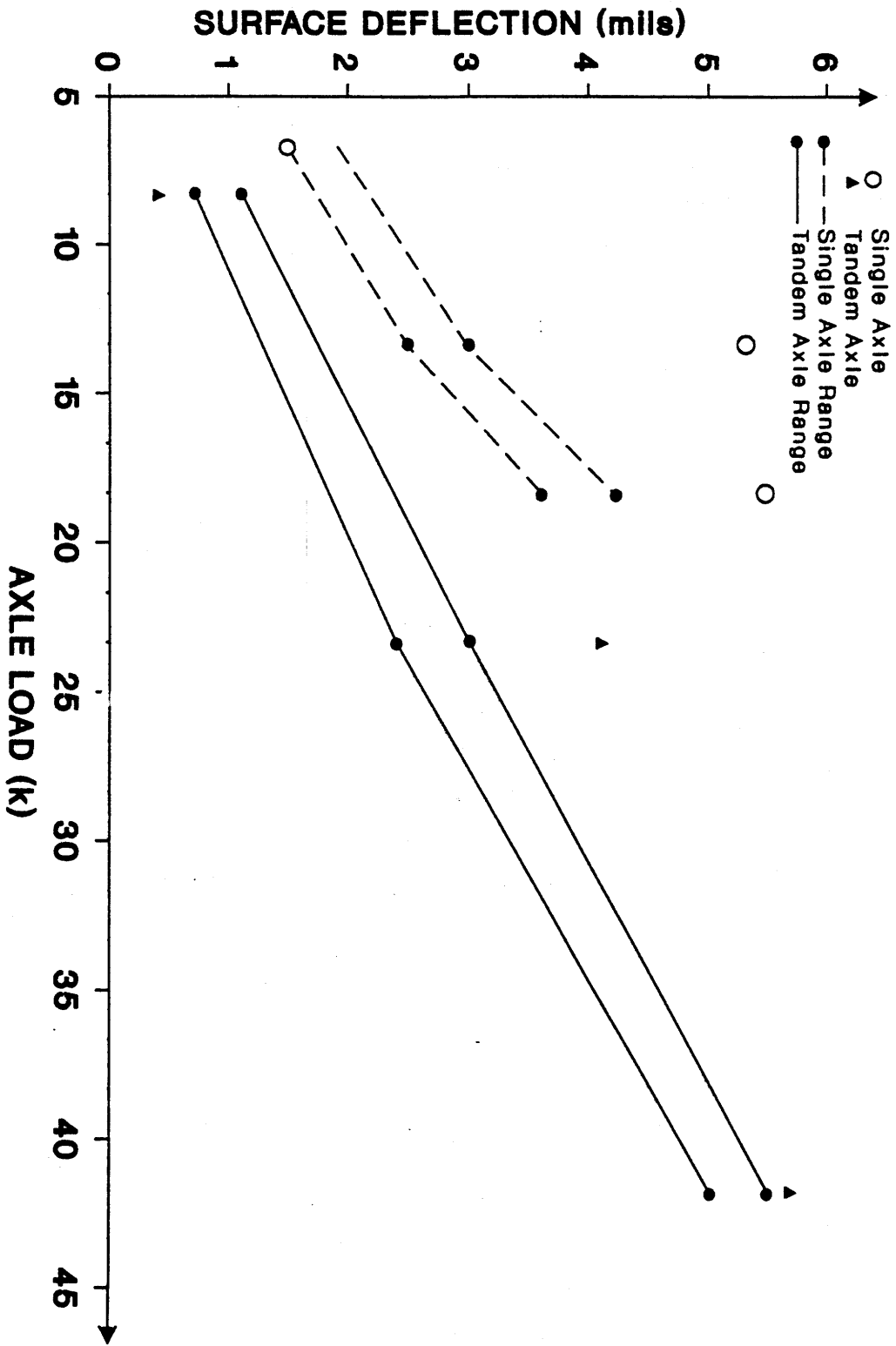


Figure 64. Comparison of measured and calculated surface deflection from the inductive displacement SID, thick section.

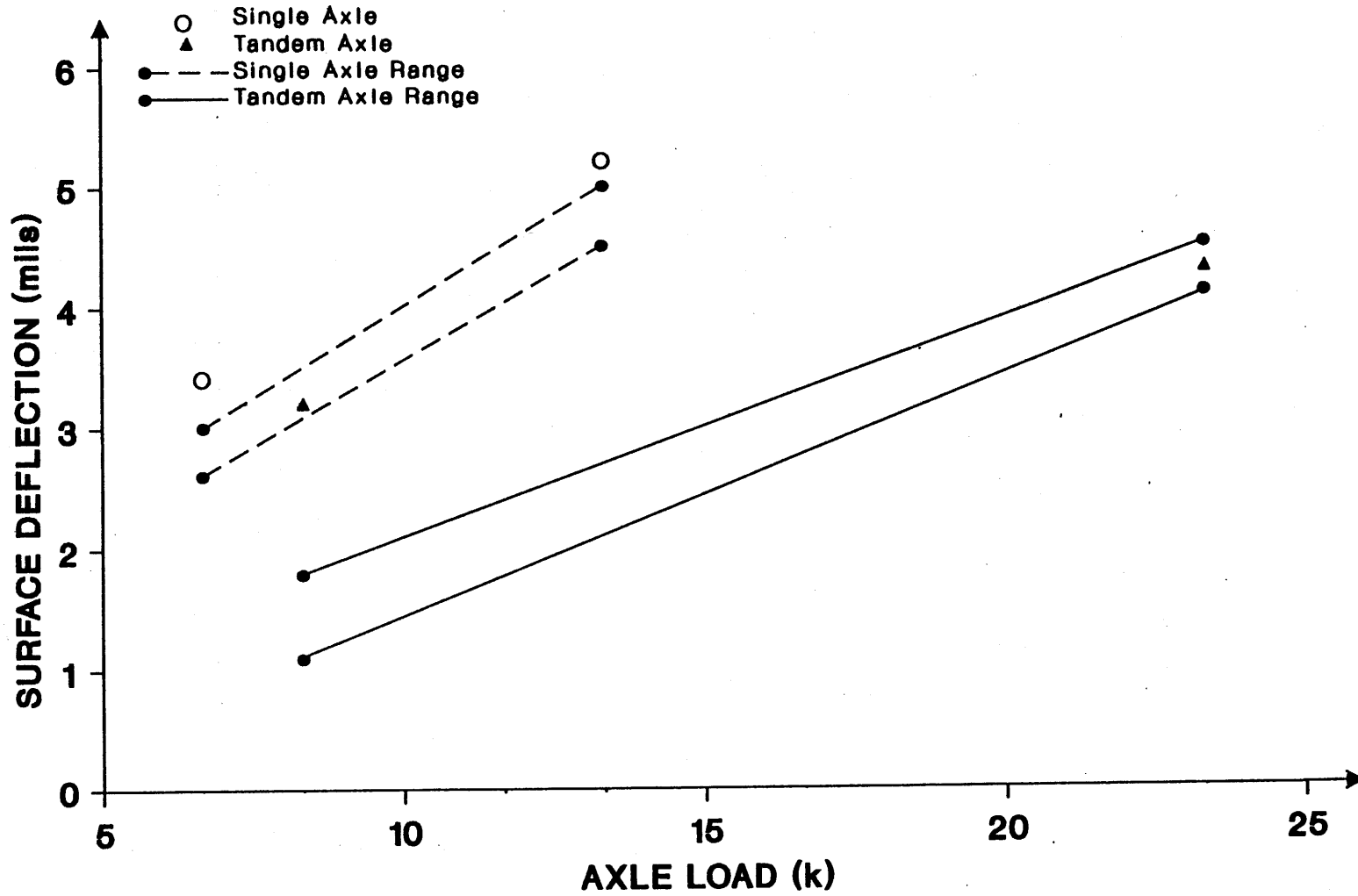


Figure 65. Comparison of measured and calculated surface deflection from the Hall effect SLD, thin section.

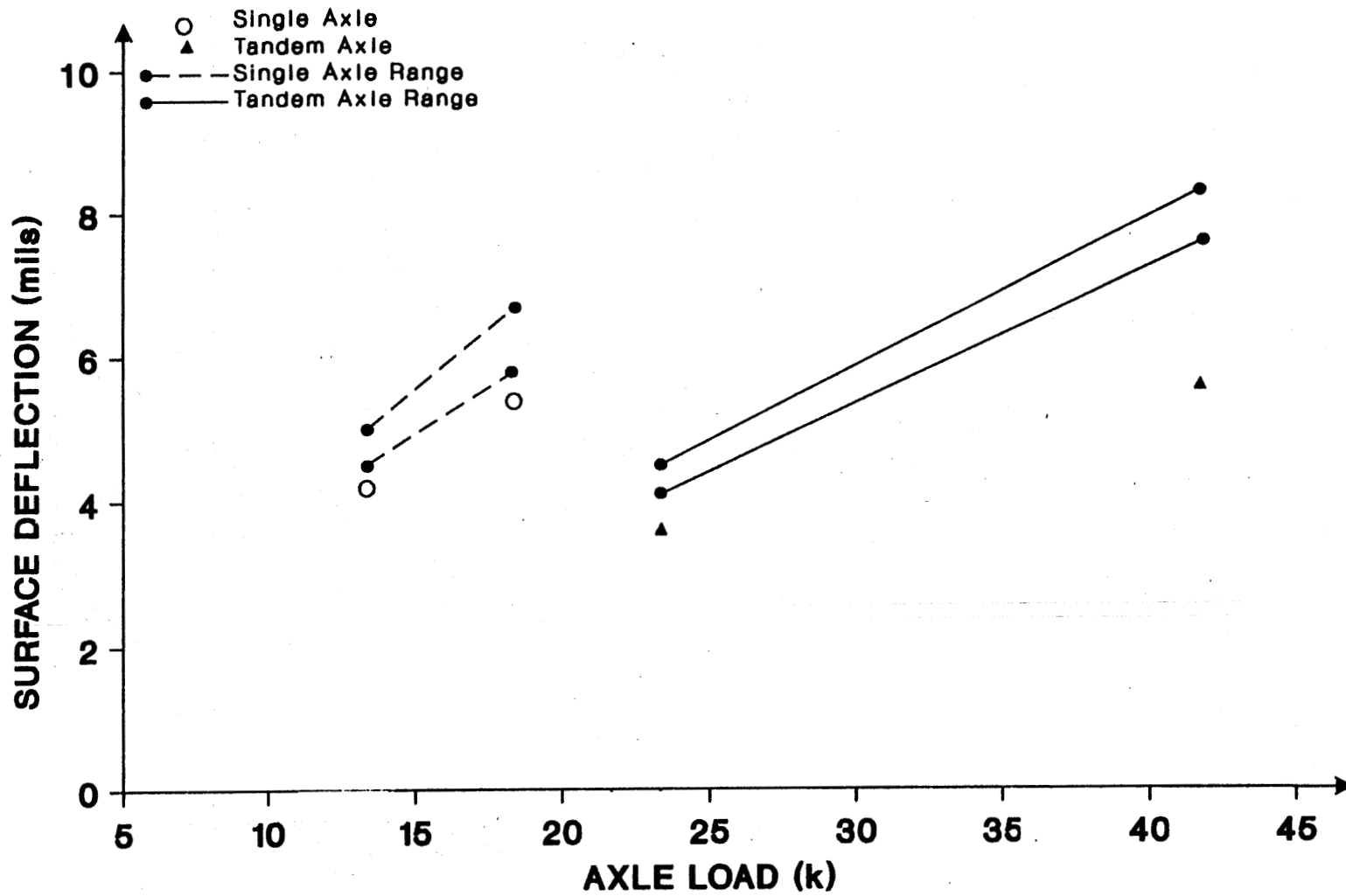


Figure 66. Comparison of measured and calculated surface deflection from the inductive displacement SLD, thin section.

COMPARISON OF SENSOR UNDER 14,528-LB FWD LOAD

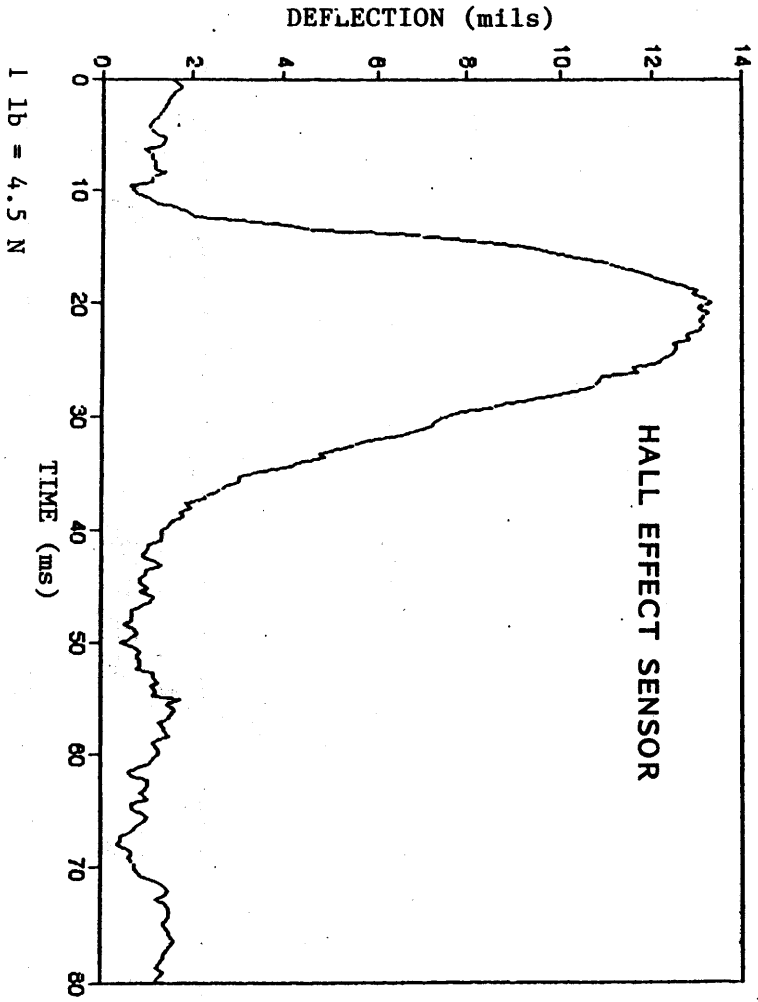
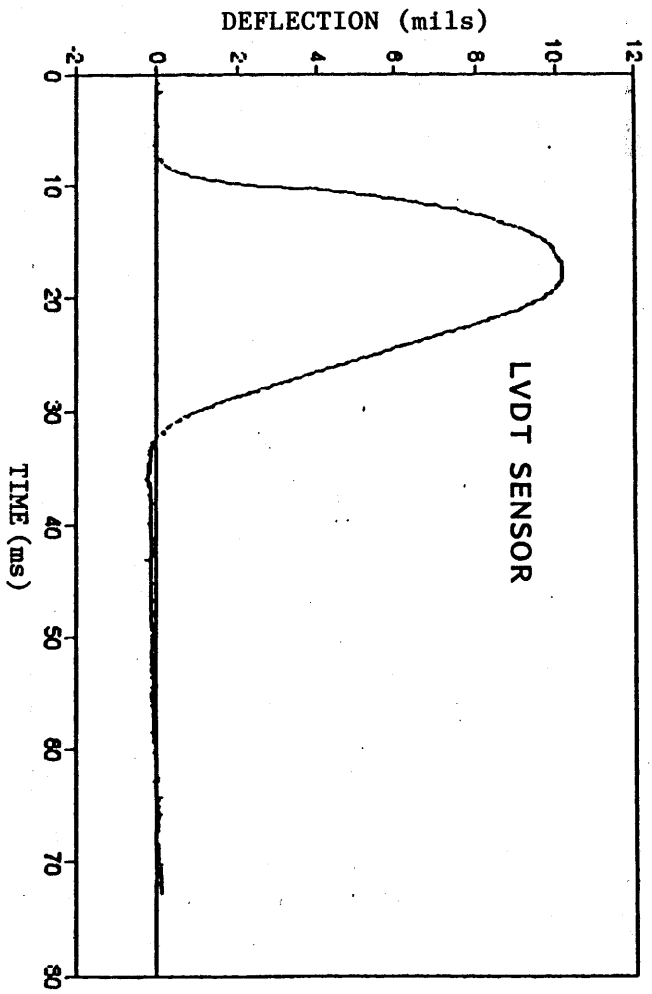


Figure 67. Typical raw sensor output for falling weight loads.

COMPARISON OF SENSOR UNDER TRUCK LOAD

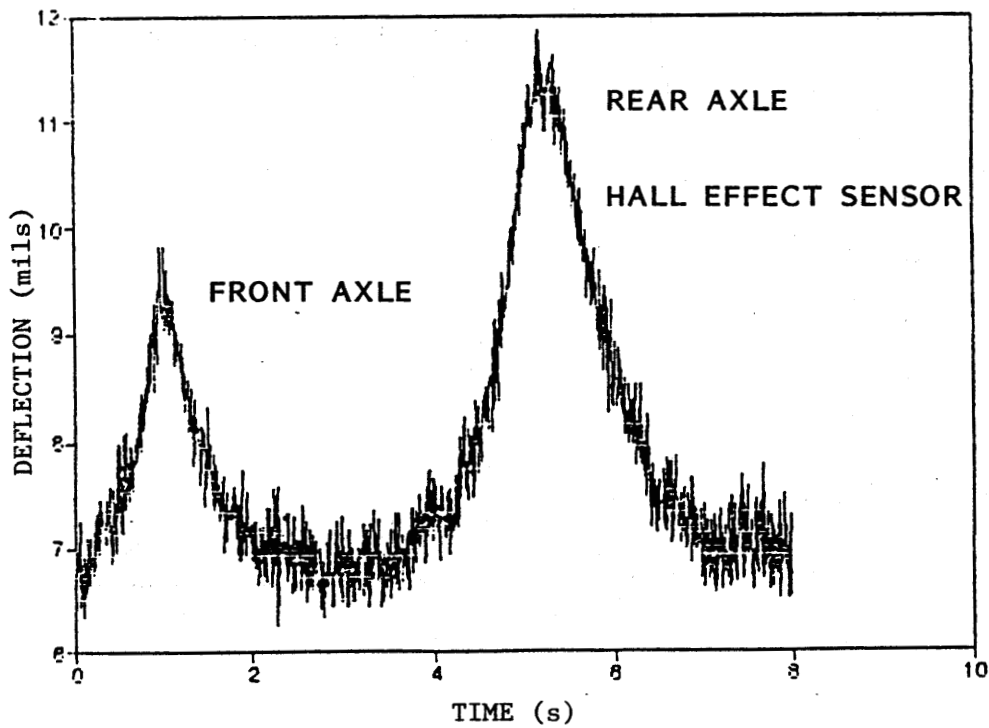
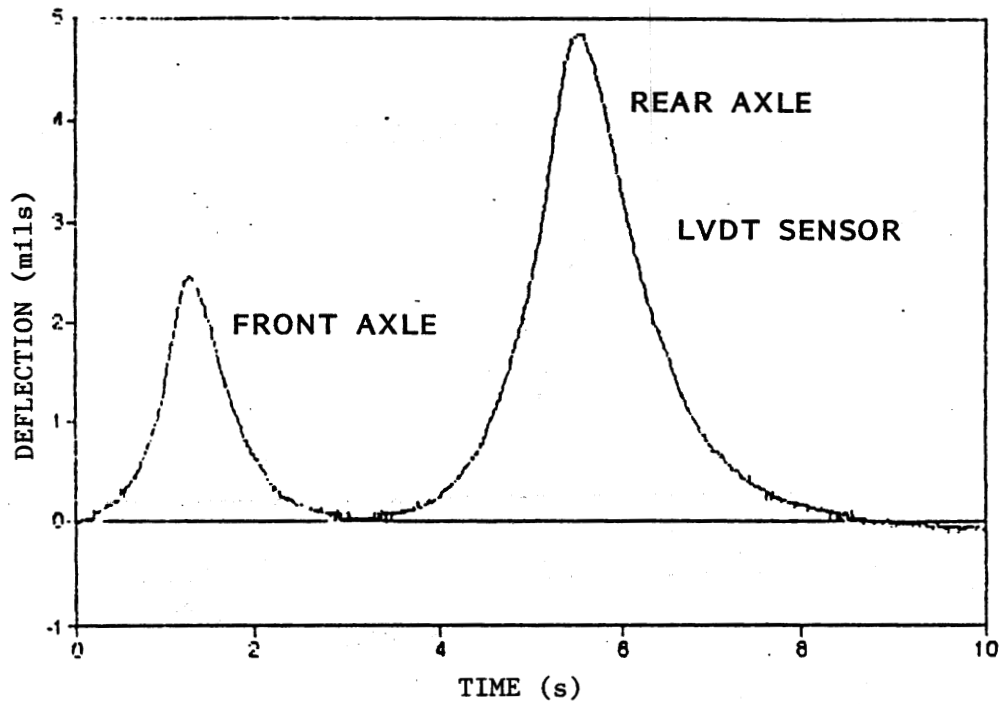


Figure 68. Typical sensor output for truck loads.

To investigate the frequency of the noise and to remove it from the signal, the FILTRUCK program developed by TTI was used. This program does a spectral analysis of the input signal, permits the user to select a low-pass frequency level, and rebuilds the signal with the high frequencies removed. The frequency spectra obtained by performing a Fast Fourier Transform on the Hall effect signals under truck loadings are shown in figure 69.

For the slow-moving truck, the relevant frequencies are in the 0- to 5-Hz range; the major noise on the truck signal is clearly shown at approximately 41 Hz. A similar spectral analysis was made of the Hall effect deflection response under FWD loading. The analysis shown in figure 70 indicated significant noise at approximately 53, 115, and 315 Hz. This presented a problem in setting a low-pass cut-off frequency for the FWD as the deflection signal itself is in the range of 0 to 50 Hz. In this analysis, the low-pass frequency was set at 50 Hz for the FWD and at 20 Hz for the truck. The filtered data are shown in figure 71. The truck plots are very smooth and similar to those measured with the LVDT. The FWD traces are significantly improved but still retain a minor low-frequency ripple in the base line.

To evaluate the repeatability of the Hall effect sensor, five identical drops were made with the FWD, and the resulting loads and measured deflections are shown in table 62. The LVDT peaks were extracted from the raw deflection signal; the Hall effect peaks were obtained after applying a 50-Hz, low-pass filter.

Both the LVDT and Hall effect sensors were highly repeatable; the coefficients of variation were less than 1 percent and of the same order of magnitude as the variation in FWD load impulse.

The Hall effect sensor can be used effectively as part of a multidepth deflectometer system. Its repeatability is similar to that measured with a typical LVDT. However, to achieve satisfactory performance, it is necessary to:

- Amplify the output signal from the Hall effect sensor.
- Use software filters to remove high-frequency noise from the signal.

HALL EFFECT FREQUENCY DISTRIBUTION TRUCK LOADING

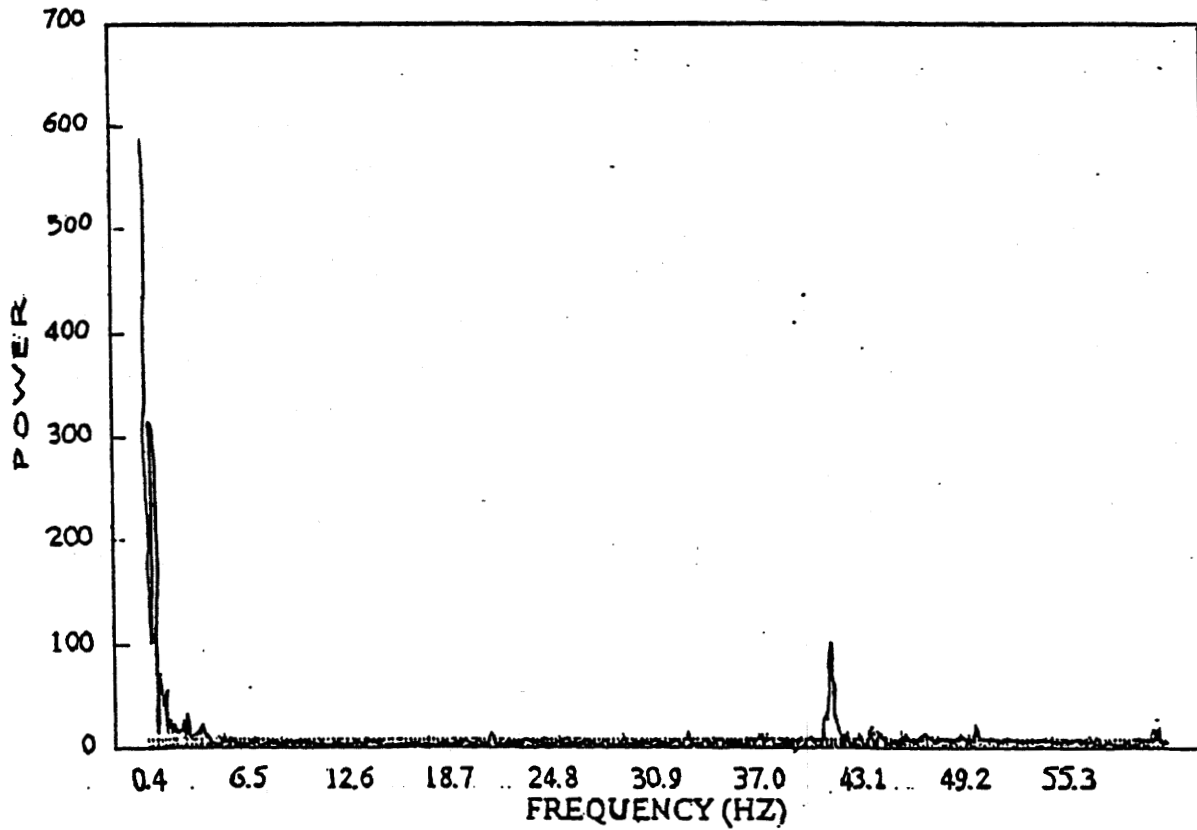


Figure 69. Power spectral analysis displaying the frequency components of the Hall effect sensors displacement output under truck loading.

FREQUENCY ANALYSIS OF HALL EFFECT

FWD LOAD 14528 LBS

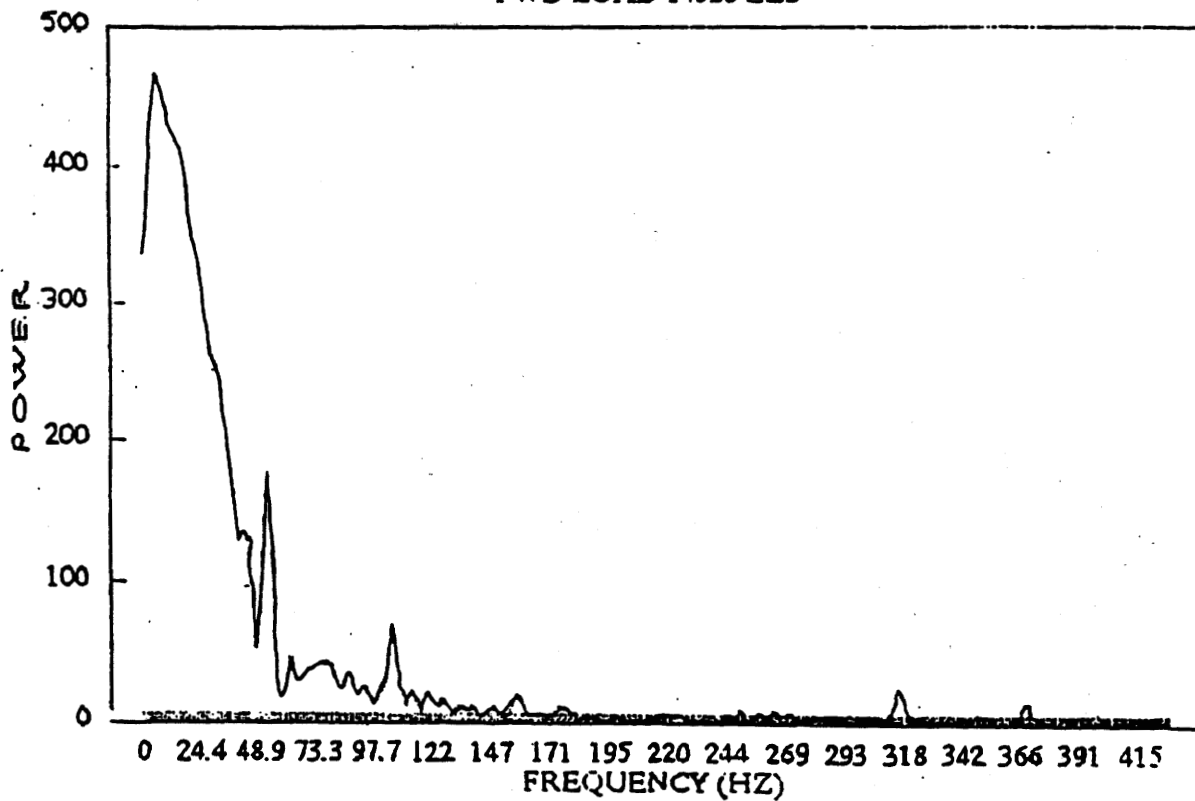
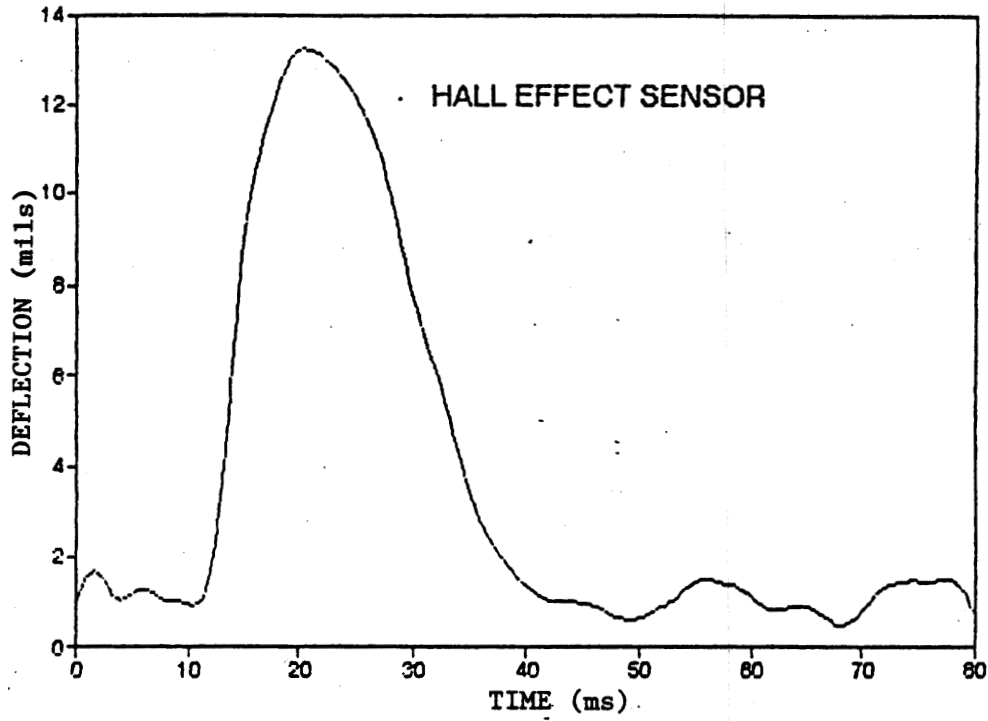
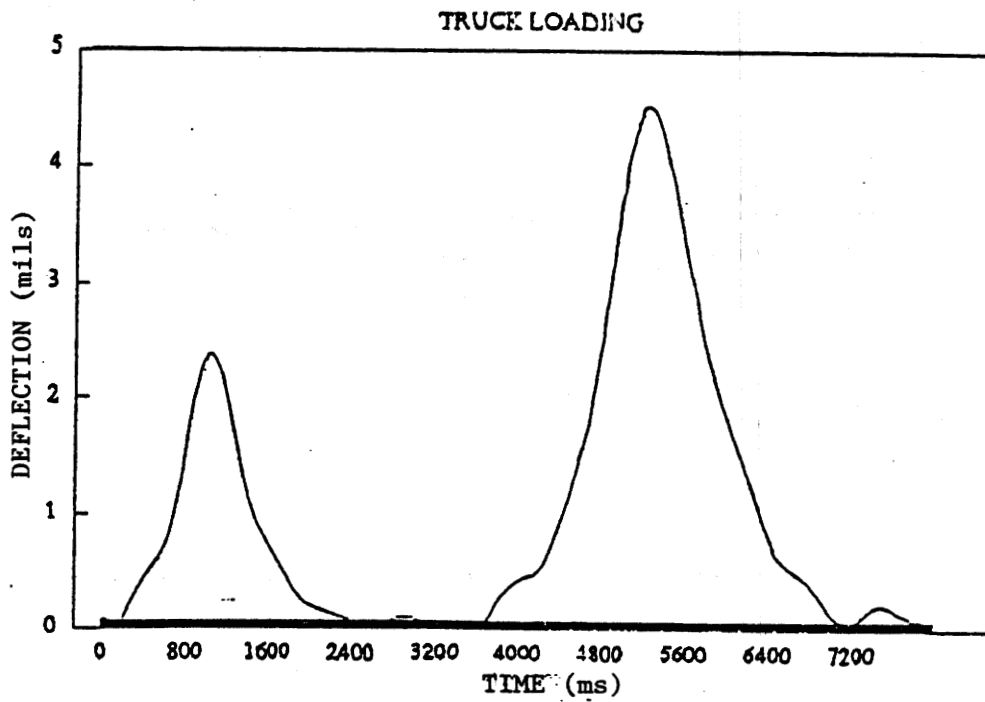


Figure 70. Power spectral analysis displaying the frequency components of the Hall effect sensors displacement output under FWD loading.



a) FWD--Low-pass filter, 50 Hz



b) Truck--Low-pass filter, 20 Hz

Figure 71. Hall effect output with high-frequency noise removed.

Table 62. Repeatability assessments of sensors.

	FWD		Maximum Deflection (mils)	
	Load (lb)	Max. Surface Deflection (mils)	Hall Effect (6 in below surface)	LVDT (13 in below surface)
	14,690	17.53	12.26	10.32
	14,663	17.50	12.36	10.27
	14,682	17.61	12.48	10.34
	14,528	17.33	12.27	10.20
	14,722	17.60	12.42	10.36
Mean	14,652	17.51	12.36	10.30
Standard Deviation	75.2	0.133	0.0950	0.0642
Coefficients of Variation (%)	.51	.77	.77	.62

1 lb = 4.5 N
 1 in = 2.54 mm

If additional work is to be done in this area, it is recommended that additional magnets be used in the MDD module. The current system uses only two magnets, and the zero position output voltage is a function of the torsion rotation of the center core rod. It is important to have the center core rod in the same exact location for testing as that used while calibrating. It is proposed that a four-magnet system may establish a more uniform magnetic field and therefore eliminate this problem.

Furthermore, the linear range on the device is very limited ± 0.05 in [± 1.27 mm]). This means it is critical that the user have access to re-zero the device should permanent deformation occur. Also, little is known about durability. The system was installed in the TTI test pavement for 1 month without any problems; the influence of wet/dry and hot/cold cycling was not evaluated in this field test.

8. SUMMARY AND RECOMMENDATIONS

This research project encompasses various aspects of in situ pavement instrumentation and the evaluation of materials properties from in situ pavement responses. The research program was divided into two phases. In the first phase, an extensive literature search was conducted to identify the existing instrumentation, select the most promising types of instrumentation, and conduct a field testing program to evaluate the gauges under actual traffic loading. In the second phase, new ideas of pavement instrumentation were investigated, prototype gauges were built and evaluated under laboratory conditions, and a field testing program was conducted to evaluate the gauges under actual traffic loading.

The pavement instrumentation investigated included gauges that measure strain in bonded and unbonded layers, stresses within the unbonded layers, and vertical deflections throughout the pavement structure. Instrumentation for temperature, moisture, and vehicle location was investigated. The field testing programs consisted of the design and construction of pavement sections and the installation of gauges throughout the test sections. Two pavement sections were constructed (thick and thin), and replicate gauges were randomly distributed throughout the 50-ft (15.25-m) long sections. A tractor-semitrailer was used to load the test sections under three levels of axle load, two levels of tire pressure, and three vehicle speeds. To ensure the statistical validity of the experimental program, four replicate measurements were collected for each combination of test variables. Finally, the data analysis consisted of the evaluation of the survivability of the gauges, the repeatability of the measurements, the effects of the test variables, and the uncertainty of the measurements.

In the second phase of research, a laboratory testing program was conducted in addition to the field testing program. The new instrumentation ideas were tested in the laboratory to evaluate the response of the gauges under dynamic loading and to develop the appropriate calibration factors to be used in the field testing program. Based on these research findings, the following recommendations are proposed.

FIELD EVALUATION OF EXISTING GAUGES

EXISTING GAUGES TO MEASURE STRAINS IN THE ASPHALT CONCRETE LAYER

The following strain gauges were installed in the asphalt concrete: Dynatest gauge, Kyowa gauge, Alberta Research Council gauge, and the instrumented core gauge. The survivability rate of all types of gauges was in excess of 70 percent, which is better than the 50 percent that is expected in such a full-scale installation. Based on the survivability data generated in the research, it can be concluded that construction activities represent the most critical stage in the life of pavement strain gauges. In general, the majority of gauge losses occurred during construction.

Based on the COV values (ratio of standard deviation to the mean), all gauges exhibited good-to-excellent within-gauge repeatability except for the ARC and core gauges under the empty load level.

The effects of the test variables on the measurement of asphalt concrete strain gauges can be summarized as follows: The effect of tire pressure on the measured strain at the bottom of the asphalt concrete layer is insignificant. The effect of vehicle speed is highly significant; a reduction on the order of 50 to 70 percent in the measured strains was observed as a function of increasing the vehicle speed from 20 to 50 mi/h (32 to 80 km/h).

The uncertainty analysis consisted of comparing the measured strains with the calculated values from the multilayer elastic solution. The data indicated that the measured strains are comparable to the calculated strains except for the ARC gauge, which is always measuring higher strains than the calculated values.

Finally, a regression analysis was conducted in which the response of the individual gauges was considered the dependent variable and the overall mean of all types of gauges was considered the independent variable. Based on the regression analyses, the performances of the Kyowa and Dynatest gauges were very good, while the core gauges performed somewhat inconsistently. The use of epoxy to glue the gauges to the cores may have been the major

contributor to the poor performance of the core gauges as compared to the other gauges. Another major contributor to the difference in the performance of the core gauges is that the retrofitted core is not an integral part of the pavement. However, it is expected that the performance of the core gauges will be greatly improved if an appropriate calibration procedure can be developed to take into consideration the effect of the epoxy on their response.

EXISTING GAUGES TO MEASURE STRAINS IN THE SUBGRADE LAYER

LVDT-type soil strain gauges were installed at various depths within the subgrade layer of both sections. The survivability of the soil strain gauges was very good; a 75-percent survival rate was attained after construction and testing. The repeatability of the LVDT soil strain gauges was good with the majority of the COV values close to 10 percent. The axle load level produced the most significant effect on the measured strains within the subgrade as compared to the effects of tire pressure and vehicle speed. Good agreement was obtained at the heavy axle load level between the measured and the calculated strains. In general, the LVDT-type soil strain gauge is a durable and repeatable instrument, and its measurements are reliable.

EXISTING GAUGES TO MEASURE STRESS

Two diaphragm-type pressure cells were installed in the thin section at the interface of the asphalt concrete layer and the crushed aggregate base. A survivability rate of 50 percent was achieved. The data reveal that all COV values are below 10 percent, indicating good repeatability. Again, the load was the only test variable that imparted a significant effect on the measurement of pressure gauges. The comparison of the measured and the calculated stresses indicated a good agreement only at the low axle load level.

EXISTING GAUGES TO MEASURE DEFLECTION

Three types of deflection-measuring devices were selected for the field testing experiment: geophones, single-layer deflectometer, and multidepth

deflectometer. The survivability of all three types of deflection gauges was very good (70- to 100-percent survival rate). The repeatability of the geophones was extremely low. The only test condition under which the geophones displayed good repeatability was the FWD loading. The geophone data collected under truck loading had COV values on the order of 25 to 45 percent. Therefore, it is obvious that the 10-Hz geophones are not sensitive enough for this kind of application. The use of the 10-Hz geophones for the measurement of pavement deflection is not recommended except when test conditions include a combination of heavy loads, high speeds, and thin pavement. The data collected from the SLD and MDD indicated very good repeatability with the majority of the COV values below 5 percent.

The effect of speed on SLD measurement differs from the single drive axle to the tandem axles. In the case of the drive axle, the effect of speed was pronounced between 20 and 35 mi/h (32 and 56 km/h); in the case of the tandem axle, the effect of speed was pronounced between 35 and 50 mi/h (56 and 80 km/h). The MDD data indicated that the effects of vehicle speed and tire pressure on the deflection at various depths are insignificant. However, this contradicts the findings of the strain data; this contradiction is suspected to be caused by the existence of the installation hole of the MDD device throughout the pavement depth, which provides free drainage for the water within the base and subgrade layers. As a result, the dynamic pore water pressure in the vicinity of the hole is greatly reduced and remains constant, independent of the loading speed.

The uncertainty of the SLD and MDD measurements was very small. Both devices measured data close to the calculated responses from the multilayer elastic solution.

EVALUATION OF IN SITU RESILIENT MODULI FROM SENSOR DATA

Based on an appraisal of the backcalculated moduli from the various analyses, the following conclusions and recommendations can be made.

The installation of instrumentation throughout the pavement structure, such as strain gauges or MDD's, will greatly enhance the capability of the

analysis to predict more realistic in situ material properties. This is supported by the comparison of backcalculated moduli from FWD sensors alone and the backcalculated moduli from FWD and MDD sensors simultaneously. The latter analysis was capable of identifying a 1-ft (.305-m) thick weak layer on top of subgrade; this result was further confirmed by the strain analyses.

The backcalculated moduli of all of the pavement layers are significantly affected by the mode of loading (i.e., FWD or truck). In the case of truck loading, the speed has a significant effect on the strain-based backcalculated moduli of the asphalt concrete layer. The modulus of the asphalt concrete layer was reduced by 50 percent as a result of reducing the speed from 50 to 20 mi/h (80 to 32 km/h). The effect of truck speed on the granular and subgrade layers was insignificant.

The effect of the magnitude of the axle load on the backcalculation moduli of all of the pavement layers was insignificant. This observation indicates that the effect of the material's nonlinearity is very small.

The effect of truck speed on the MDD-based backcalculated moduli of the asphalt concrete was insignificant. This contradicts the data from the strain-based backcalculated moduli.

The combined analysis of strain and MDD data indicated that the speed has a significant effect on the modulus of the asphalt concrete layer. The backcalculated moduli from these combined analyses have high merit since they satisfy two independently measured pavement response parameters (strains and depth deflections).

INVESTIGATION OF NEW INSTRUMENTATION IDEAS

The investigation of new instrumentation covered two major groups: gauges currently used in portland cement concrete and entirely new instrumentation ideas. Each of the gauges within both groups was evaluated in terms of principles of measurement, cost, availability, operating temperature, moisture effects, linearity, and applications.

The Carlson gauge and the TML embedment gauge were investigated within the first group; the Hall effect sensor, the piezoelectric film, and the inductive displacement transducer were investigated within the second group. Based on this evaluation, the Carlson gauge, the TML gauge, the Hall effect sensor, and the inductive displacement transducer were recommended for further testing under laboratory and field conditions. The research has uncovered several serious problems with the piezoelectric film with regard to pavement instrumentation applications. Therefore, it was recommended that no further investigations or evaluations of piezoelectric film be conducted.

LABORATORY TESTING OF NEW INSTRUMENTATION

The gauges from the portland cement concrete category were subjected only to a single laboratory testing to determine their modulus of elasticity in the direction of the applied strain. The gauges under the new instrumentation concepts category were subjected to several laboratory tests in order to evaluate the various characteristics of the new gauges.

The modulus of elasticity of the TML gauges was around 250,000 psi (1,725 MPa), which is well within the range of the asphalt concrete modulus at normal pavement temperatures. The modulus of elasticity of the Carlson gauge was not measured because of the undefined cross-sectional area of the gauge.

The laboratory evaluation of the Hall effect sensor consisted of the following tests:

- Effect of temperature (construction and inservice).
- Dynamic characteristics (sinusoidal and pulse).
- Modulus of elasticity.
- Effect of bending.

The Hall effect sensor performed excellently in all of the tests, which warrants the development of strain gauges and deflection-measuring devices using the Hall effect sensor for field evaluation. Furthermore, the Hall effect sensor was used in the MDD device and evaluated under FWD loading.

FIELD EVALUATION OF NEW INSTRUMENTATION

NEW GAUGES TO MEASURE STRAINS IN THE ASPHALT CONCRETE LAYER

Based on the laboratory evaluation of new instrumentation, it was recommended that the Hall effect sensor, the TML embedment gauge, and the PML gauge be included in a field evaluation program. In addition, the Kyowa gauges were installed as reference gauges since they performed extremely well in the first phase. The survivability rate of all types of gauges was in excess of 75 percent except for the TML type of strain gauge.

Based on the COV, all gauges exhibited good-to-excellent within-gauge repeatability. The majority of the COV values are in the range of 1 to 6 percent.

The effects of the test variables on the measurement of asphalt concrete strain gauges manifested similar trends to the ones produced from the existing gauges tested in the first phase. The majority of the data exhibited a linear relationship between the strain and axle load. The measurements indicated that the speed of the test vehicle has a significant effect on the measured strains for all types of strain gauges.

The uncertainty of the measured strains was also evaluated. In this phase, the dynamic loads were measured by a portable WIM unit. Therefore, the range of measured dynamic loads was used in conjunction with the variation in asphalt concrete thickness and in situ moduli to generate a range of calculated strain response. The measured strains varied around the range of calculated strains. Less agreement was observed between the measured and calculated strains in phase II as compared to the data in phase I. However, this could be expected since most of the gauges tested in phase II represented new instrumentation ideas.

NEW GAUGES TO MEASURE STRAINS IN UNBONDED LAYERS

In general, the application of new instrumentation ideas in the crushed aggregate base course and subgrade layers was unsuccessful. The Hall effect

sensor, Carlson gauge, and TML soil strain gauge were installed into the base and subgrade layers. The survivability rate of the base and subgrade strain gauges was very low, which indicates that some major improvements must be made in the design and installation procedures of these new concept soil strain gauges. The repeatability of the survived soil strain gauges was good, with the majority of the COV values below 10 percent.

NEW GAUGES TO MEASURE DEFLECTION

The new deflection gauges consisted of an SLD with a Hall effect sensor, an SLD with an inductive displacement sensor, and an MDD with a Hall effect sensor. The survivability of all three types of new deflection gauges was very good. Only one Hall effect SLD (out of a total of three units) failed during the testing period. All of the inductive displacement SLD's and the MDD's survived the entire testing program.

The repeatability of the deflection gauges was variable from one type of gauge to another. In general, the repeatability of the SLD's on the thick sections was poor, and the repeatability of the Hall effect SLD on the thin section was good. The repeatability of the inductive displacement SLD on the thin section was poor. The repeatability of the MDD was good.

The effect of test variables on the response of SLD's was measured by varying the load, tire pressure, and vehicle speed. The data indicated highly inconsistent relationships among the measured deflections, axle load, and vehicle speed. This indicates that there are some serious problems with this type of SLD. In addition, the uncertainty analysis did not show any good agreement between the measured and calculated deflection data.

Finally, the evaluation of the Hall effect sensor in the MDD indicated that a multiple magnets system must be used to increase the linear range and establish a more uniform magnetic field.

APPENDIX A: GENERAL PURPOSE MODULUS BACKCALCULATION (PENMOD) USER MANUAL

INTRODUCTION

The modulus backcalculation system called PENMOD described below was assembled for the FHWA Project DTFH61-88-C-00052, "In Situ Instrumentation for Resilient Modulus Measurement." The program operates under the following considerations:

1. Modulus values are calculated from deflection, strain, or stress measurements made in the horizontal or vertical plane.
2. Can have up to seven sensor measurements at various distances from the load horizontally and at various depths in the pavement.
3. Allows the user to set the weighting factors for each sensor.
4. Uses the WESLEA program to generate the deflection, strain, and stress data base.
5. The load can be modeled as a single wheel or as dual wheels.

This modulus back calculation system is a user-friendly, microcomputer-oriented system that allows the user to obtain the modulus of pavement layers from observed multidepth deflectometer deflections, strain gauge measurements, or stress measurements made with pressure cells. The user can model the load on a single wheel or on dual wheels. The user also has the option to make more modulus backcalculations at a later time with out recreating the deflection-strain-stress data base for the same pavement section.

The modulus backcalculation system is run from a batch file called PENMOD.BAT. It is only necessary for the user to type `PENMOD`, press Enter, and respond to the screens to input data, and the remaining steps of the backcalculation analysis are performed. The user is aware of the status of the analysis at each stage because an appropriate message is

displayed on screen. The modulus backcalculation system consists of three separate computer programs. ISMB (for In Situ Modulus Backcalculation) is the screen input program that allows the user to quickly and easily input data for the analysis. WESLEA is the linear elastic program that calculates the deflection-strain-stress data base from the input data. GSER is the function optimization search program that calculates the modulus values for the pavement section from the initial input supplied by the user. Each of these programs is discussed in more detail below.

The screen input program ISMB.EXE provides the user with a quick and easy way to enter observed data for the backcalculation analysis. Several options are available to the user. The user can select single or dual wheel load input. The user can elect to generate the deflection-strain-stress data base or to enter additional deflection, strain, or stress sensor measurements only. The user is asked to specify the type of measurement (deflection, strain, or stress). Then the user is prompted for the data inputs for the geometry of the pavement (layer thicknesses), the load configuration (tire pressure, load, and load spacing), and sensor placement (horizontal and vertical distances from the load). The user is asked to input the range of modulus values for each pavement layer in KSI and the Poisson's ratio of the material. Note that if the user chooses to input additional sensor readings only and not generate the data base, the screen described above will not be used. Instead the user will be prompted for the number of points for which observed sensor readings on the section were recorded and the individual sensor readings at each point.

These input data are used to create two files for subsequent use. One file, called TMP.WES (figure 72), is a correctly formatted input file for the WESLEA program to make the required number of runs to produce the deflection-strain-stress data base. The other file is called TMP.DEF (figure 73) and contains the observed sensor readings and other data needed by the search program. Note that if the user wishes to retain either of these files for later use, these files should be re-named before the next problem is run to avoid over-writing the files.

TITLE

PENN MDD TEST RUN W/NEW PROGRAM

NO. OF PROBLEMS

27

E, PSI	NU	THICK., IN	SLIP
200.0	0.35	6.0	1.
5.0	0.35	8.0	1.
5.0	0.45	136.0	1.
5.0	0.45	1.0	1.
1000.0	0.45		

NO. OF LOADED AREAS

1

LOAD, LBS	RAD., IN	X, IN	Y, IN
4220.	3.278	0.00	0.00

NO. OF EVALUATION POSITIONS

4

LAYER	X, IN	Y, IN	Z, IN
2	0.00	7.25	6.50
3	0.00	7.25	14.50
3	0.00	7.25	26.50
3	0.00	7.25	73.00

E, PSI	NU	THICK., IN	SLIP
489.9	0.35	6.0	1.
5.0	0.35	8.0	1.
5.0	0.45	136.0	1.
5.0	0.45	1.0	1.
1000.0	0.45		

Figure 72. Example of TMP.WES file.

```

PENN MDD TEST RUN W/NEW PROGRAM
3.278 6.00 8.00 0.00 136.00 3 3 3 1 3 0 1
0.200000D+03 0.120000D+04 0.35
0.500000D+01 0.500000D+02 0.35
0.500000D+01 0.500000D+02 0.45
3 7.25 4220.0 125.000 1
0.00 0.00 0.00 0.00
6.50 14.50 26.50 73.00
1.00 1.00 1.00 1.00
1 1 3.18 1.68 0.63
2 2 3.40 1.81 0.68
3 3 2.64 1.42 0.54

```

Figure 73. Example of TMP.DEF file.

The WESLEA program produces the deflection-strain-stress data base from the input data supplied by the user. For the single wheel load, this is the vertical deflection, tangential strain, and vertical stress computed by WESLEA for the load configuration and modulus values provided by the user. For the dual wheel load, this is the vector sum of the vertical deflection, tangential strain, and vertical stress from both loads computed by WESLEA from the user's input data. The WESLEA program writes the deflection-strain-stress data base to a file called WES.RES (figure 74). This file should be re-named if the user wishes to save the data base for a later analysis.

The search program GSER.EXE is a function optimization routine based on the Hooke and Jeeves function optimization algorithm. The program makes repeated calculations of deflection, strain, or stress basins using varying combinations of the elastic moduli values input by the user until the smallest mean squared error (MSE) between the observed and calculated basin is found. The program then prints out the elastic modulus values for the pavement layers that produced this smallest MSE (figure 75).

The calculated deflection, strain, or stress basin is obtained using a three-point LaGrange interpolation of the WESLEA data base for the combination of elastic moduli values for any one iteration.

It is possible for the experienced microcomputer user to run the analysis by executing each program as separate steps. For the first time, or for the less experienced user, it is suggested that the PENMOD program be run from the batch file to obtain quick results.

The detailed steps for installing and running PENMOD are listed and described below.

GETTING STARTED

The PENMOD modulus backcalculation system is furnished on a high-density 5.25-in (133-mm) floppy diskette. The diskette contains 15 files, including 3 example data files and an example output file. The

200.0	5.0	5.0	5.0	0.198334D+02	0.238502D+00	-0.365397D+01
200.0	5.0	5.0	5.0	0.153923D+02	0.189706D+00	-0.250019D+01
200.0	5.0	5.0	5.0	0.114581D+02	0.119326D+00	-0.143664D+01
200.0	5.0	5.0	5.0	0.524769D+01	0.296487D-01	-0.326136D+00
489.9	5.0	5.0	5.0	0.157579D+02	0.129074D+00	-0.240303D+01
489.9	5.0	5.0	5.0	0.128474D+02	0.118204D+00	-0.174597D+01
489.9	5.0	5.0	5.0	0.101060D+02	0.853181D-01	-0.110108D+01
489.9	5.0	5.0	5.0	0.505160D+01	0.265355D-01	-0.297556D+00
1200.0	5.0	5.0	5.0	0.122009D+02	0.660077D-01	-0.149474D+01
1200.0	5.0	5.0	5.0	0.104028D+02	0.689031D-01	-0.115319D+01
1200.0	5.0	5.0	5.0	0.861935D+01	0.565424D-01	-0.793380D+00
1200.0	5.0	5.0	5.0	0.476560D+01	0.223742D-01	-0.258909D+00
200.0	15.8	5.0	5.0	0.165581D+02	0.171248D+00	-0.441118D+01
200.0	15.8	5.0	5.0	0.143101D+02	0.204087D+00	-0.228505D+01
200.0	15.8	5.0	5.0	0.105893D+02	0.109095D+00	-0.125685D+01
200.0	15.8	5.0	5.0	0.505330D+01	0.269688D-01	-0.298994D+00
489.9	15.8	5.0	5.0	0.139461D+02	0.105993D+00	-0.306414D+01
489.9	15.8	5.0	5.0	0.123535D+02	0.138808D+00	-0.169504D+01
489.9	15.8	5.0	5.0	0.957039D+01	0.836284D-01	-0.101249D+01

Figure 74. Example of WES.RES file. (Columns are: E_1 , E_2 , E_3 , E_4 , deflection, strain, and stress.)

PENN MDD TEST RUN W/NEW PROGRAM

LATERAL OFFSET TO LOAD : 7.250 (IN.) (SINGLE TIRE)
 RADIUS OF LOAD AREA (IN.) : 3.278 INITIAL MODULI VALUES POISSON'S
 MINIMUM MAXIMUM RATIOS
 SURFACE THICKNESS (IN.): 6.000 200000. 1200000. .35
 BASE THICKNESS (IN.): 8.000 5000. 50000. .35
 SUBGRADE THICKNESS (IN.): 136.000 5000. 50000. .45

READING : 1 2 3
 OFFSET : .00 .00 .00
 DEPTH : 6.50 14.50 26.50

73.00 DEPTH OF ANCHOR

WT FACTOR : 1.00 1.00 1.00

 STATION: 1 1 1 2 3 LOAD (LBS): 4220
 MEASURED DEFLECTION: 3.18 1.68 .63 PRESSURE (PSI): 125.00
 CALCULATED DEFLECTION: 3.11 1.26 .78
 % ERROR 2.19 24.85 -24.12 ABS SUM OF % ERROR: .512E+02

LAYER: SURFACE BASE SUBGRADE ERROR SQUARED: .120E+00
 MODULI VALUES (PSI): 656972. 11878. 50000.

 STATION: 2 2 1 2 3 LOAD (LBS): 4220
 MEASURED DEFLECTION: 3.40 1.81 .68 PRESSURE (PSI): 125.00
 CALCULATED DEFLECTION: 3.31 1.42 .84
 % ERROR 2.56 21.31 -24.11 ABS SUM OF % ERROR: .480E+02

LAYER: SURFACE BASE SUBGRADE ERROR SQUARED: .104E+00
 MODULI VALUES (PSI): 402816. 14778. 50000.

 STATION: 3 3 1 2 3 LOAD (LBS): 4220
 MEASURED DEFLECTION: 2.64 1.42 .54 PRESSURE (PSI): 125.00
 CALCULATED DEFLECTION: 2.63 1.06 .69
 % ERROR .19 25.52 -27.49 ABS SUM OF % ERROR: .532E+02

LAYER: SURFACE BASE SUBGRADE ERROR SQUARED: .141E+00
 MODULI VALUES (PSI): 1199997. 10206. 50000.

Figure 75. Example output.

user is urged to copy the diskette before beginning to use the PENMOD system.

SYSTEM REQUIREMENTS

The minimum system requirements to run the PENMOD system are:

- IBM AT or compatible microcomputer.
- 640 Kb of RAM.
- DOS (Version 3.00 or later) operating system.
- Math coprocessor chip (80287 or similar).
- One high-density 5.25-in (133-mm) 1.2 Mb floppy diskette drive.
- One hard disk drive.
- An EGA graphics card with 256 Kb of screen memory and a compatible RGB color monitor.
- A line printer.

It is recommended that an advanced microcomputer such as a 286 or 386 be used to minimize program execution time when running analyses with more than 20 observations. Note that a color monitor is not essential to run the program; this enhances the fields on the screen for data input. The line printer is also not needed unless the user wants a hard copy of the results of the analysis.

FILE-NAMING CONVENTION

The 15 files comprising the PENMOD system consist of command files, executable files, and data files. Listed below are descriptions of the types of files, which can be identified by the three-character DOS file extension name:

- **PENMOD.BAT** DOS batch file that runs the programs of the PENMOD system.
- **DISPLAY.COM** Command file for the screen input program that manages the data input from the screen.
- **.AID** These files contain the screens displayed by the PENMOD system.

- .EXE The executable files for data input (ISMB.EXE), data base generation (WESLEA.EXE), and modulus calculation (GSER.EXE).
- TMP.WES The file produced by the data input program that is used by WESLEA to calculate the deflection-strain-stress data base.
- TMP.DEF The file produced by the data input program that is used by the search program to calculate the modulus values.
- WES.RES The deflection-strain-stress data base produced by the WESLEA program and used by the search program for the LaGrange interpolation procedure to calculate the modulus values.
- .OUT A user-named file for storing the results if a line printer is not available.

The user should note that the files TMP.WES, TMP.DEF, and WES.RES are created each time the program is run, and if the user wants to save the data in one of these files, that file should be re-named by the user before the program is run again.

INSTALLING PENMOD

The user should create a directory on a hard disk and copy the 15 files from the distribution diskette to the directory on the hard disk.

Listed below are the steps to install PENMOD on a directory on hard disk D.

1. D:\ MD PMOD <enter>
2. D:\ CD PMOD <enter>

With the distribution diskette in floppy drive A:

3. D:\ PMOD COPY A: *.* <enter> This copies the files from the distribution diskette to the PMOD directory on hard disk drive D.
4. D:\ PMOD DIR/W <enter>

Check to see that all 15 files are in the PMOD directory.

RUNNING THE PROGRAM

The PENMOD system consists of three steps: data input, data base generation, and modulus calculation. These steps are performed automatically for the user when the program is run from the batch file. (See the Special Notes section for information on how to run the program manually.) It is suggested that the user run PENMOD from the batch file until he or she becomes familiar with the program.

To run the PENMOD system, the user should make the directory containing the PENMOD system the active directory by typing `CD D:\PMOD` and pressing Enter at the DOS prompt. When the user is in the PMOD directory, type `PENMOD` and press Enter to use the batch file that runs the PENMOD system. Several screens will be displayed for the user to select various program options and to input data for the analysis to be made. These screens and the program options and data input required to make modulus calculations with the PENMOD system are described below.

DATA INPUT

WHEEL LOAD CONFIGURATION SCREEN

The first screen the user will see displayed is for the purpose of selecting the single wheel load or dual wheel load option (figure 76). The user should enter a 1 for single wheel or a 2 for dual wheels and press Enter to validate the entry. Note that for any time prior to pressing the Enter key, the user can press the Esc key and the cursor will go to the first field on the screen. This allows the user to change any entry before the entry is accepted (or read) by the input program. Pressing the Enter key validates the entry in the field where the cursor is positioned, and the entry is entered (or read) by the input program.

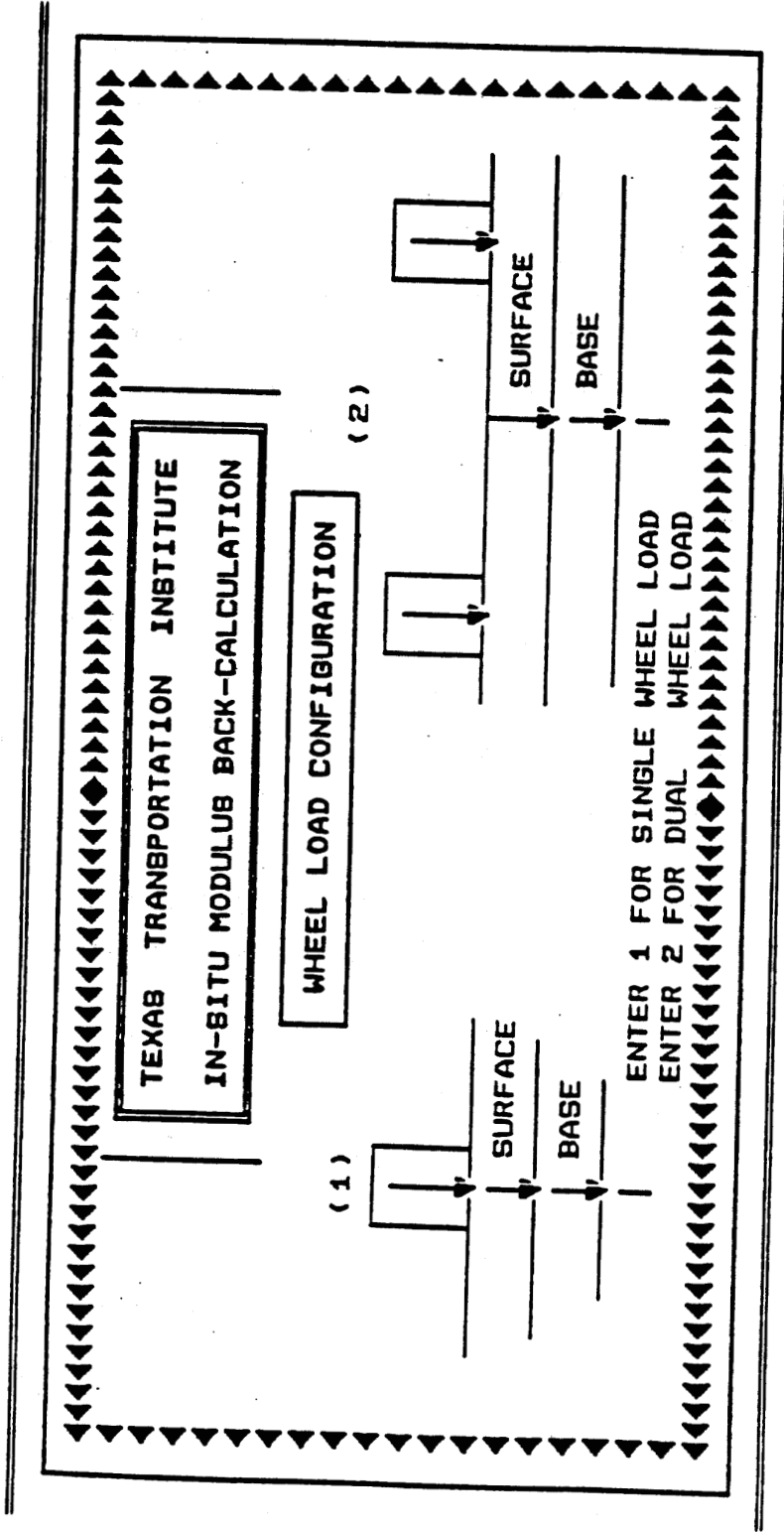


Figure 76. Example of output LOADOPT.

DATA INPUT OPTION

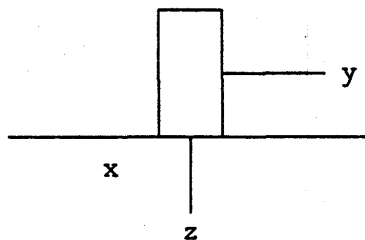
This screen (figure 77) gives the user the option to create a deflection-strain-stress data base (enter 1) or to make additional calculations using the existing data base (enter 2). If option 2 is chosen, the user is only required to enter additional observed deflection, strain, or stress measurements only, and the data base does not have to be re-created. This option should be run from the manual procedure since the batch file always runs the WESLEA program. See the Special Notes section for information on how to run the program manually.

SELECT SENSOR TYPE

The user is asked to identify the type of observed data: enter 1 for MDD deflection measurements, 2 for strain gauge measurements, or 3 for stress measurements (figure 77).

X, Y, Z COORDINATE SYSTEM

Inside PENMOD, the user is prompted to specify wheel spacings and sensor locations in terms of the X, Y, Z coordinate system. This system is sketched below:



x, y, z Coordinate System

The surface is the zero z position. The wheel travels along the x axis, and wheel spacing for dual tires is specified along the y axis.

DATAOPT Enter text or [Esc] to invoke the Main menu F10=HELP

<p>TEXAS TRANSPORTATION INSTITUTE IN-SITU MODULUS BACK-CALCULATION GENERAL PURPOSE PROGRAM</p>	
<p>SELECT DATA INPUT OPTION</p> <ol style="list-style-type: none">1. CREATE THE WESLEA DATA BASE2. INPUT OBSERVED SENSOR READINGS ONLY. <p>ENTER THE NUMBER OF YOUR CHOICE</p>	<p>SELECT SENSOR TYPE</p> <ol style="list-style-type: none">1. MULTI-DEPTH DEFLECTOMETER2. STRAIN GAGE3. PRESSURE CELL <p>ENTER THE NUMBER OF YOUR CHOICE</p>

Figure 77. Example of output DATAOPT.

SINGLE WHEEL LOAD CONFIGURATION

This screen is displayed for wheel load option 1 and data input option 1 (figure 78). The user is asked to enter the data values necessary to run the WESLEA program to create the deflection-strain-stress data base. These inputs are (see Data Inputs section):

1. Title.
2. Layer thicknesses (in inches).
3. Tire pressure (in psi).
4. Lateral offset (in inches), used when the single wheel is not directly over the sensors.
5. Axle load (in lb).
6. Number of readings (up to seven).
7. X-offset of sensors from the center of the load.
8. Depth of sensors (in inches).
9. Weighting factors (set = 1).
10. Minimum and maximum subgrade modulus values and Poisson's ratio (in ksi) limit range to a factor of 5, for example: 10 ksi to 50 ksi.
11. Minimum and maximum subbase modulus values and Poisson's ratio (in ksi) range ≤ 5 , typical Poisson's ratio (0.2 to 0.45).
12. Minimum and maximum base modulus values and Poisson's ratio (in ksi), range ≤ 10 , for example: 10 ksi to 100 ksi.
13. Minimum and maximum surface modulus values and Poisson's ratio (in ksi) ≤ 10 , for example: 100 ksi to 1,000 ksi, typical Poisson's ratio = 0.35.

The user should note that if there is no subbase layer, a zero should be entered for H3. If the user is entering an infinite layer for the subgrade, a zero should be entered for H4. For the case where the user is entering a rigid layer at some depth, the user should enter the depth to the rigid layer for H4. Note that the cursor is positioned at

SINGLE WHEEL LOAD CONFIGURATION						
TITLE						
H1	H2	H3	H4	TIRE PRESSURE (PSI)	LATERAL OFFSET-Y	AXLE LOAD
NUMBER OF READINGS						
READING NO.				X - OFFSET FROM CENTER OF LOAD		
1	2	3	4	5	6	7
Z - DEPTH OF SENSOR						
WEIGHTING FACTORS						
SUBGRADE MODULUS (MOST PROBABLE VALUE IN KSI)						
MINIMUM			MAXIMUM		AND POISSON'S RATIO	
MODULUS OF THIRD LAYER (IN KSI)						
MINIMUM			MAXIMUM		AND POISSON'S RATIO	
MODULUS OF SECOND LAYER (IN KSI)						
MINIMUM			MAXIMUM		AND POISSON'S RATIO	
MODULUS OF FIRST LAYER (IN KSI)						
MINIMUM			MAXIMUM		AND POISSON'S RATIO	

249

Figure 78. Example of output SINGLINPT.

the correct fields for the minimum and maximum values for the layers entered by the user.

For the stress and strain gauges, the number of readings represents the number of locations at which stress and strains are measured for a single pass on a single gauge. Typically, strains from a single gauge are input when the test wheel is 0, 6, 12, 18, and 24 in (0, 152, 305, 457, and 610 mm) from the gauge ($x = 0, 6, 12, 18, \text{ and } 24$) and number of readings equal 5.

For the multidepth deflectometer, the "number of readings" entry refers to the number of MDD sensors plus one for the anchor position. If the site has three MDD's, then the 4 would be entered. When processing MDD frequently, only peak deflections are analyzed ($x = 0$). The user must specify the MDD locations and the anchor depth, for example, $z = 6, 12, 24, \text{ and } 78$ in (152, 305, 610, and 1 981 mm). In the computation process, movements of the anchor are automatically accounted for.

DUAL WHEEL LOAD CONFIGURATION

The dual wheel load input screen (figure 79) is the same as the single wheel load screen with one exception. Instead of the lateral offset of the sensor from the load, the user is asked for the distance between the dual wheels.

Regardless of the wheel configuration, the data input program produces the input file for the WESLEA program to generate the deflection-strain-stress data base.

SENSOR READING INPUT

At this screen (figure 80), the user can enter the observed sensor measurements as listed below:

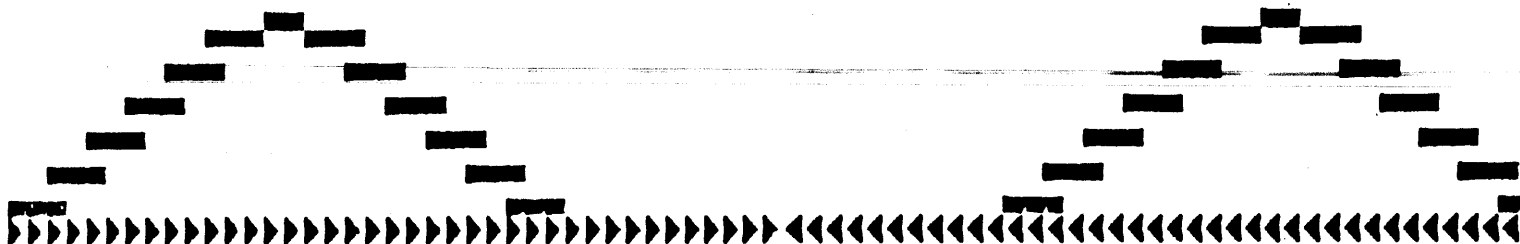
Screen print ISMBDEFL



TEXAS TRANSPORTATION INSTITUTE
IN-BITU MODULUS BACK-CALCULATION

NUMBER OF TESTS TO BE ANALYZED (NPTS)

STATION	DEFLECTIONS AT OFFSET NO.						
No.	1	2	3	4	5	6	7
	SENSOR READINGS						



252

Figure 80. Example of output ISMBDEFL.

1. Number of tests (measurements).
2. Station (location).
3. Sensor readings.

Note that the "number of readings" value entered on the previous screen determines the number of sensor inputs allowed for each test and that the "number of tests" value entered on this screen is the number of observed deflection, strain, or stress measurements used to determine the layer moduli. For stress and strain, if the number of readings equals five, the five values will need to be input on this screen. For MDD, if the number of readings equals four, this includes the anchor position, so only three values of MDD deflection data need to be input on this screen.

DATA BASE GENERATION

After the pavement geometry, estimated modulus, and observed sensor measurements have been entered, the WESLEA program is run to generate the deflection-strain-stress data base. A screen (figure 81) with the number of WESLEA runs to be made is displayed while the WESLEA program is running. Creating the data base can be the most time-consuming part of the analysis. In general, the shorter the range between the minimum and maximum estimated modulus values, the fewer runs of the WESLEA program will be required.

MODULUS CALCULATION

Prior to performing the pattern search to obtain the moduli values, the user is prompted to either send the output to a file or direct it to the printer (shown in figure 82). The third part of the PENMOD system is the modulus calculation. The modulus calculation program (GSER.EXE) will print a message to the screen giving the number of modulus calculations being made (figure 83). This should be the same as the number of observed sensor measurements entered on the previous screen. The output from the search program includes the station, observed measurements (deflection, strain, or stress), and the calculated values (deflection, strain, or stress) with the percent error for each sensor and the

F10=HELP

Enter text or [Esc] to invoke the Main menu

WESS



Figure 81. Screen displayed while WESLEA is running.

OUTFILE

Enter text or [Esc] to invoke the Main menu

F10=HELP

IF YOU DO NOT HAVE A PRINTER AVAILABLE OR IF YOU WISH TO SAVE THIS OUTPUT FOR PRINTING AT A LATER TIME, ENTER A FILE NAME IN THE BOX AND PRESS "ENTER". IF YOU WANT TO PRINT THE OUTPUT AS USUAL, JUST PRESS "ENTER" WITHOUT GIVING A FILE NAME.

NOTE: ENTER A VALID DOS FILE NAME OF UP TO EIGHT CHARACTERS AND/OR NUMBERS AND USE .OUT AS THE EXTENSION.

Figure 82. Screen displaying the option for the user to define if the output should go to a file or to the printer.

SEARCH

Enter text or [Esc] to invoke the Main menu

F10=HELP



Figure 83. Display of the number of bowls being used in backcalculation.

calculated modulus values. These output data are printed on the line printer with appropriate column headings, or the user can have this output written to a file for later use if a line printer is not available.

SPECIAL NOTES

The steps listed above are the simplest and easiest way to run the PENMOD system. Because not all users have the same level of expertise in using microcomputers or have access to the same computer equipment, the individual steps to run an analysis (data input, data base generation, and modulus calculation) will be given below. Also listed below is the batch file PENMOD.BAT.

- PENMOD.BAT
- DISPLAY
- ISMB
- WESLEA
- GSER

To run PENMOD as individual programs, the user should type **DISPLAY** and press Enter to invoke the command file to manage the data inputs from the screen to the data input program. This only has to be done the first time the user boots up the system or runs the program. Then type **ISMB** and press Enter to run the data input program and respond to the screens to enter pavement geometry, sensor spacing, estimated modulus values, and observed sensor measurements. The data input program creates the TMP.WES and TMP.DEF files. The user can create several TMP.WES (WESLEA input files) and TMP.DEF (GSER input files) by running the data input program successively and re-naming the TMP.WES and TMP.DEF files before the next data input program run.

To generate the deflection-strain-stress data base, type **WESLEA** and press Enter.

To run the modulus calculation program, type **GSER** and press Enter. For the case where the user does not have a line printer available or where the user wants to save the analysis output, any correct DOS file name should be entered at the program prompt.

DATA INPUTS

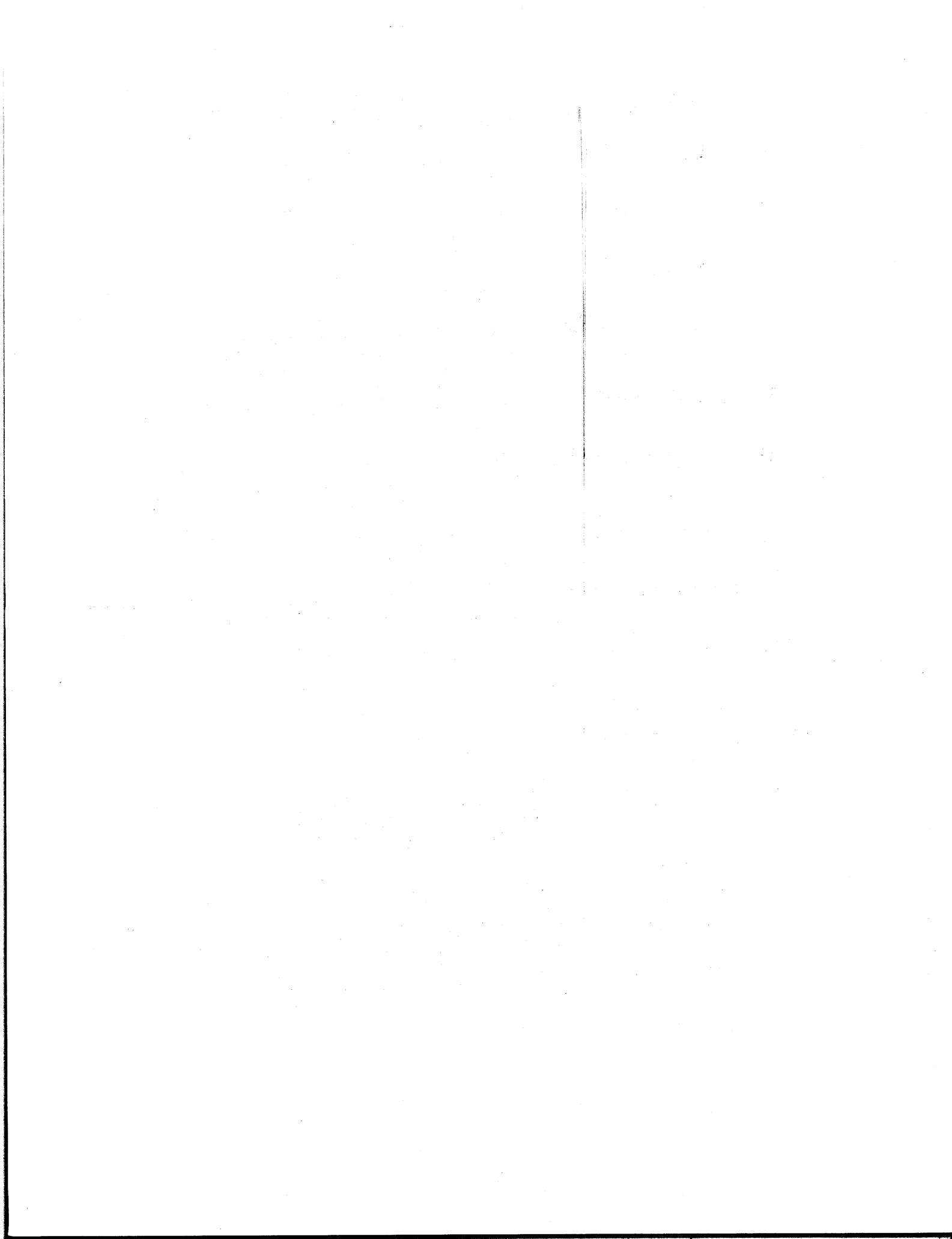
The following is the list of data inputs the user is asked to make to perform an analysis with the PENMOD system:

1. TITLE Up to 60 characters to identify the analysis.
2. H1 Thickness of the surface layer, in inches.
3. H2 Thickness of the second layer, in inches (enter 0.0 if there is no second layer).
4. H3 Thickness of the third layer, in inches (enter 0.0 if there is no third layer).
5. H4 Thickness of the subgrade layer, in inches (enter 0.0 for semi-infinite subgrade).
6. TIRE PRESSURE Enter the tire pressure, in psi.
7. WHEEL SPACING For the dual wheel load, the distance in inches between the dual wheels.
8. LATERAL OFFSET For the single wheel load, the distance in inches from the wheel to the sensor.
9. AXLE LOAD The total load, in pounds (whether dual or single wheel).
10. NUMBER OF READINGS The total number of sensors. Note that for the multidepth deflectometer, this includes the anchor sensor.
11. X-OFFSET For dual wheel loads, the horizontal distance of the sensor from the center of the dual wheels. For single wheel loads, the horizontal distance of the sensor from the wheel.

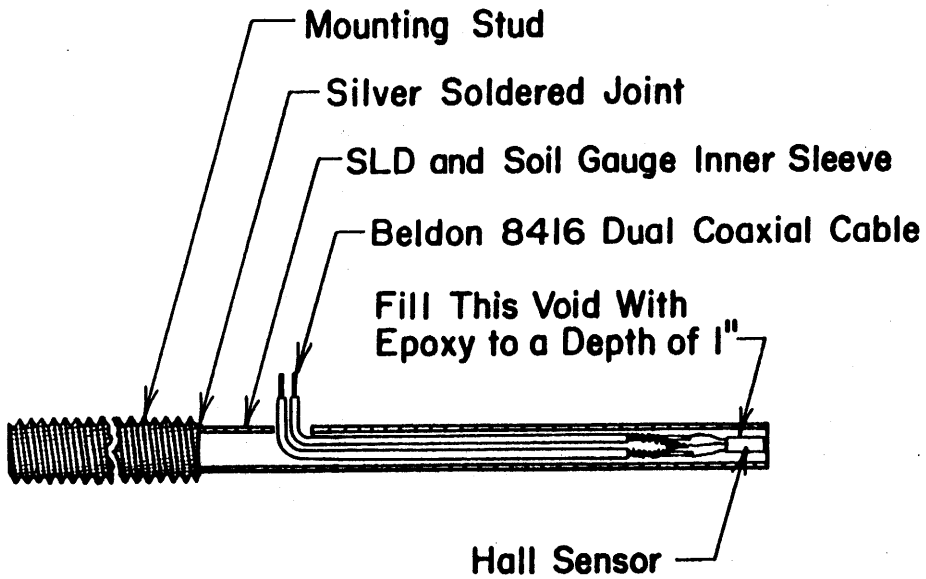
- | | |
|--------------------------|---|
| 12. Z-DEPTH | The vertical placement of the sensor within the pavement layer. |
| 13. WEIGHTING FACTOR | Used to adjust questionable sensor readings. |
| 14. SUBGRADE MODULUS | Enter a range (minimum and maximum) in ksi for the subgrade modulus. |
| 15. POISSON'S RATIO | Enter the Poisson's ratio for the subgrade. |
| 16. THIRD LAYER MODULUS | Enter a range (minimum and maximum) for the third layer modulus, in ksi (this field is skipped if H3 is 0.0). |
| 17. POISSON'S RATIO | Enter the Poisson's ratio for the third layer, if used. |
| 18. SECOND LAYER MODULUS | Enter a range (minimum and maximum) in ksi for the second layer modulus (this field is skipped if H2 is 0.0). |
| 19. POISSON'S RATIO | Enter the Poisson's ratio for the second layer, if used. |
| 20. FIRST LAYER MODULUS | Enter a range (minimum and maximum) in ksi for the first layer modulus. |
| 21. POISSON'S RATIO | Enter the Poisson's ratio for the first layer. |

The next data inputs are for entering the observed sensor measurements for an analysis.

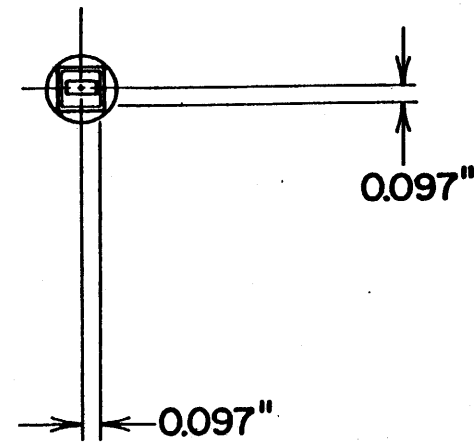
- | | |
|--------------------|--|
| 1. NPTS | Number of tests to be analyzed. The total number of deflection, strain, or stress sensor measurements made on the section. |
| 2. STATION NO. | The identification (location) of an individual measurement test on the section. |
| 3. SENSOR READINGS | The multidepth deflectometer reading, the strain gauge reading, or the pressure cell reading of each sensor. Note that for the multidepth deflectometer, this reading will be the corrected (sensor - anchor) reading. |



261

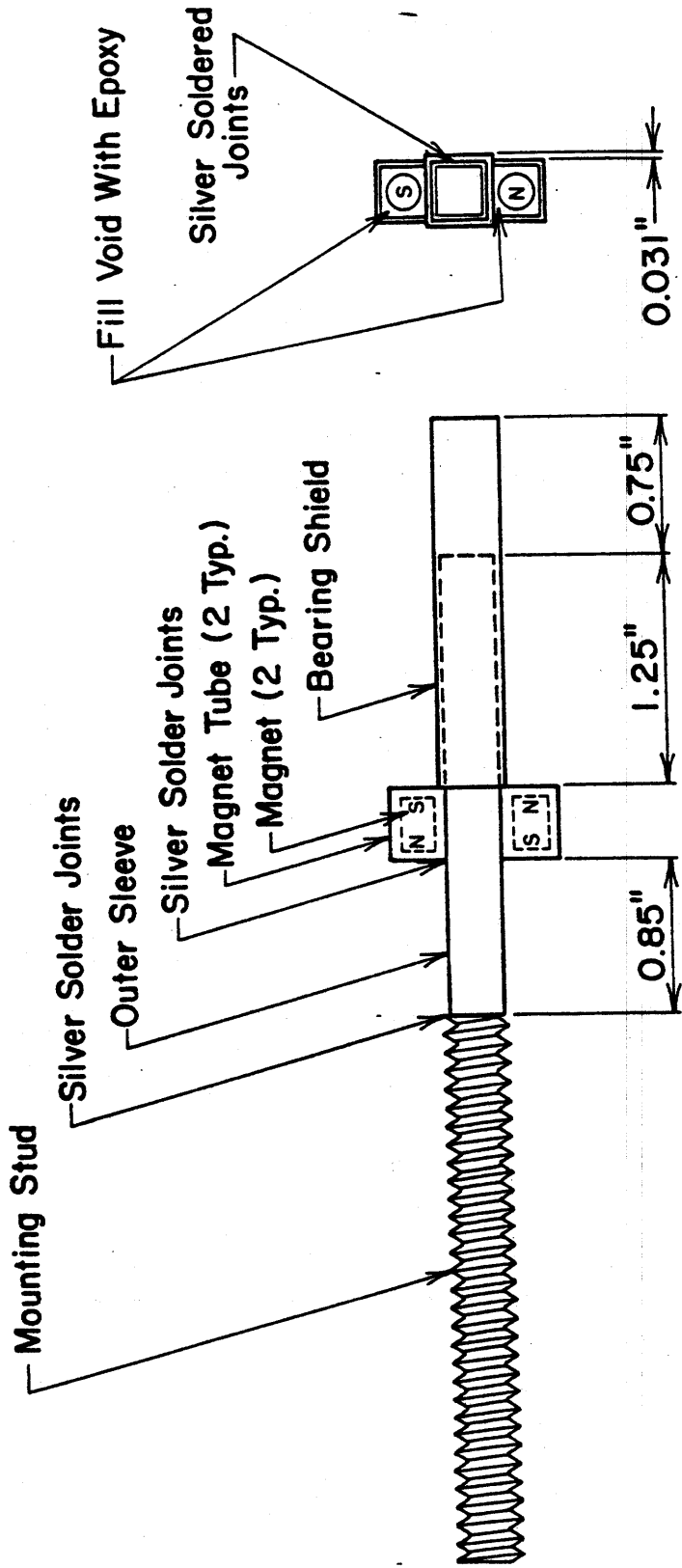


1 in - 25.4 mm



COMPLETED SENSOR ASSEMBLY

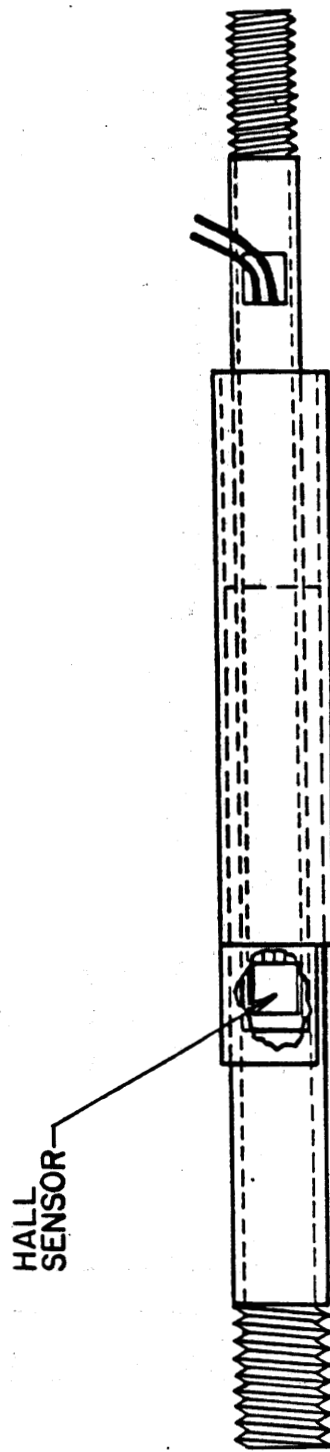
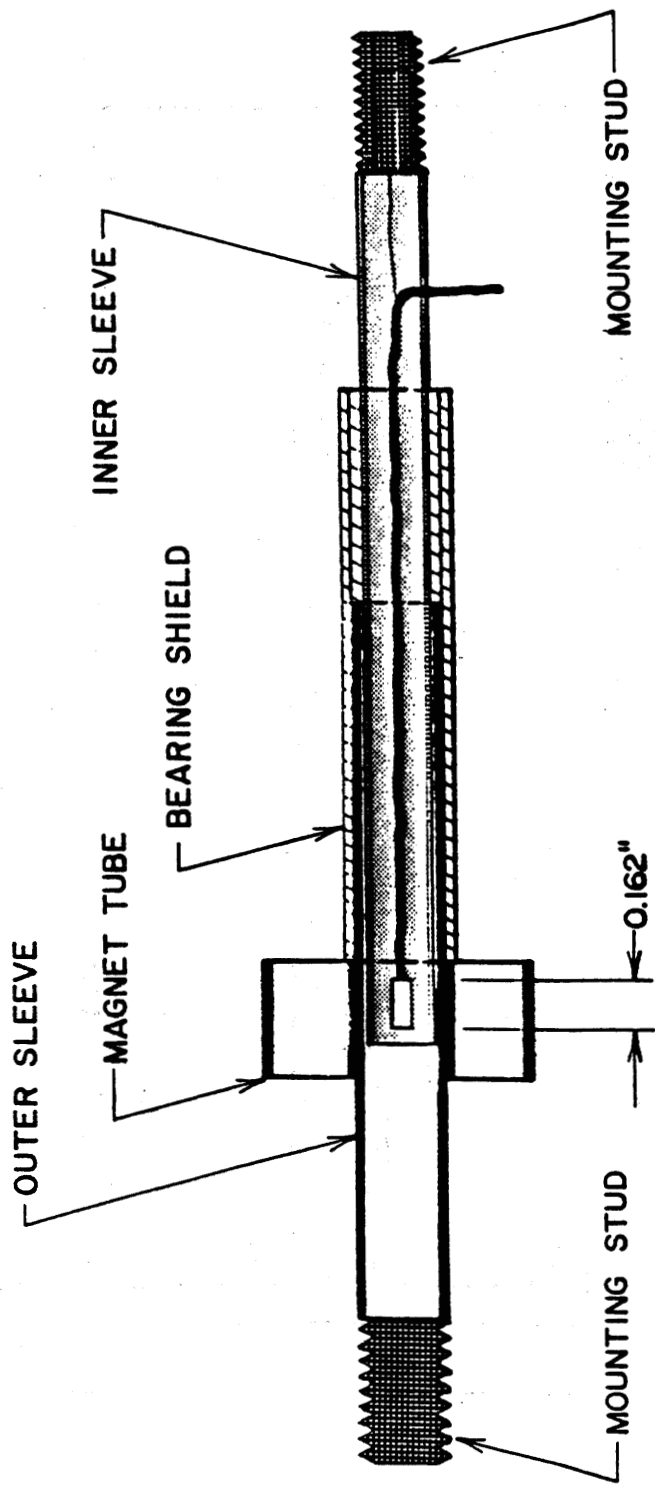
Figure 84. Completed sensor assembly drawings--SLD and soil transducer.



1 in - 25.4 mm

MAGNET ASSEMBLY DRAWING

Figure 85. Magnet assembly drawings--SLD and soil transducer.



1 in - 25.4 mm

ALL MAT'LS BRASS SILVER SOLDERED JOINTS

Figure 86. Assembly drawings--SLD and soil transducer.

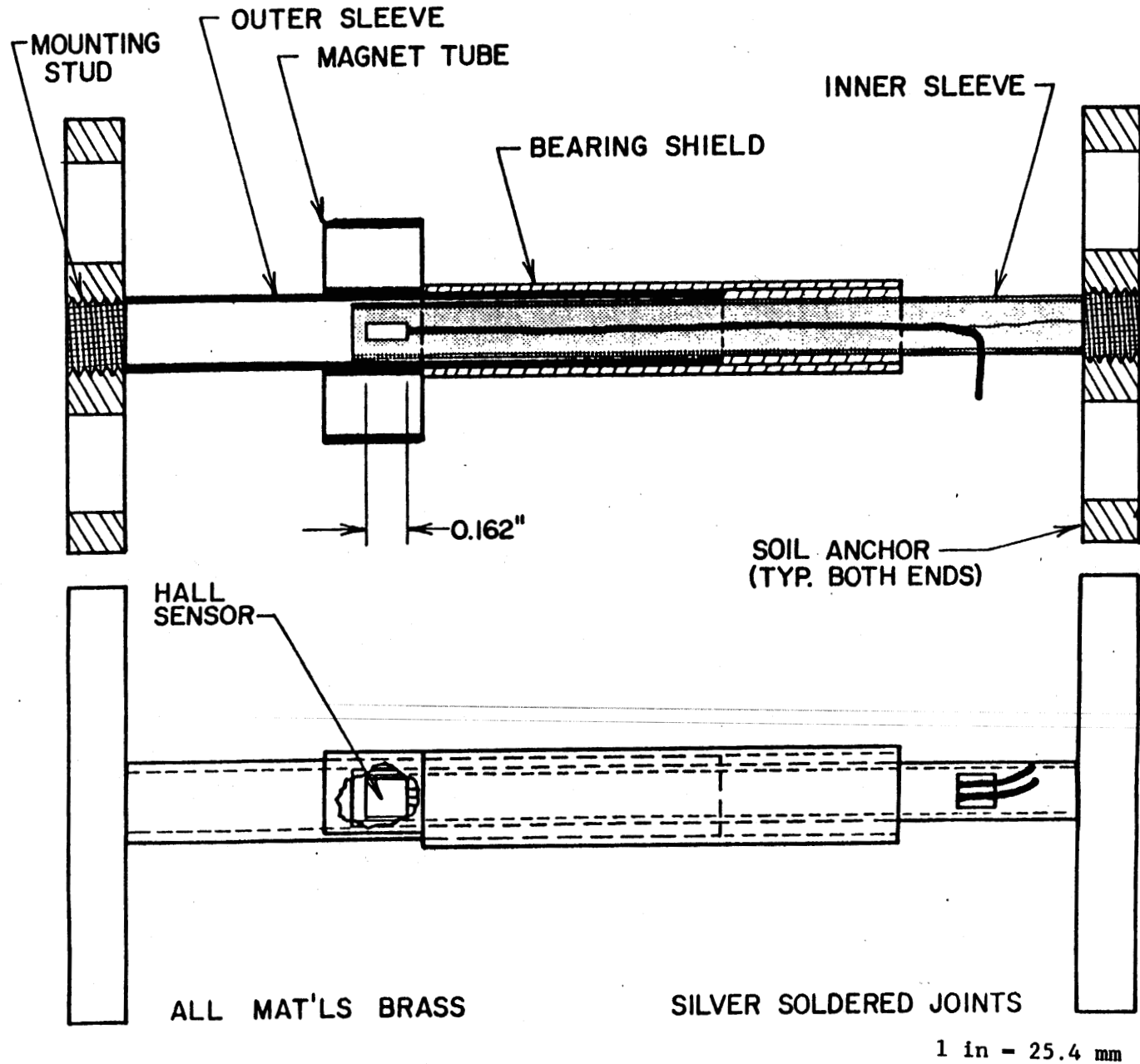
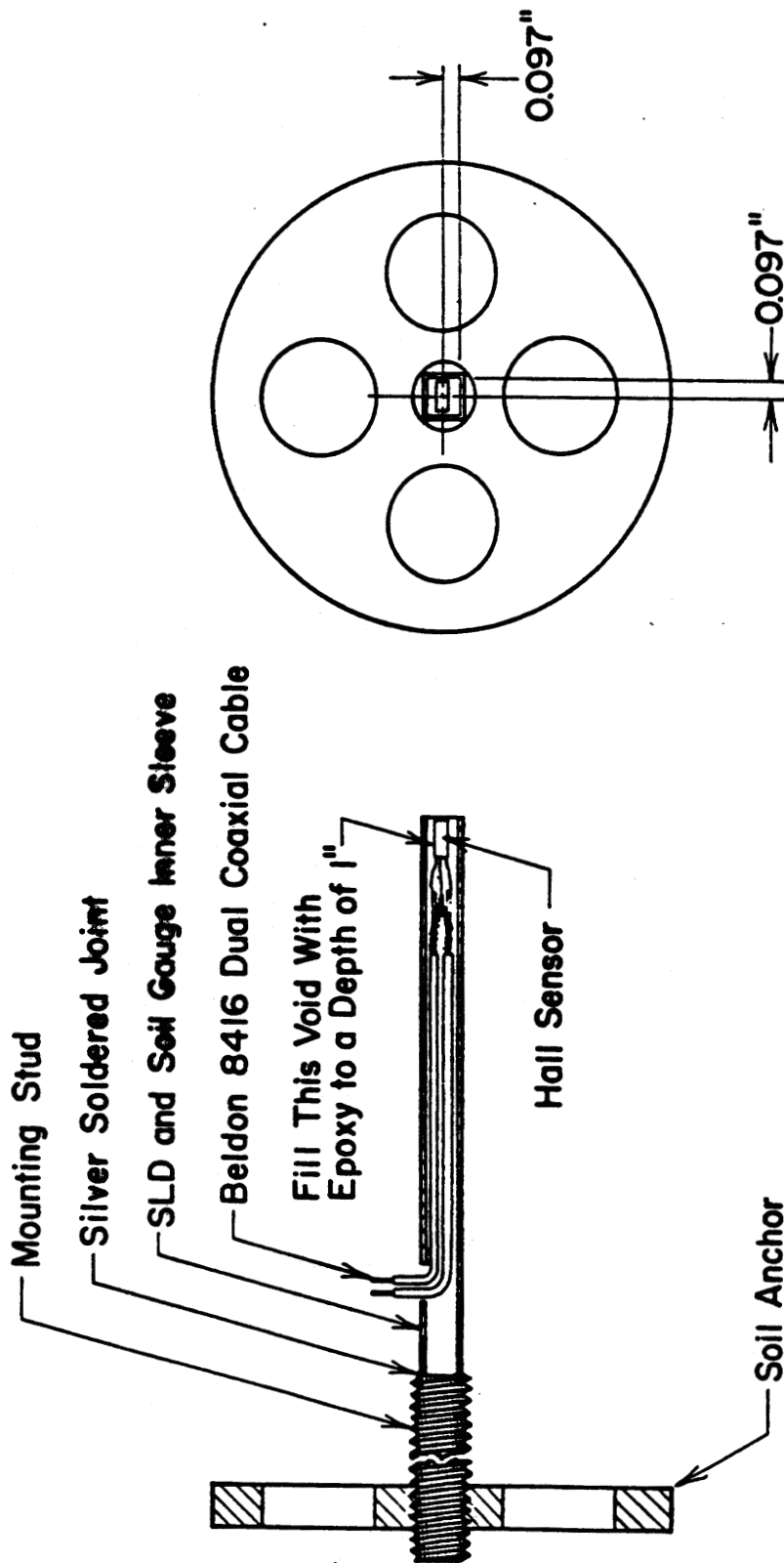


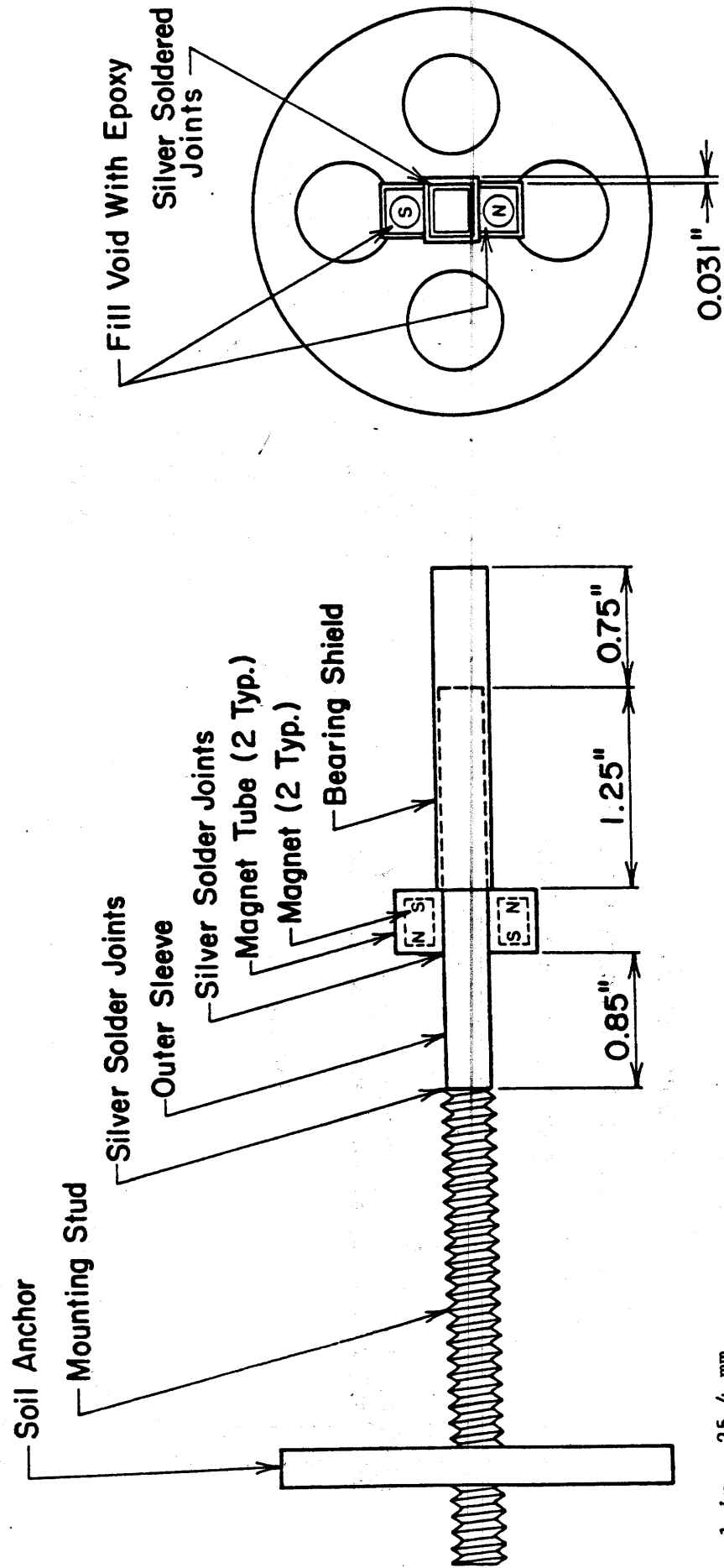
Figure 87. Assembly drawings--soil transducer.



1 in - 25.4 mm

COMPLETED SENSOR ASSEMBLY

Figure 88. Completed sensor assembly drawings--soil transducer.



1 in = 25.4 mm

MAGNET ASSEMBLY DRAWING

Figure 89. Magnet assembly drawing--soil transducer.

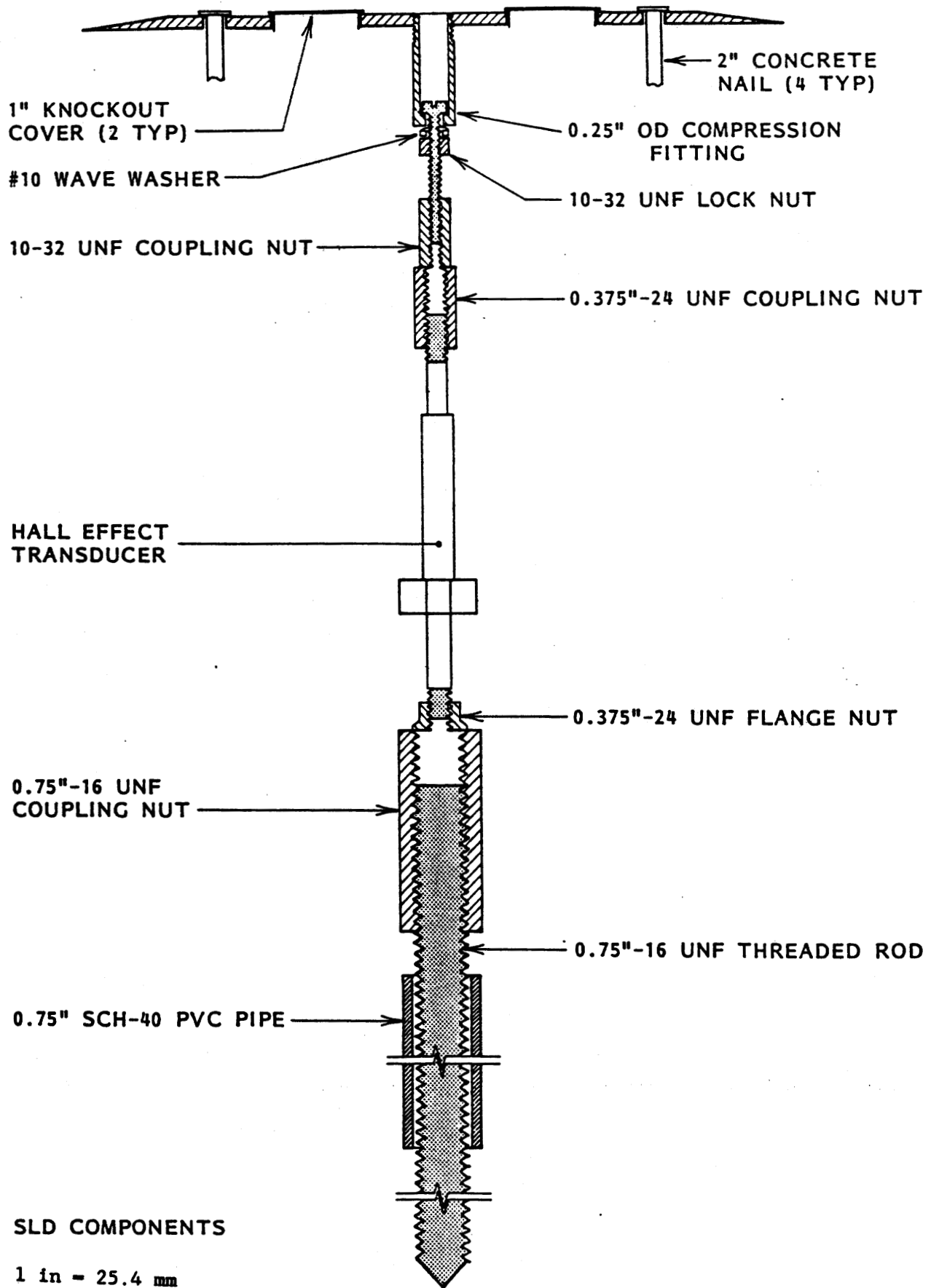


Figure 90. Assembly drawings--SLD transducer (components).

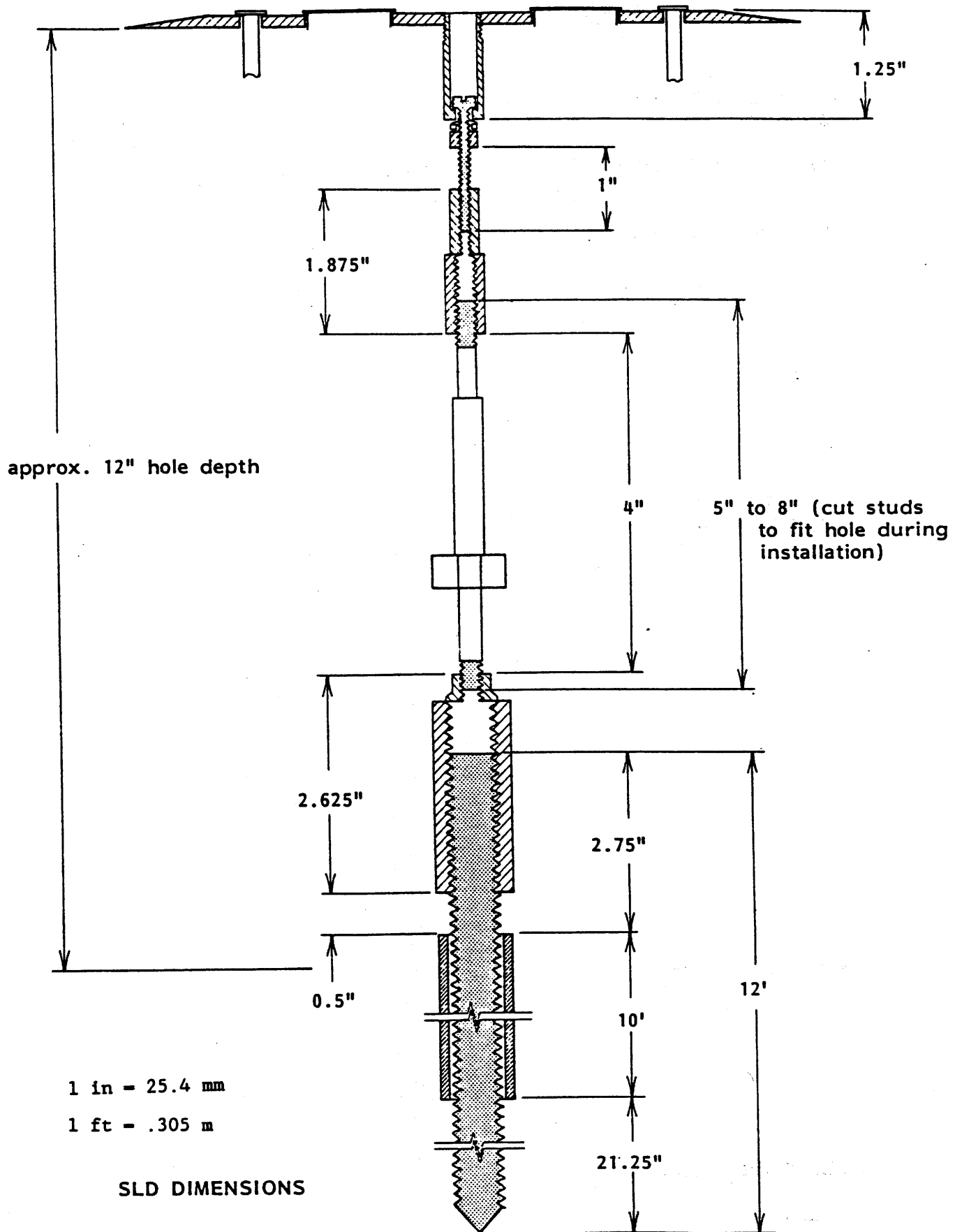


Figure 91. Assembly drawings--SLD transducer (dimensions).

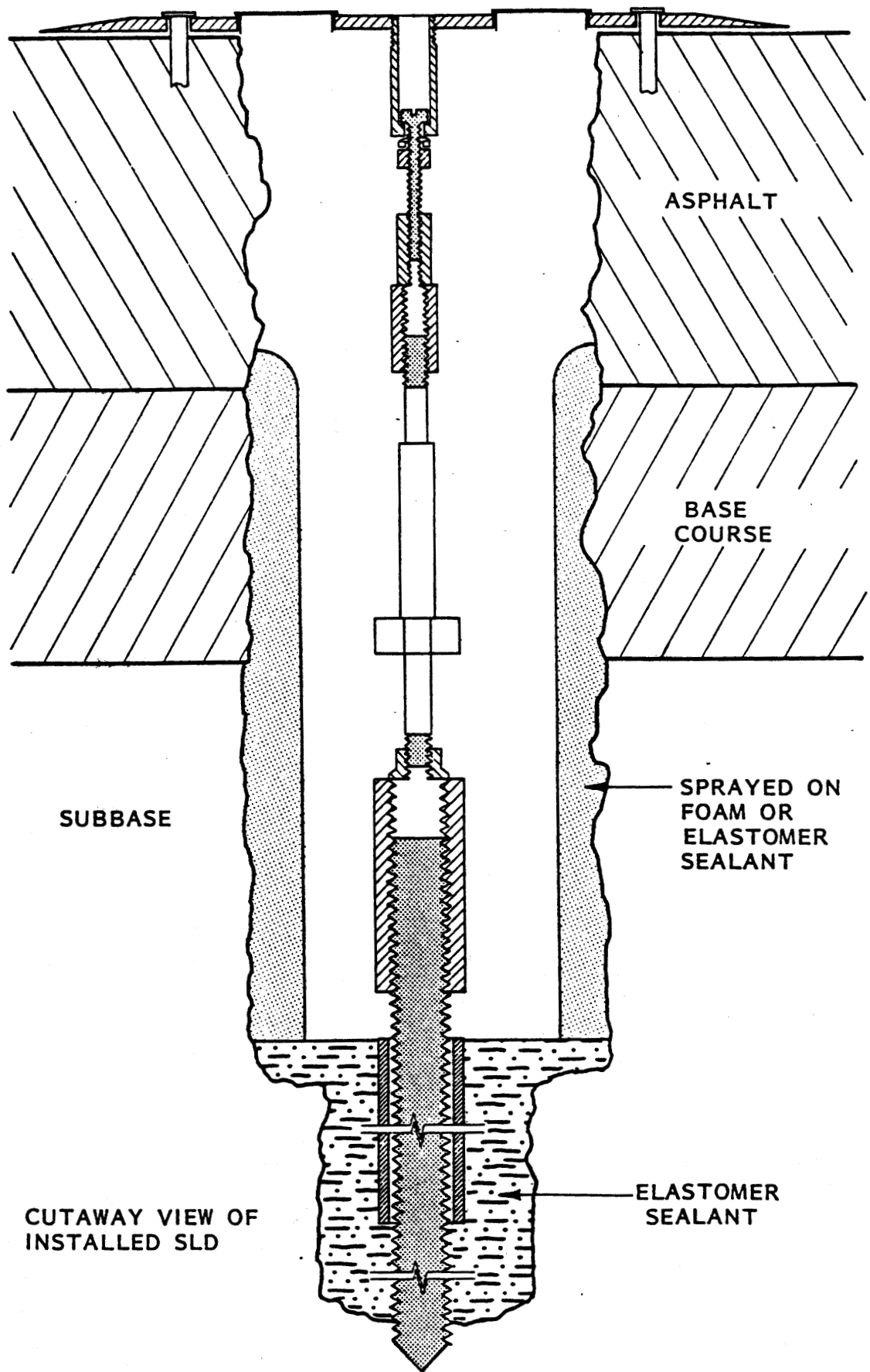
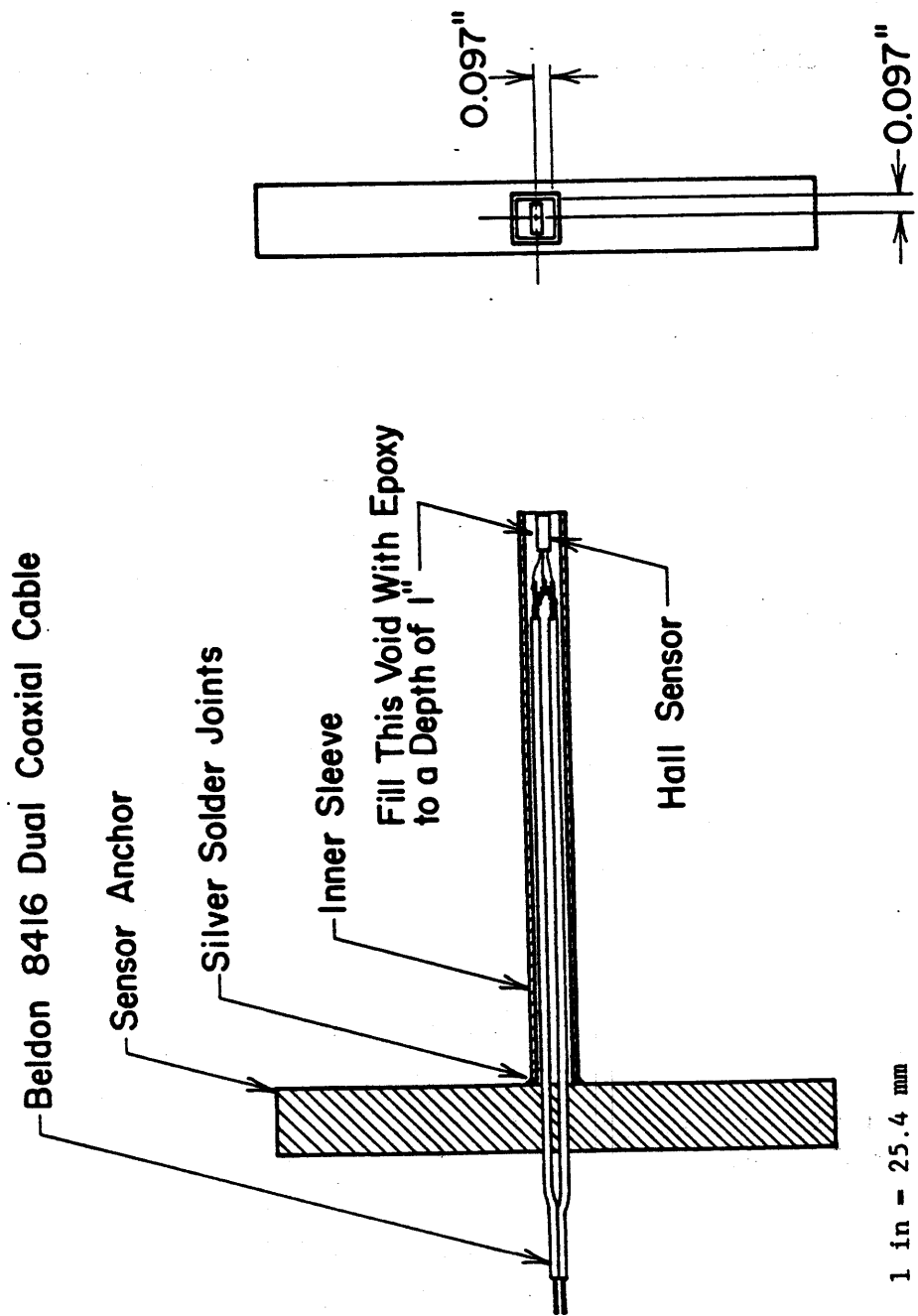
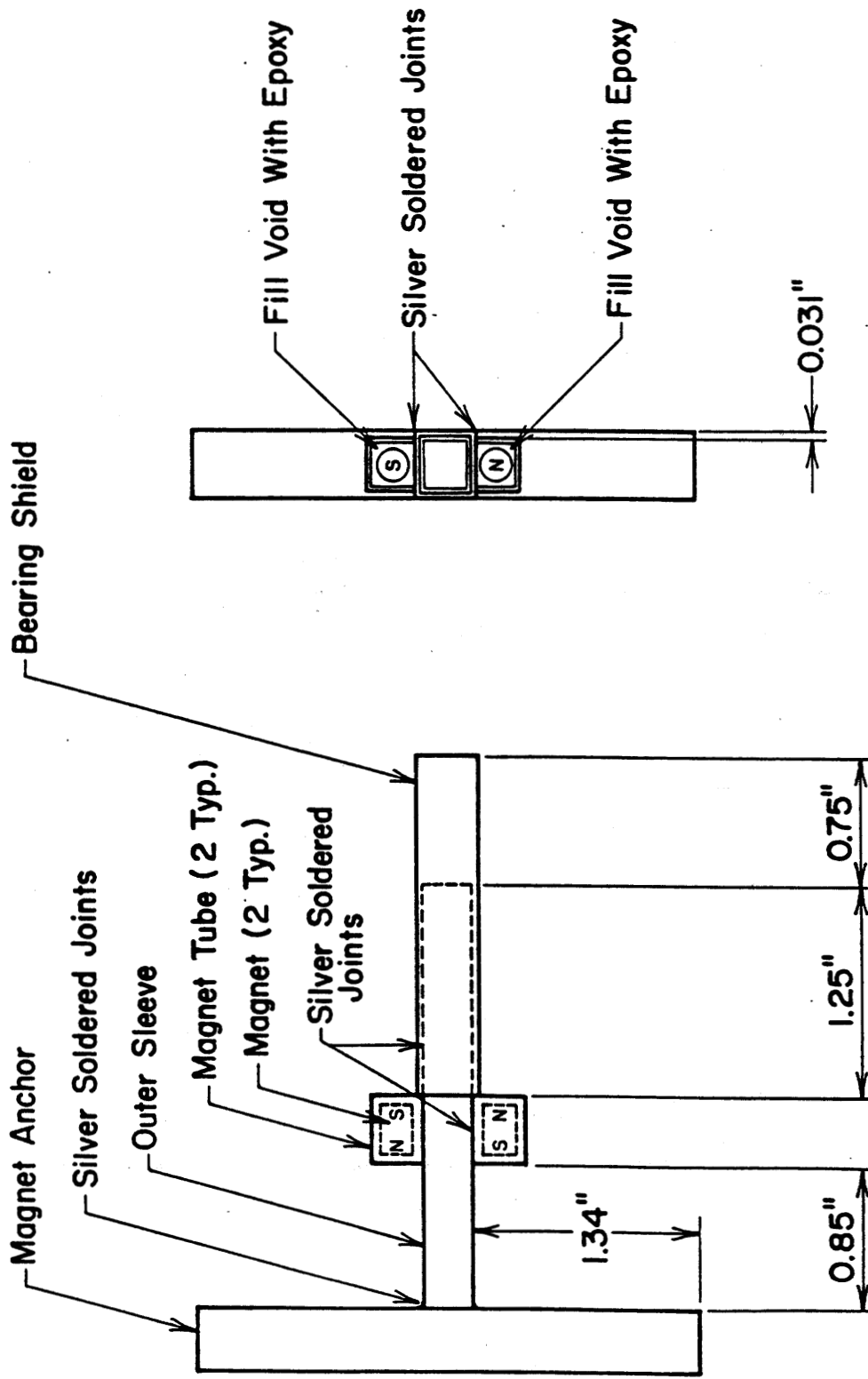


Figure 92. Assembly drawings--SLD transducer (installed).



COMPLETED SENSOR ASSEMBLY

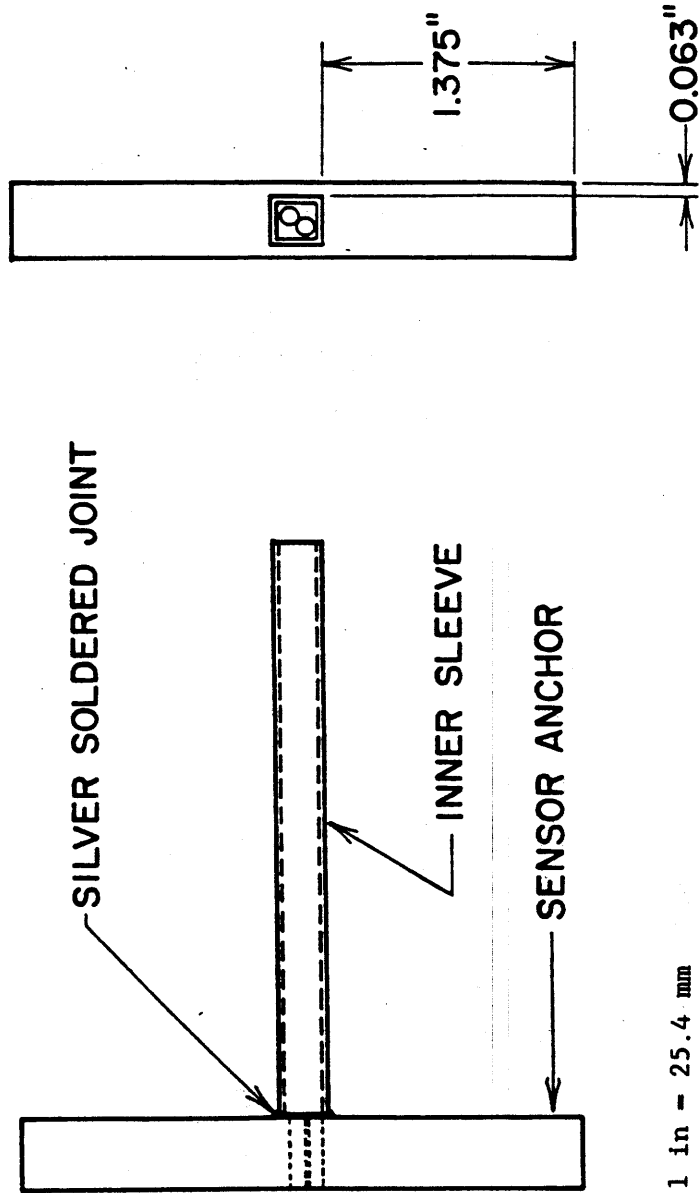
Figure 93. Completed sensor assembly drawings--asphalt transducer.



1 in - 25.4 mm

MAGNET ASSEMBLY DRAWING

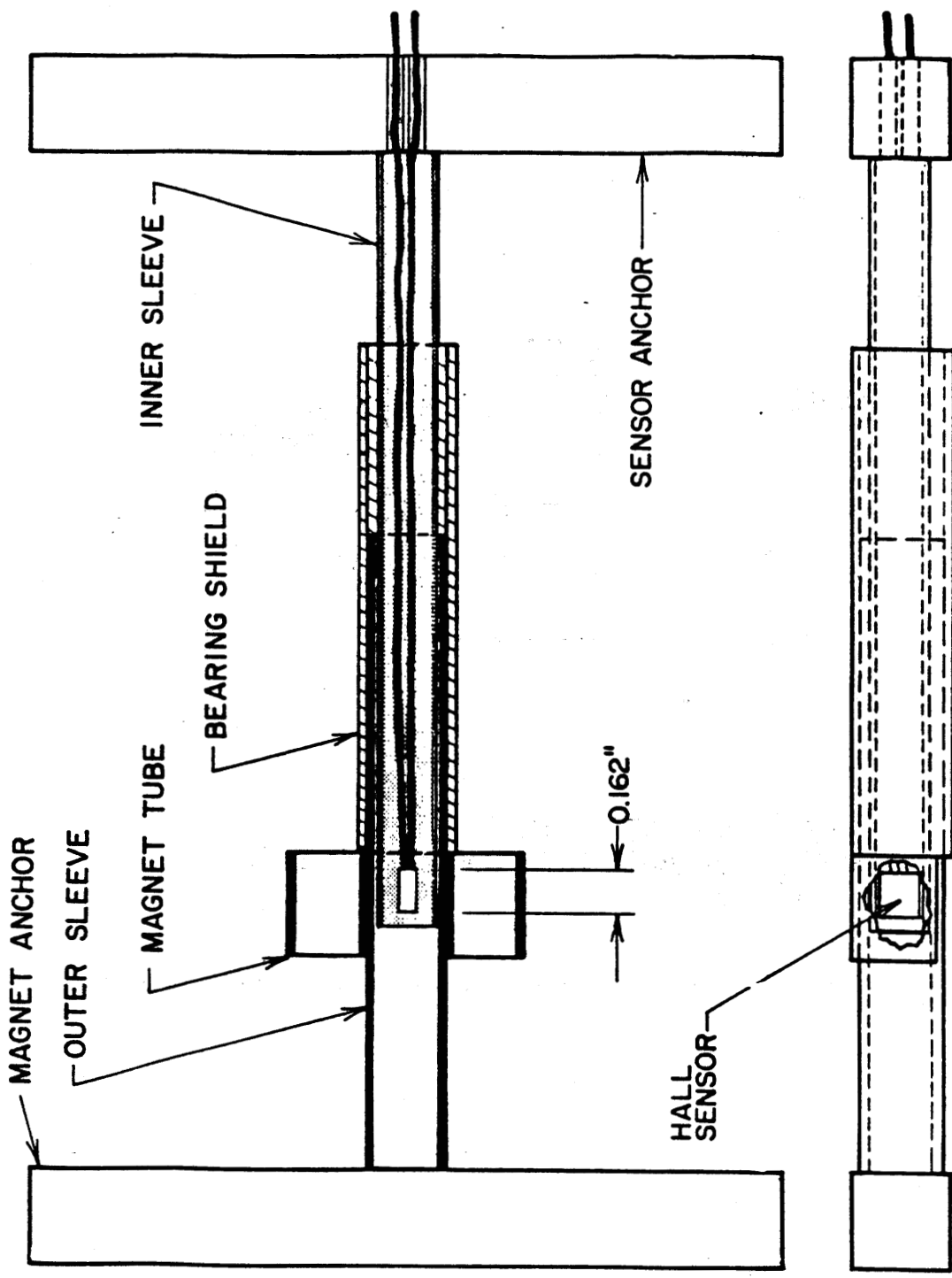
Figure 94. Magnet assembly drawings--asphalt transducer.



1 in - 25.4 mm

SENSOR ASSEMBLY DRAWING WITHOUT SENSOR AND CABLES

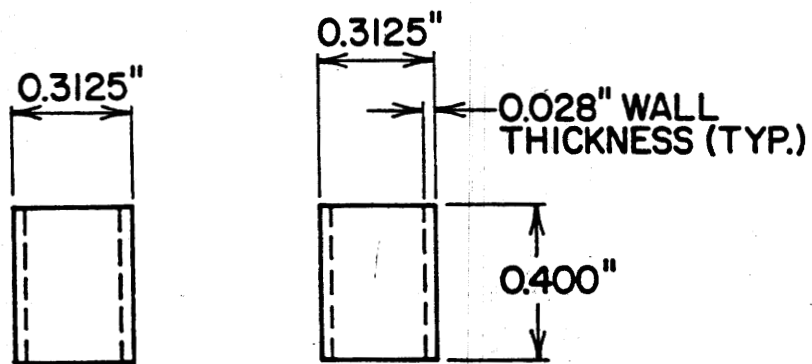
Figure 95. Assembly drawings (without sensor and cables)--asphalt transducer.



SILVER SOLDERED JOINTS

ALL MAT'LS BRASS

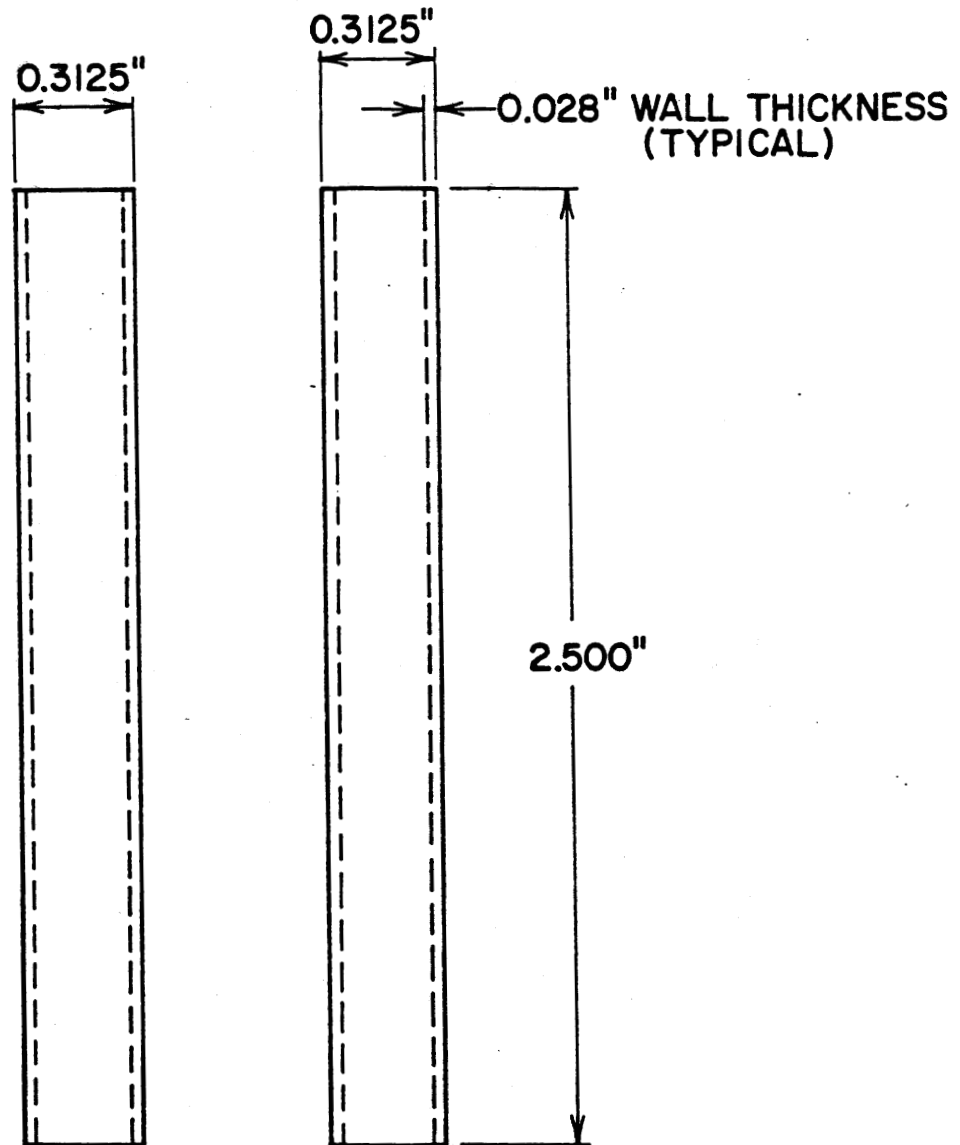
Figure 96. Assembly drawings--asphalt transducer.



1 in = 25.4 mm

ITEM: MAGNET TUBE
 MAT'L: SQUARE HOLLOW BRASS TUBE
 QTY: 2

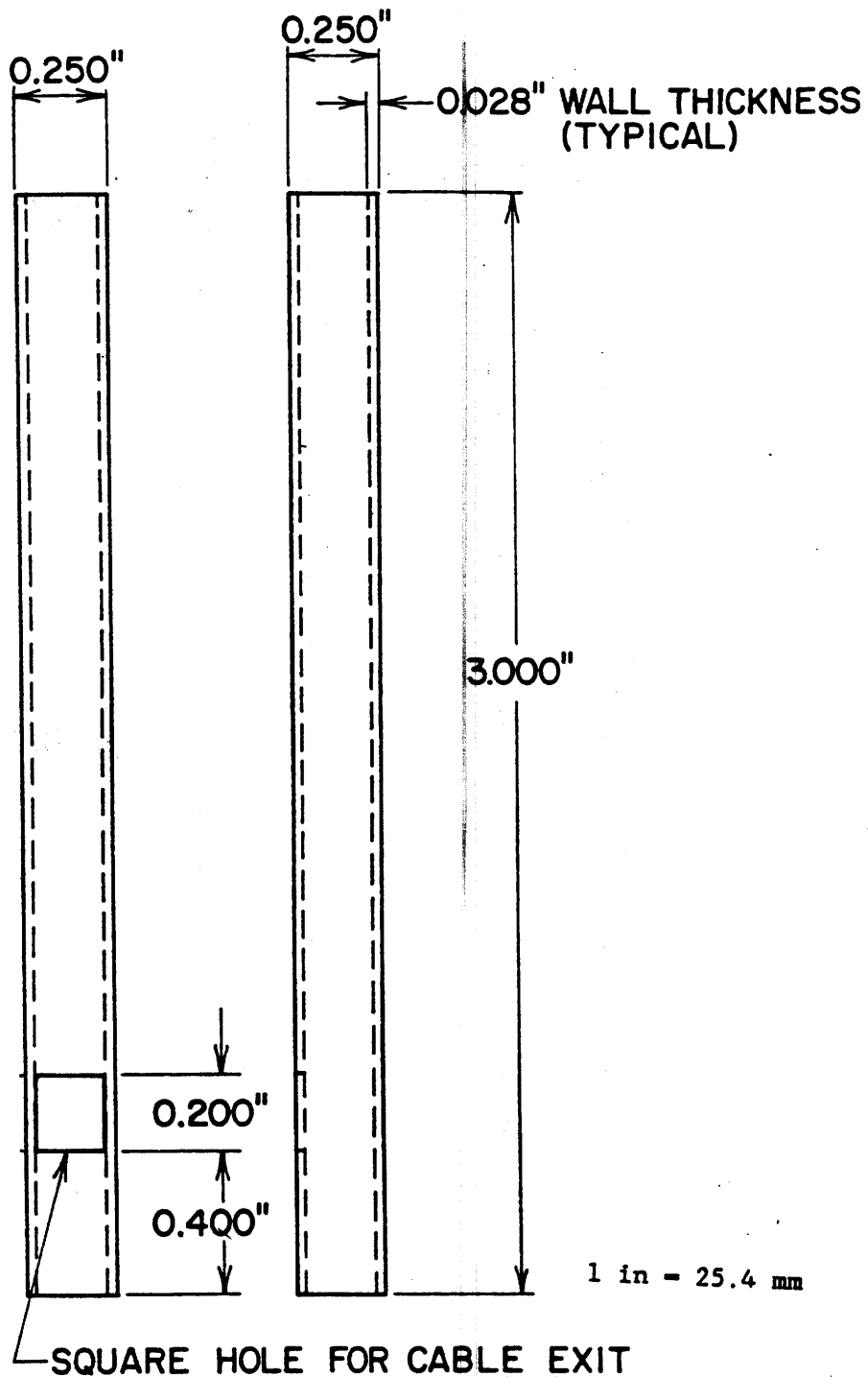
Figure 97. Manufacturing drawings--transducer assembly (magnet tube).



1 in = 25.4 mm

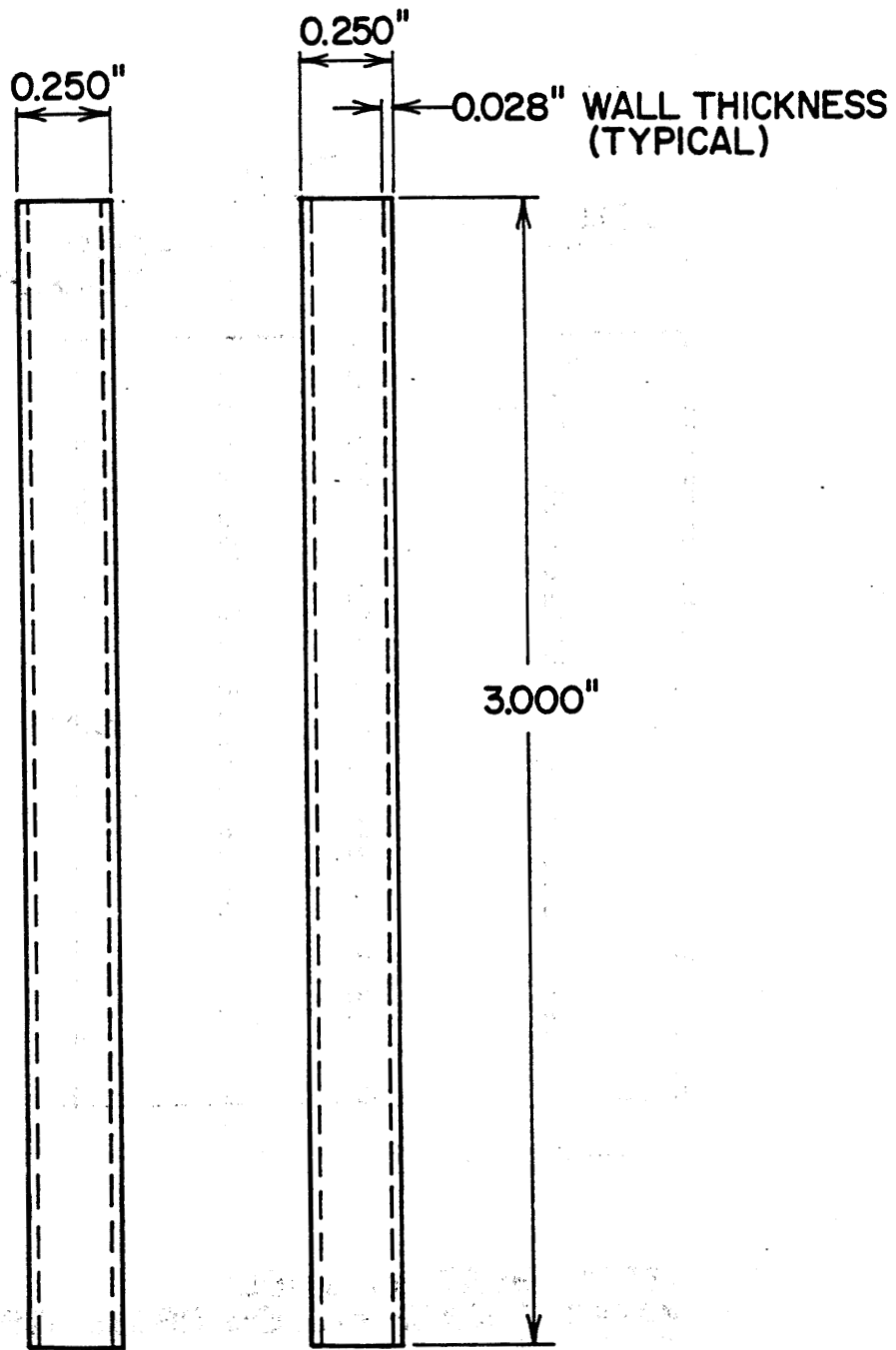
ITEM: OUTER SLEEVE
 MAT'L: SQUARE HOLLOW BRASS TUBE
 QTY: 1

Figure 98. Manufacturing drawings--transducer assembly (outer sleeve).



ITEM: SLD AND SOIL GAUGE INNER SLEEVE
 MAT'L: SQUARE HOLLOW BRASS TUBE
 QTY: 1

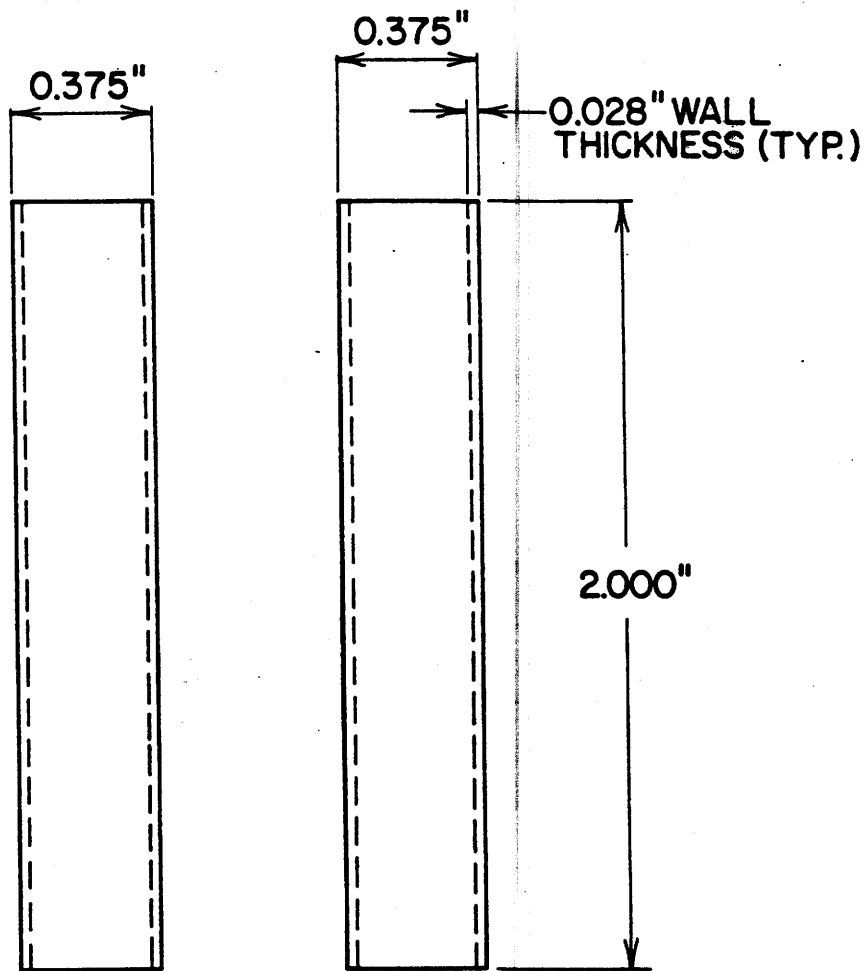
Figure 99. Manufacturing drawings--transducer assembly (SLD and soil gauge inner sleeve).



1 in = 25.4 mm

ITEM: INNER SLEEVE
 MAT'L: SQUARE HOLLOW BRASS TUBE
 QTY: 1

Figure 100. Manufacturing drawings--basic transducer assemblies.

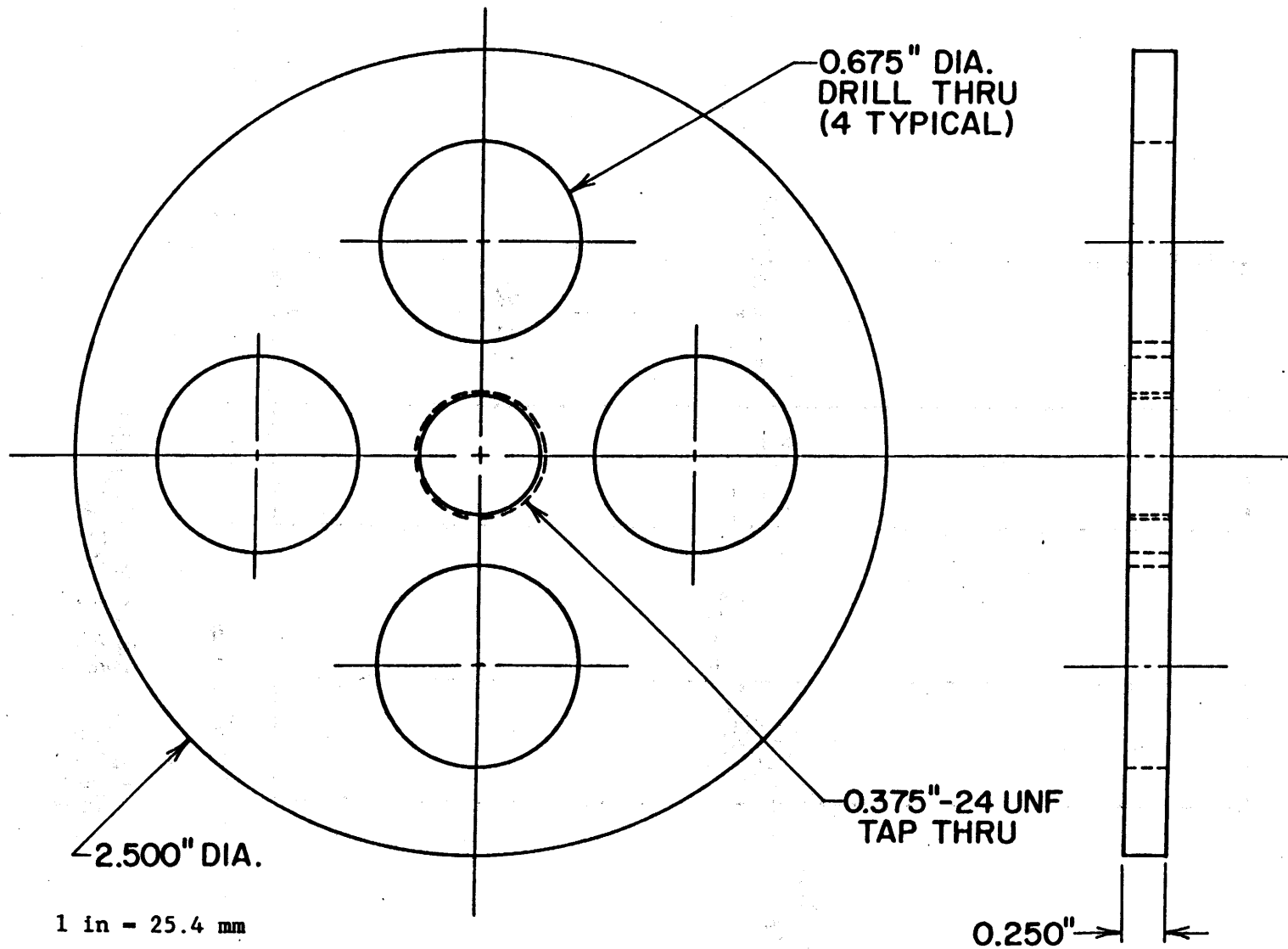


1 in = 25.4 mm

ITEM: BEARING SHIELD
MAT'L: SQUARE HOLLOW BRASS TUBE
QTY: 1

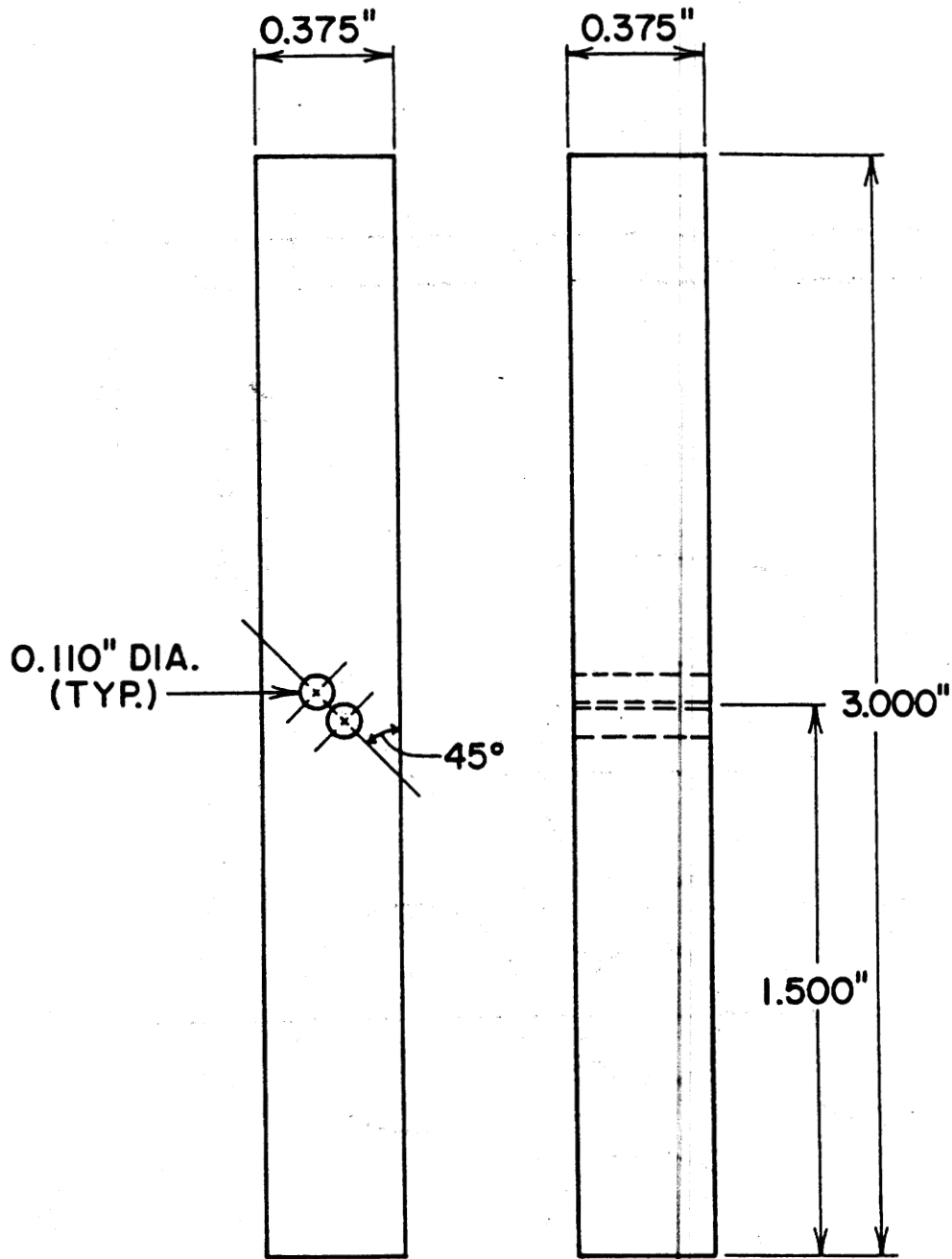
Figure 101. Manufacturing drawings--transducer assembly (bearing shield).

279



ITEM: SOIL ANCHORS
MAT'L: BRASS
QTY: 2

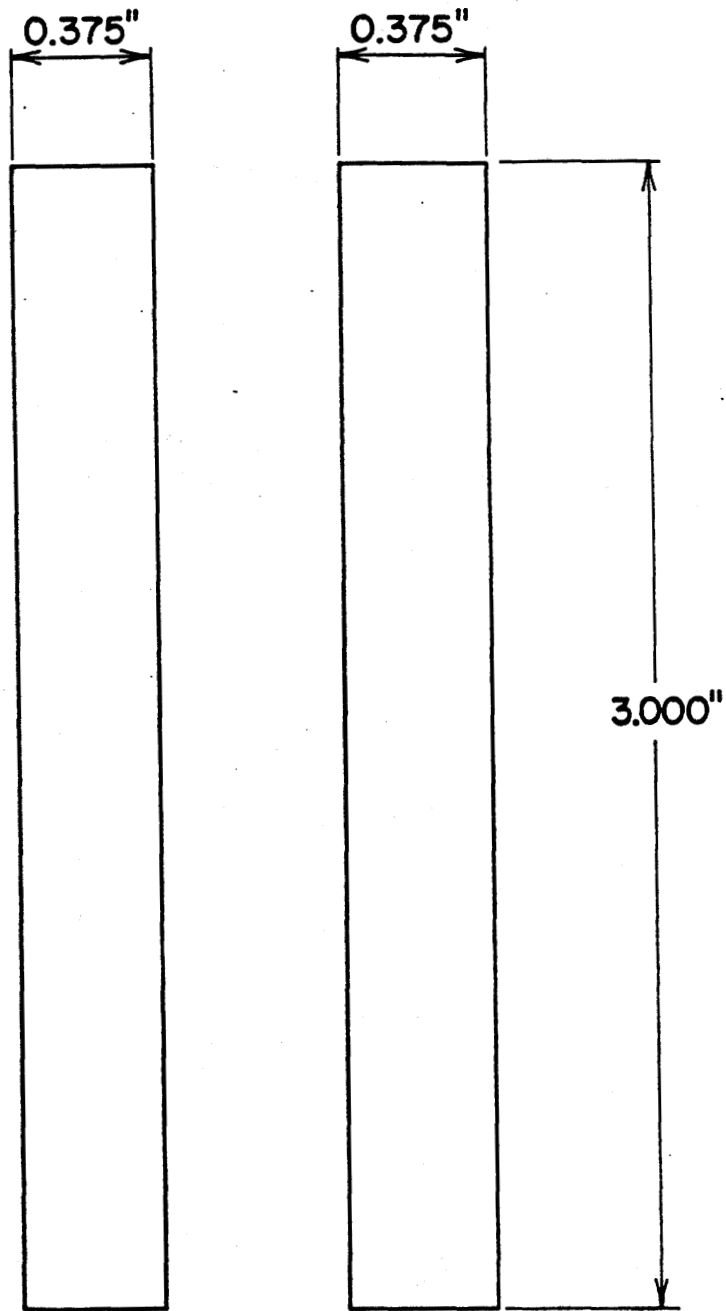
Figure 102. Manufacturing drawings--transducer assembly (soil anchors).



1 in = 25.4 mm

ITEM: SENSOR ANCHOR
 MAT'L: SOLID BRASS
 QTY: 1

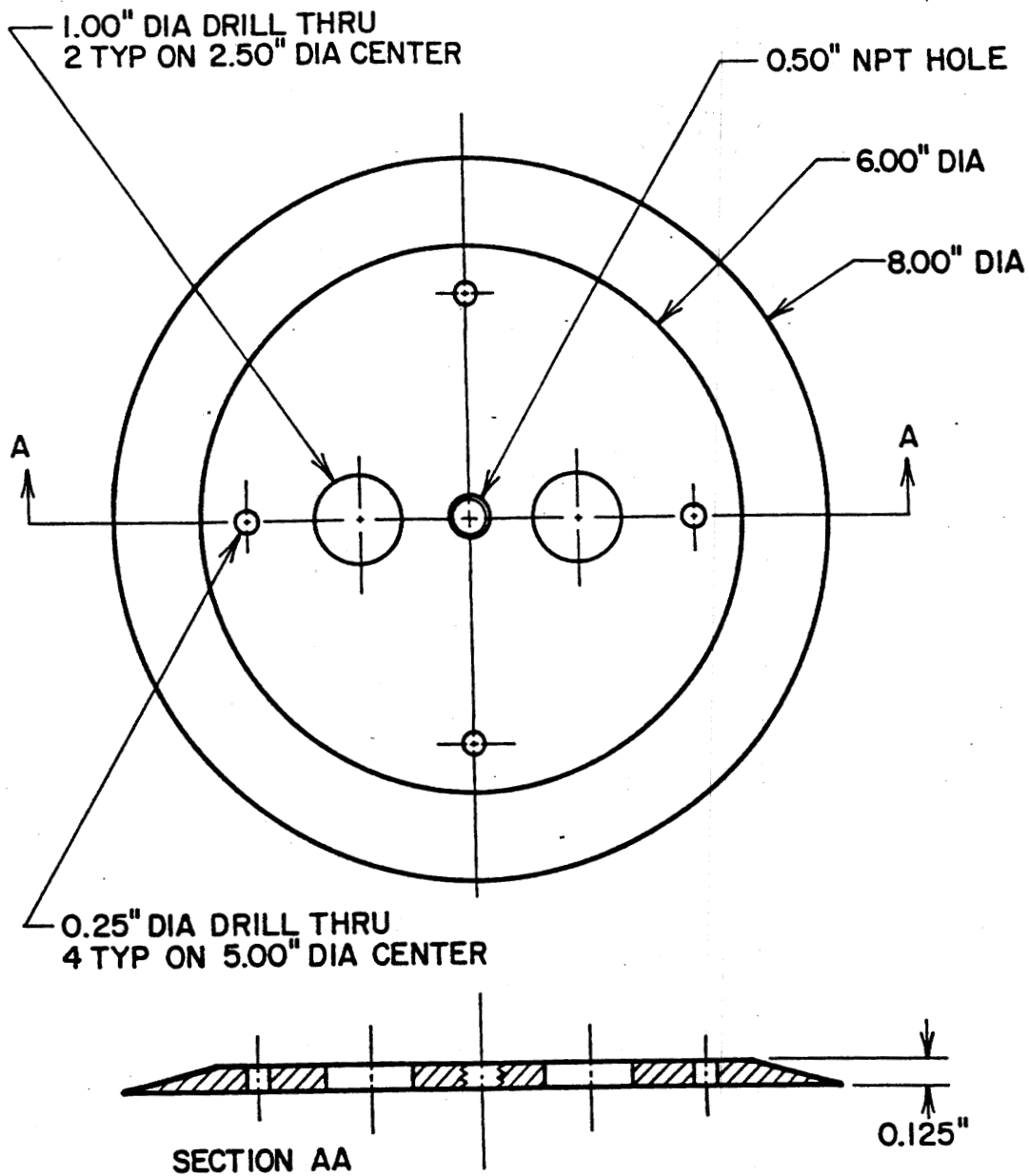
Figure 103. Manufacturing drawings--transducer assembly (sensor anchor).



1 in = 25.4 mm

ITEM: MAGNET ANCHOR
MAT'L: SOLID BRASS
QTY: 1

Figure 104. Manufacturing drawings--transducer assembly (magnet anchor).



ITEM: SLD DISK
MAT'L: STEEL

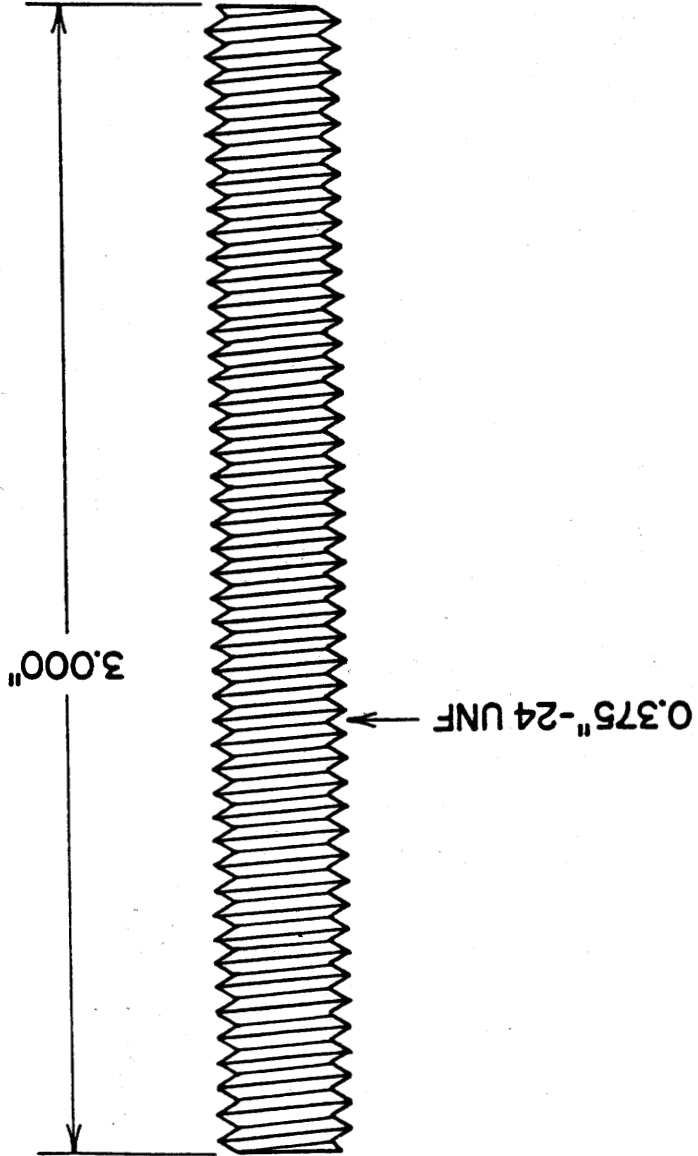
1 in = 25.4 mm

Figure 105. Manufacturing drawings--transducer assembly (SLD disk).

Figure 106. Manufacturing drawings--transducer assembly (SLD and soil gauge mounting stud).

ITEM: SLD AND SOIL GAUGE MOUNTING STUD
MAT'L: THREADED BRASS ROD
QTY: 2

1 in - 25.4 mm



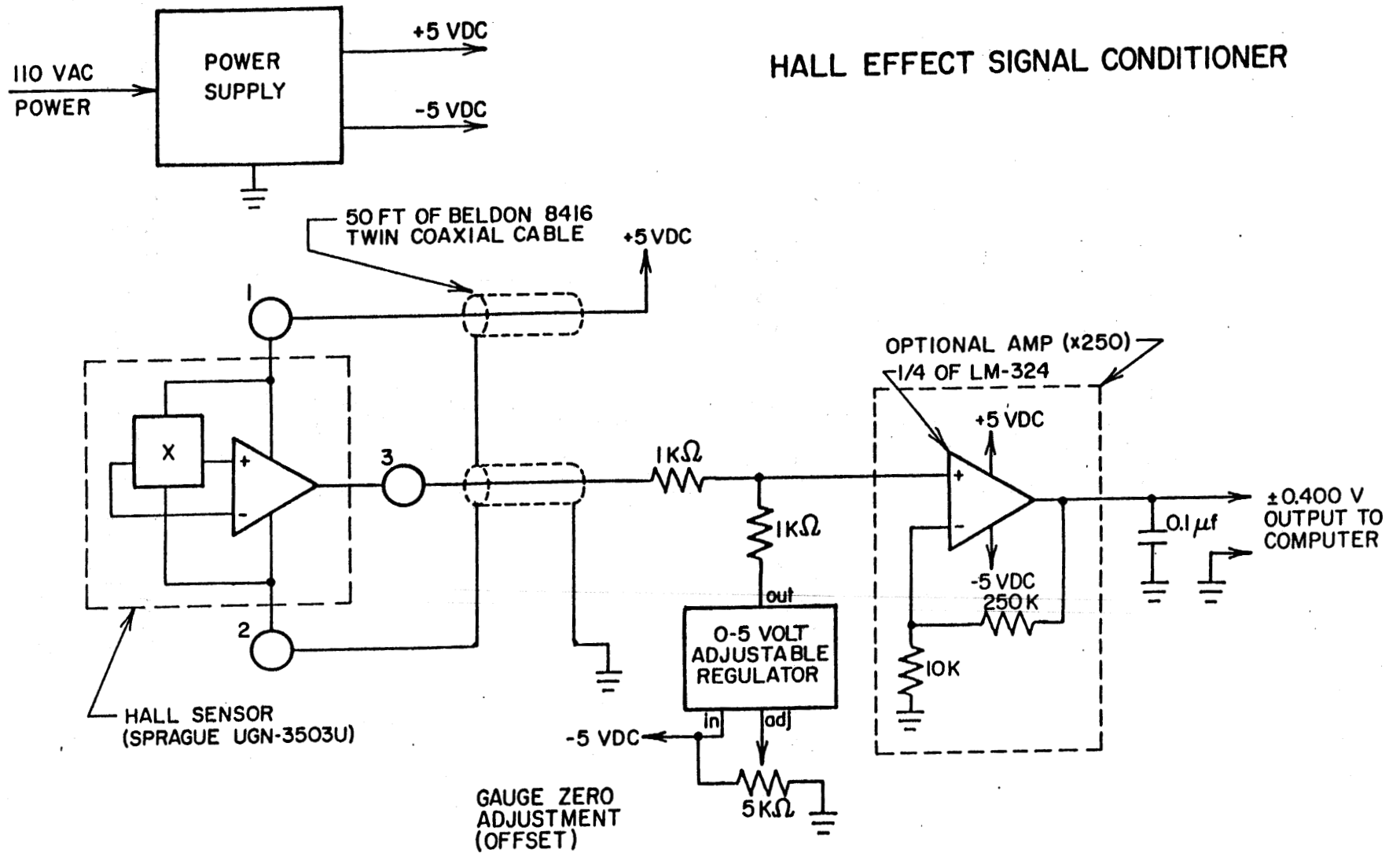


Figure 107. Assembly drawings--transducer conditioner for all three variations of transducers.

REFERENCES

1. American Association of State Highway and Transportation Officials, *AASHTO Guide for Design of Pavement Structures*, AASHTO, Washington, DC, 1986.
2. P. Sebaaly, N. Tabatabaee, and T. Scullion, *Instrumentation for Flexible Pavements--Interim Report*, Publication No. FHWA-RD-89-084, Federal Highway Administration, Washington, DC, April 1989.
3. P. Sebaaly, N. Tabatabaee, C. E. Antle, and B. T. Kulakowski, *Statistical Analysis of the Field Data*, PTI Report No. 9038, Pennsylvania Transportation Institute, University Park, PA, March 1990.
4. J. F. Potter, H. C. Mayhew, and A. P. Mayo, *Instrumentation of the Full Scale Experiment on A1 Trunk Road at Conington, Huntingdonshire*, Report LR296, Road Research Laboratory, 1969.
5. S. Nazarian and A. Bush, "Determination of Deflection of Pavement Systems Using Velocity Transducers," paper presented at the Annual Meeting of the Transportation Research Board, Washington, DC, 1989.
6. A. J. Bush, *Nondestructive Testing of Light Aircraft Pavements, Phase II, Development of the Nondestructive Evaluation Methodology*, Publication No. FHWA/RD-80/911, Federal Highway Administration, Washington, DC, 1980.
7. J. Uzan, R. L. Lytton, and F. P. Germann, "General Procedures for Backcalculating Layer Moduli," paper presented at the First Symposium on NDT of Pavements and Backcalculation of Moduli, ASTM, Baltimore, MD, July 1988.
8. J. Uzan, T. Scullion, C. H. Michalek, M. Parades, and R. L. Lytton, *A Microcomputer Based Procedure for Backcalculating Layer Moduli from FWD Data*, TTI Research Report 11-23-1, Texas Transportation Institute, College Station, TX, July 1988.
9. J. T. Christison and B. P. Shields, "Pavement Elastic Moduli by the Surface Wave Method Correlated with In-Situ Measurements of Elastic Response under Moving Vehicle Loads," in *Proceedings of the 19th Annual Conference of the Canadian Technical Asphalt Association*, Regina, Saskatchewan, pp. 229-252.

